

---

# **Validation of a Real-Time Engineering Simulation of the UH-60A Helicopter**

---

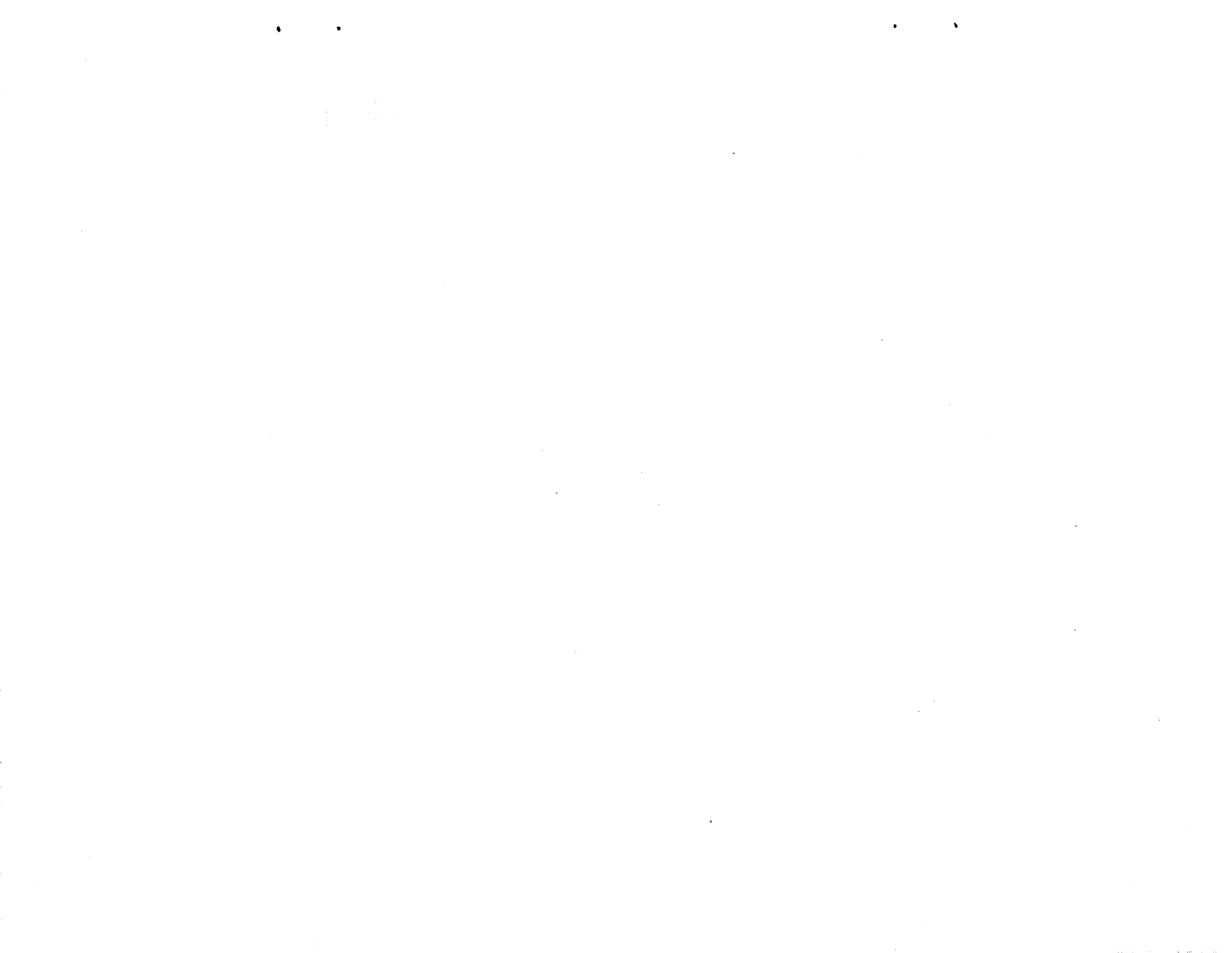
Mark G. Ballin, Ames Research Center, Moffett Field, California

February 1987



National Aeronautics and  
Space Administration

**Ames Research Center**  
Moffett Field, California 94035



## SUMMARY

A real-time simulation of the UH-60A Black Hawk Helicopter based on the Sikorsky Gen Hel mathematical model is compared with flight test data and Sikorsky's nonreal-time computer program. An overview of the mathematical model is given, including a description of updates and expansion of the model by NASA. Also, real-time programming requirements and techniques are explained. The simulation displays very good agreement with flight test data and excellent agreement with the nonreal-time program on which it is based. The large dedication of effort required to develop the real-time program suggests a need for development of generalized techniques for real-time simulation of high-fidelity physical models of rotorcraft.

## INTRODUCTION

High fidelity modeling of helicopter dynamics is increasingly becoming a requirement for pilot-in-the-loop handling qualities research. Dynamics once considered to be of secondary importance, such as vehicle response to rotor speed variations, are now seen to be areas where improvement is desirable for future generations of rotorcraft. In addition, high-gain feedback control systems require considerable model sophistication. If careful consideration is not given to high-order dynamics, possible instabilities of the actual closed-loop system will not be reproduced. Simulation models are therefore required which provide the fidelity necessary to reproduce higher-order effects over a large flight envelope in real time.

High-fidelity engineering simulations which are based on physical representations of dynamic systems have advantages over linear-map or parametric equation representations for many simulation investigations. In this type of model, internal physical quantities such as individual rotor blade positions or shear forces at a hinge are determined. The dynamics of each helicopter subsystem and its effects on other subsystems are modeled in physical terms. This allows a user to modify a component subsystem, such as a lag damper, based on tests of the actual hardware. If an interaction between two or more subsystems has an effect on handling qualities (for example, the torque-balance interaction of the main rotor, tail rotor, engines, and fuel control system), the high-fidelity physical model may be used to investigate this effect over a wide range of flight conditions. Simpler models may correctly simulate the interaction only about a narrow range of conditions for which estimates of each interacting quantity are valid. High-fidelity piloted simulation may also be used to investigate handling qualities or controllability of the modeled aircraft outside the normal range of operation. Because vehicle systems are modeled physically, internal quantities can be observed which may be important for reasons

not related to handling qualities, such as flight safety. For example, the proximity of each blade tip to the tail boom may be monitored as the pilot operates in an off-design condition.

A high-fidelity real-time model of the Sikorsky UH-60A Black Hawk helicopter has been under development for several years at NASA Ames Research Center for use on the Vertical Motion Simulator (VMS). Validation of the mathematical model of the helicopter was initially performed by Sikorsky Aircraft (ref. 1). Validation of the real-time model is necessary to establish that real-time computer coding considerations do not dynamically alter the model and that subsequent updates to the model have in fact further improved the fidelity of the model.

The real-time simulation is first demonstrated to be statically valid over a typical envelope of operation. Examples of dynamic response to pilot input are then used to show concurrence with the previous validation study and to illustrate the effects of improvements by comparison with flight-test data. The work presented here should not be interpreted as a complete validation over the entire operating range of the simulation.

#### MATHEMATICAL MODEL DESCRIPTION

The real-time mathematical model of the UH-60A is based on the generalized, modularized programs developed by the manufacturer for time-domain analysis of total helicopter systems. These programs make up the Sikorsky General Helicopter Flight Dynamics Simulation (Gen Hel). A real-time version of this mathematical model was provided to NASA Ames under contract (ref. 2). From this model, a computer program was written to execute in real time on the CDC 7600 computer. In addition, the fidelity of the model was increased as needed, notably in the area of engine and drive train modeling.

The model is a nonlinear representation of a single main rotor helicopter that is accurate for a full range of angles of attack, sideslip, and rotor inflow. Six rigid-body degrees of freedom as well as the main rotor flapping, lagging, air-mass, and hub-rotational-speed degrees of freedom are modeled. Because of its modular nature, each major force- and moment-producing component of the aircraft is treated as an independent entity. The underlying framework of the program is the interfacing between these components. All of the interfaces are physical quantities such as forces, moments, attitudes, body-fixed velocities, and downwash velocities. In this way, interaction between the components is modeled while maintaining the flexibility to modify or replace any one component without modification to the other components. Figure 1 is a block diagram representation of the simulation components.

A blade-element approach is used to model each main rotor blade. Total rotor forces and moments are produced by summations of forces from each blade, which are determined from aerodynamic, inertial, and gravitational forces. Aerodynamic forces are computed from angle of attack and dynamic pressure acting on each blade segment based on the orthogonal velocity components. These components are determined as

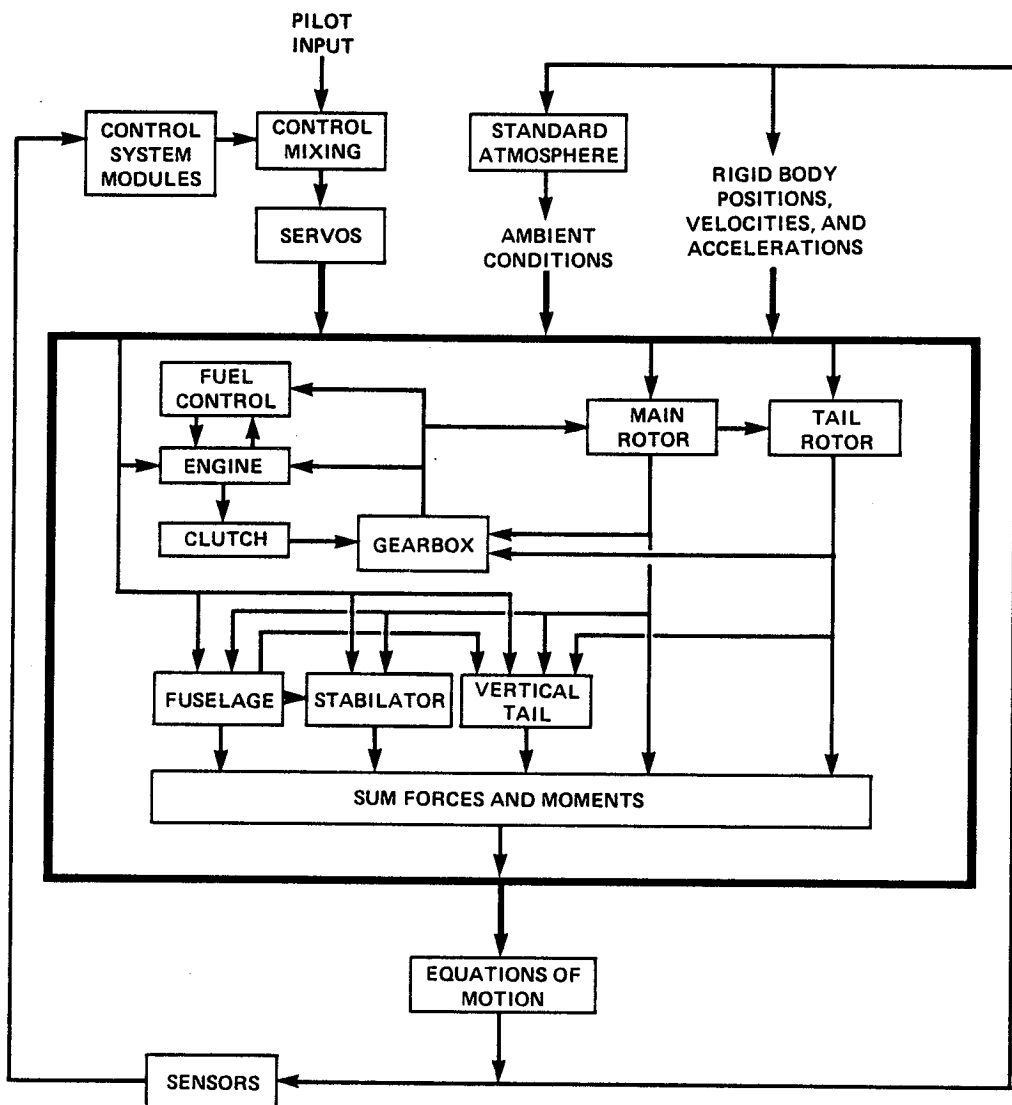


Figure 1.- Gen Hel simulation components.

functions of blade azimuth, lag and flap angles, local velocity of the blade segment, and local downwash. Downwash is approximated to have a first harmonic distribution as a function of wake skew angle. Blade inertial and gravitational forces are computed from blade rotational velocity, lagging and flapping velocities and accelerations, and blade position. No dynamic twisting or bending of the blades is modeled, although a preformed blade twist is represented through adjustment of the geometric pitch of each segment. The summations of forces act on the airframe at the blade hinge and lag damper locations. Rotor moments result from blade hinge and lag damper offsets from the main rotor shaft.

The tail rotor thrust is represented by linearized Bailey theory. Interference effects from the aerodynamic modules are accounted for as empirically determined blockage factors. The main rotor downwash is used to modify the tail rotor inflow. The aerodynamics of the fuselage, stabilator, and vertical tail pylon are each represented in separate modules so that the nonlinear interference effects of the main rotor and the interference between the components are modeled separately. The aerodynamic function tables were developed from wind-tunnel test data, and reference 3 was used to extrapolate and modify the available data.

#### MODEL UPDATES

Some inertial terms of the blade flapping acceleration equation had been dropped by Sikorsky under simplifying assumptions. During real-time implementation of the RSRA mathematical model (ref. 4), it was found to be necessary to complete the inertial terms. The Gen Hel RSRA blade-element rotor model is identical in formulation to the UH-60A model; all additional terms were therefore incorporated in the UH-60A simulation. A complete description of the added flapping-equation inertial terms may be found in reference 5.

As part of an ongoing VMS effort to explore the improvements attainable in helicopter handling qualities by improving rotor speed control, a real-time digital simulation for the GE T700 engines and their hydromechanical and electrical fuel control systems was developed by NASA Ames. Based on a simplified hybrid computer program developed by NASA Lewis, it was expanded to a level of sophistication necessary for compatibility with the Sikorsky Gen Hel mathematical model. Rather than using a partial derivative representation (as was done in ref. 2), the major engine components and dynamics of several internal engine states are modeled on the basis of physical laws relating to transfer of energy and mass flow. The simulation is a close representation of T700 performance and dynamics over the full operating range and its component formulation allows great flexibility.

Because of this increased level of detail, it was necessary to incorporate a modified version of the expanded gearbox model developed by Sikorsky for the RSRA. It allows an accurate representation of power dissipation by the main rotor, tail rotor, accessories, and transmission. The inertias of all of the major rotating components are also modeled. The tail rotor module was expanded to include a torque-required computation by the addition of Bailey drag terms (described in ref. 6). A new formulation of the engine-overrunning clutch was also developed by NASA Ames to allow correct operation at flight idle and in situations involving loss of engine power.

In early real-time qualitative assessments, the pilots commented about unrealistic lags between collective control input and vehicle response and their inability to perform precision hover tasks without causing pilot-induced oscillation. After examination of total-system and model delays and lags, it was determined that the bandwidth of the transfer function representing primary servo dynamics was too

low. The swashplate angle of the actual aircraft is controlled by three primary servos which exhibit nonlinear characteristics, both individually and when working together. However, the linear transfer function representation is considered to be a level of sophistication which is appropriate for use with Gen Hel. After consultation with the manufacturer, a bandwidth which is based on the no-load acceptance testing of the actuator was used in place of the original math model implementation. As will be shown, the time histories of the transient responses reflect the improvement. Pilot comments also suggest that collective response characteristics are much improved.

Appendix A contains the complete equations describing the model updates implemented on the Ames real-time simulation. Variables used in the appendix are Sikorsky Gen Hel variable names (ref. 2).

#### REAL-TIME CONSIDERATIONS

Real-time simulation of a blade-element rotor requires that time steps be as small as possible. Modeling of high bandwidth dynamics also requires small time steps. In addition, delays from cockpit input to visual- and motion-system output must be minimized. The outputs from each program module must be computed from one pass through the module. Internal iteration is used only when it is unavoidable, because a constant time step must be based on the maximum number of iterations needed. For each program pass, forces and moments from each component are computed and summed, from which the net translational and angular accelerations acting on the airframe are determined. The resulting body-fixed velocities and positions are used sequentially in the succeeding intervals to emulate a continuum solution to the total system.

The time-step size has a large effect on the output from the blade-element rotor program. The rotor model contains its own integration algorithms, tuned to give correct flapping and lagging positions and velocities in the rotating reference frame of the rotor hub. Because each rotor blade is modeled at its azimuth orientation, each update results in an azimuthal transition which, if too great, causes integration errors within the rotor that result in contaminated rotor outputs. Also, as in actual rotors, the total rotor outputs contain high frequency harmonics with a fundamental frequency equal to the number of rotor blades times the angular velocity of the hub (referred to as the N/rev frequency). A maximum step size must therefore be set to prevent aliasing of the fundamental frequency into lower frequencies.

The sequential nature of the "one-pass requirement" leads to algebraic loops in digital simulation. Algebraic loops are a result of sequential computation of interdependent parameters and must be prevented wherever possible through careful designing of code sequence and hierarchy. A discrete model must necessarily provide a value for a variable at the end of a time interval based on both its previous value and the values of parameters upon which it is dependent at the beginning of

the interval. In the real world, the variable is dependent on the values of other parameters at the same instant in time. The occurrence of an algebraic loop can result in significant differences in phase compared to the continuous system and the dynamic stability of the system can be affected. The real-time program has been sequenced, integration algorithms have been chosen, and the time-index corrections have been used to minimize these effects.

For example, the rotor speed degree-of-freedom results in an algebraic loop between the rotor, engine, and fuel control system which causes a significant propagation of error with increasing time step. Changes of rotor speed are a result of an imbalance of the main rotor torque required and the engine torque available. The hub angular acceleration is integrated to obtain hub velocity for each pass in the gearbox module, which is sequentially executed after the rotor and engine modules. At the beginning of each pass through the rotor, blade lag velocities and positions are computed from the integration algorithms. Lag acceleration, which is functionally dependent on hub acceleration, is then computed. However, the hub acceleration is actually an output from a previous pass through the gearbox and is therefore delayed by one interval. As explained in reference 7, rotor torque harmonic variations are largely a function of blade lag angles. Because rotor torque is used in the gearbox to determine the value of hub acceleration, an algebraic loop is formed. Real-time coding therefore requires that lag accelerations be corrected before their use in the blade-lag integration algorithms. The latest value of hub acceleration, calculated after the previous rotor pass, is used to modify the lag accelerations, and the effects of the previous hub acceleration used are subtracted out. This results in sequentially correct values of lag angle and resultant torque. Figure 2 illustrates the effect of this change for a time step of 20 msec. An abrupt decrease of collective pitch at 60 knots causes a variation in rotor hub speed and acceleration as shown in figure 2(a). Hub acceleration oscillates at the N/rev frequency, corresponding to the physical changes of torque at the hub. Without the correction, the algebraic loop causes a spurious 10-Hz oscillation at a large amplitude (fig. 2(b)).

Implementation of the blade-element rotor model also led to a reexamination of the basic kinematic model used at NASA Ames for all piloted simulation (ref. 8). Body translational and angular accelerations are computed by this module, but they are not normally updated for synchronization with the following time interval whereas velocities and positions are. Because the rotor module must use body accelerations as well as velocities and positions to determine hub accelerations, an algebraic loop is generated. It was found that sensitivity of the rotor module to errors in phase is greater than its sensitivity to small magnitude errors. The kinematic model was therefore modified to provide extrapolated accelerations, thereby eliminating much contamination of rotor output.

The "mixed time indices" which are the inevitable result of sequential one-pass coding have been minimized for the entire program using methods as described above. Correction of mixed indices alleviates the need for filtering or special numerical techniques for attenuation of rotor noise as were used in McFarland (ref. 9). The program can be executed with time steps as great as 20 msec with no

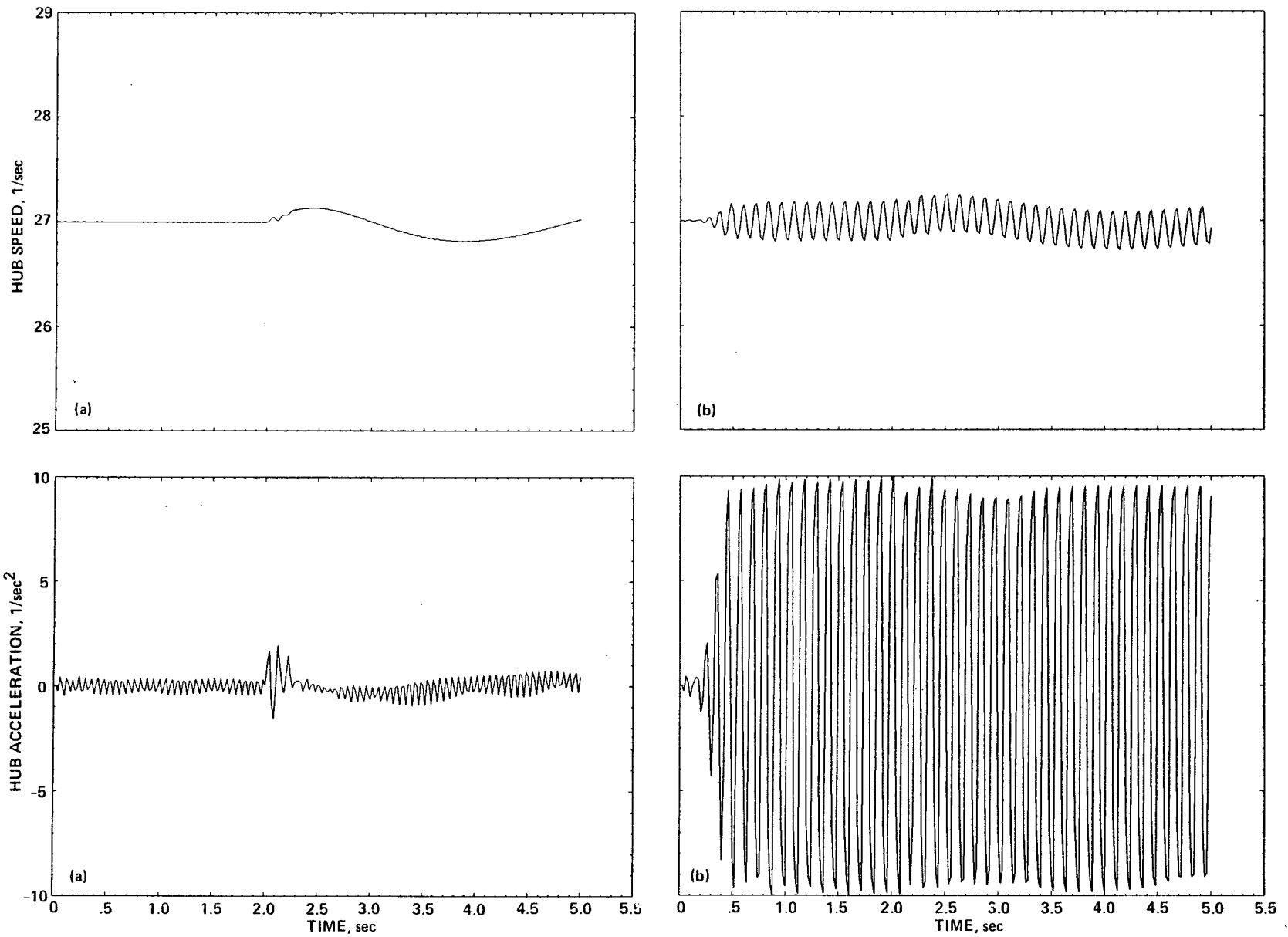


Figure 2.- Rotor hub speed and acceleration response to a 2-inch down collective step at 60 knots (0.02 sec time step). (a) With blade lag acceleration computation sequence correction; (b) without correction.

measurable effect on blade dynamics. Temporally mixed index values that still exist were determined to be too computationally costly to correct, but their influence on system dynamics is minimal. The real-time program sequence and hierarchy are shown in figure 3.

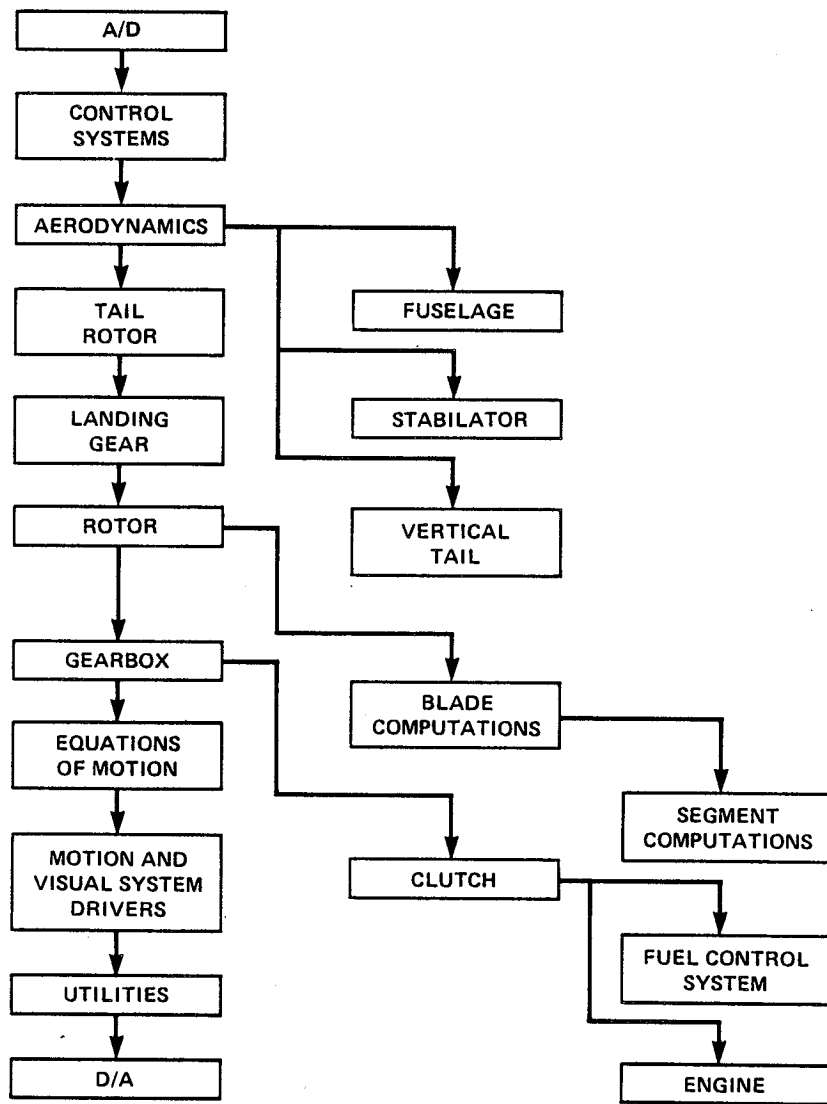


Figure 3.- Real-time program sequence and hierarchy.

## FLIGHT-TEST DATA

The test data used for comparison were obtained in a series of tests conducted by USAAEFA for use in validation of the Rotorcraft Systems Integration Simulator. A detailed description of the testing is given in reference 10. The trim data and selected transient-response time histories were provided to Sikorsky for use in their validation of the mathematical model (ref. 1). The test aircraft, S/N 77-22716, was an early production Black Hawk containing USAAEFA test instrumentation. An airspeed boom was mounted forward of the nose, and a movable ballast cart was used to adjust the longitudinal center of gravity as needed. In addition, blade pitch, flap and lag instrumentation was provided by Sikorsky.

Data were obtained while maintaining a constant thrust coefficient at specified vehicle and blade-tip Mach numbers. The altitude was increased as fuel was expended and the rotor speed was varied as a function of temperature. Fuel crossfeeding and the ballast cart were used to maintain constant lateral and longitudinal c.g.'s, while the waterline c.g. was allowed to vary.

No stability augmentation was used during transient-response data runs. Analog and digital stability augmentation systems, the flightpath stabilization system, and the stabilator control system were disabled and the pitch bias actuator was centered and locked. The stabilator was fixed for each run; its position was determined as the stabilator control system would have set it for the aim airspeed and collective determined by the specified thrust coefficient. This is a highly degraded configuration; the results are not representative of a UH-60A in normal operation. The configuration, however, allows a validation of the basic vehicle model without masking model deficiencies, as may occur when control system models are operating.

The transient responses consisted of individual-axis steps, pulses, or doublets of one inch or less in both directions. The velocities varied from hover to 140 knots true airspeed. The test procedure normally consisted of stabilizing in trim with one of the two redundant stability augmentation systems on; this was disabled one second before the control input. Unsatisfactory stability characteristics of the unaugmented aircraft, especially in pitch, required the pilot to initiate recovery within a few seconds of the input.

## STATIC TRIM

The steady-state trim characteristics of the two simulations and the flight test data are given in appendix B. A general six degree-of-freedom trimming algorithm was used to determine iteratively the steady-state flight conditions by adjusting aircraft attitude and control positions to zero all net forces and moments acting on the aircraft. The rigid-body equations of motion were bypassed during trim, but the rotor module was allowed to step forward in time. The aircraft configuration was set up to duplicate static-trim cases performed by Sikorsky to match

USAAEFA test data. Flight test values of aircraft weight, c.g. location, and trim main rotor speed were used. Comparisons of flight test values of stabilator incidence angle with known values based on Sikorsky experience indicate that the test data are in error by as much as 5°, so the stabilator control system was used to determine stabilator position for all static-trim comparisons. This method was also used in the Sikorsky validation (ref. 1).

Level-flight trims were determined for airspeeds from 0 to 160 knots in 10-knot increments. The control positions, aircraft attitude, stabilator position, and main-rotor required power are presented in figure B1. The trim points from the Sikorsky simulation were provided by Sikorsky for comparison. Agreement between the two simulations is excellent for all airspeeds. As indicated in reference 1, agreement between the simulation and the flight test is good except for a nearly constant pedal bias of approximately 0.5 in. to the right. There is less agreement at lower speeds, caused in part by the pilot's difficulty in achieving trimmed flight on the back side of the power-required curve and also by the simplified modeling of the impingement of the main rotor downwash on the fuselage and stabilator. This also results in an underestimation of collective stick trim position by both simulations when in hover.

The climb and descent comparisons are shown in figures B2 through B4 for airspeeds of 60, 100, and 137.5 knots. The Sikorsky simulation data are from reference 1. Discrepancies exist between Ames and Sikorsky simulations because Sikorsky used a level-flight trim value of stabilator position for each speed. Again, agreement is good, with the greatest differences occurring in pedal positions. Figure B5 contains comparisons for steady high-g coordinated turns for 60 and 100 knots. Because Sikorsky positioned the stabilator based on level-flight trim, differences between the simulations exist in pitch attitude and longitudinal cyclic position.

#### DYNAMIC RESPONSE

For transient response comparisons, the model configuration and test conditions were set up to duplicate those of the flight tests. All stability augmentation and flightpath stabilization was disabled and the pitch bias actuator was disabled and centered. As was done for static trim comparisons, the stabilator control system was used during the program trimming sequence to determine stabilator position, which was then held fixed. Because no information concerning moments and products of inertia of the test aircraft was available, the inertia terms used were those of the Sikorsky validation; they represent those of a typically configured and loaded Black Hawk. The ambient pressure, density, and temperature were determined from density and pressure-altitude test data.

After trimming to the test conditions, time histories of test-aircraft control inputs were used as direct input to the simulation. Constant biases were added to the control inputs to correct for small discrepancies between the test aircraft and simulation trim positions. In this way, the simulation begins each transient

response in trim and simulation trim errors have a minimal influence on dynamic response comparisons. The test data as received were already processed and no additional adjustments were performed. In a few of the test time-histories, spurious data and obviously incorrect offsets can be seen. They are attributed to instrument biases or recording errors, but no effort has been made at correction.

All simulation runs performed by Sikorsky in their nonreal-time validation used a time step of 0.01 sec. The simulation output was recorded only in time steps of 0.03 to 0.05 sec because of plotting limitations as described in reference 1. The N/rev frequency characteristic of the simulation is higher than the Nyquist criterion frequency corresponding to these sample rates, resulting in aliased output. The aliased frequencies seen in the Sikorsky simulation plots are 2.8 and 7.8 Hz and are especially prevalent in acceleration plots. Because of this, Sikorsky chose to base their simulation fidelity assessments on rate- and attitude-response data (ref. 1). A complete documentation of flight-test transient responses and Sikorsky simulation comparisons may be found in reference 11.

Appendix C contains aircraft configuration and sensor location information. Appendix D presents transient-response time-history comparisons between flight test data and the Ames real-time simulation. The flight-test velocity and acceleration time-histories represent values measured at a sensor location on the aircraft. Simulation velocities and accelerations were computed at these locations so that a direct comparison can be made. It should be noted that blade lag- and flap-angle time histories represent the motion of one instrumented rotor blade. Because there is no direct correspondence in blade azimuth between simulation and flight test, only relative amplitudes and frequencies should be compared.

#### Response to Control Inputs

The transient responses contained in appendix D serve as examples of response to control inputs for hover, 60-knot, and 100-knot initial level-flight conditions. Initial responses compare well with flight-test data, with somewhat less damping of simulation rates in general. Aerodynamic damping of the fuselage is not modeled in the simulation; this may have some effect on vehicle response involving large angular rates. Because of pilot difficulty in maintaining trim of the unaugmented aircraft, in many cases flight-test data had drifted from trim at the time of the control input, causing differences between test and simulation responses. There is also evidence of control input hysteresis in flight test data. Small inputs sometimes produced no flight test response. Because there is no modeling of control freeplay, simulation response may be expected to be faster with greater magnitude. The simulation also produces off-axis responses of greater magnitude than flight-test responses, caused at least partly by model approximations to the mechanical control linkages. Control mixing is approximated as linear cross-couplings between control inputs in the simulation, whereas in fact the mechanical linkages are not linear. A list of model deficiencies may be found in reference 1, most of which are considered to be of minimal importance. Some of the deficiencies

listed have been eliminated by model expansion and improvements, as described in the following section.

### Effects of Model Improvements

Appendix E contains example time-history comparisons between the Ames real-time simulation and the Sikorsky simulation. Figure E1, showing the response to a 0.5-in. aft cyclic step in hover, illustrates the very good agreement between the two simulations under circumstances in which model updates have a small influence. The trim control positions are identical for both simulations and the velocity, position, and attitude responses are very similar. The small differences between the two simulations are caused by the modification to the primary servo dynamics. As explained previously, aliasing of output is evident in Sikorsky acceleration plots and amplitudes of oscillation differ between the two simulations because of differing coding implementations. The control input caused little variation of rotor speed, so blade motions and directional axis responses are in agreement.

The response to a 1-in. down collective input at hover illustrates the improvements caused by program expansion and modifications (fig. E2). Modification to the primary servo bandwidth causes large improvements in all acceleration plots. As is most clearly seen in vertical-acceleration time histories, the Sikorsky simulation response lags the flight test response by approximately 0.1 sec, resulting in a simulation which causes pilot induced oscillation during hover. Increasing the servo bandwidth results in a very good agreement between the Ames simulation and flight-test data.

Several of the simulation deficiencies described in reference 1 are a direct result of insufficient detail in engine- and drive-train modeling. Improvements to the Ames real-time model are shown by figure E2 in rotor speed, engine-related time histories, and yaw-related histories. The Sikorsky-simulation rotor speed varies adversely in response to a collective input because of an insufficient level of sophistication of the partial derivative engine model and fuel control system (detailed in ref. 2). Its response is also too fast and is of the wrong magnitude. These rotor speed errors manifest themselves in yaw-acceleration, rate-, and heading-time histories as well as altering blade-lag response. Both engine models appear to trim at an incorrect level of power when compared with the flight test. This is a direct result of error in modeling of the main rotor torque in hover, as previously described. However, the NASA-developed engine shows slightly better agreement because of the more detailed representation of power required in the Ames real-time model. The simplified Sikorsky model always estimates tail-rotor required power to be 10% of main rotor power. In this hover case, tail rotor power of the real-time simulation is determined to be 13% of the main rotor power, which is a better approximation of the actual aircraft.

An example of response at high speed is shown in figure E3. Again, acceleration and rate responses to the lateral input are lagged in the Sikorsky simulation whereas those of the Ames simulation are in good agreement with test data. Ames

simulation engine trim is in slightly better agreement with test results, as evidenced by gas generator speed. The figure also illustrates the effect of slightly differing stabilator incidence angles on aircraft trim. The Sikorsky validation used the recorded flight test value of stabilator position for all transient response comparisons. Because the recorded stabilator data are suspected to be incorrect, the Ames validation was performed with an incidence angle determined by the stabilator control system during program trim. Blade-flap- and lag-time-histories, as well as trim control positions, suggest that this is a better approximation to stabilator position. In this example, the control system positioned the stabilator at  $3.75^\circ$  trailing edge down, while the flight test data indicated a value of  $7.8^\circ$ . This caused a larger nose-down trim attitude in the Sikorsky simulation, resulting in lower magnitudes of first-harmonic flapping and lagging of the main rotor. The conclusion in reference 1 that lagging amplitudes are too small is actually the result of differing stabilator positions between simulation and flight-test data.

#### RECOMMENDATIONS FOR IMPROVEMENT

Several deficiencies noted in reference 1 have been eliminated by the more detailed representation of the rotor speed degree-of-freedom and modification to the linear representation of the primary servo dynamics. Those eliminated include the incorrect fuel flow, main rotor torque, and main-rotor-speed response to a collective input, incorrect blade-flap and lag response to rotor control inputs, adverse yaw response to collective inputs, and delayed vehicle response to all control inputs.

The minor off-axis couplings may be caused in part by a linear representation of the mechanical control linkages. The couplings are reduced by the stability augmentation system; they produced very few pilot complaints during a recent VMS simulation. Differences in trim pedal position and trim collective position in hover probably have little adverse effect, but they do point to areas where increased model detail may be desired.

However, validation results and pilot opinion suggest that there is some need for further refinement and expansion of the model. Reference 1 states that large control inputs produce exaggerated model responses. Control freeplay should be modeled and a more sophisticated nonlinear representation of primary servo response, including rate and travel limits for each servo, may be warranted. This requires addition of the geometry that relates primary servo positions to swashplate angles. Pilot comments also suggest the need for simulation of the increased N/rev vibration level during quick-stops and in the speed range of 18 to 25 knots. This has been reported as a shortcoming of the actual aircraft (ref. 10), but pilots have found it to be an important cue, especially in the reduced visual environment of flight simulators. The simplified model of main rotor dynamic inflow may prevent physical modeling of the phenomenon, but an adequate representation may be achieved

through a flight-test-derived modification factor, as was done to simulate ground effect.

## CONCLUSIONS

Real-time simulation of rotorcraft is achievable at the level of sophistication of the UH-60A version of Gen Hel, although a high-speed computational capability is required. Blade-element rotor models with rigid blades which are used in conjunction with rigid-body airframe models may be executed in real time with no loss of model fidelity. Considerable effort is required to solve procedural and numerical problems which arise from the necessity to execute in the most computationally efficient manner possible. Because of the increasing use of high-fidelity modular programs, some form of generalized methodology is needed to decrease the development effort for each new program. Documentation of special correction techniques, such as that applied to the blade-lag-acceleration term, is necessary. Because it is generally not possible to achieve temporally perfect one-pass coding, the areas which must have correct temporal indices should be documented and incorporated into a generalized real-time modular program structure.

## APPENDIX A

### MODEL UPDATES

Modifications to the manufacturer-supplied mathematical model (ref. 2) are presented below. Symbols and program variable mnemonics follow the convention of the reference.

#### ADDITIONS TO THE FLAPPING ACCELERATION EQUATION

Additions to reference 2 are underlined.

$$\begin{aligned}
 \ddot{\beta} = & \frac{M_b}{I_b} \left\{ \cos \beta [\dot{V}_{zs} + e\{2\Omega(p_s \cos \psi - q_s \sin \psi) + \dot{p}_s \sin \psi + \dot{q}_s \cos \psi\}] \right. \\
 & + \sin \beta \cos \delta [\dot{V}_{y_s} \sin \psi - \dot{V}_{x_s} \cos \psi - e(r_s - \Omega)^2] \\
 & + \sin \delta \sin \beta [\dot{V}_{x_s} \sin \psi + \dot{V}_{y_s} \cos \psi - e(\dot{r}_s - \dot{\Omega})] \left. \right\} \\
 & + \cos^2 \beta \{ \cos \delta [2(\Omega + \dot{\delta})(p_s \cos \psi - q_s \sin \psi) + \dot{p}_s \sin \psi + \dot{q}_s \cos \psi] \\
 & - \sin \delta [2(\Omega + \dot{\delta})(p_s \sin \psi + q_s \cos \psi) + \underline{\dot{q}_s \sin \psi - \dot{p}_s \cos \psi}] \} \\
 & - \sin \beta \cos \beta [(r_s - \Omega)^2 - 2\dot{\delta}(r_s - \Omega) + \dot{\delta}^2] + \frac{1}{I_b} (M_{FAB} + M_{FFD} + M_{FLD}) \quad (A1)
 \end{aligned}$$

where

$\beta$  blade flapping angle, rad

$\delta$  blade lagging angle, rad

$e$  blade hinge offset from center of rotation, ft

$I_b$  inertia of blade about the hinge, slug·ft<sup>2</sup>

$M_b$  first mass moment of blade about the hinge, slug·ft

$M_{FAB}$  aerodynamic moment about hinge (blade span axis), ft·lb  
 $M_{FFD}$  flapping moment caused by flap damper, ft·lb  
 $M_{FLD}$  flapping moment caused by lag damper, ft·lb  
 $\Omega$  rotor shaft speed, rad/sec  
 $\Psi$  rotor blade azimuth position, deg  
 $p_s$  angular rate about shaft x-axis, rad/sec  
 $q_s$  angular rate about shaft y-axis, rad/sec  
 $r_s$  angular rate about shaft z-axis, rad/sec  
 $v_{x_s}$  shaft x-axis velocity, ft/sec  
 $v_{y_s}$  shaft y-axis velocity, ft/sec  
 $v_{z_s}$  shaft z-axis velocity, ft/sec

#### Engine and Fuel Control Models

Real-time General Electric T700 engine and fuel control models are described in Ballin, Mark G., "A High Fidelity Real-Time Simulation of a Small Turboshaft Engine" (in preparation).

#### Drive Train Model

The following description of the drive train and tail rotor torque computation is modified from unpublished Sikorsky documentation (D. G. C. Ruttledge, personal communication, Sikorsky Aircraft, United Technologies Corp., 1986). Simplifications made for real-time implementation include rigid drive shafts and a single-engine and clutch representation of the propulsion system.

The drive train model consists of an idealized gearbox which sums the torque loads of a variety of components. Torque is provided by the engine module through a clutch interface. The gearbox model applies its torque load to the body c.g. via the rotor force and moment transformations rather than directly. All component loads other than internal torque balances are handled in the same manner as before.

Gearbox- The idealized gearbox is represented by a large ring-gear which has inertia and oil-drag damping. All component torques are summed at this ring-gear. A body-centered axis set is employed--thus body yaw acceleration ( $r$ ) terms are seen in the equations.

The ring gear inertia represents all the gear trains actually employed in the system, referred to a speed OMGBX which is the main-rotor-output shaft speed (rad/sec). To preserve the modularity concept of Gen Hel, components are specified with inertias including their associated shafting up to (an arbitrary) junction with the gearbox. This inertia is referred to the component operational speed. A gear ratio ( $n$ ) between the component operating and the gearbox main-rotor output speed is also specified. The gearbox algorithm then sums the  $n^2J$  appropriately, to represent the component inertia. If a component contains a clutch mechanism (e.g., engines usually have overrunning clutches) the module representing that component must have the ability to add the additional inertia when the clutch is fully engaged and conversely to remove it as soon as the clutch begins to slip.

In initial-condition mode:

If  $OMGIBX = 0$ ,  $OMGBX = OMRMR \cdot OMGTMR$   
 Else  $OMGBX = OMGIBX$   
 In any case  $OMRBX = OMGBX / OMGTMR$

In operate mode:

$$SQENBX = \sum_{i=1}^{\text{no. of engines}} QQENG$$

$$QGBX = \sum_{k=1}^{\text{no. of loads}} QQ_k - SQENBX + OMGBX \cdot DAMPBX$$

$$FACIBX = \sum_{k=1}^{\text{no. of loads}} FAC_k$$

$$OMGDBX = \frac{RS.MR - QGBX/JGBX}{1 + FACIBX/JGBX} \quad (A2)$$

$$OMGBX = OMGBX_0 + \int OMGDBX dt \quad (A3)$$

$$OMRBX = OMGBX / OMGTMR \quad (A4)$$

$$HPDBX = DAMPBX \cdot OMGBX^2 / 550.0 \quad (A5)$$

While trimming, use  $OMGDBX$  as a criterion.

Note. Torque load modules called by GEARBOX must contain:

$$1. \dot{\omega}_i = n_i \cdot \text{OMGDBX} \quad (\text{A6})$$

$$2. \omega_i = n_i \cdot \text{OMGBX} \quad (\text{A7})$$

$$3. Q\dot{Q}_i = n_i \cdot \text{QLOAD}_i \quad (\text{A8})$$

$$4. \text{FAC}_i = J_i \cdot n_i^2 \quad (\text{A9})$$

Where

DAMPBX viscous damping component of the gearbox caused by oil drag and other factors, ft·lb·sec

FAC<sub>i</sub> inertia of the *i*th component with reference to the gearbox speed

FACIBX partial sum of the gearbox inertias

HPDBX horsepower absorbed in the gearbox, hp

JGBX the rotating inertia of the gearbox components referred to the output speed OMGBX (defined later), slug·ft<sup>2</sup>

J<sub>j</sub> rotating inertia of the *j*th component referred to the component operating speed, slug·ft<sup>2</sup>

n<sub>j</sub> gearing ratio between component-*j* operating speed and gearbox output speed OMGBX

OMGBX speed of the ring gear (output speed of main rotor gearbox), rad/sec

OMGDBX acceleration of the ring-gear, rad/sec<sup>2</sup>

OMGTMR trimmed main-rotor speed (defined as input), rad/sec

OMRRMR main-rotor-speed ratio (defined with respect to OMGTMR)

OMRBX gearbox-output-speed ratio (defined with respect to OMGTMR)

QLOAD<sub>i</sub> torque load of the *i*th component at the component operating speed, ft·lb

QQ<sub>i</sub> torque load of the *i*th component on the ring gear, ft·lb

QQENG output torque of an individual engine (measured at the ring-gear), ft·lb.

QGBX total torque load on the ring gear, ft·lb

RS.MR body yaw acceleration, rad/sec<sup>2</sup>

SQENBX sum of the engine torques transmitted to the gearbox, ft.lb

#### Tail Rotor Torque Transfer

The tail rotor is treated as a typical torque-load submodule except that the gear ratio is not entered directly; rather it is computed from the nominal-trim rotor rotational speeds.

In initial condition mode:

$$n_{TR} = \text{OMEGTR}/\text{OMGTMR} \quad (\text{A10})$$

In operate mode:

$$QQTR = n_{TR} * QTR$$

$$QGBX = QGBX + QQTR$$

$$FAC_{TR} = n_{TR}^2 * JSHTR$$

Note that all forces and moments (including the pitching moment due to QTR) are transferred to the c.g. by the tail-rotor module itself.

Where

FAC<sub>TR</sub> inertia of the tail rotor with reference to the gearbox speed, slug·ft<sup>2</sup>

JSHTR inertia of the tail rotor and associated shafts and gears as reflected at the tail rotor hub, slug·ft<sup>2</sup>

n<sub>TR</sub> overall gear ratio between tail rotor and gearbox main rotor output

OMEGTR nominal tail-rotor rotational speed (defined as input), rad/sec

OMGTMR nominal main-rotor trimmed speed (defined as input), rad/sec

QGBX torque load of the gearbox ring-gear, ft·lb

QQTR torque load of the tail rotor, reflected at the ring gear, ft·lb

QTR torque load of the tail rotor, at the tail rotor hub, ft·lb

### Main Rotor Torque Transfer

The main rotor is treated as a typical torque-load submodule except that the gearing is assumed to be unity.

$$\text{OMR.MR} = \text{OMRDBX}$$

$$\text{OMRMR} = \text{OMRBX}$$

$$\text{FAC}_{\text{MR}} = \text{JSHMR}$$

$$\text{QQMR} = \text{QHMR}$$

$$\text{QGBX} = \text{QGBX} + \text{QQMR}$$

Additionally,  $\text{QHEG} = \text{QQMR}$  (this allows the transfer of QQMR to the body c.g. in rotor code).

Where

$\text{FAC}_{\text{MR}}$  inertia of the main rotor shafting and hub with reference to the gearbox speed,  $\text{slug}\cdot\text{ft}^2$

$\text{JSHMR}$  inertia of the main rotor shafting and hub,  $\text{slug}\cdot\text{ft}^2$

$\text{OMR.MR}$  nondimensional acceleration of the main rotor

$\text{OMRDBX}$  nondimensional acceleration of the main rotor, gearbox output,  $1/\text{sec}^2$

$\text{OMRMR}$  main-rotor-speed ratio (defined with respect to  $\text{OMGTMR}$ )

$\text{OMRBX}$  gearbox-output-speed ratio (defined with respect to  $\text{OMGTMR}$ )

$\text{QQMR}$  torque load of the main rotor at the ring-gear,  $\text{ft}\cdot\text{lb}$

$\text{QHMR}$  torque load of the main rotor at the hub,  $\text{ft}\cdot\text{lb}$

$\text{QGBX}$  total torque-load at the gearbox ring gear,  $\text{ft}\cdot\text{lb}$

$\text{QHEG}$  yawing moment applied to the c.g. caused by the main rotor,  $\text{ft}\cdot\text{lb}$

Accessory loads- The accessory load is a rather arbitrary torque load which represents an average load caused by accessories such as generators and hydraulic pumps. The nominal accessory hp is converted to a torque at trimmed rotor speed and a variation of 10% load per 100% rotor-speed change is assumed.

In initial condition mode:

$$QQTACC = ACCHP * 550.0/OMGBX \quad (A11)$$

In operate mode:

$$QQACC = QQTACC (1.0 + 0.1 (OMRBX - 1.0)) \quad (A12)$$

$$QGBX = QGBX + QQACC$$

$$FAC_{ACC} = J_{ACC} * n_{ACC}^2 \quad (A13)$$

where

ACCHP nominal accessory load in trim, hp

FAC<sub>ACC</sub> inertia of the accessories with reference to the gearbox speed, slug·ft<sup>2</sup>

J<sub>ACC</sub> inertia of the accessories referred to the accessory drive speed, slug·ft<sup>2</sup>

n<sub>ACC</sub> gear ratio between accessory drive speed and gearbox output speed

OMAMGBX gearbox output speed, rad/sec

OMRBX nondimensional gearbox-output speed

QGBX cumulative total-torque load at the gearbox ring gear, ft·lb

QQACC actual accessory torque-load at gearbox ring gear, ft·lb

QQTACC torque load at the gearbox ring gear caused by accessories in nominal trim conditions, ft·lb

Multiple engine clutch- This is modeled as a triple-channel overrunning clutch which allows the hub to freewheel at higher speed than the engine-shaft-output speed while never allowing gearbox speed to be greater than hub speed.

The speeds are checked to see if they are in close proximity. If they are close, the accelerations are checked to see that the engine is applying a driving torque to the gearbox. Clutch chatter is reduced by delaying QPTE by one interval so that there are no mixed temporal indices in the clutch-logic equations.

The clutch logic is:

If OSEG < N<sub>E</sub> \* OMGBX, the clutch is disengaged

Else, if N<sub>E</sub> \* OMDBX > QPTE/JE, the clutch is disengaged

Else, the clutch is engaged

Whereupon

If the clutch is engaged,

$$FAC_E = n_E^2 J_E \quad (A14)$$

$$OSEG = OMGBX \cdot n_E \quad (A15)$$

$$OS.EG = OMGDBX \cdot n_E \quad (A16)$$

$$QQSTO = QPTE \cdot n_E \quad (A17)$$

but if the clutch is disengaged, FACIBX is not changed and

$$OS.EG = QPTE/JE \quad (A18)$$

$$OSEG = OSEG_O + \int OS.EG dt \quad (A19)$$

$$QQSTO = 0$$

In either case, QGBX = QGBX + QQSTO.

All of the steps are repeated for the number of engines required or the QGBX equation is modified to:

$$QGBX = QGBX + ENCOMP * QQSTO$$

Also, if the clutch is engaged,

$$FAC_E = (ENCOMP - 1.0) \cdot n_E^2 J_E \quad (A20)$$

and the clutch logic is executed only once.

ENCOMP number of identical engine/clutch combinations in simulation

FAC<sub>E</sub> inertia of engine and associated shafting with reference to the gearbox speed, slug·ft<sup>2</sup>

J<sub>E</sub> engine and associated shafting inertia, slug·ft<sup>2</sup>

n<sub>E</sub> gear ratio between engine output and gearbox ring gear

OMGBX gearbox-ring-gear-output speed

OMGDBX acceleration of the ring gear

OSEG engine-shaft-output speed, rad/sec

OS.EG engine-shaft-output acceleration, rad/sec<sup>2</sup>  
 QGBX cumulative total of ring-gear torques, ft·lb  
 QPTE engine-output torque (referred to engine speed), ft·lb  
 QQSTO engine torque (referred to the ring gear speed), ft·lb

#### Drive Train Constants

The drive train constants that were used for the UH-60A Black Hawk are as follows.

DAMPBX = 50.0  
 JGBX = 208.4  
 JSHMR = 41.85  
 JSHTR = 19.69  
 OMEGTR = 124.62  
 ACCHP = 40.0  
 J<sub>ACC</sub> = 0.004  
 n<sub>ACC</sub> = 51.4  
 n<sub>E</sub> = 81.042  
 JE = 0.124  
 ENCOMP = 2

#### ADDITIONS TO TAIL ROTOR MODEL (Modified from unpublished Sikorsky documentation)

The tail-rotor torque coefficient is defined as

$$\begin{aligned}
 CQTR = & \frac{\sigma}{2} [(\delta_2 t_{5.5} - a_{TR} t_{4.1}) \lambda^2 + (\delta_2 t_{5.6} - a_{TR} t_{4.2}) \theta_{TR} \lambda + (\delta_2 t_{5.7} - a_{TR} t_{4.3}) \theta_1 \lambda \\
 & + (\delta_2 t_{5.8} - a_{TR} t_{4.4}) \theta_{TR}^2 + (\delta_2 t_{5.9} - a_{TR} t_{4.5}) \theta_1 \theta_{TR} \\
 & + (\delta_2 t_{5.10} - a_{TR} t_{4.6}) \theta_1^2 + \delta_0 t_{5.1} + \delta_1 t_{5.2} \lambda + \delta_1 t_{5.3} \theta_{TR} + \delta_1 t_{5.4} \theta_1]
 \end{aligned}$$

where  $\sigma = bc/\pi R_{TR}$  and  $\theta_1 = TWSTTR/57.3$ . Tail rotor torque is then computed as

$$QTR = CQTR \cdot \pi \rho \Omega_{TR}^2 R_{TR}^5 OMGBX^2$$

The coefficients used in the above equations are defined as

$$t_{4.1} = \frac{B^2}{2} + \frac{5}{4} + \frac{\gamma^2 B^2}{1296} \mu_{TR}^2$$

$$t_{4.2} = \frac{B^3}{3} + \frac{8B}{3} + \frac{\gamma^2 B^9}{864} \mu_{TR}^2$$

$$t_{4.3} = \frac{B^4}{4} + 2B^2 + \frac{\gamma^2 B^{10}}{1080} \mu_{TR}^2$$

$$t_{4.4} = \frac{8}{9} B^2 + \frac{\gamma^2 B^{10}}{2304} \mu_{TR}^2$$

$$t_{4.5} = \frac{4B^2}{3} + \frac{\gamma^2 B^{11}}{1440} \mu_{TR}^2$$

$$t_{4.6} = \frac{B^4}{2} + \frac{\gamma^2 B^{12}}{3600} \mu_{TR}^2$$

$$t_{4.7} = \frac{-B^5}{108} \mu_{TR}^2$$

$$t_{4.8} = \frac{-B^6}{144} \mu_{TR}^2$$

$$t_{4.9} = \frac{-B^7}{180} \mu_{TR}^2$$

$$t_{4.10} = \frac{B^2}{36} \mu_{TR}^2$$

$$t_{5.1} = \frac{1}{4} + \frac{1}{4} \mu_{TR}^2$$

$$t_{5.2} = \frac{1}{3}$$

$$t_{5.3} = \frac{1}{4} + \frac{1}{4} \mu_{TR}^2$$

$$t_{5.4} = \frac{1}{5} + \frac{1}{6} \mu_{TR}^2$$

$$t_{5.5} = \frac{1}{2} + \frac{-1}{4} + \frac{1}{B^2} + \frac{1}{2B^4} + \gamma^2 \frac{B^4}{162} - \frac{B^5}{81} + \frac{B^6}{144} \mu_{TR}^2$$

$$t_{5.6} = \frac{2}{3} + \frac{4}{3B} + \frac{4}{3B^3} + \gamma^2 \frac{B^5}{108} - \frac{B^6}{54} + \frac{B^7}{96} \mu_{TR}^2$$

$$t_{5.7} = \frac{1}{2} + 1 + \frac{1}{B^2} + \gamma^2 \frac{B^6}{135} - \frac{2B^7}{135} + \frac{B^8}{120} \mu_{TR}^2$$

$$t_{5.8} = \frac{1}{4} + \frac{1}{4} + \frac{8}{9B^2} + \gamma^2 \frac{B^6}{288} - \frac{B^7}{144} + \frac{B^8}{256} \mu_{TR}^2$$

$$t_{5.9} = \frac{2}{5} + \frac{1}{3} + \frac{4}{3B} + \gamma^2 \frac{B^7}{180} - \frac{B^8}{90} + \frac{B^9}{160} \mu_{TR}^2$$

$$t_{5.10} = \frac{1}{6} + \frac{5}{8} + \gamma^2 \frac{B^8}{450} - \frac{B^9}{225} + \frac{B^{10}}{400} \mu_{TR}^2$$

for which

$$\gamma = \frac{\rho a_{TR} C_{TR} R_{TR}^4}{IB_{TR}}$$

where

$a_{TR}$  blade-section lift curve slope, 1/rad

$b$  number of tail rotor blades

$B$  blade-tip-loss factor

$c$  tail-rotor-blade chord, ft

CDTR	tail rotor hub drag, $\text{ft}^2$
$IB_{TR}$	mass moment of inertia of rotor blade, $\text{slug}\cdot\text{ft}^2$
OMGBX	gearbox ring gear output speed, rad/sec
QTR	tail rotor torque, ft-lb
$R_{TR}$	tail rotor radius, ft
TWSTTR	linear blade twist, deg
$\delta_0, \delta_1, \delta_2$	coefficients in power series which express section profile-drag coefficient as a function of lift coefficient
$\gamma$	mass constant of tail rotor blade
$\lambda$	tail rotor inflow
$\mu_{TR}$	tail-rotor-tip-speed ratio
$\Omega_{TR}$	tail-rotor trim speed, rad/sec
$\rho$	air density, slugs/ $\text{ft}^3$
$\sigma$	tail rotor solidity
$\theta_1$	linear blade twist, rad

#### ADDITIONAL TAIL ROTOR CONSTANTS FOR UH-60A BLACK HAWK

The constants necessary to incorporate the tail rotor torque model are as follows:

$$\delta_0 = 0.0087$$

$$\delta_1 = -0.0216$$

$$\delta_2 = 0.4$$

$$IB_{TR} = 3.1$$

In addition, the value of CDTR in reference 2 has been changed:

$$CDTR = 0.4$$

## PRIMARY SERVO DYNAMICS MODIFICATION

The transfer function as it appears on pp. 5.5-14, 5.5-15, 5.5-16, and 5.5-17 of reference 2 is as follows.

$$\frac{\delta_{MX}}{\delta_{MIX}} = \frac{1}{0.00114 s^2 + 0.0473 s + 1}$$

The primary servo dynamics modification as based on no-load acceptance testing of actuators:

$$\frac{\delta_{MX}}{\delta_{MIX}} = \frac{1}{0.0002041 s^2 + 0.020 s + 1}$$

## APPENDIX B

### STATIC TRIM CHARACTERISTICS

Steady-state trim characteristics of the Ames and Sikorsky versions of Gen Hel are compared with USAAEFA test data contained in reference 10.

GROSS WEIGHT	16000 lb	— SIKORSKY GEN HEL
CG STATION	351.0 in.	- - - AMES GEN HEL
CG WATERLINE	231.5 in.	○ AEFA TEST
DENSITY ALTITUDE	5250 ft	

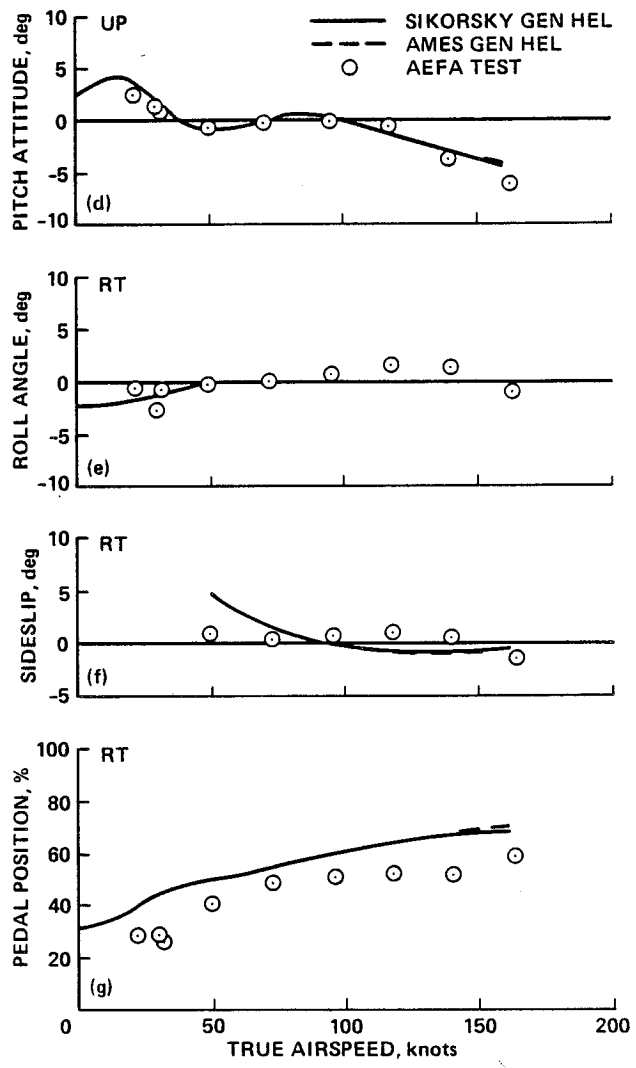
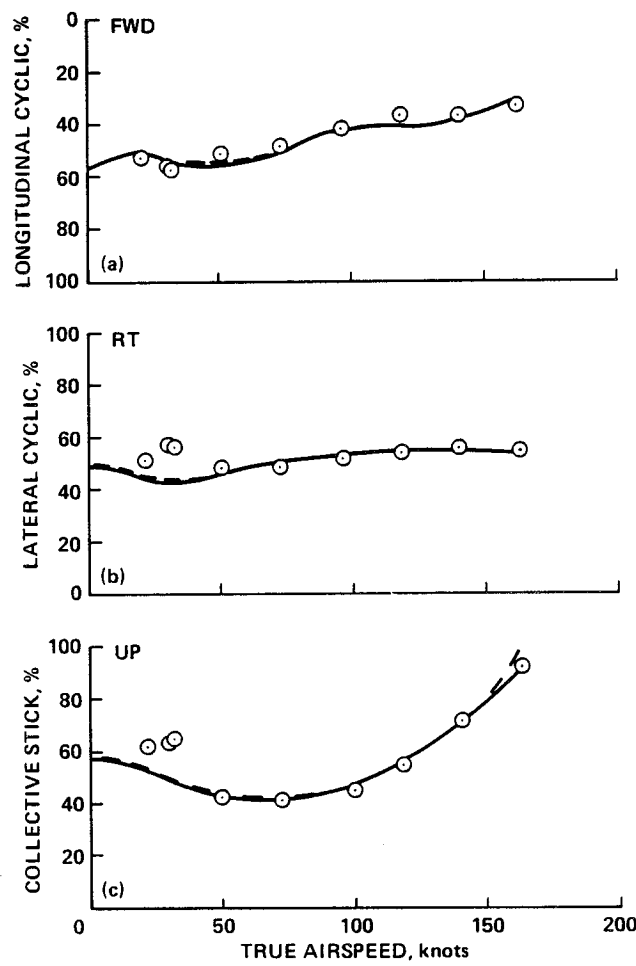


Figure B1.- UH-60A Black Hawk level-flight static trim.

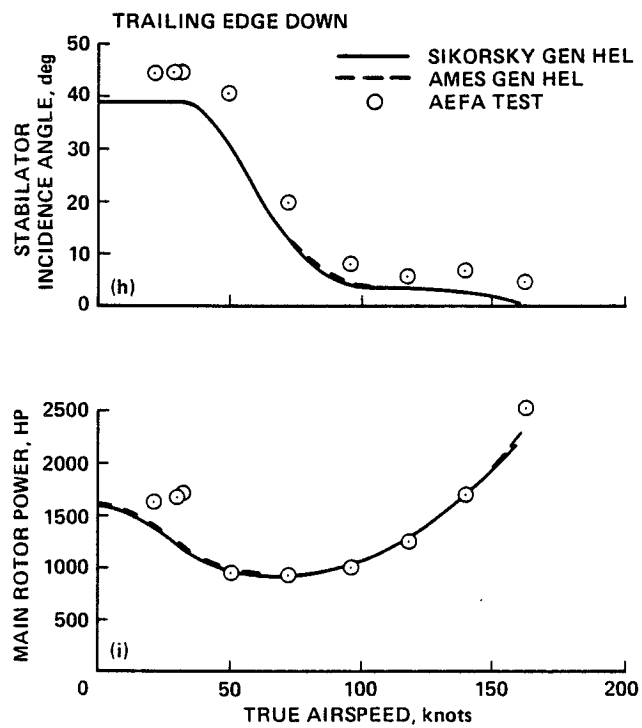


Figure B1.- Concluded.

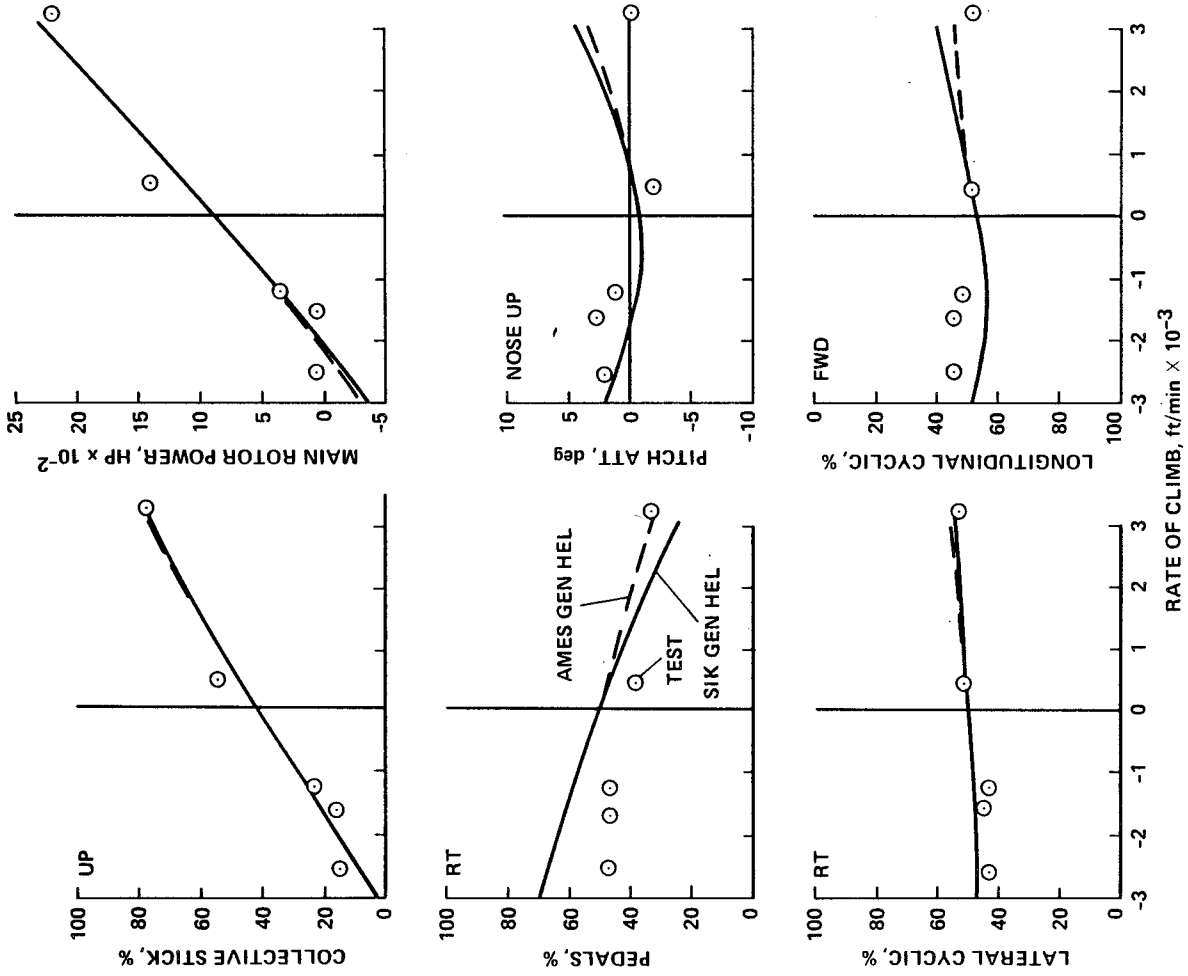


Figure B2.- UH-60A Black Hawk steady-climb and descent trim, 60 knots.

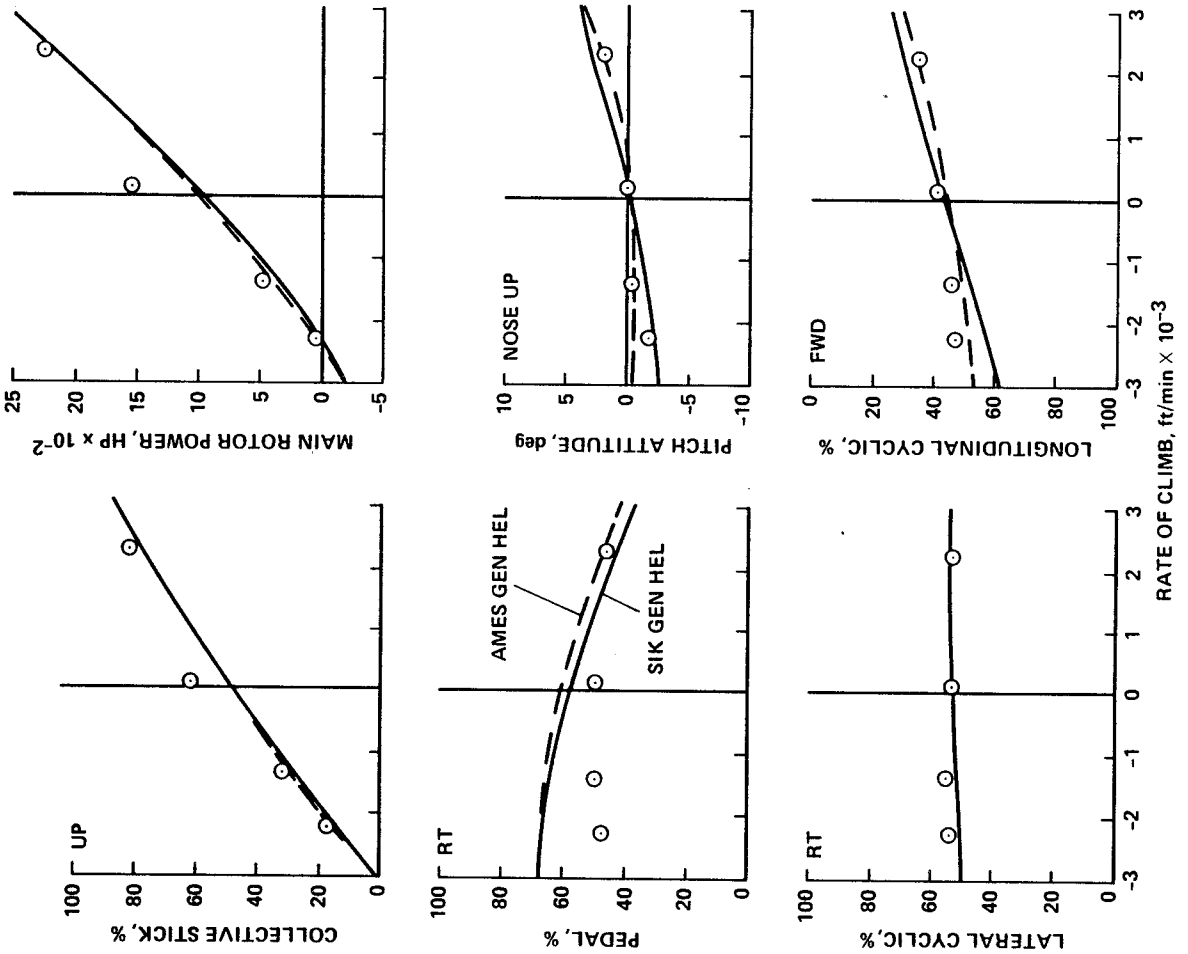


Figure B3.- UH-60A Black Hawk steady-climb and descent trim, 100 knots.

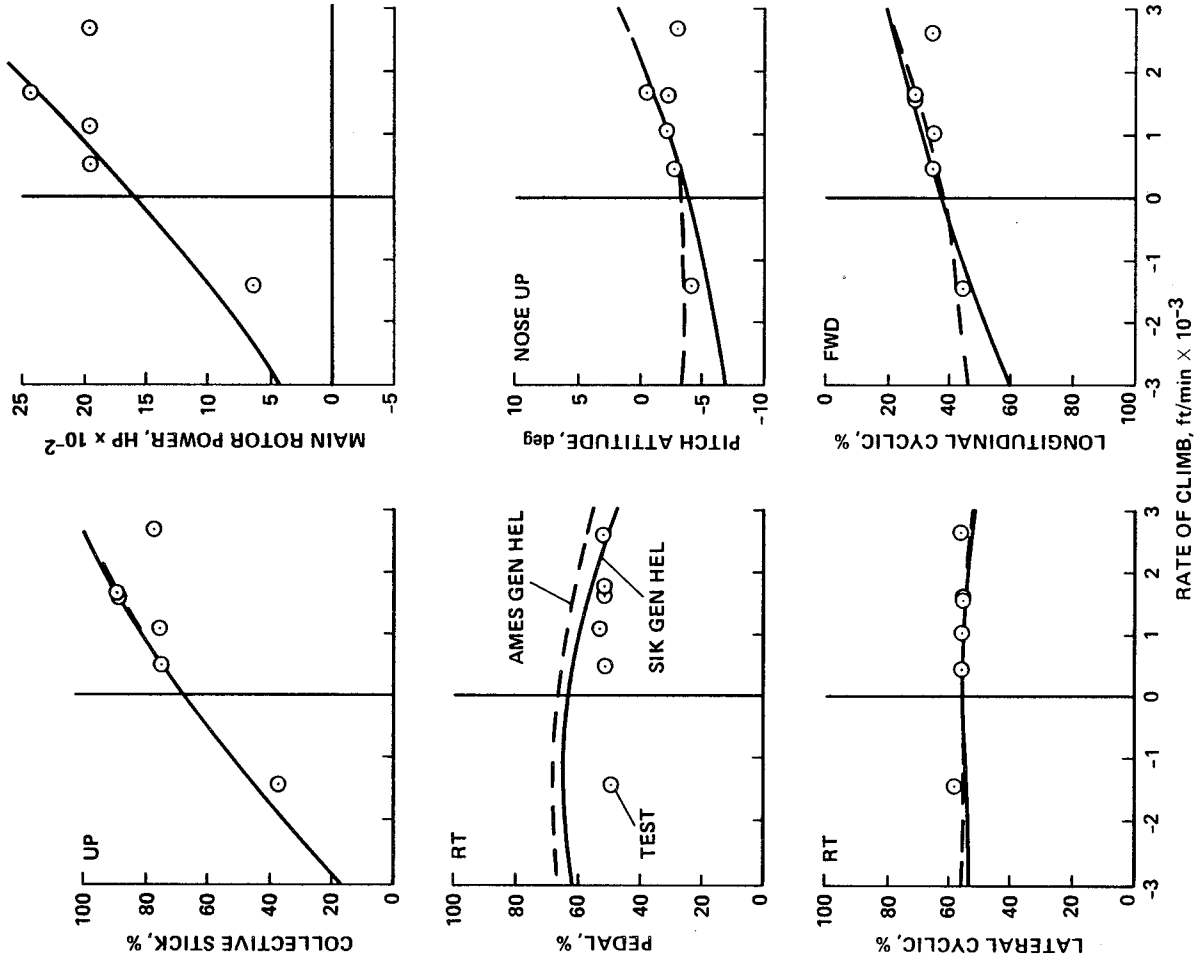


Figure B4.- UH-60A Black Hawk steady-climb and descent trim, 137.5 knots.

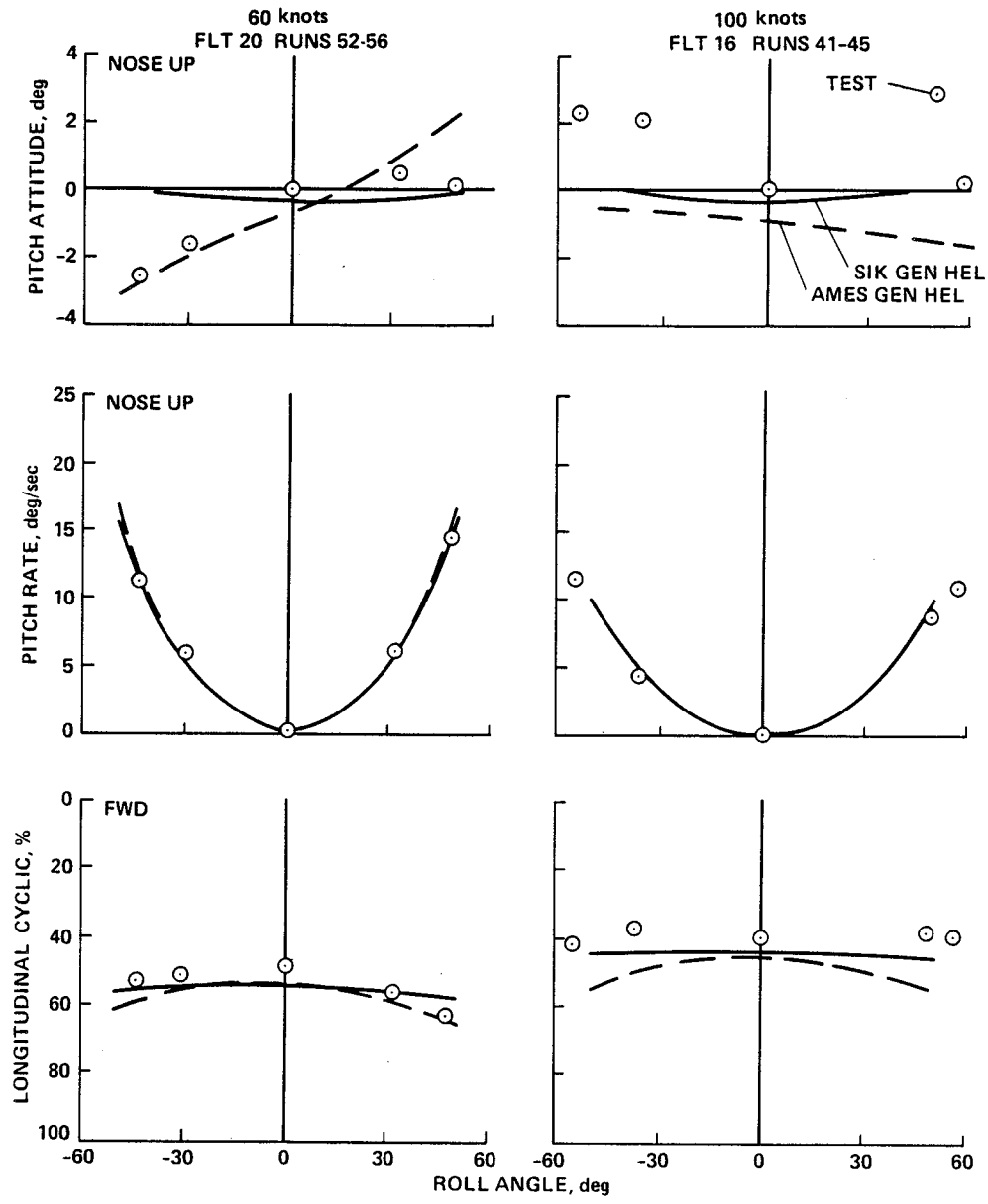


Figure B5.- UH-60A Black Hawk steady coordinated-turn trim, 60 knots and 100 knots.

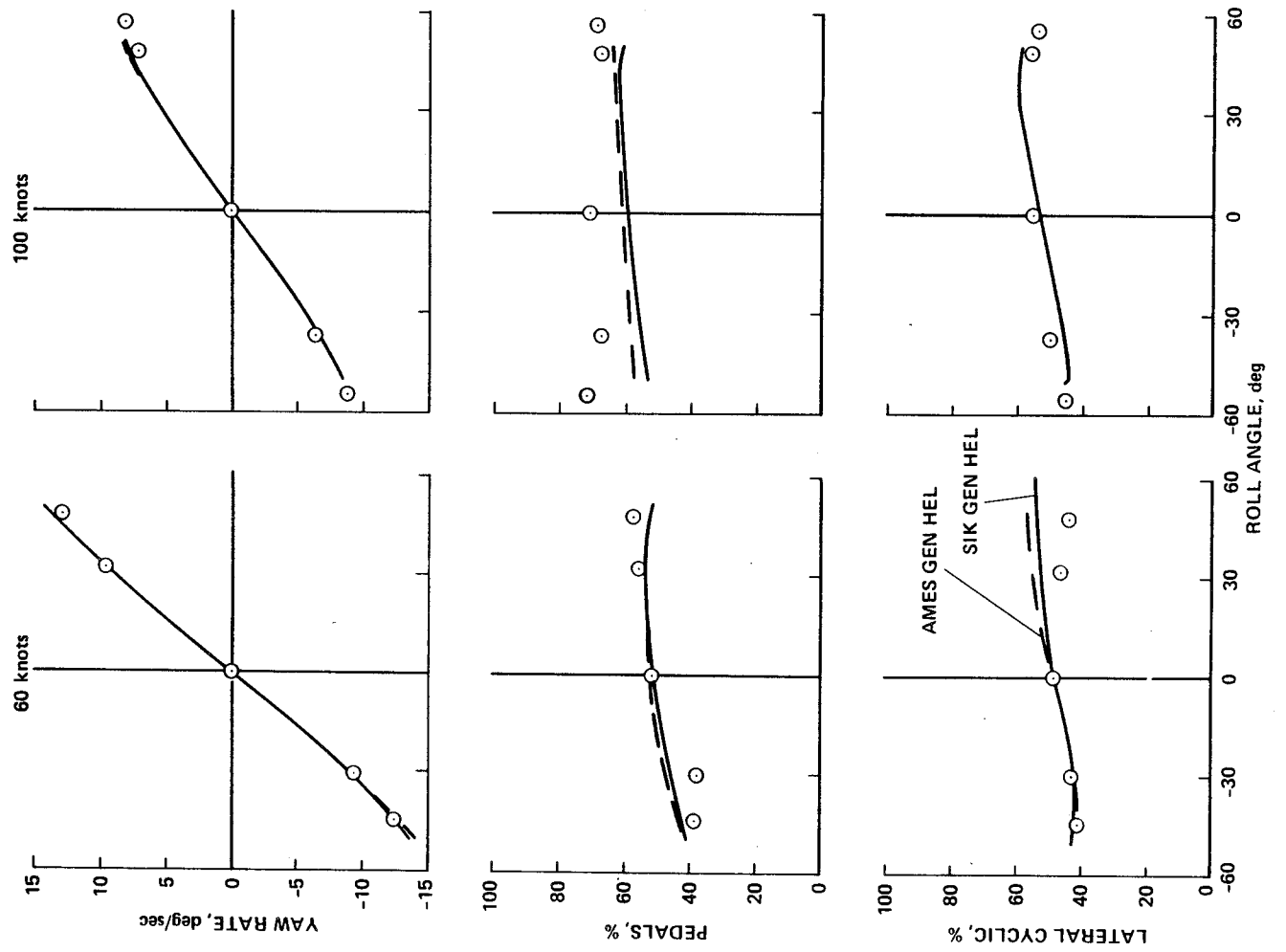


Figure B5.- Continued.

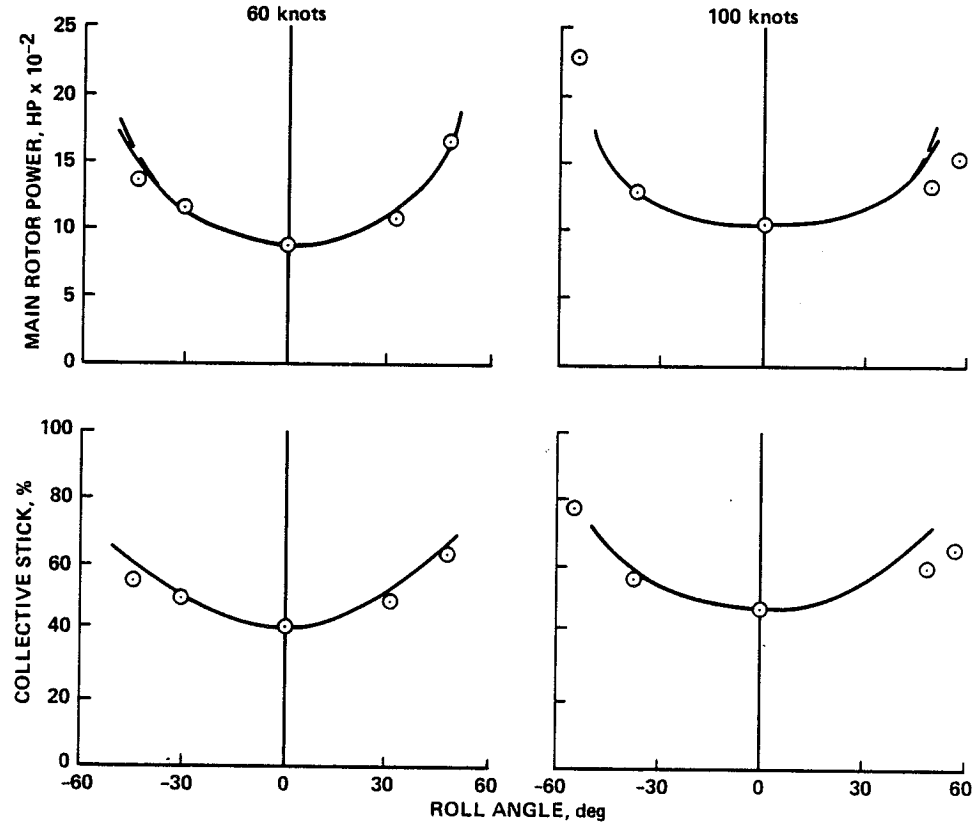


Figure B5.- Concluded.

## APPENDIX C

### TEST CONDITIONS FOR TRANSIENT RESPONSES

Test conditions and aircraft configuration information are presented below for each of the transient-response time histories of appendices D and E. Pertinent inputs to the simulations are also given when they differ from or are estimates of flight-test values.

#### SENSOR LOCATIONS

##### CG Accelerometer

Station.....389 in.  
Buttline.....-31 in.  
Waterline.....207.7 in.

##### Translational Velocity Transducer

Station.....248 in.  
Buttline.....70 in.  
Waterline.....265 in.

#### TEST DATA CONDITIONING

Samples per second.....100  
Filter break frequency....30 Hz

#### TEST CONFIGURATION FOR ALL TRANSIENT RESPONSE COMPUTATIONS

$$\begin{aligned} I_{xx} &= 4659 \dots \text{slug}\cdot\text{ft}^2 \\ I_{yy} &= 38512 \dots \text{slug}\cdot\text{ft}^2 \\ I_{zz} &= 36796 \dots \text{slug}\cdot\text{ft}^2 \\ I_{xz} &= 1882 \dots \text{slug}\cdot\text{ft}^2 \end{aligned}$$

Buttline CG location	- 0 in.
Pitch bias actuator	- disabled and centered
Flightpath stabilization	- disabled
Stability augmentation system	- disabled
Stabilator position	- fixed to the trim value set by control system

TABLE C1.- AIRCRAFT CONFIGURATIONS AND TEST CONDITIONS  
FOR TRANSIENT RESPONSES

File	Flight	Run	Gross Weight, lb	CG Station, in.	CG Waterline, in.	Density Altitude, ft	Pressure Altitude, ft	Equivalent Airspeed, knots	Rotor Speed, rad/sec
102	18	20	15990	348.8	231.7	6809	5500	93.0	27.0
103	18	10	16150	349.5	231.6	6565	5256	91.9	26.86
201	47	27	15870	359.3	232.6	6658	5582	0	27.0
202	47	31	15760	359.2	232.7	6673	5493	0	27.0
204	48	21	15950	359.4	232.5	6510	5370	0	27.0
205	48	23	15870	359.4	232.6	6777	5584	0	27.0
206	48	26	15720	359.2	232.7	6834	5562	0	27.0
209	49	35	15750	359.3	232.7	6659	5742	0	26.93
210	50	27	15940	359.4	243.8	6705	5776	0	26.90
212	50	24	16030	359.4	232.5	6296	5411	0	26.87
401	45	16	16530	359.6	232.3	5084	4484	93.3	27.0
403	45	44	15840	359.5	232.6	6270	5641	91.0	27.05
404	46	12	16540	359.5	232.3	5001	4455	92.8	27.0
405	46	14	16490	359.5	232.3	4872	4401	55.8	27.01
409	43	15	16410	359.6	232.3	4360	4556	93.3	26.53
412	49	16	16470	359.7	232.3	4995	4554	92.8	26.95
502	69	18	16110	351.1	232.4	6268	4969	56.9	27.0
503	69	20	16050	351.1	232.4	6313	5020	54.6	27.0
504	14	23	15770	348.3	231.7	5718	4514	54.4	26.57
505	14	24	15760	348.3	231.7	5796	4636	55.0	26.59
509	25	47	15510	352.0	232.0	6969	5953	53.1	26.85
510	29	30	15720	351.4	231.8	5930	5515	53.96	26.90
512	29	36	15600	351.4	231.9	5631	5948	53.1	26.90
706	17	48	15410	351.9	232.1	7427	6450	92.8	26.90
710	18	33	15740	347.6	231.8	7015	5636	89.8	27.03
711	18	37	15690	347.4	231.8	6988	5615	90.3	27.01

## APPENDIX D

### DYNAMIC RESPONSE CHARACTERISTICS

Transient responses of the Ames real-time simulation and USAAEFA flight test data of reference 11 are compared for small step-inputs of each control. No stability augmentation or flightpath stabilization was used. One primary control was input for each case while other controls were held fixed as long as possible. If a step input was not possible for reasons of instability or safety, a pulse input was used.

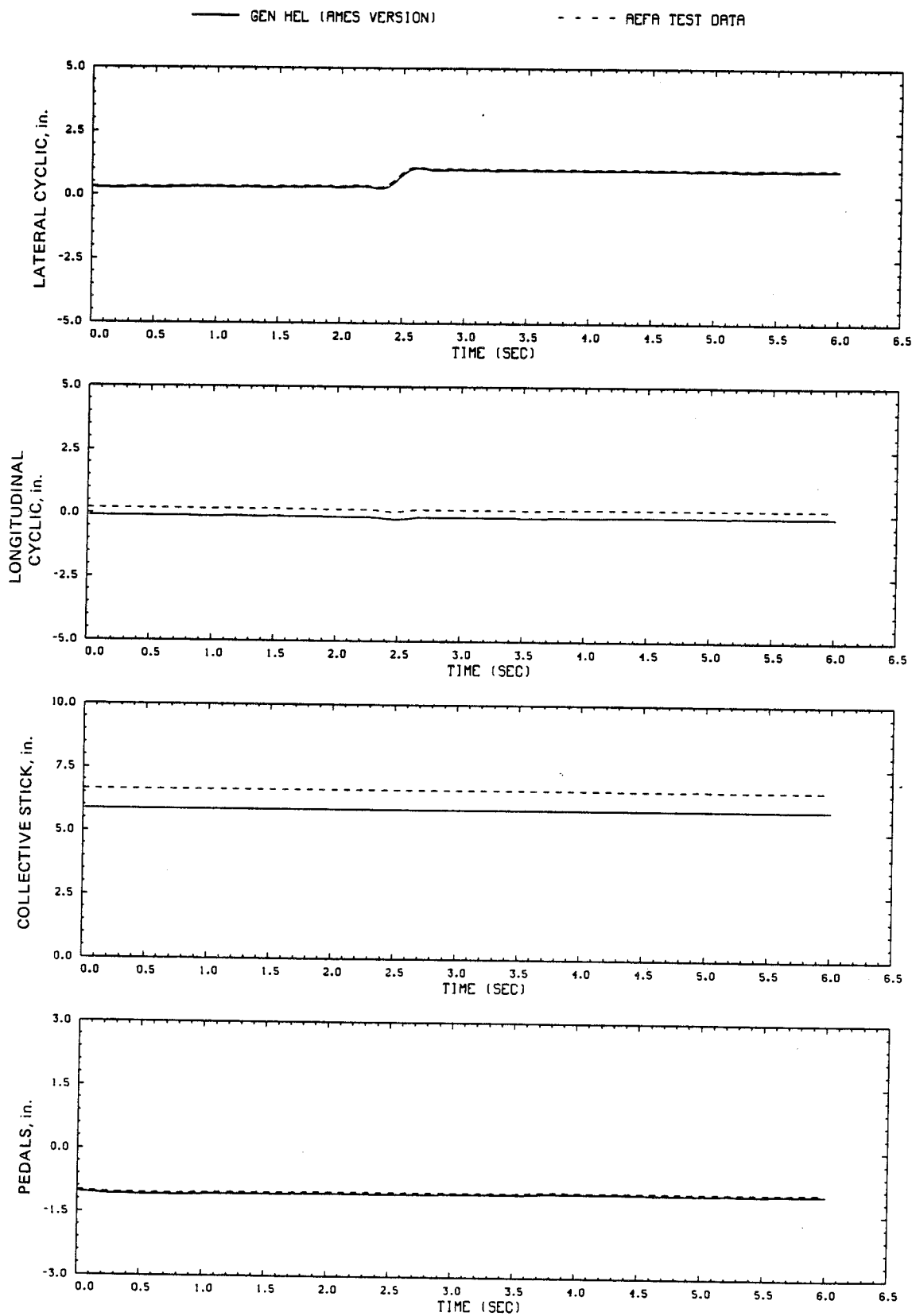


Figure D1.- Comparison of Ames real-time simulation and flight-test data.  
(File 201: 1-in. right cyclic input at hover)

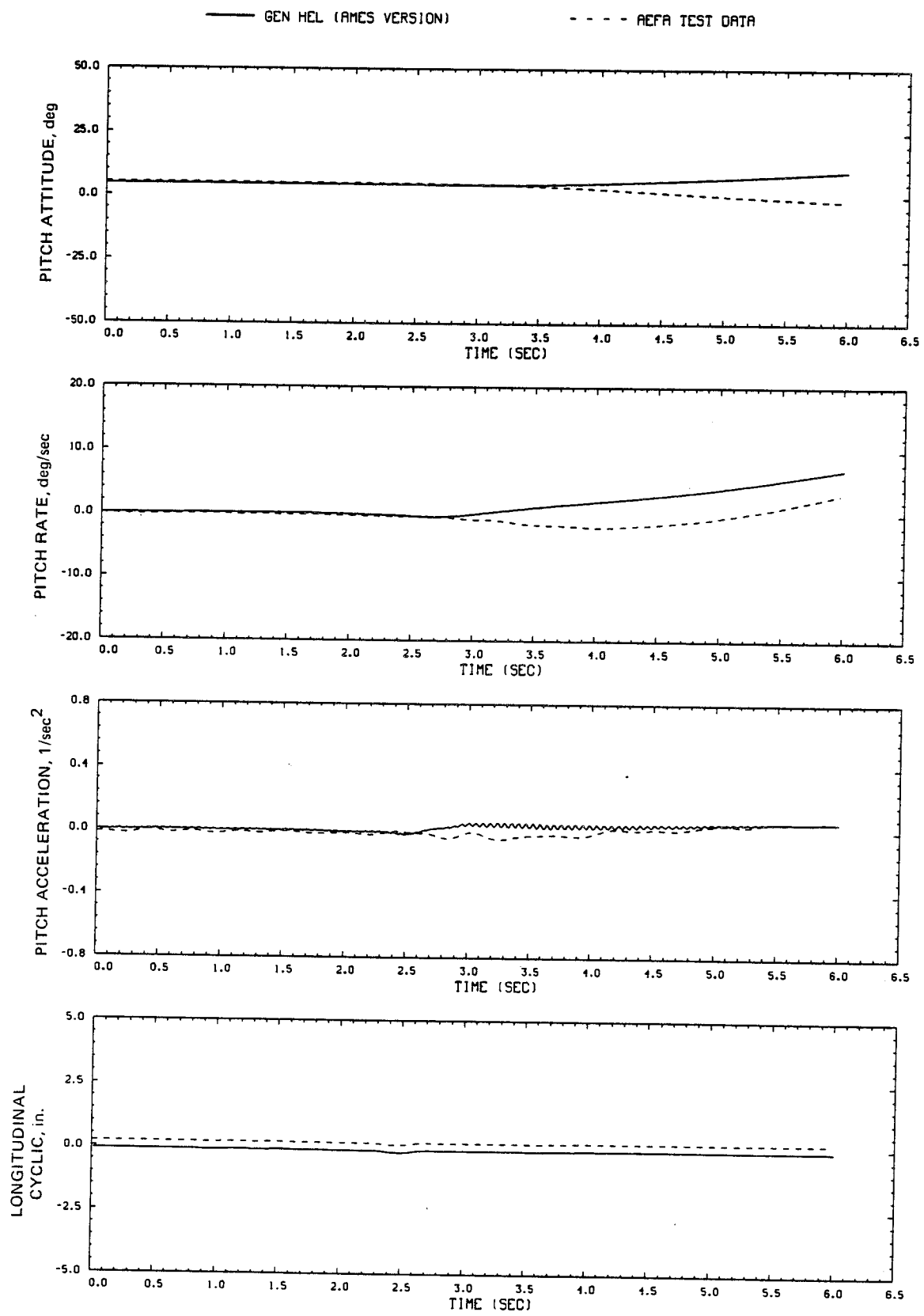


Figure D1.- Continued.

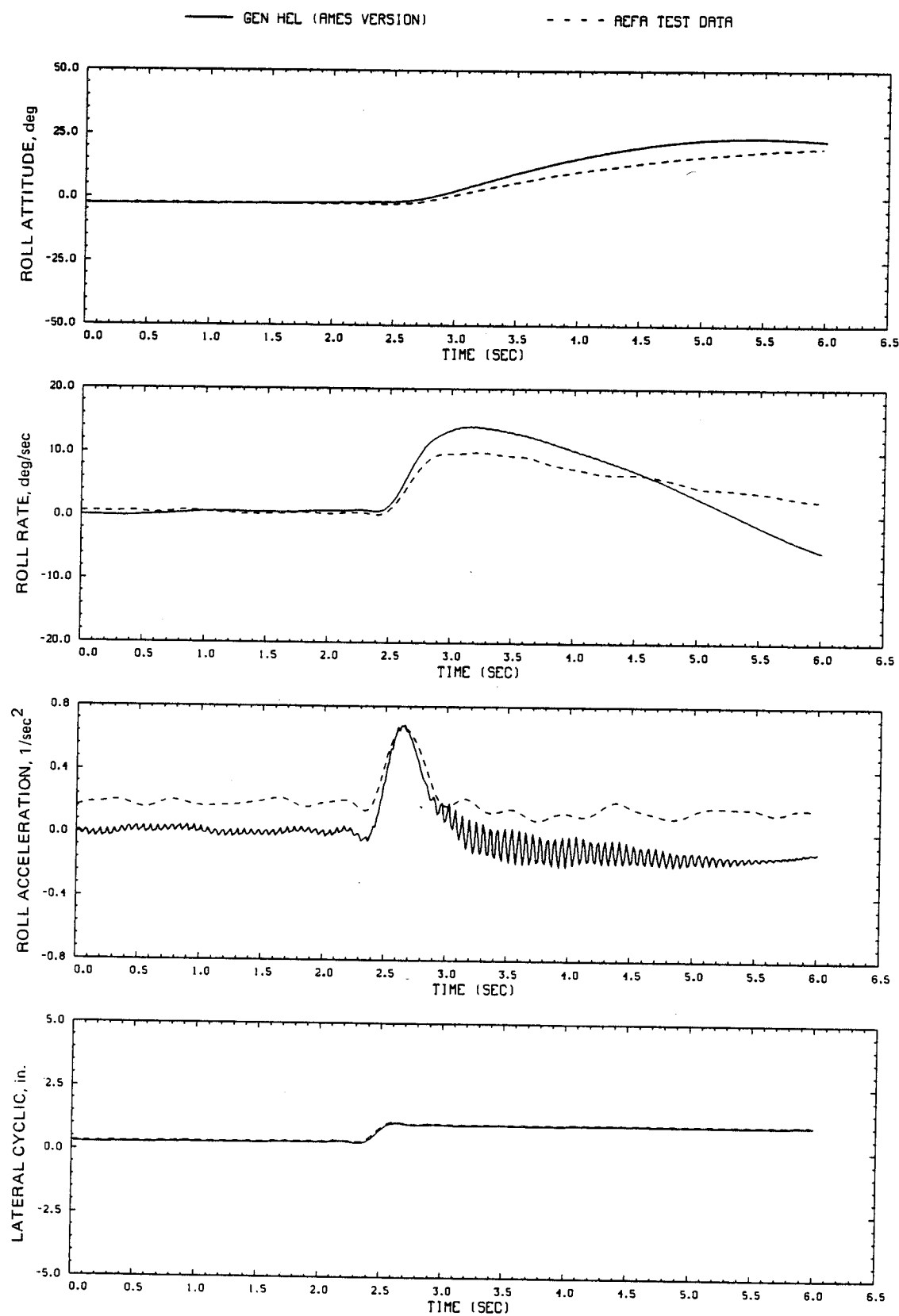


Figure D1.- Continued.

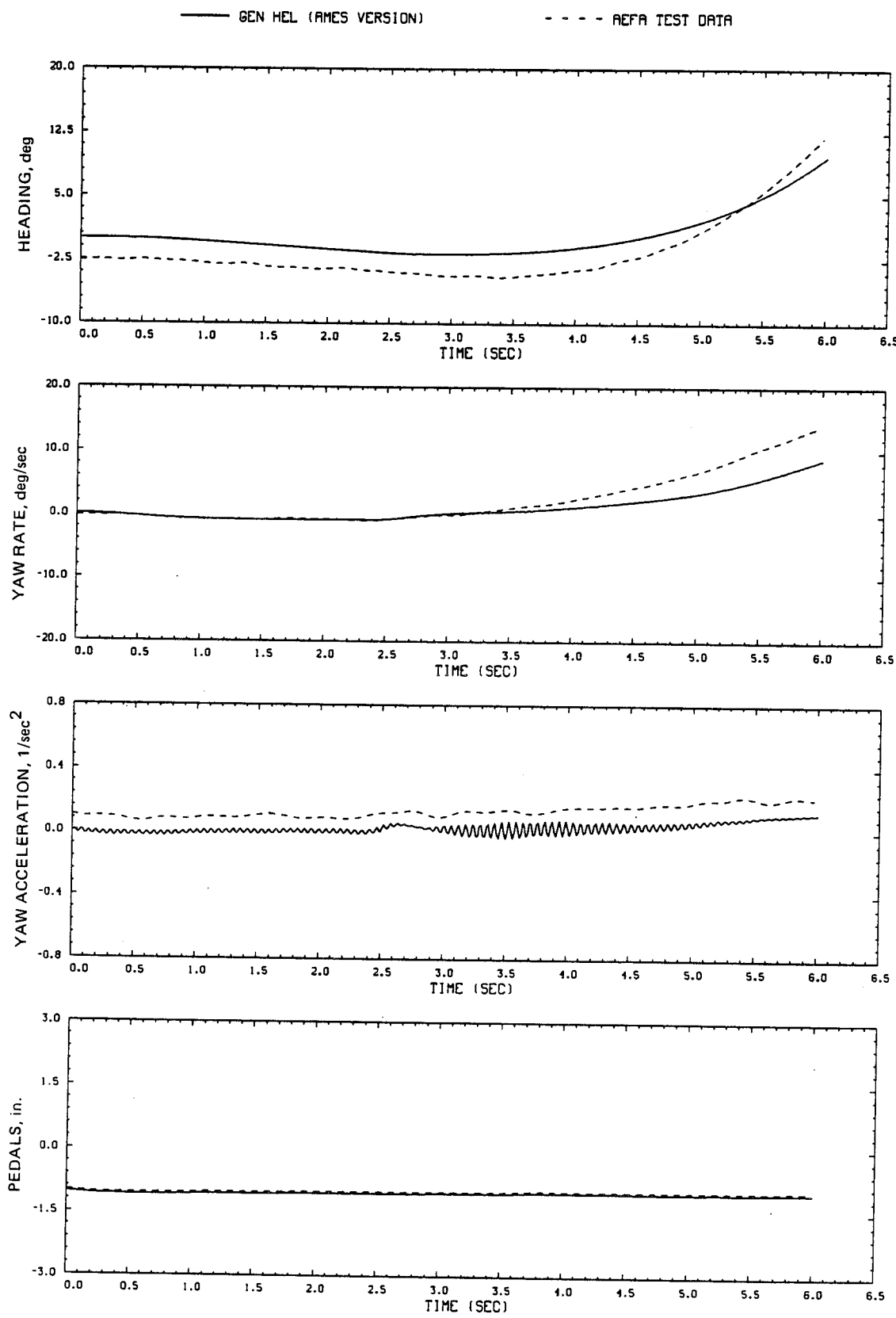


Figure D1.- Continued.

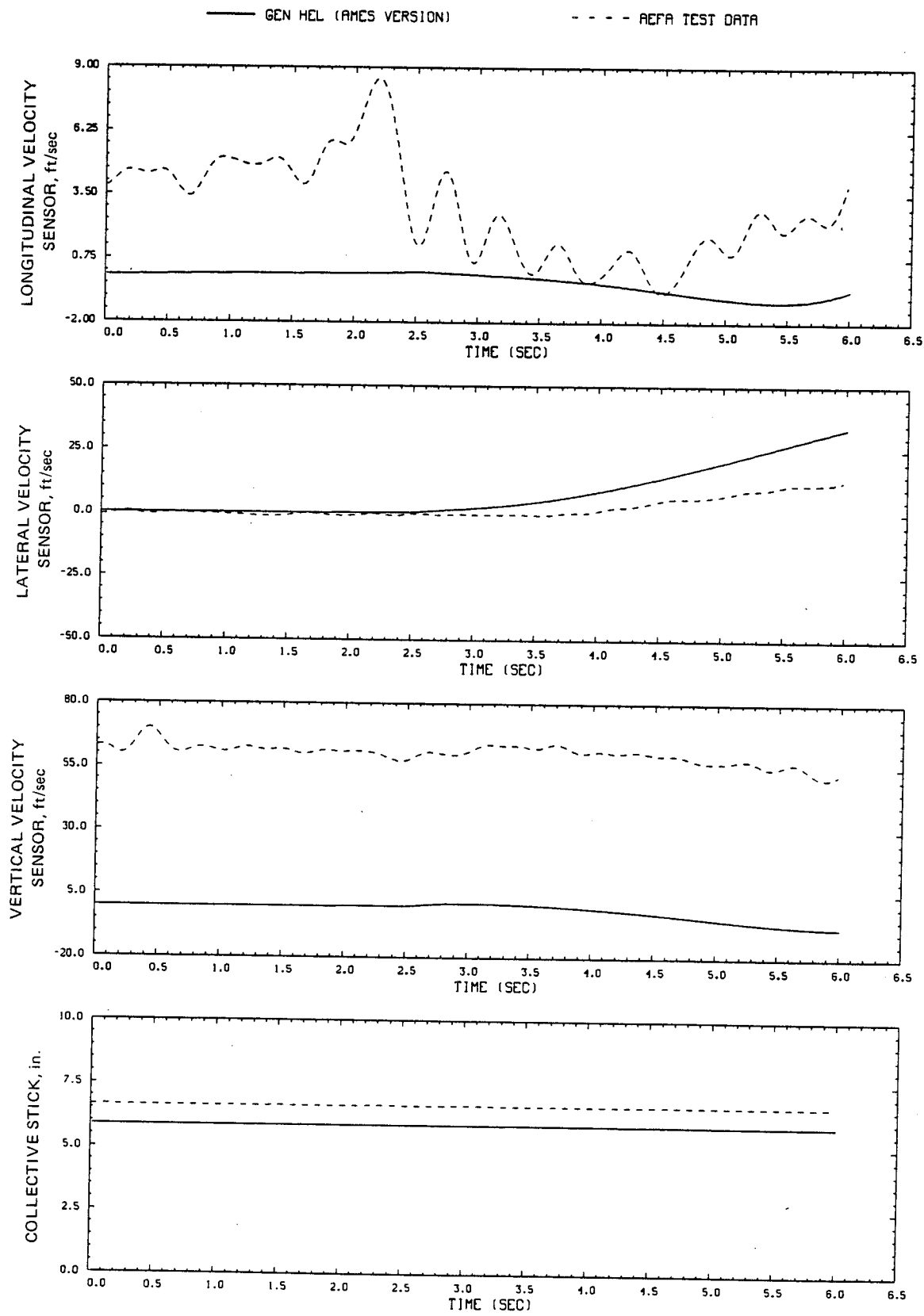


Figure D1.- Continued.

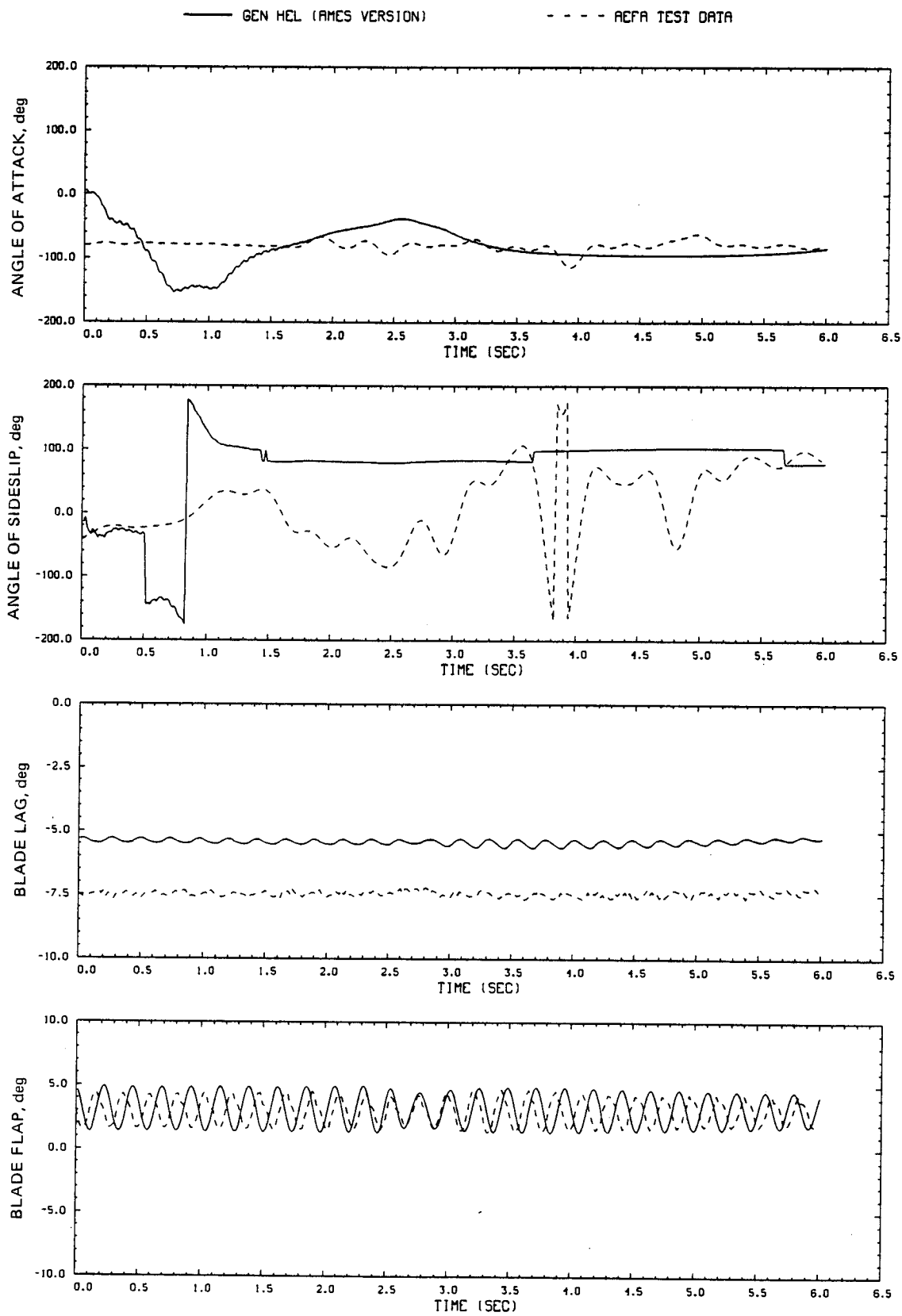


Figure D1.- Continued.

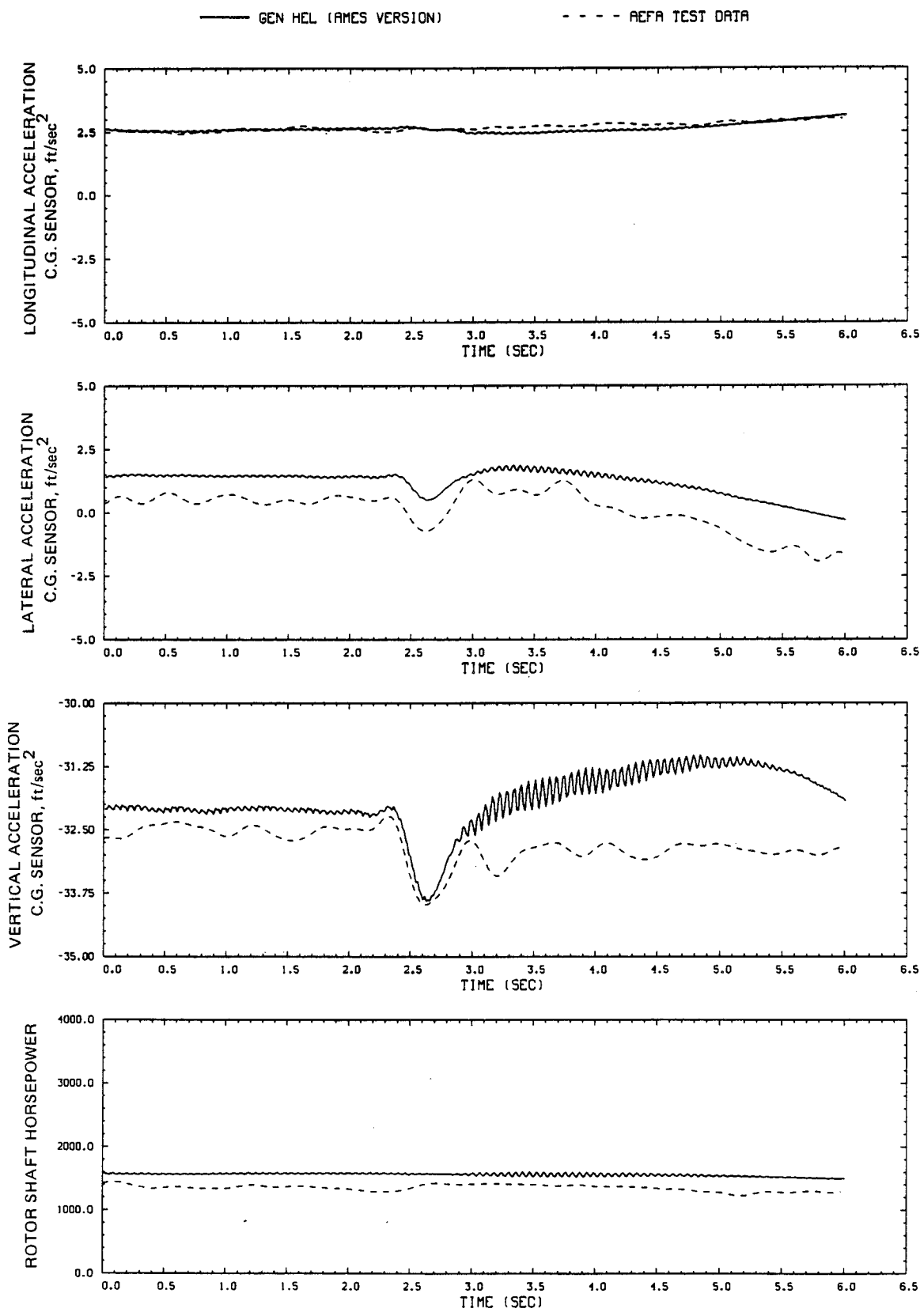


Figure D1.- Continued.

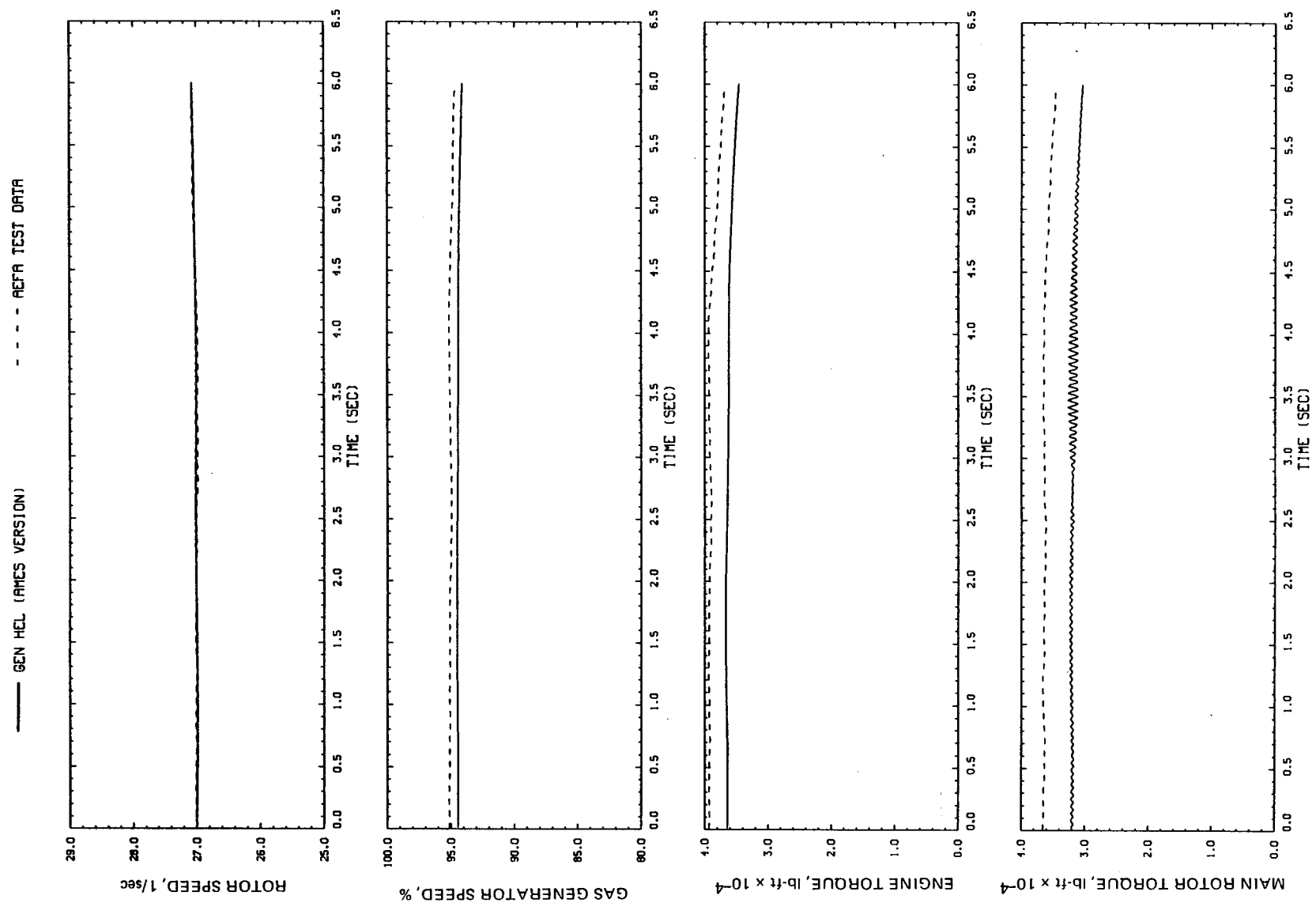


Figure D1.- Concluded.

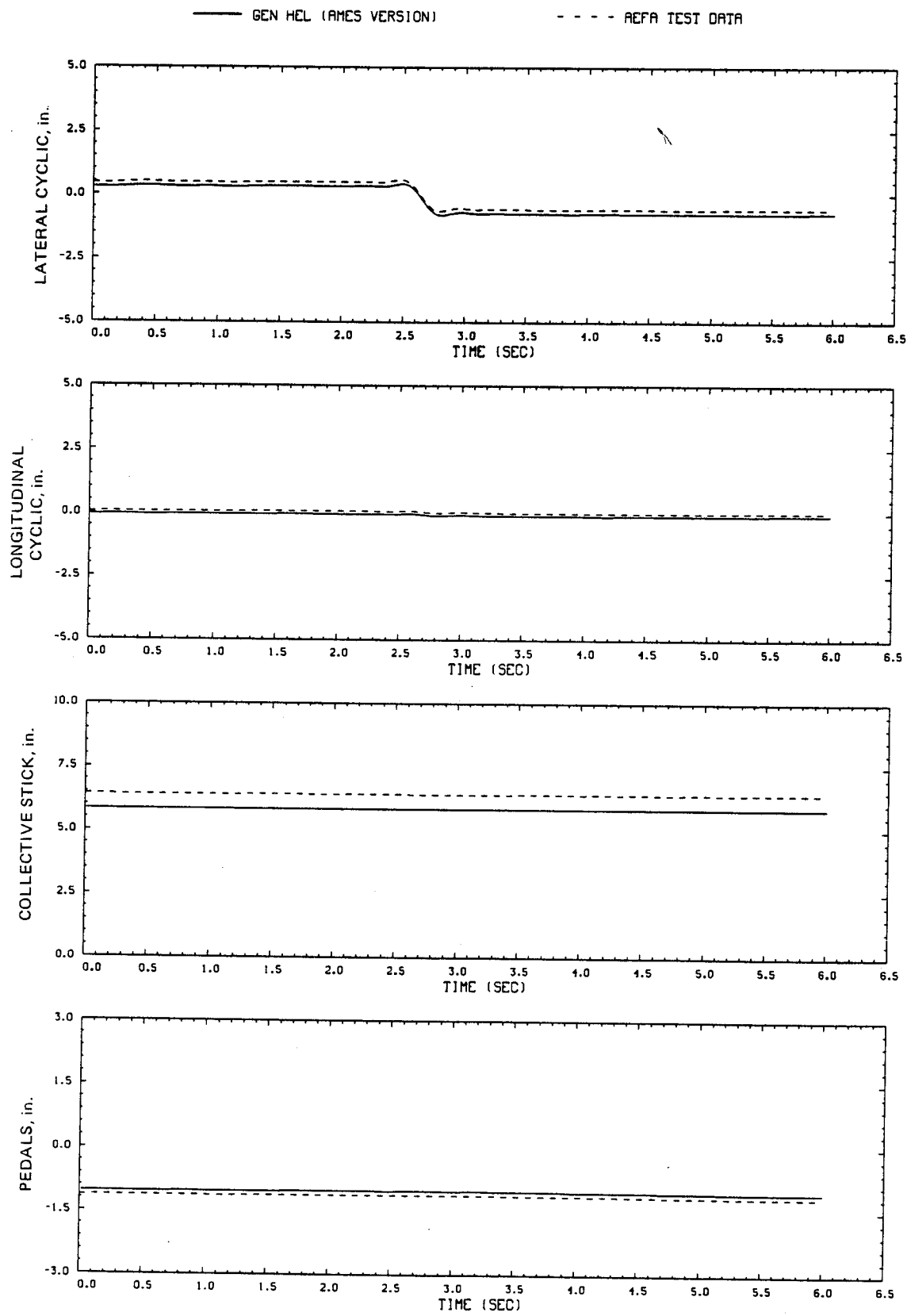


Figure D2.- Comparison of Ames real-time simulation and flight-test data.  
(File 202: 1-in. left cyclic input at hover)

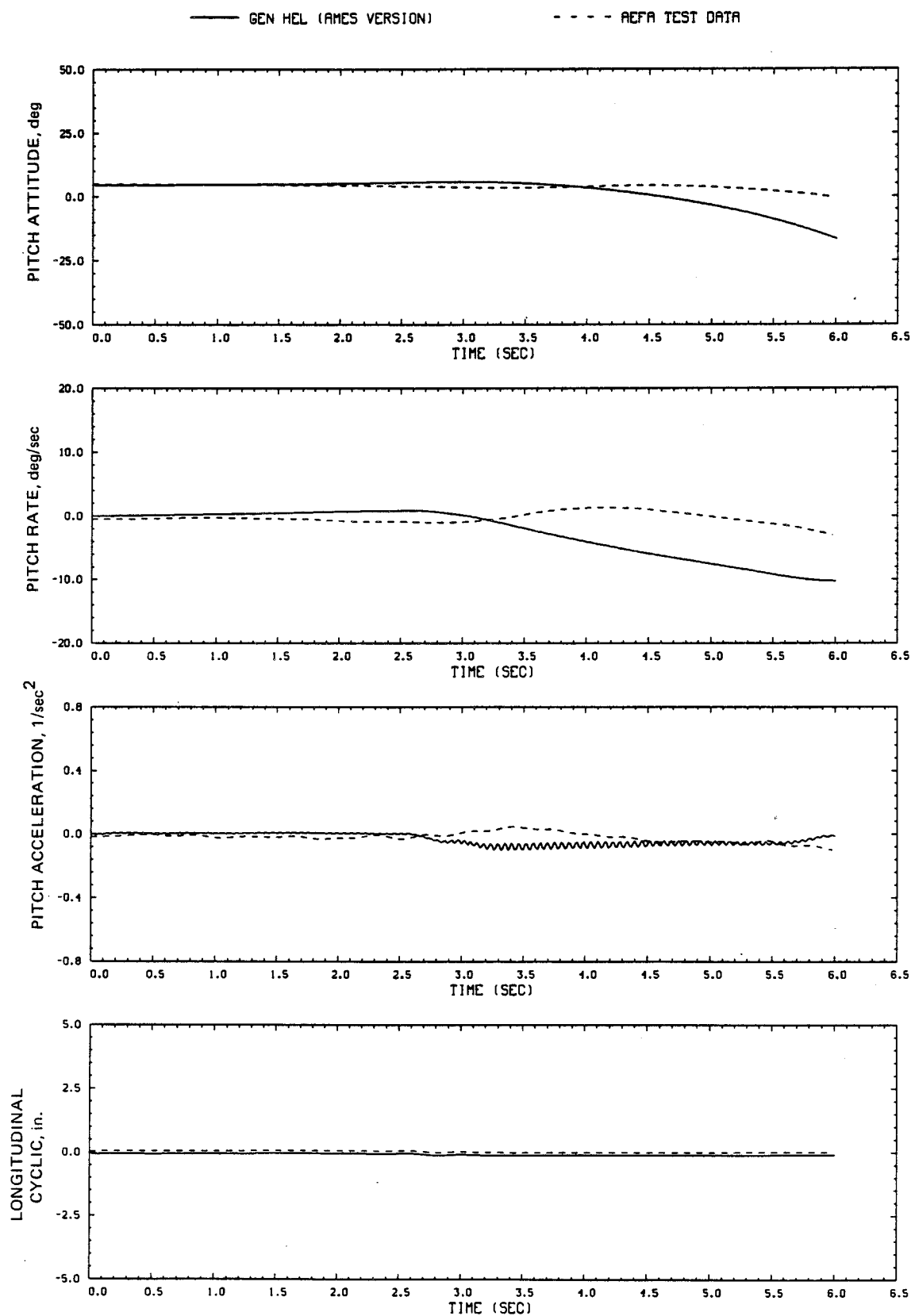


Figure D2.- Continued.

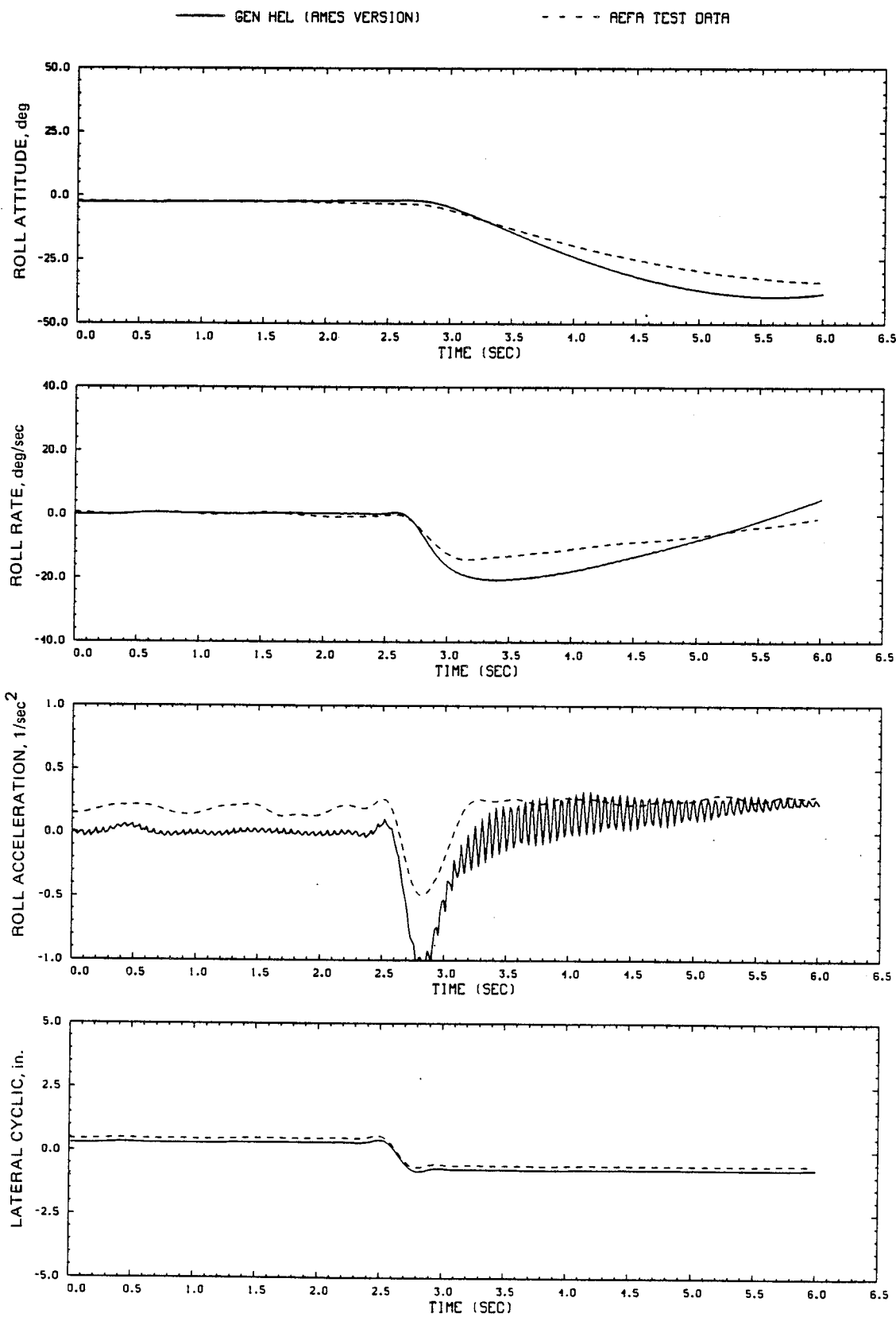


Figure D2.- Continued.

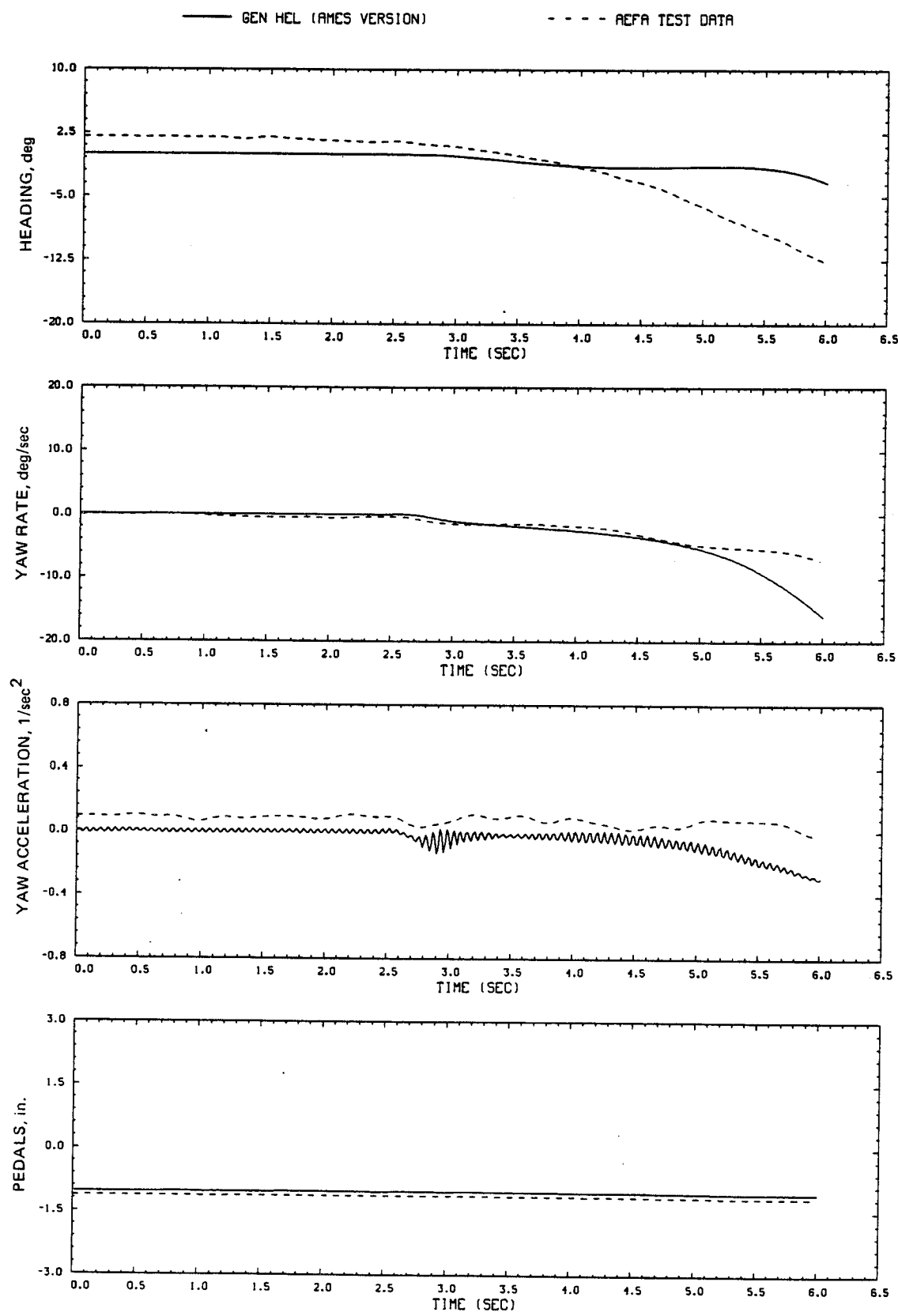


Figure D2.- Continued.

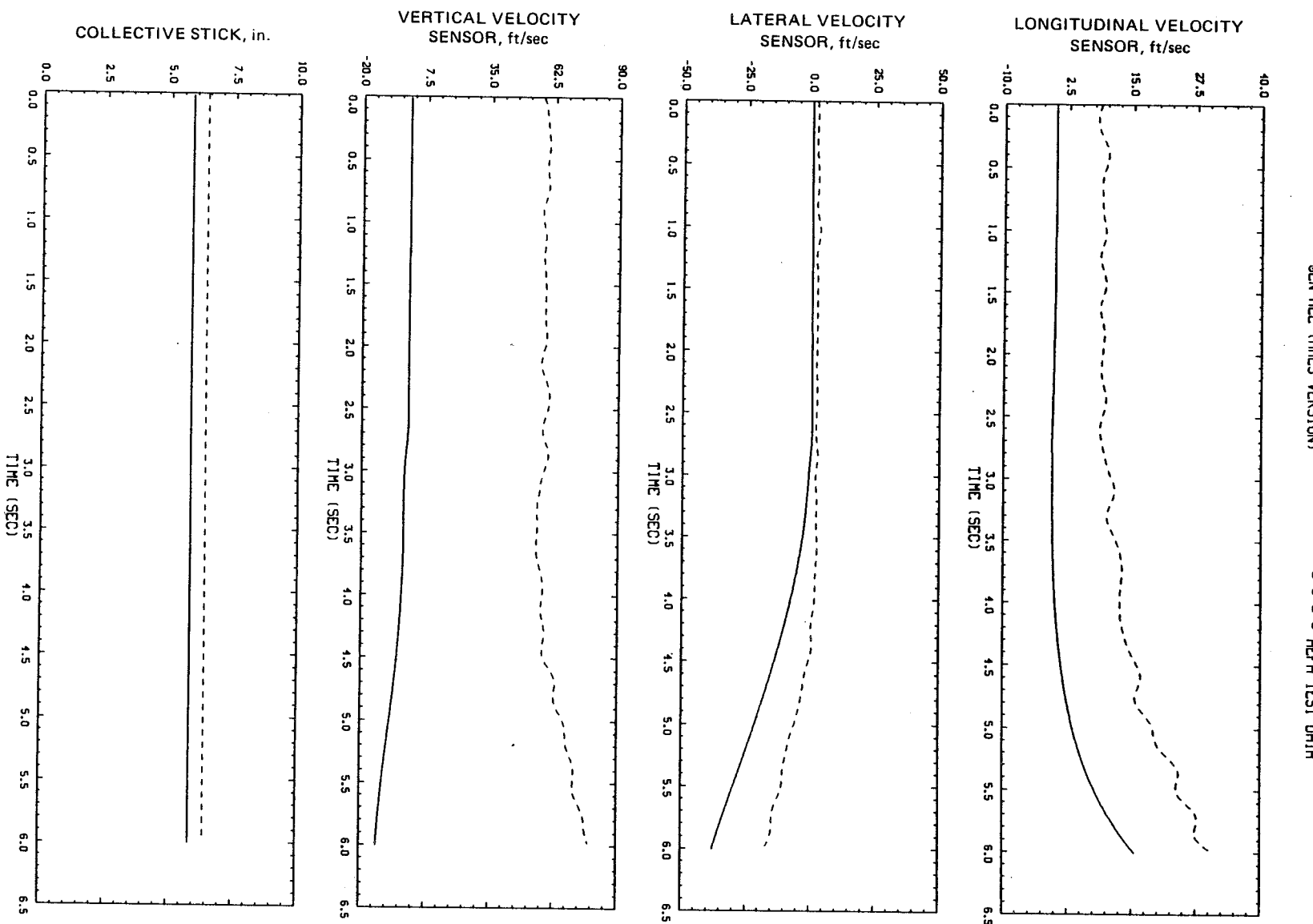


Figure D2.- Continued.

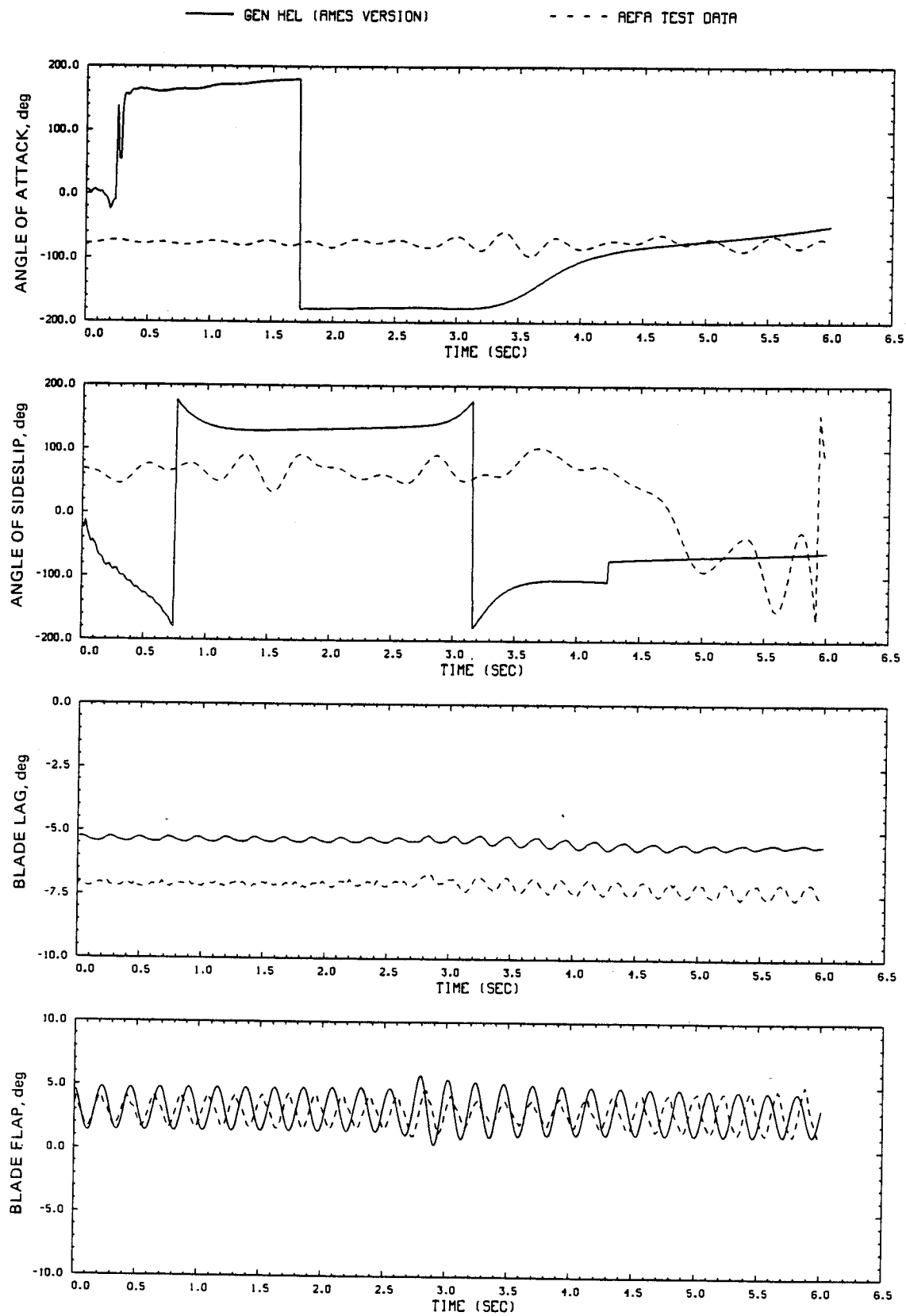


Figure D2.- Continued.

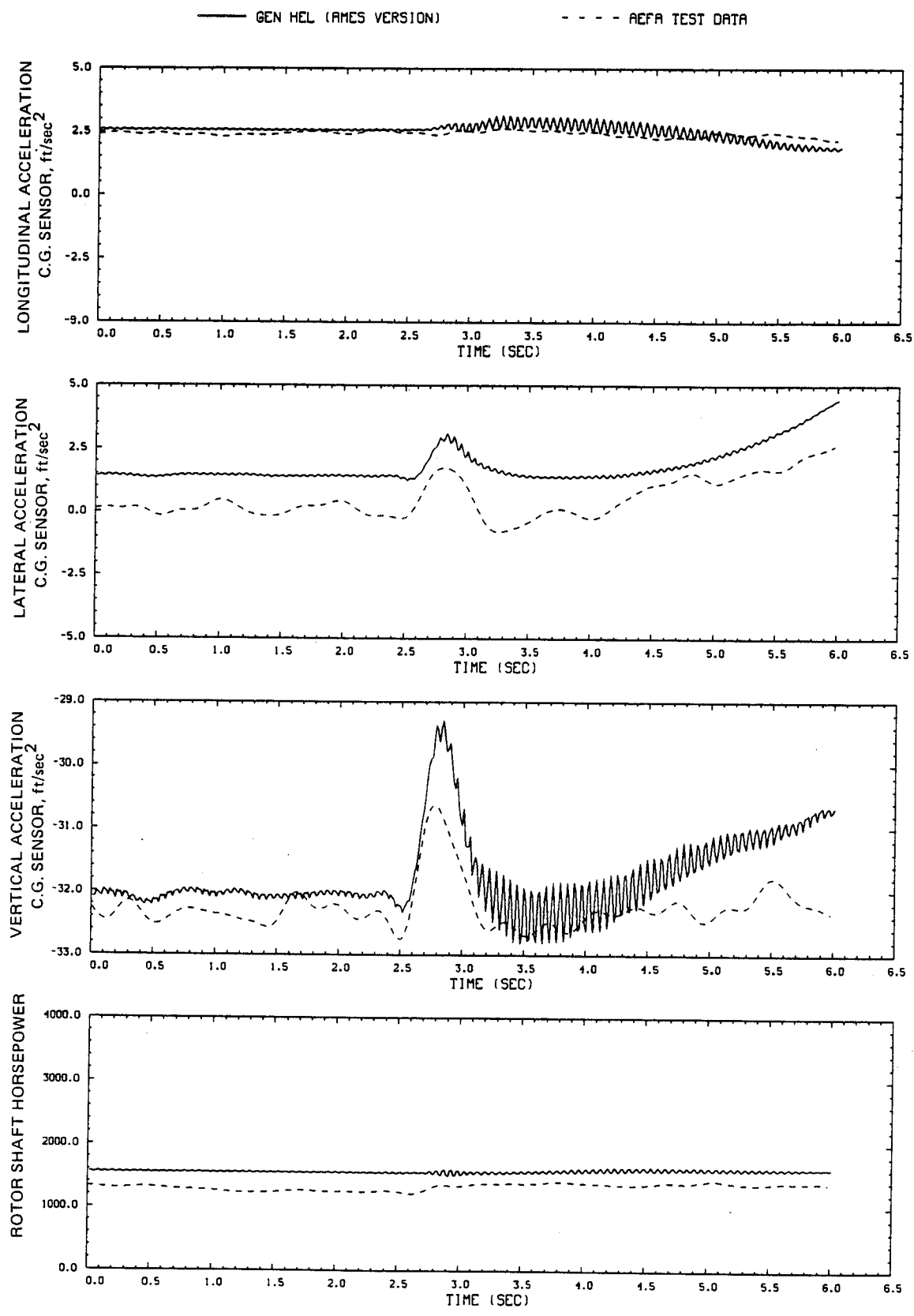


Figure D2.- Continued.

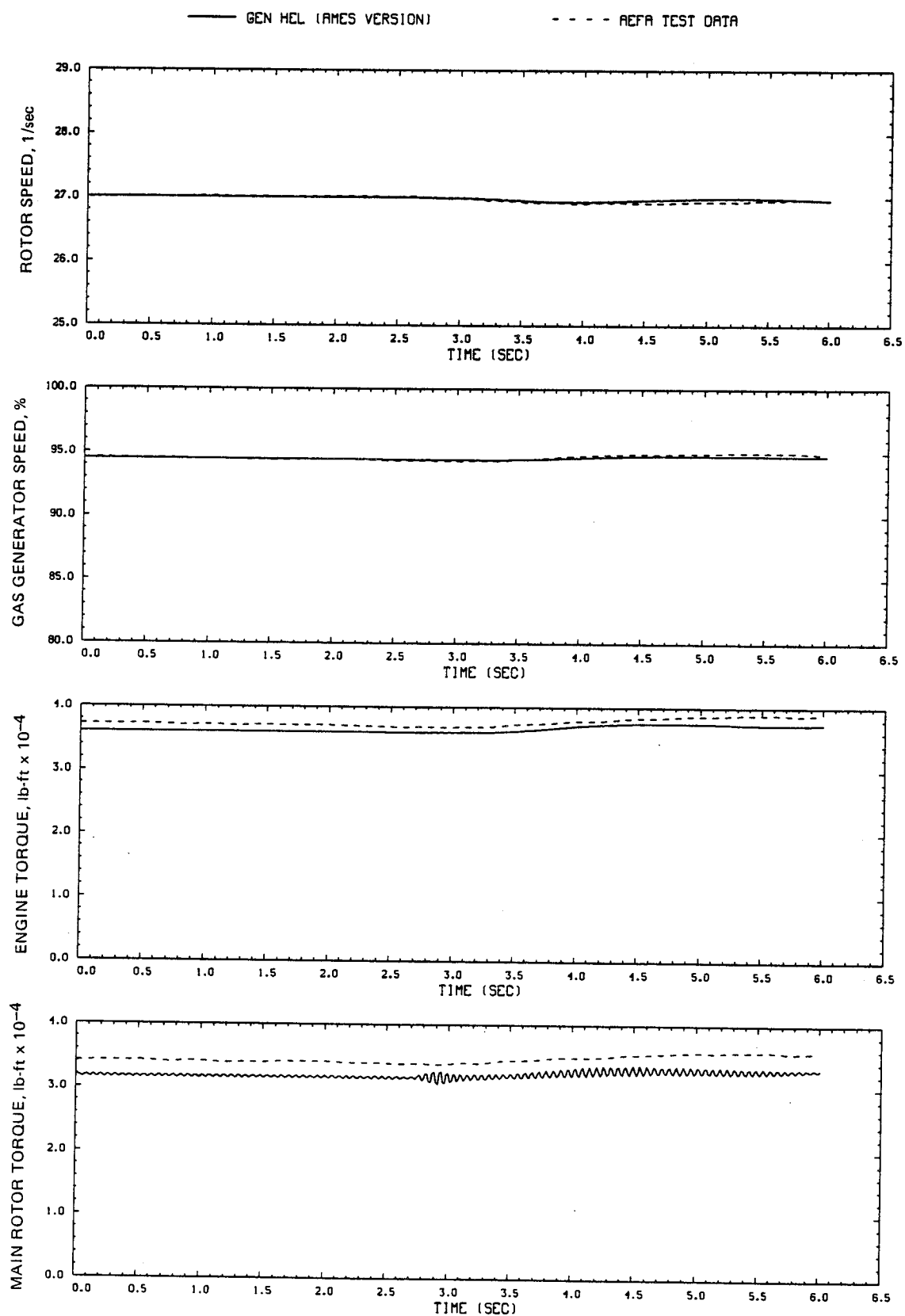


Figure D2.- Concluded.

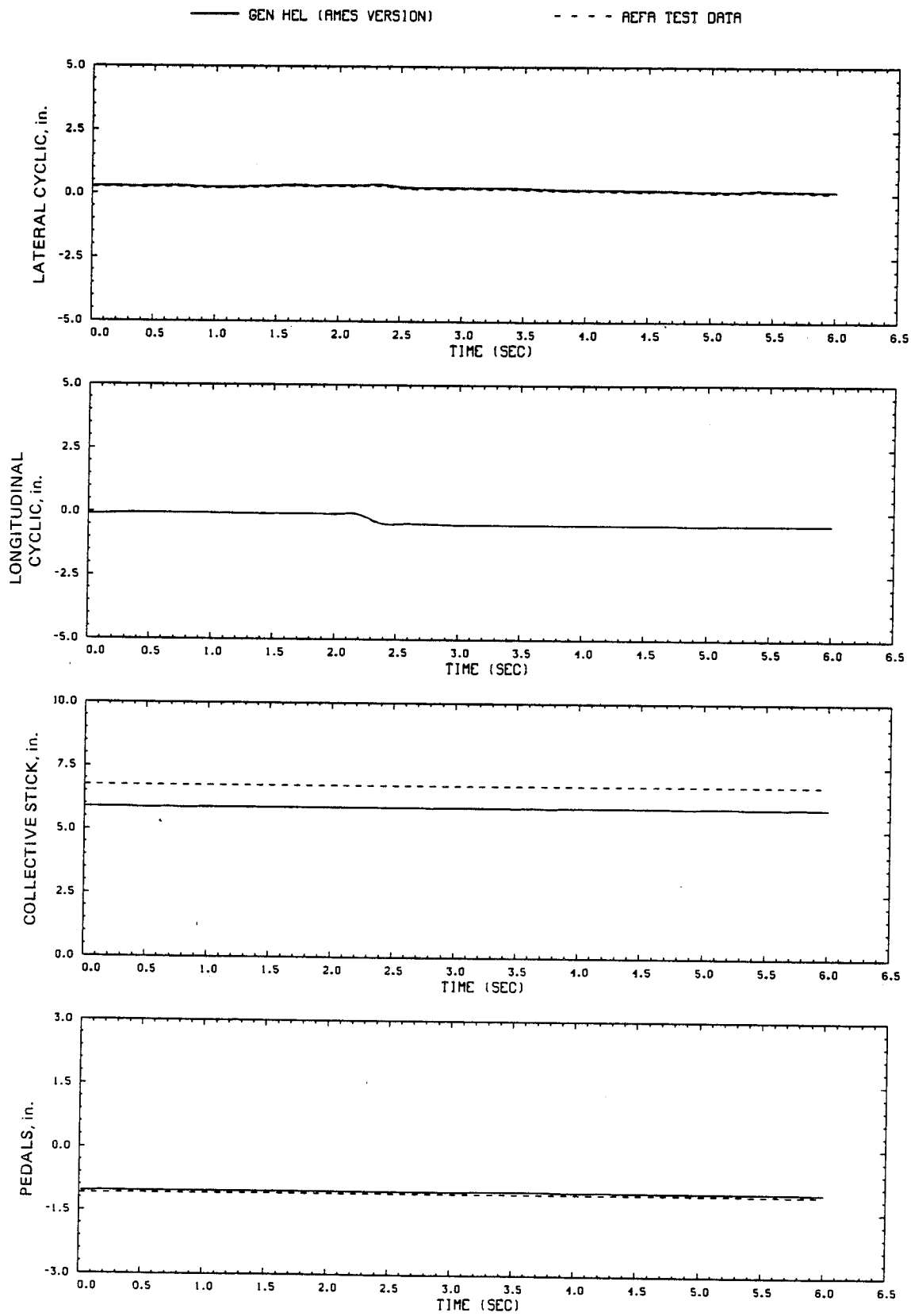


Figure D3.- Comparison of Ames real-time simulation and flight-test data.  
(File 204: 0.5-in. forward cyclic input at hover)

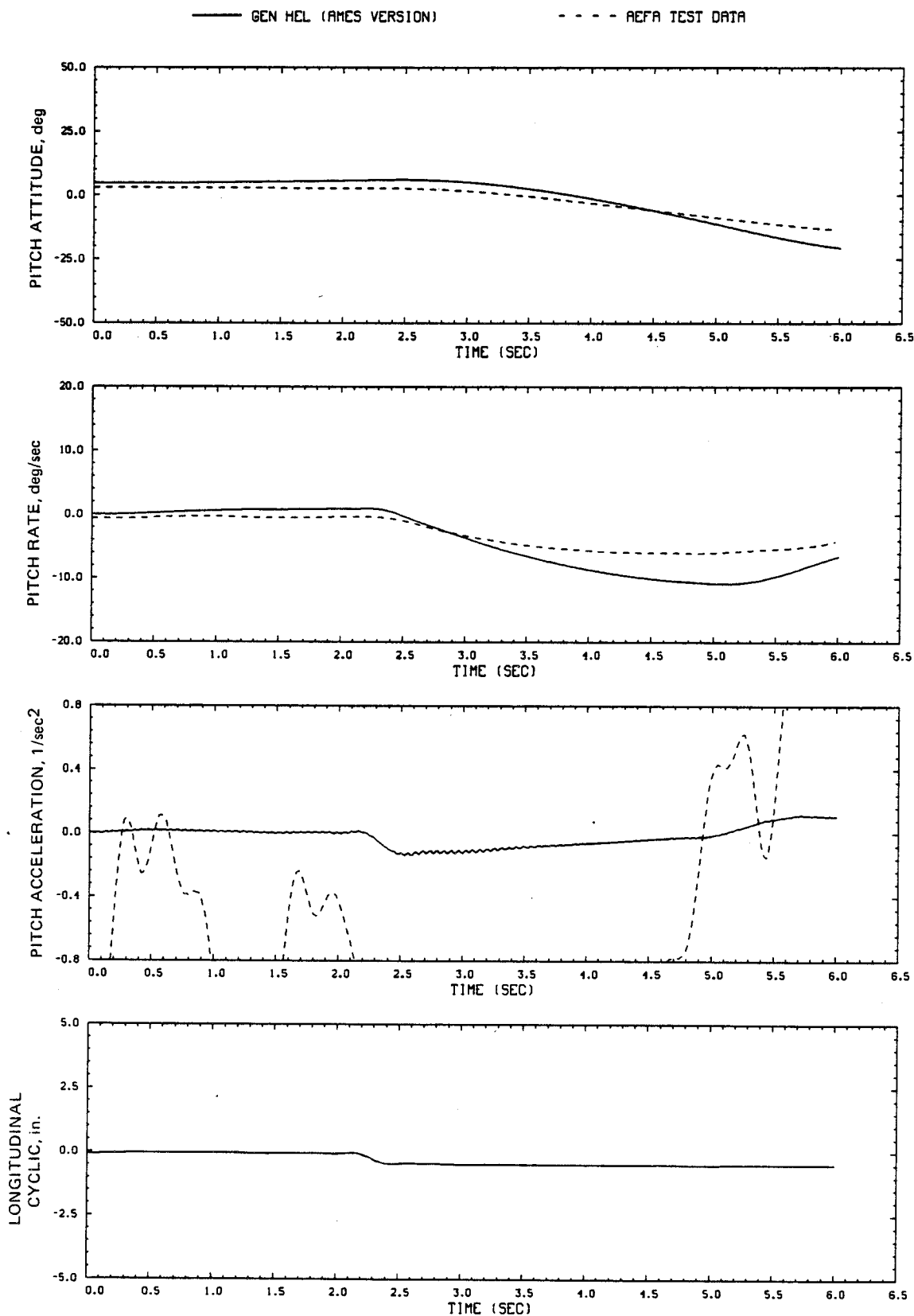


Figure D3.- Continued.

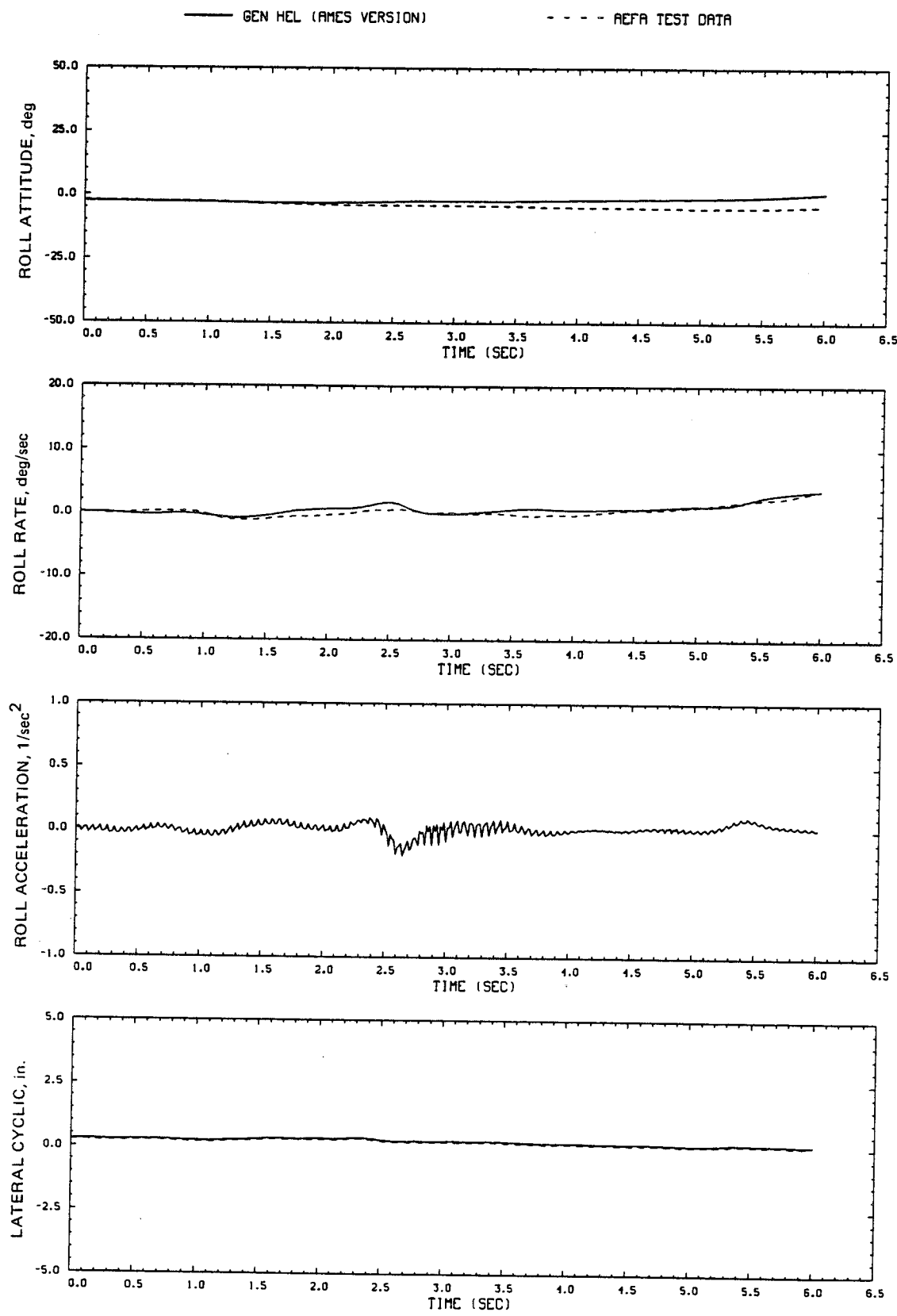


Figure D3.- Continued.

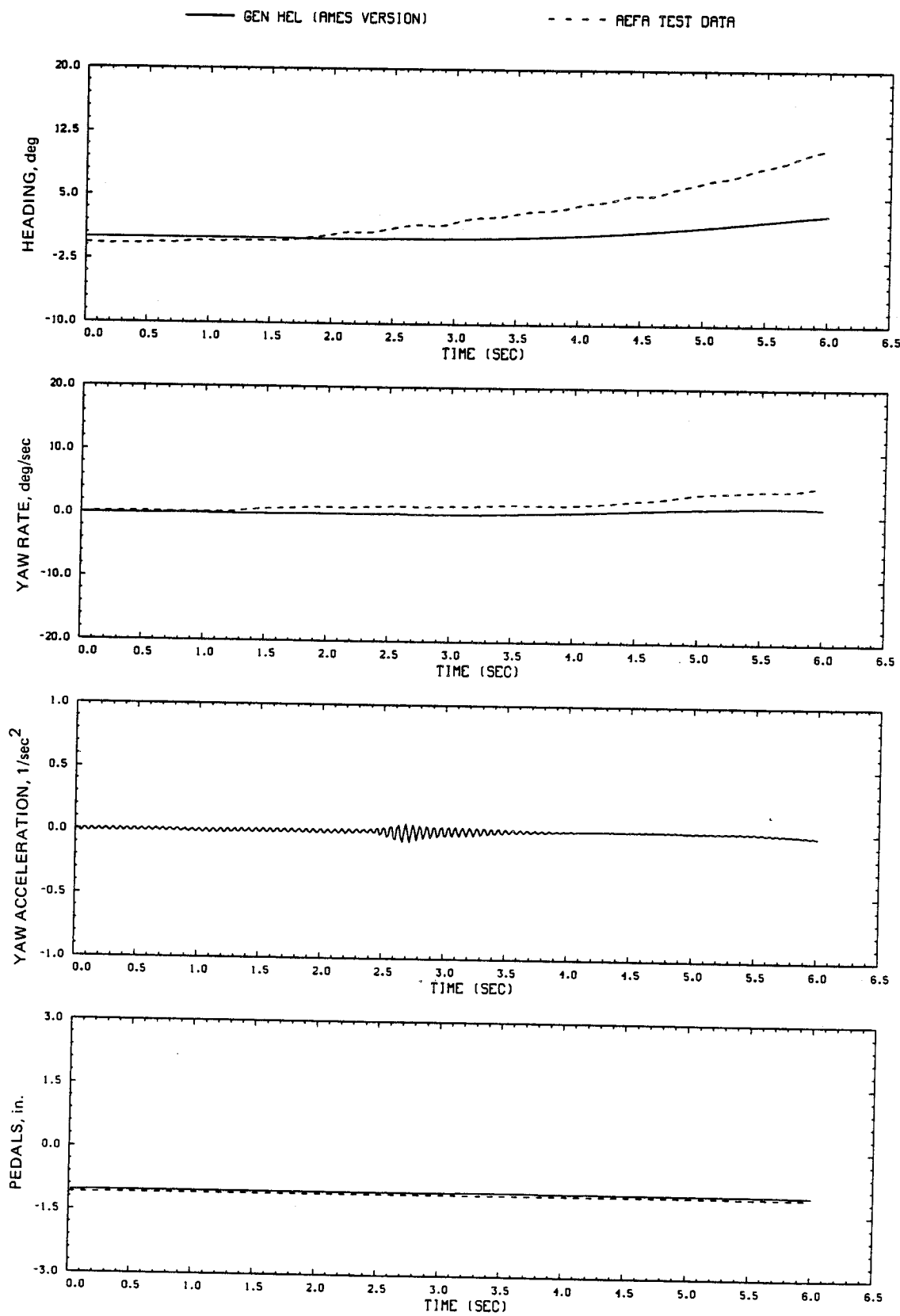


Figure D3.- Continued.

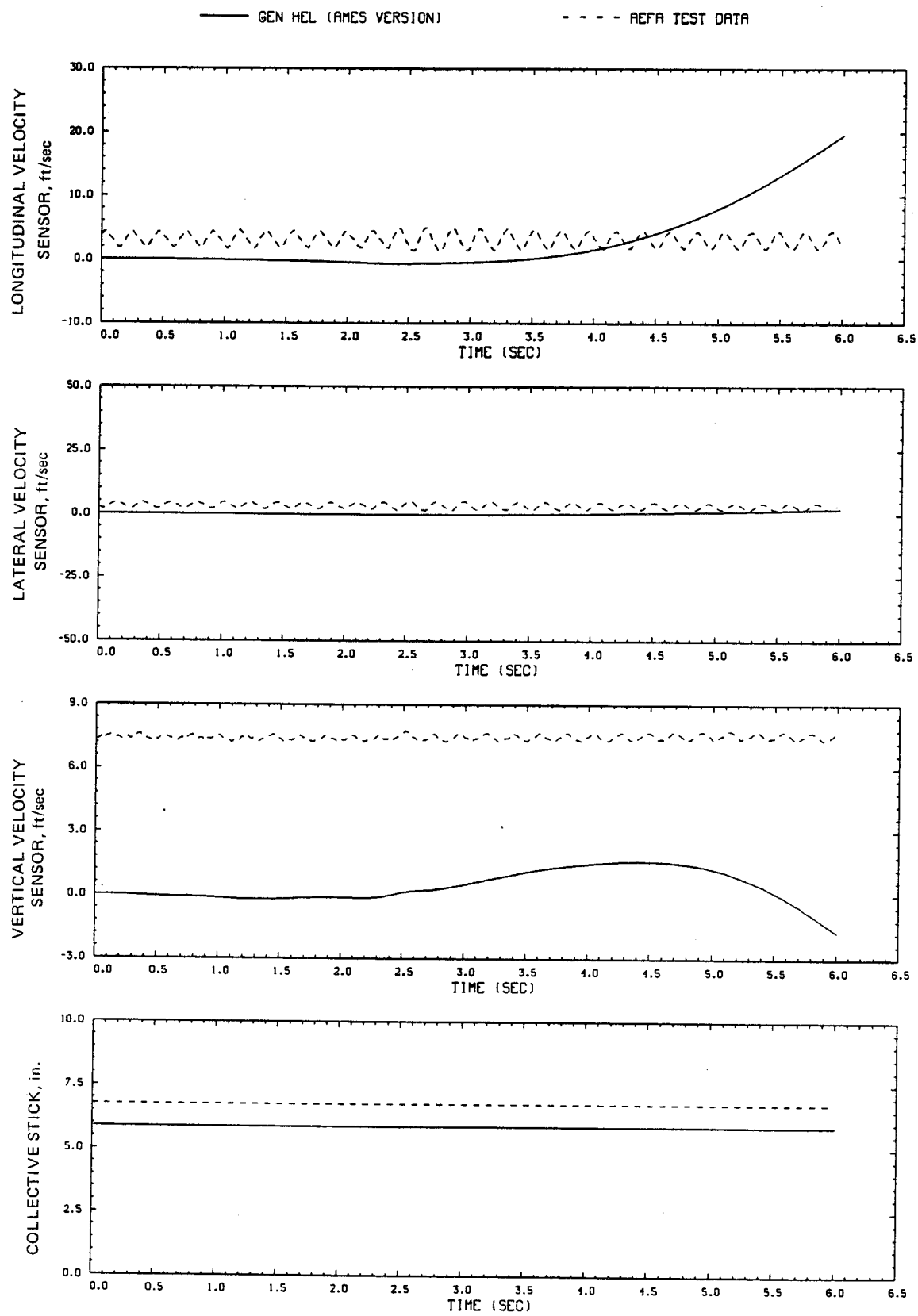


Figure D3.- Continued.

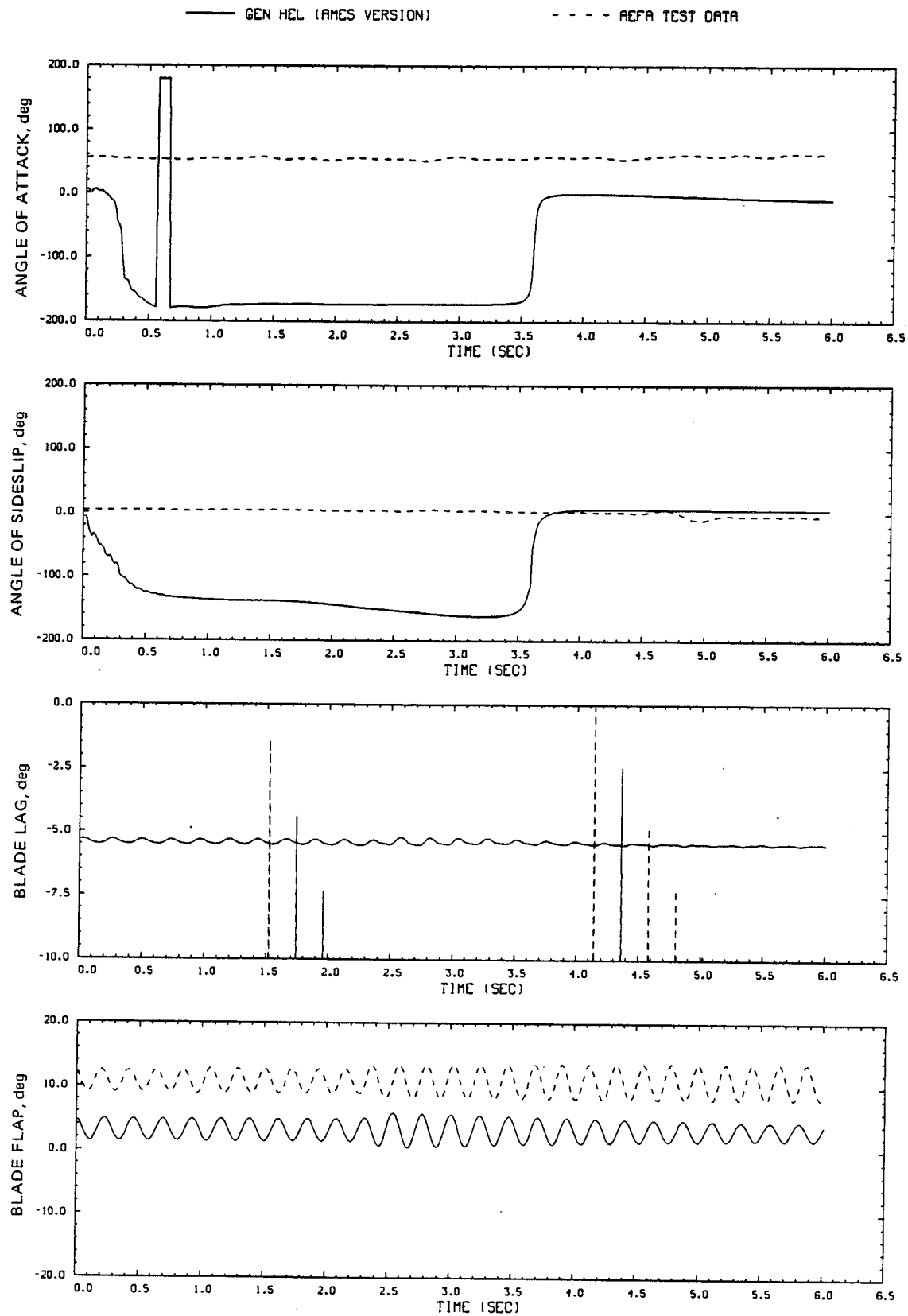


Figure D3.- Continued.

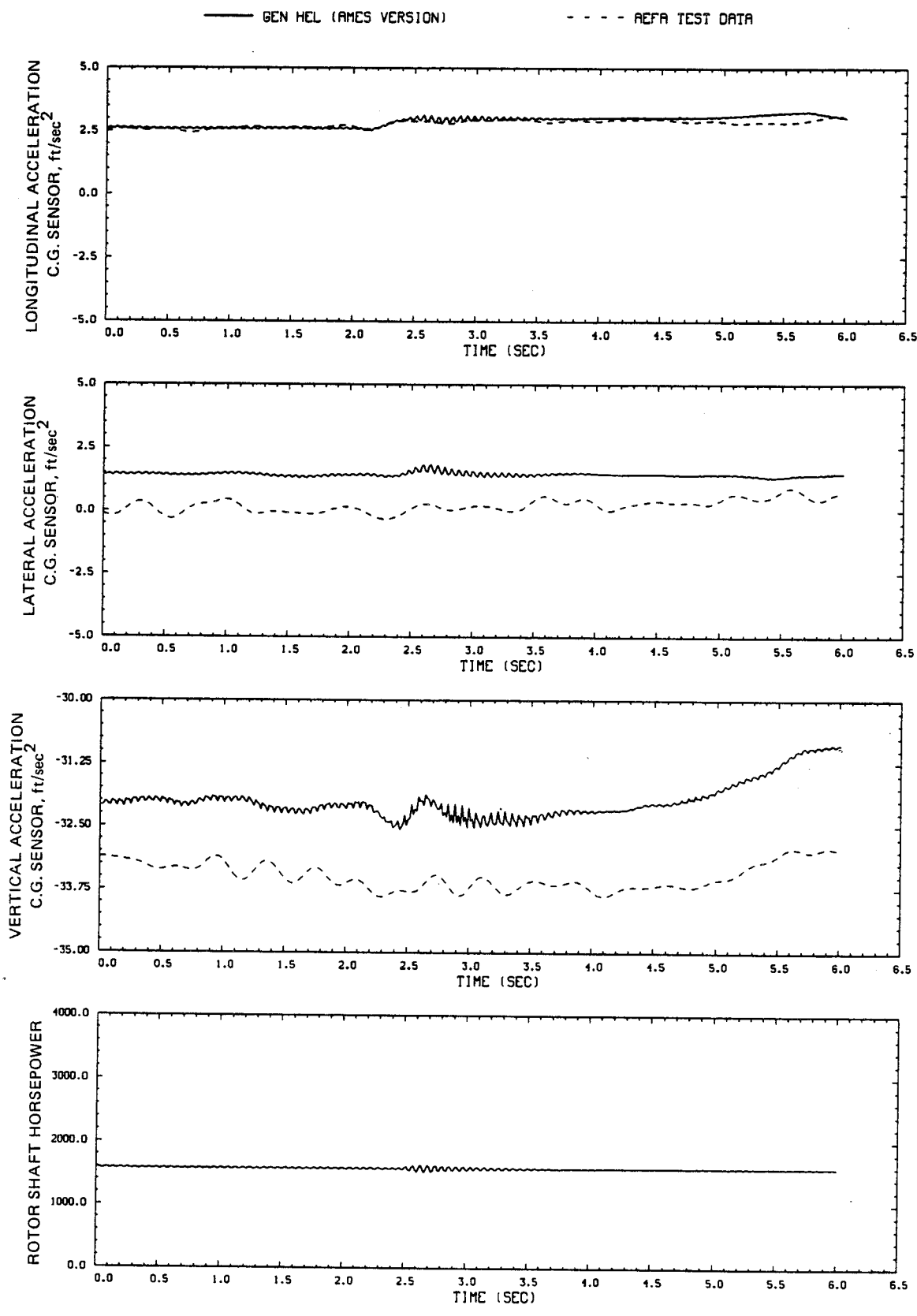


Figure D3.- Continued.

— GEN HEL (AMES VERSION)

- - - REFA TEST DATA

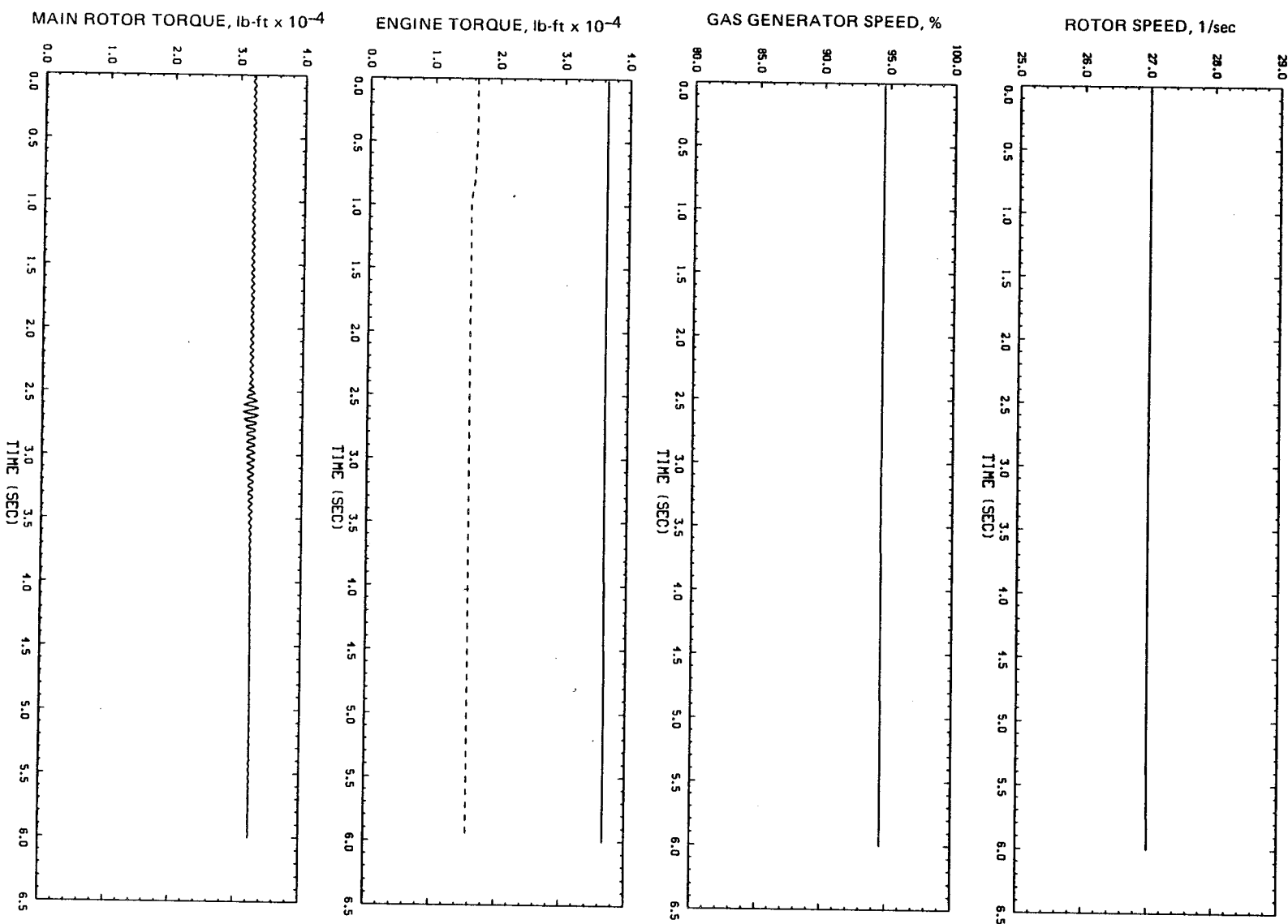


Figure D3.- Concluded.

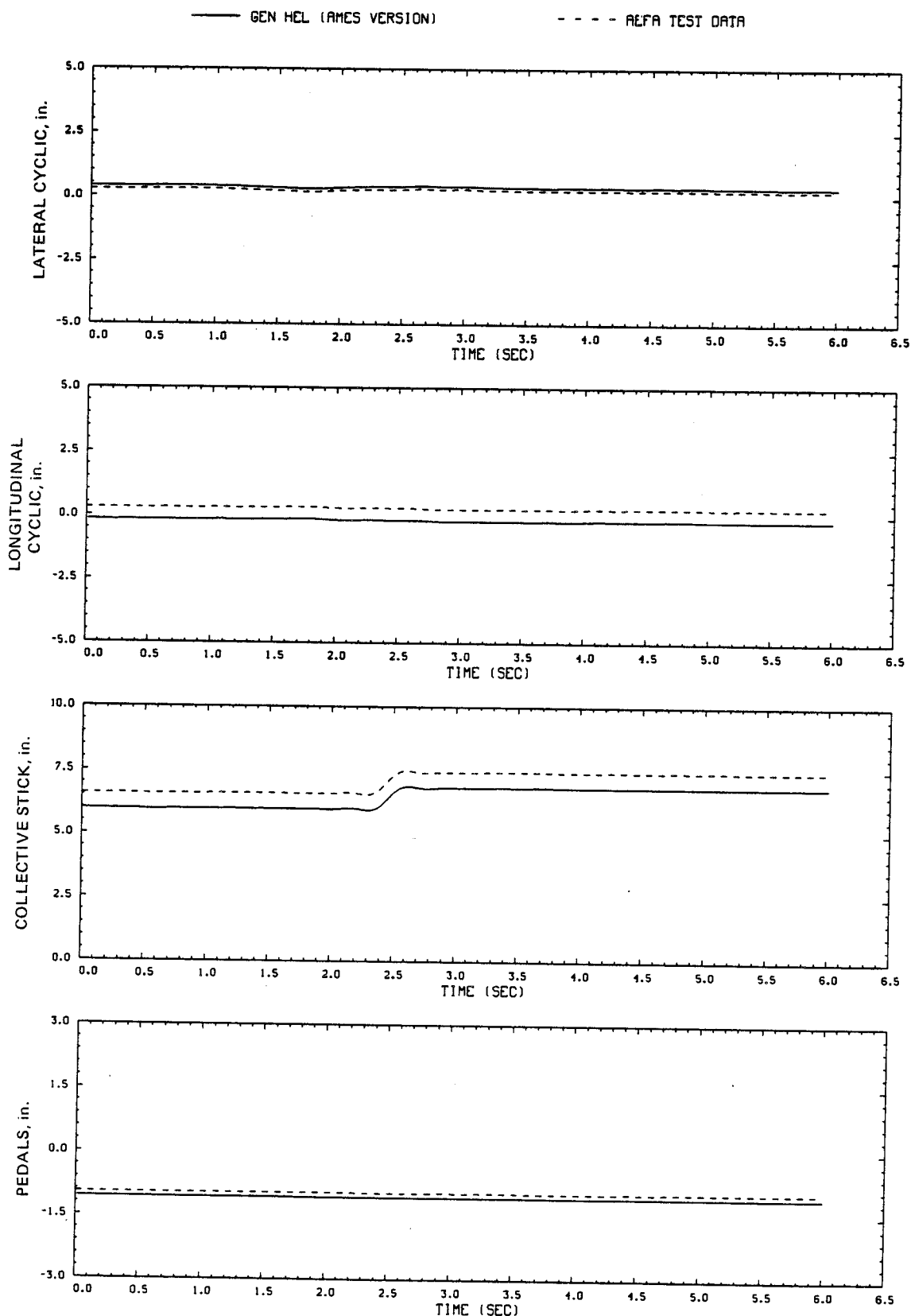


Figure D4.- Comparison of Ames real-time simulation and flight-test data.  
(File 212: 1-in. up collective input at hover)

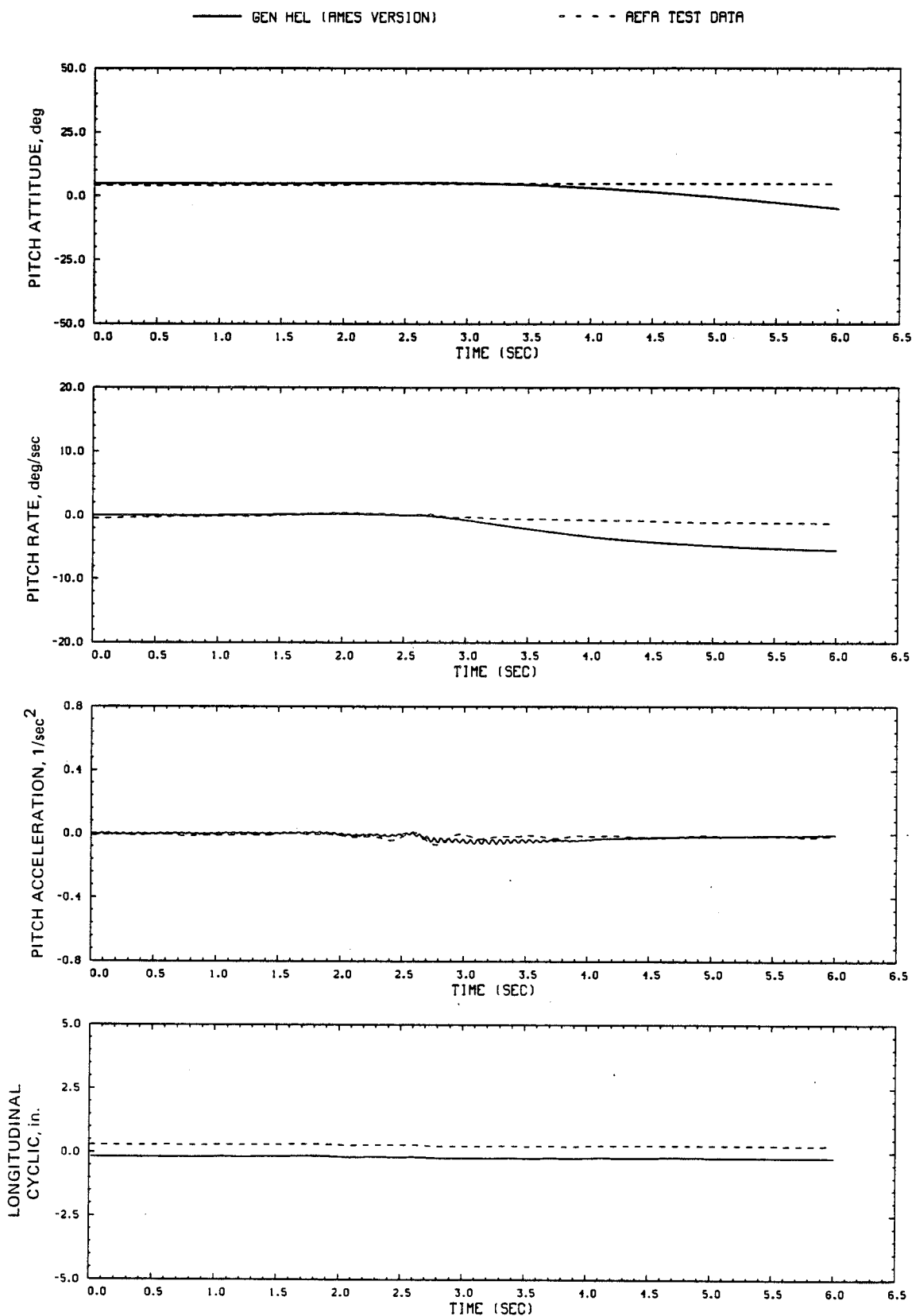


Figure D4.- Continued.

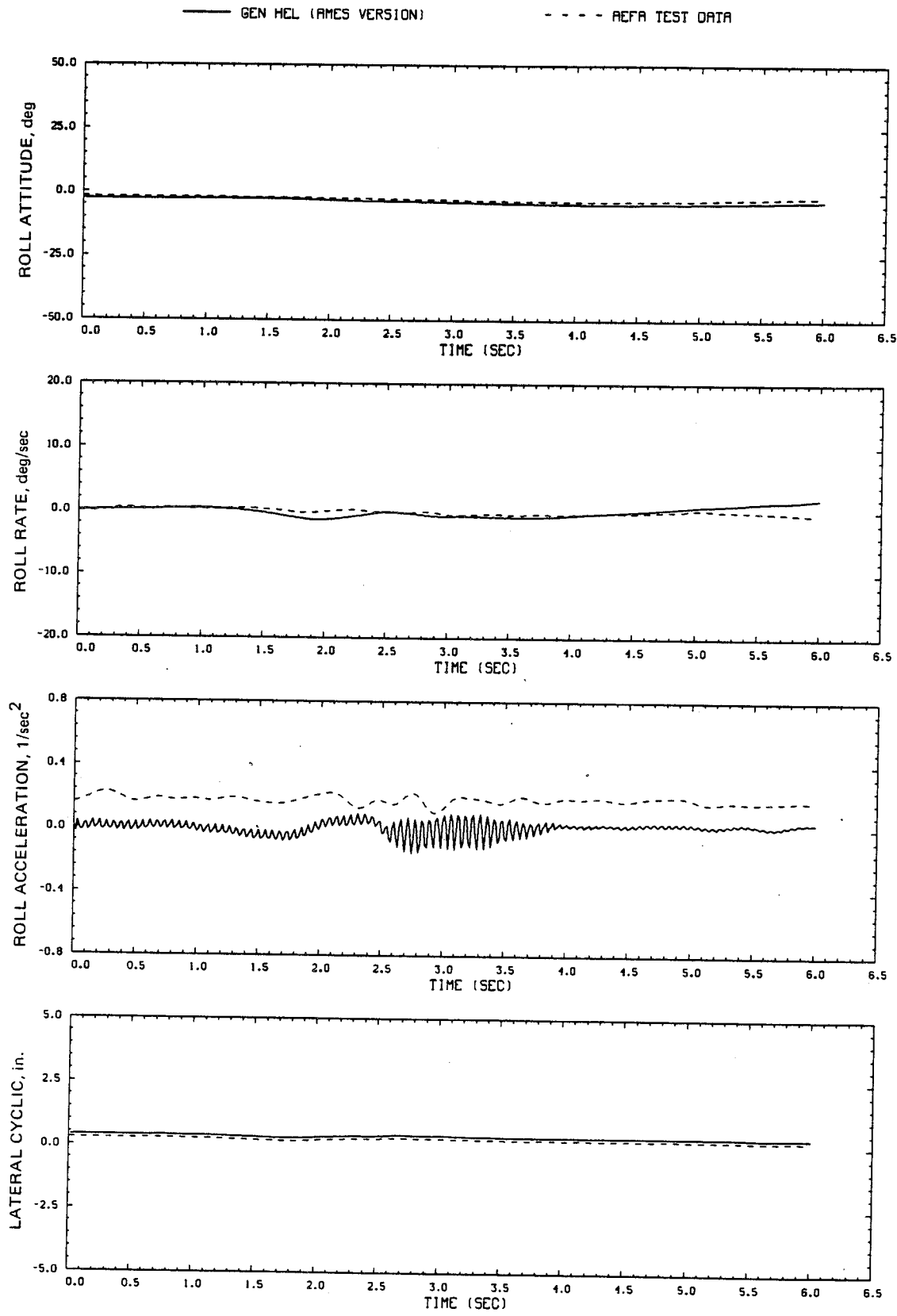


Figure D4.- Continued.

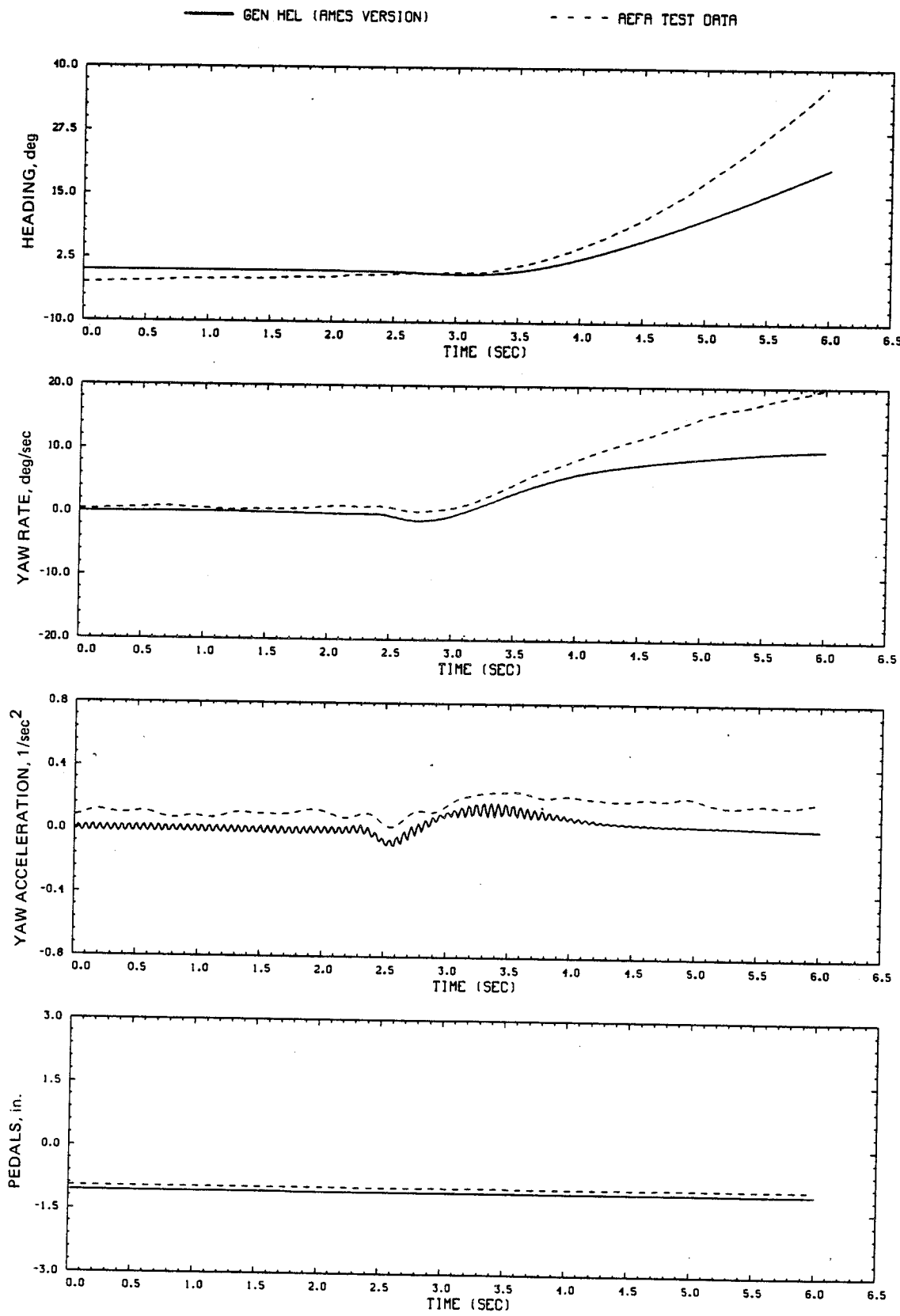


Figure D4.- Continued.

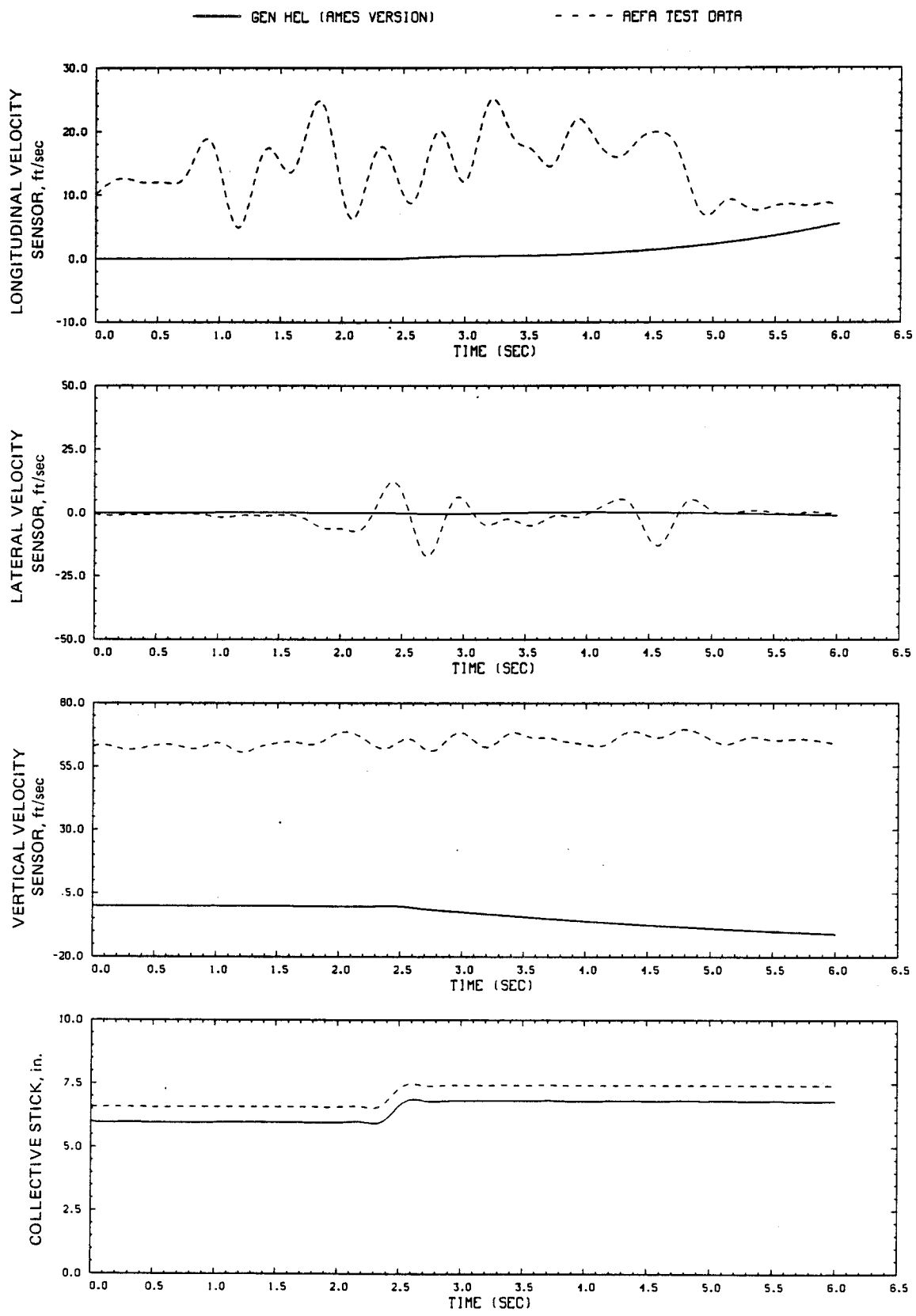


Figure D4.- Continued.

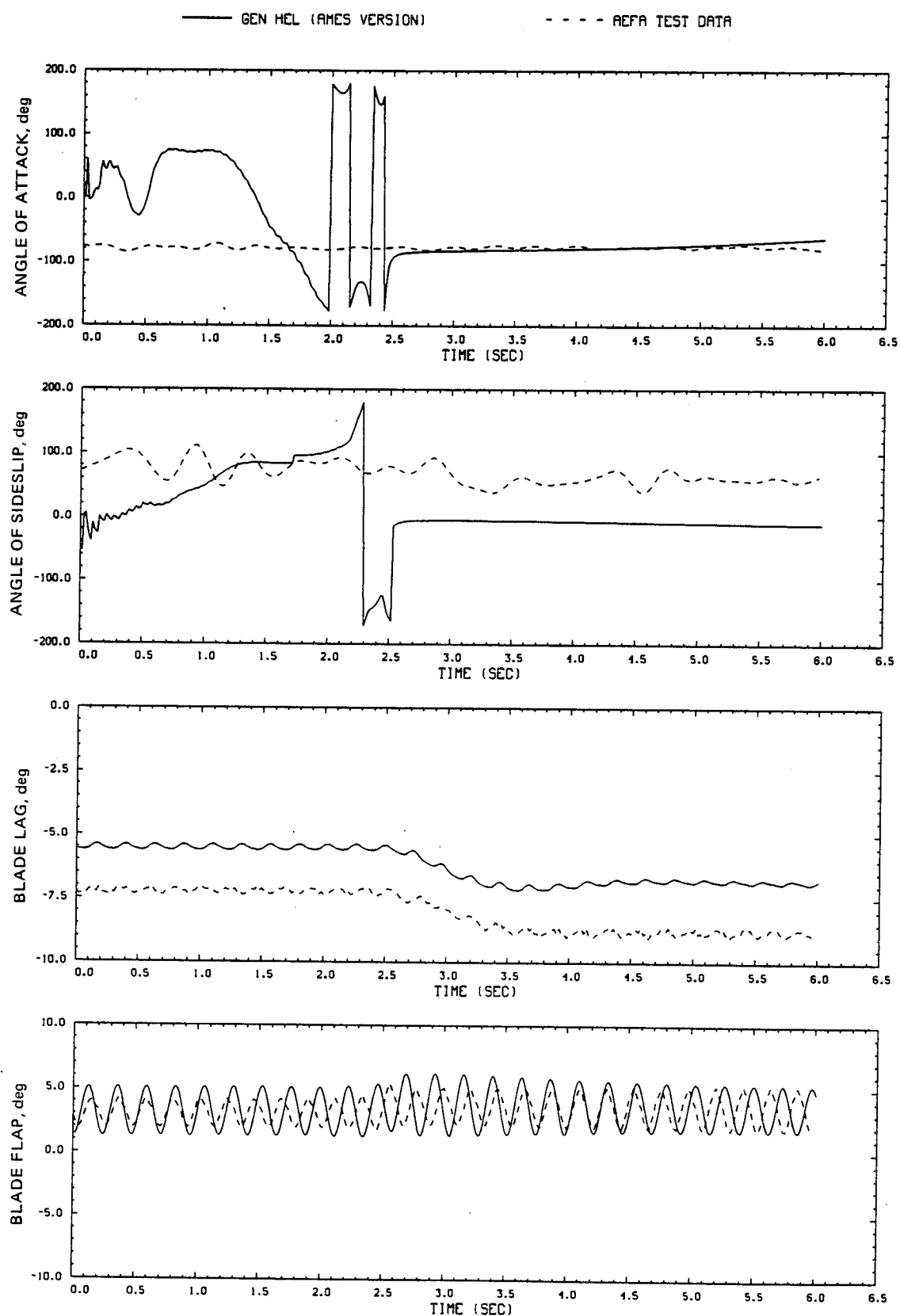


Figure D4.- Continued.

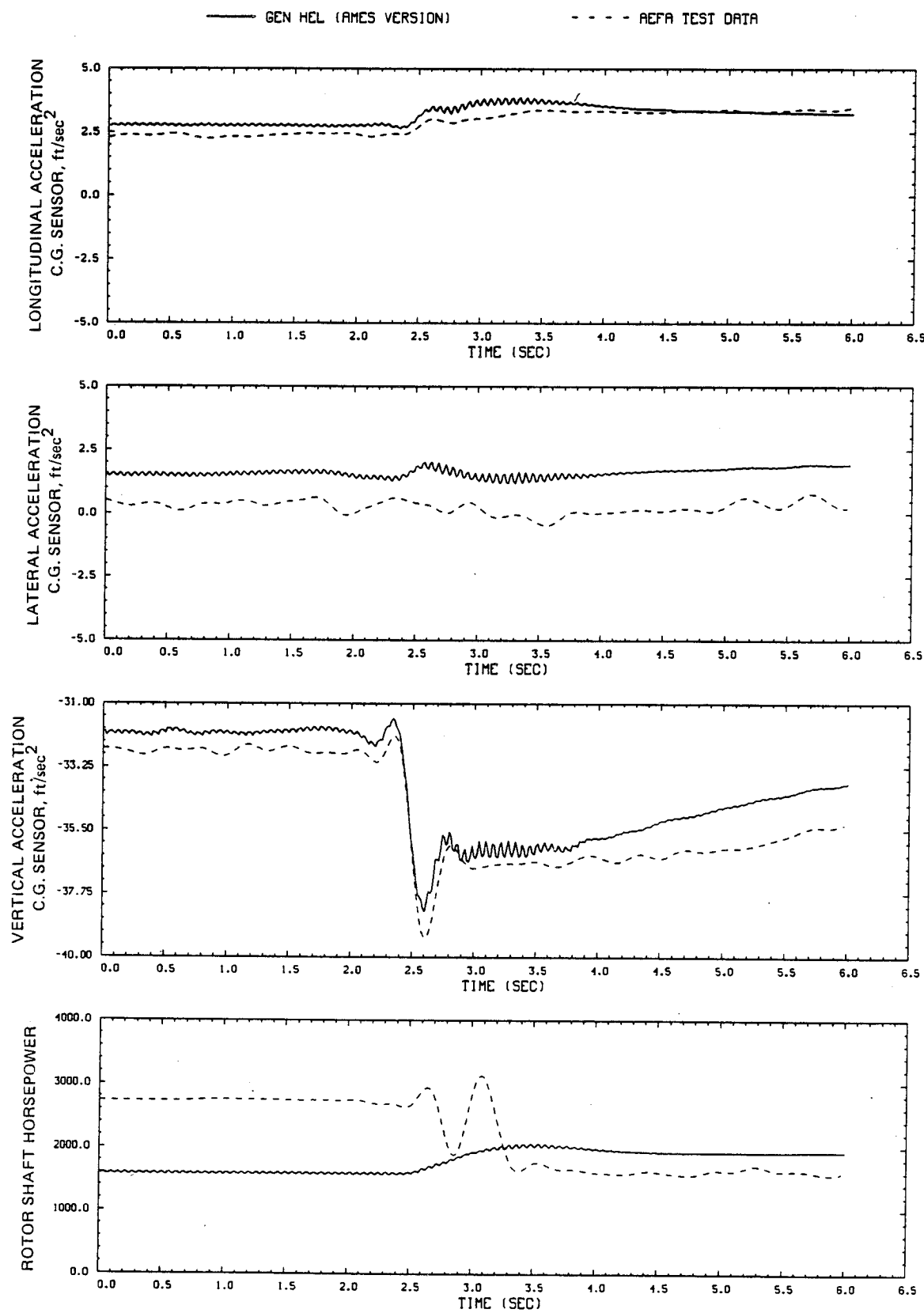


Figure D4.- Continued.

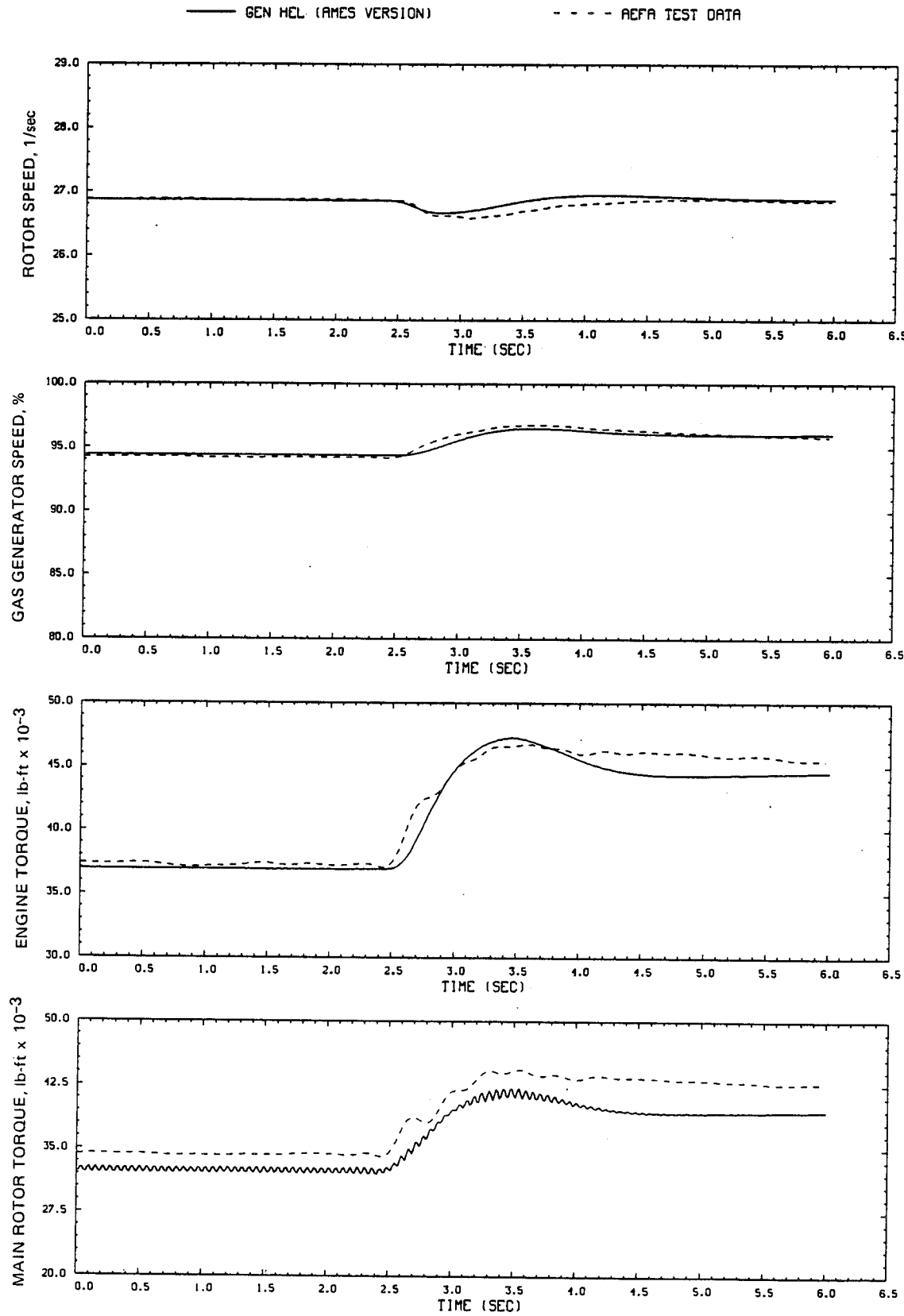


Figure D4.- Concluded.

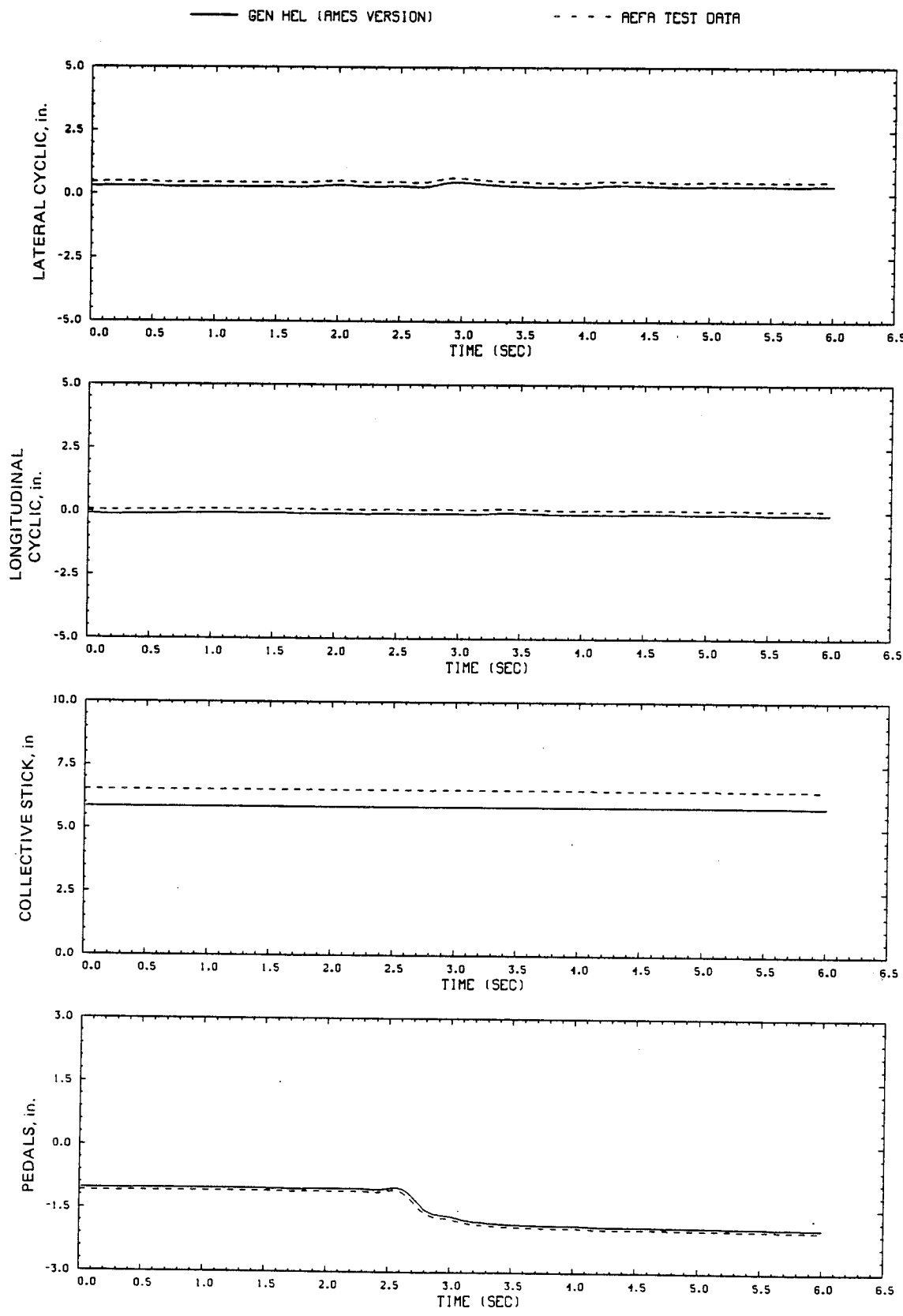


Figure D5.- Comparison of Ames real-time simulation and flight-test data.  
(File 209: 1-in. left pedal input at hover)

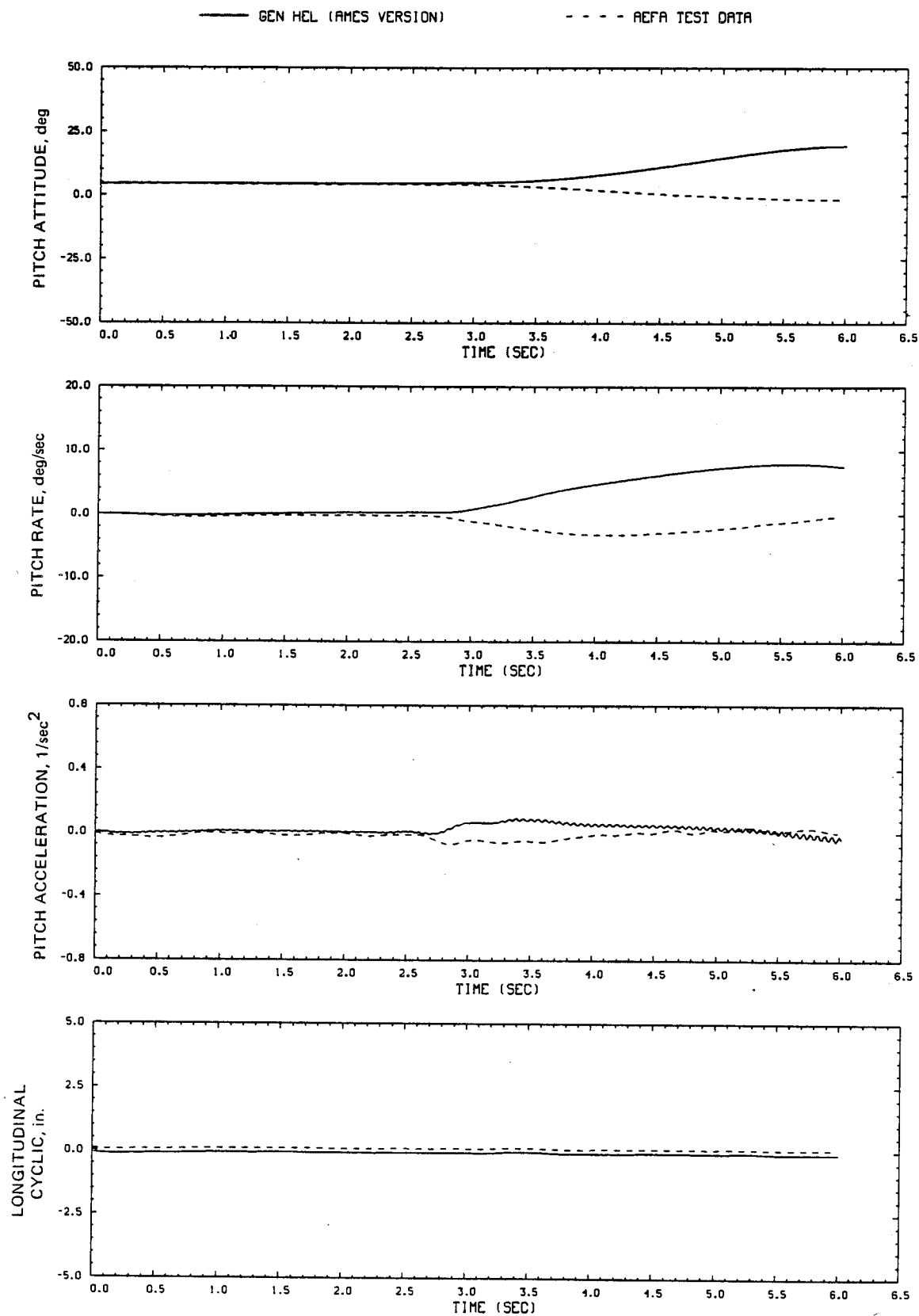


Figure D5.- Continued.

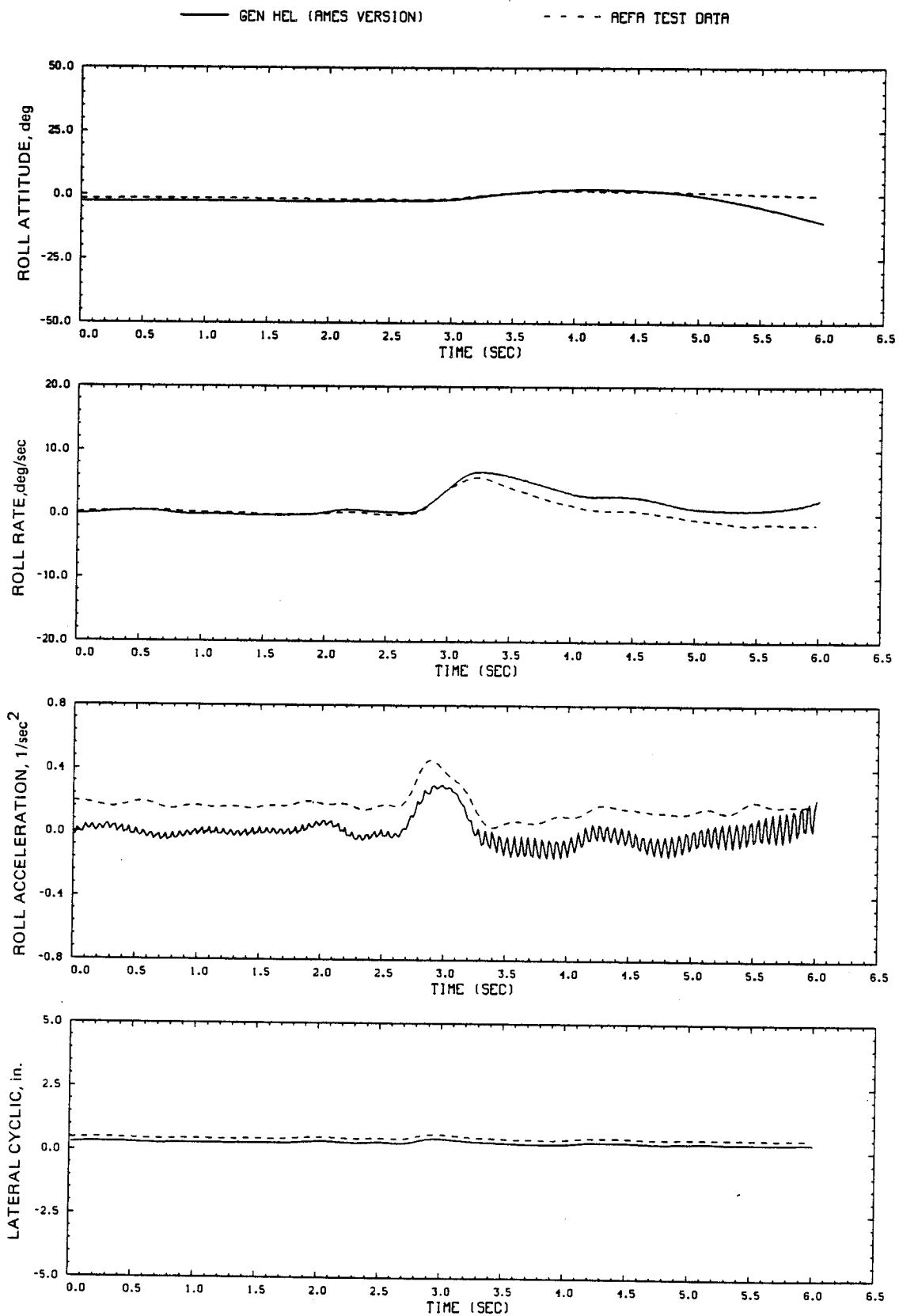


Figure D5.- Continued.

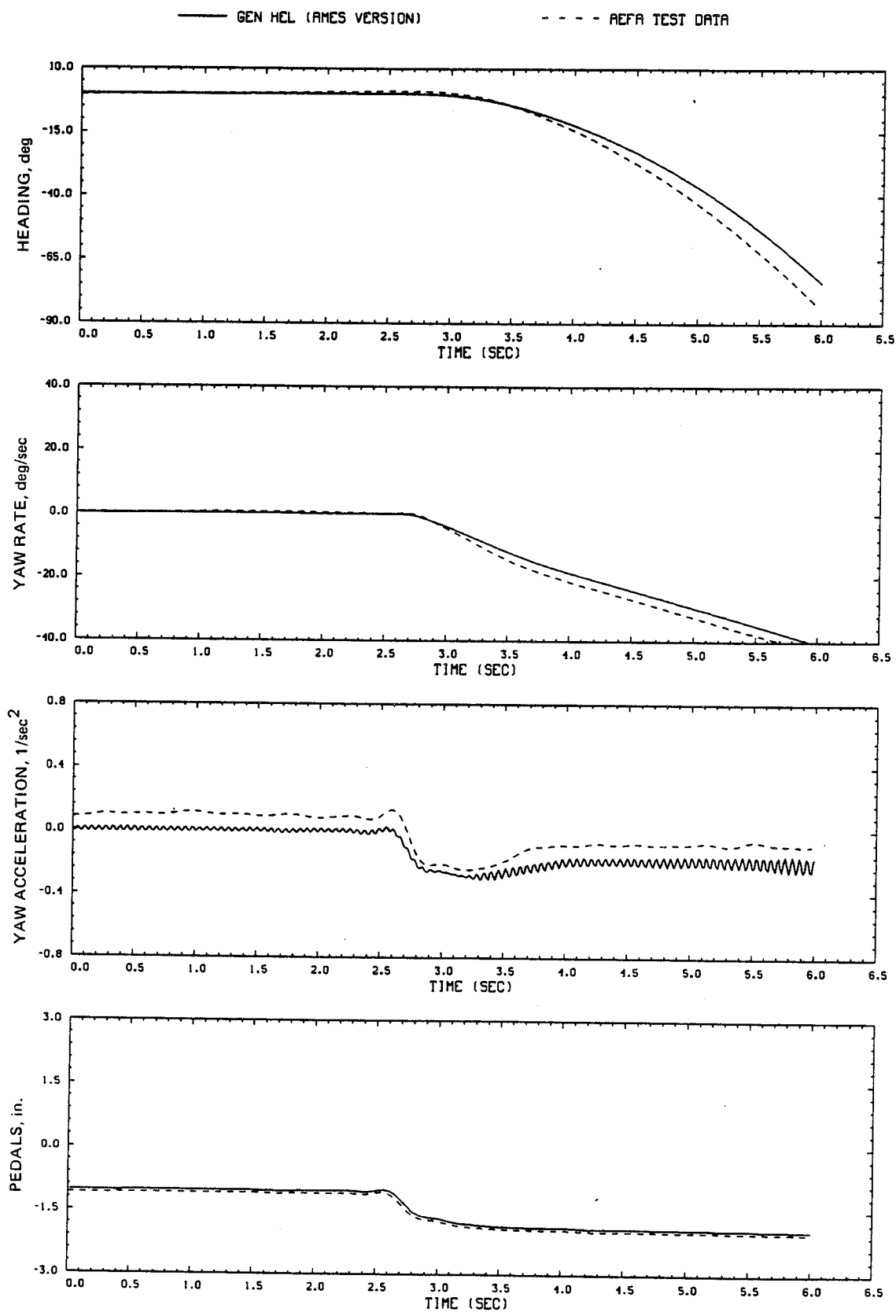


Figure D5.- Continued.

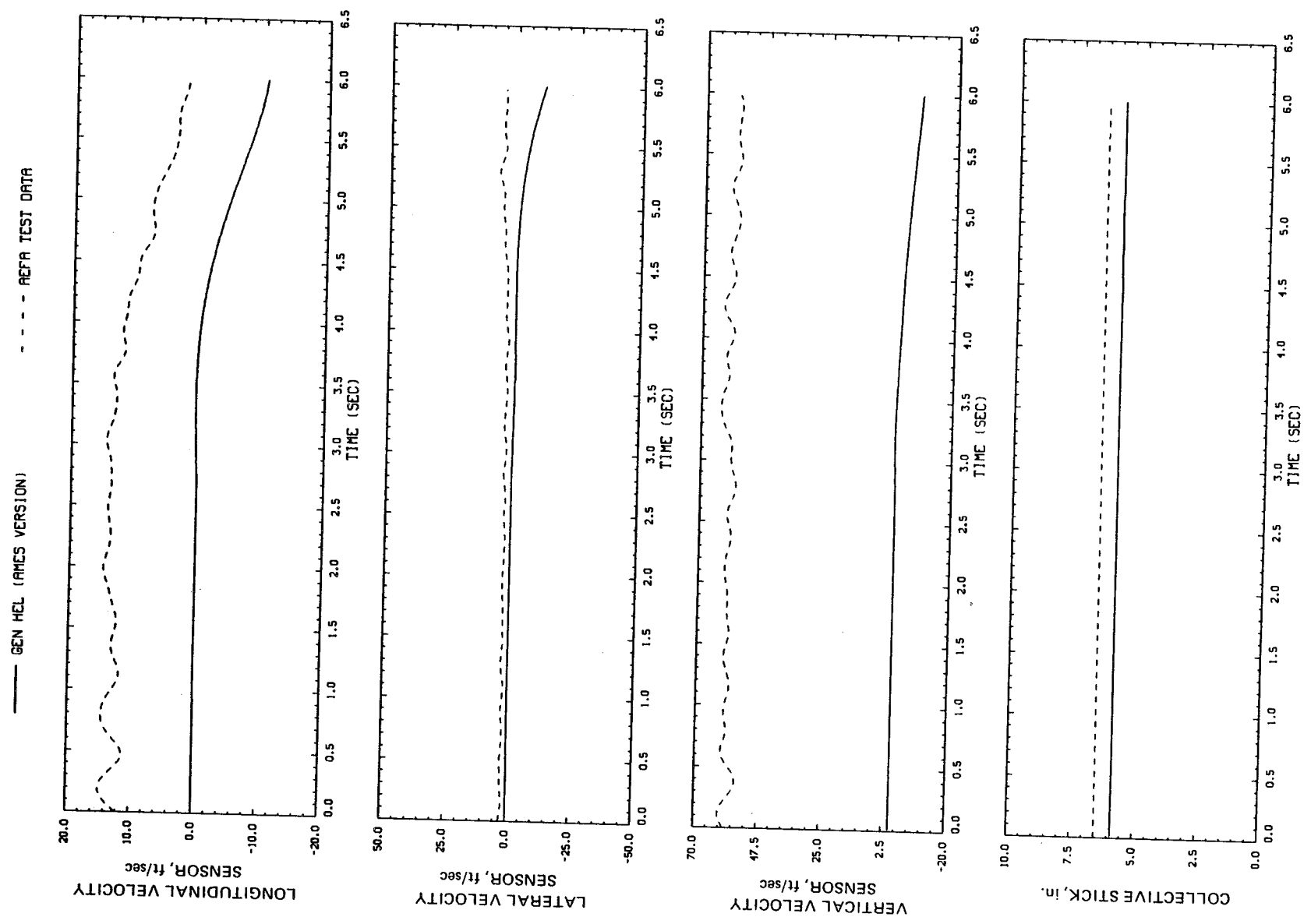


Figure D5.- Continued.

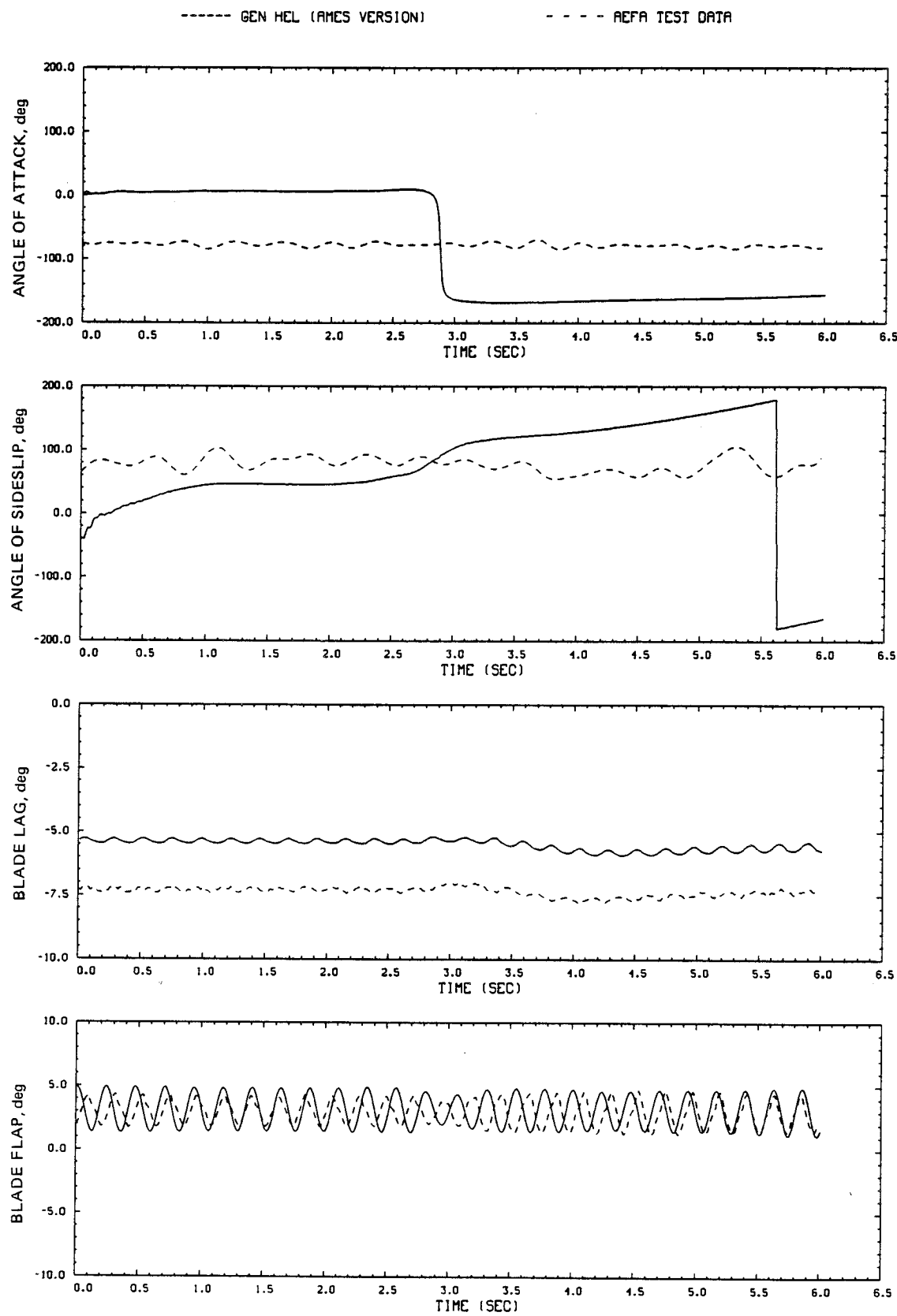


Figure D5.- Continued.

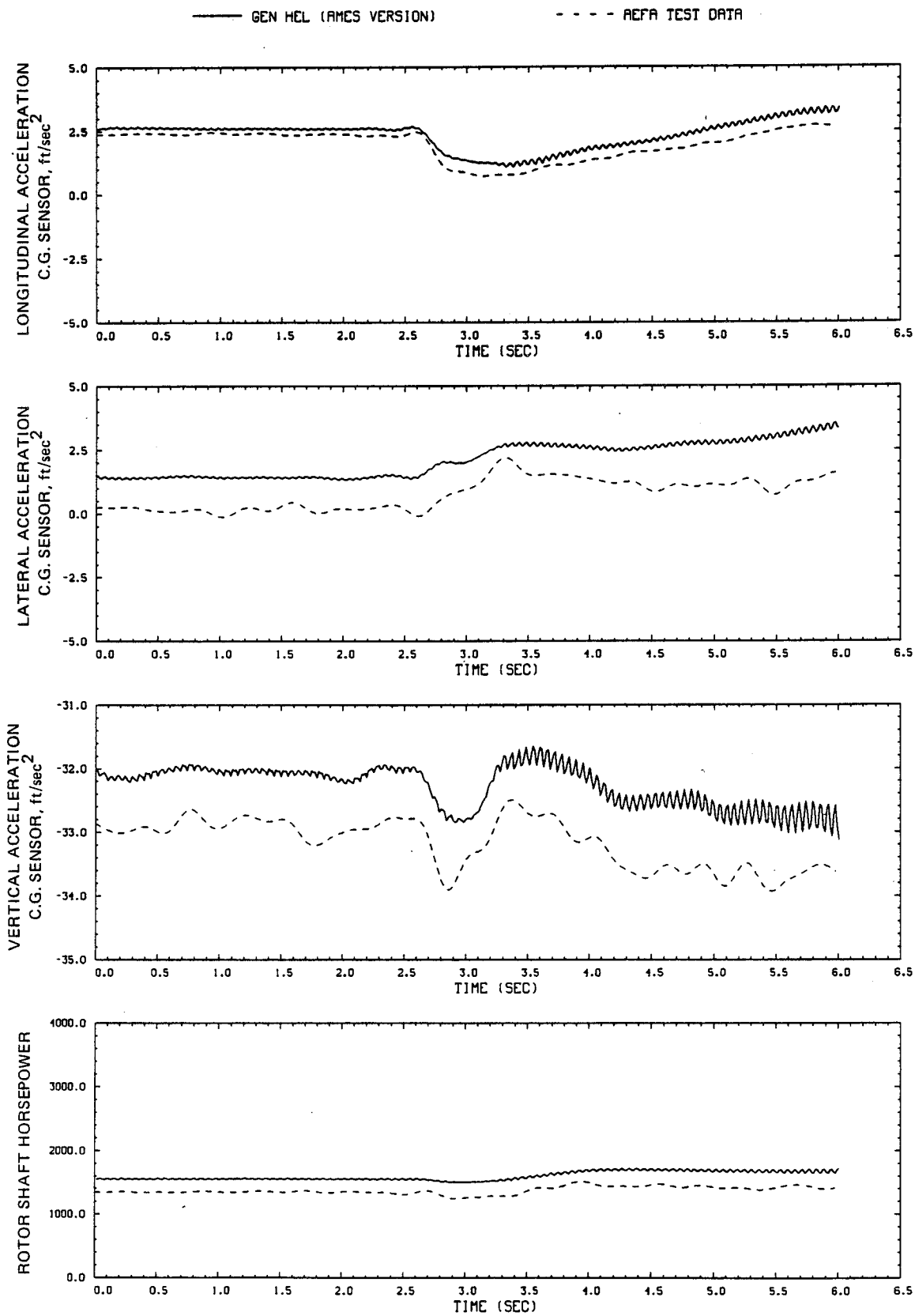


Figure D5.- Continued.

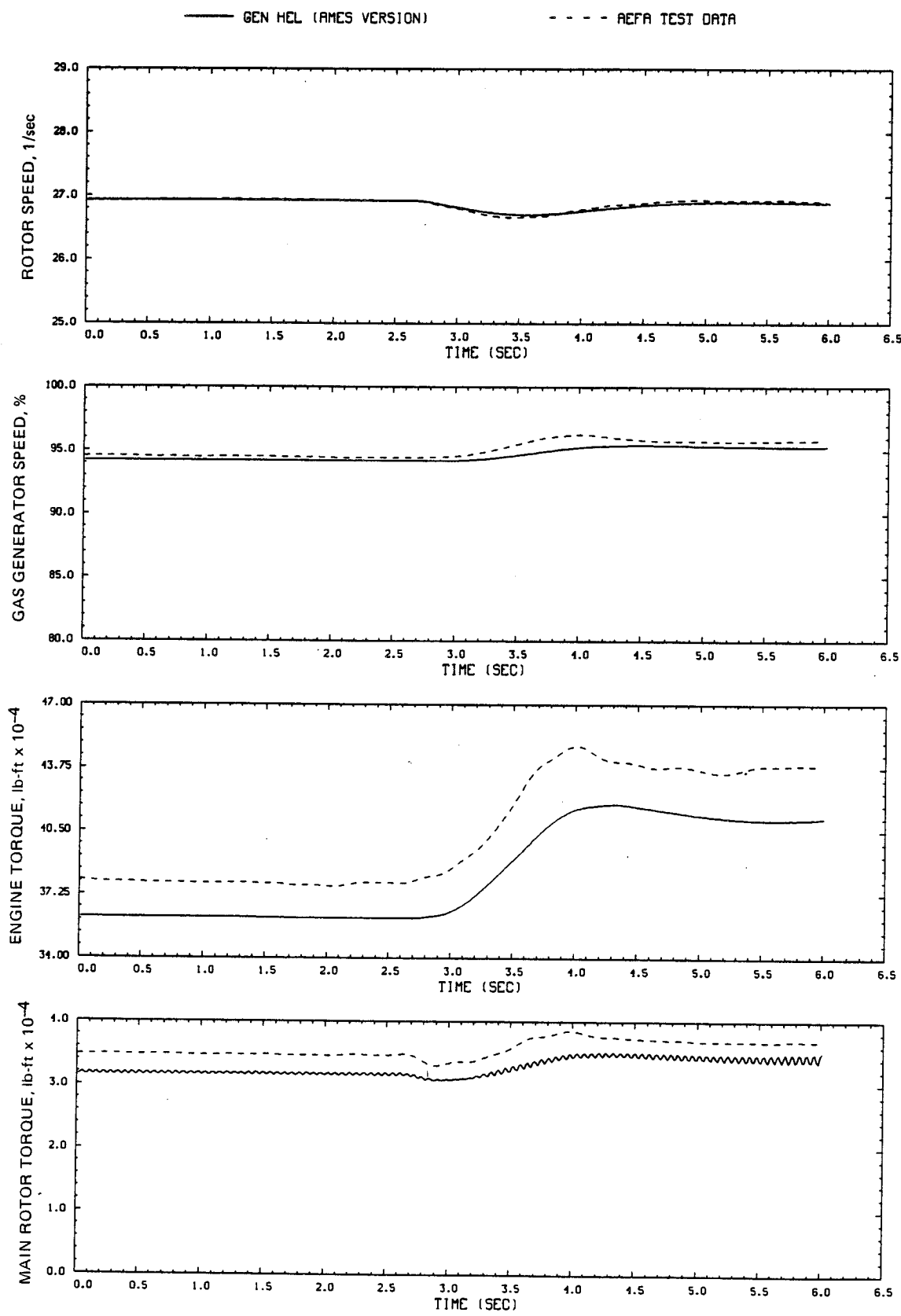


Figure D5.- Concluded.

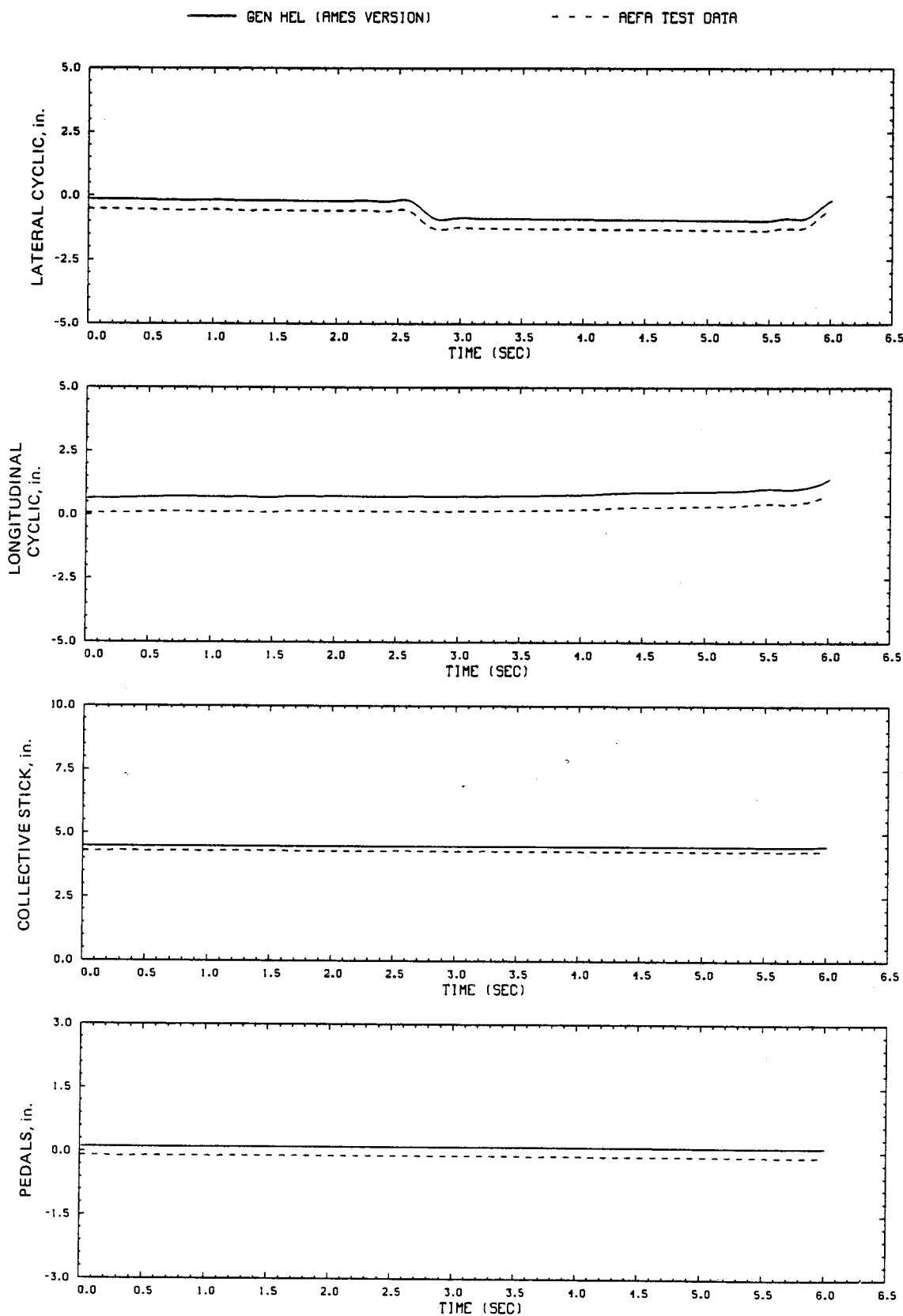


Figure D6.- Comparison of Ames real-time simulation and flight-test data.  
(File 504: 1-in. left cyclic input, 60 knots)

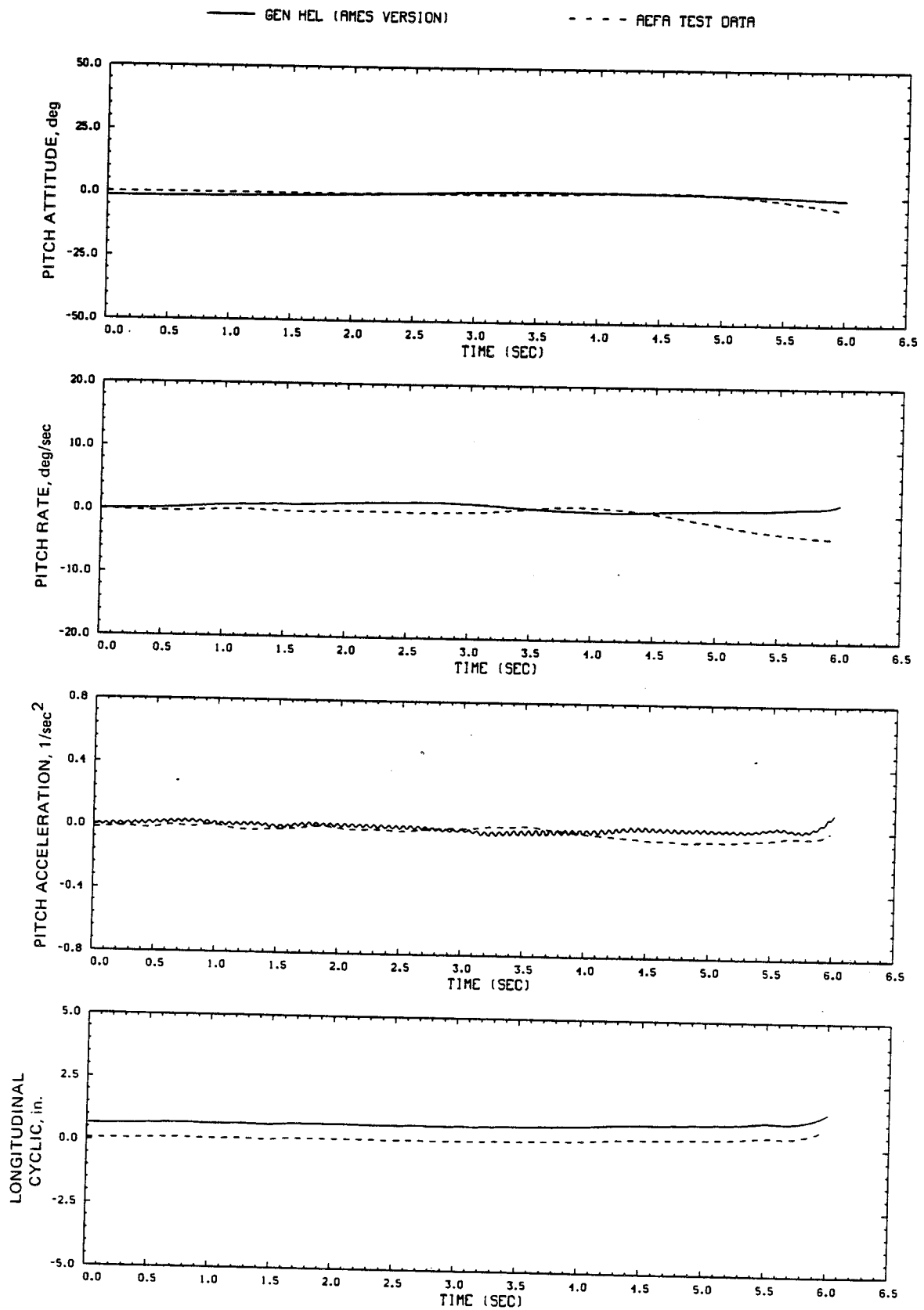


Figure D6.- Continued.

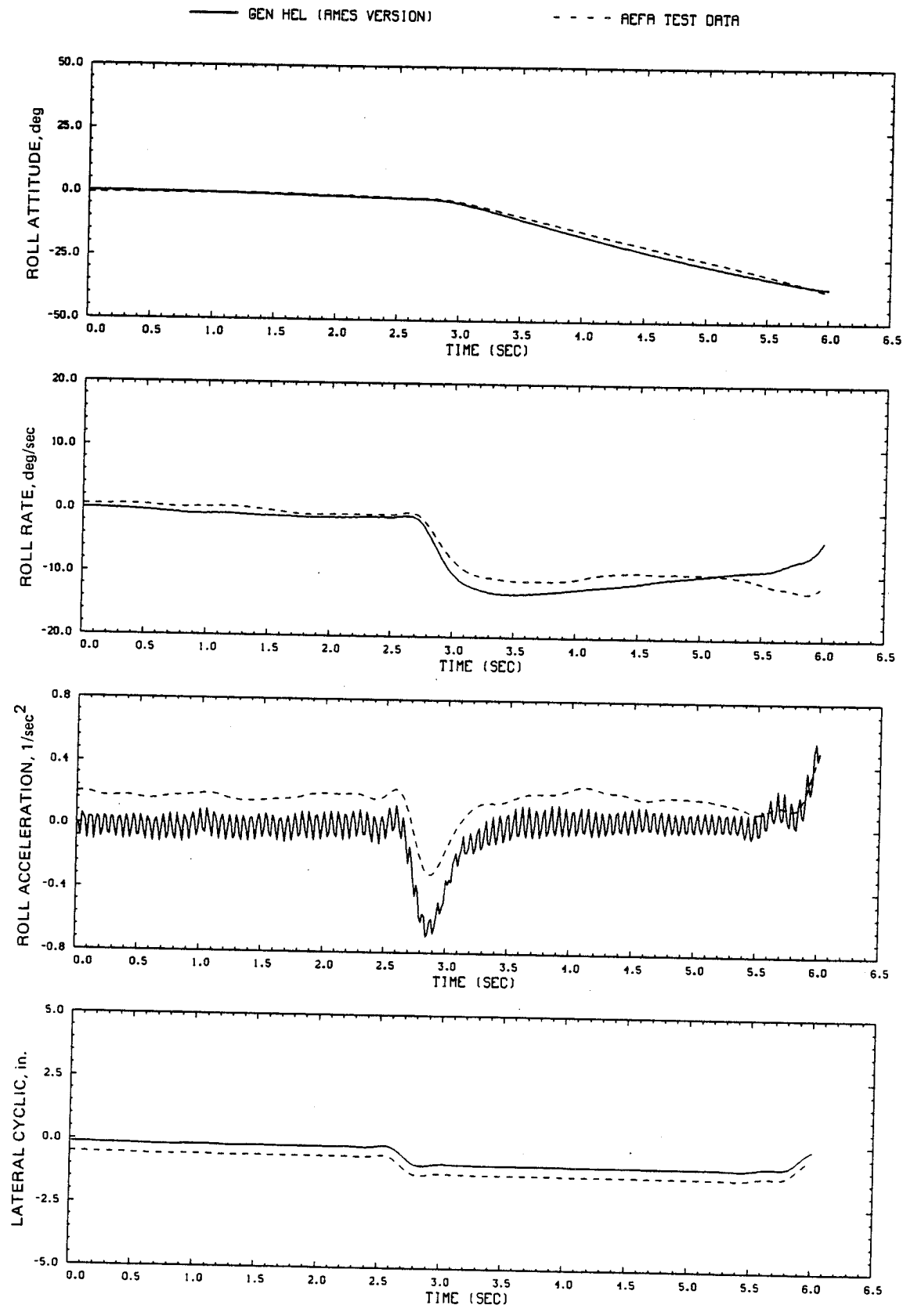


Figure D6.- Continued.

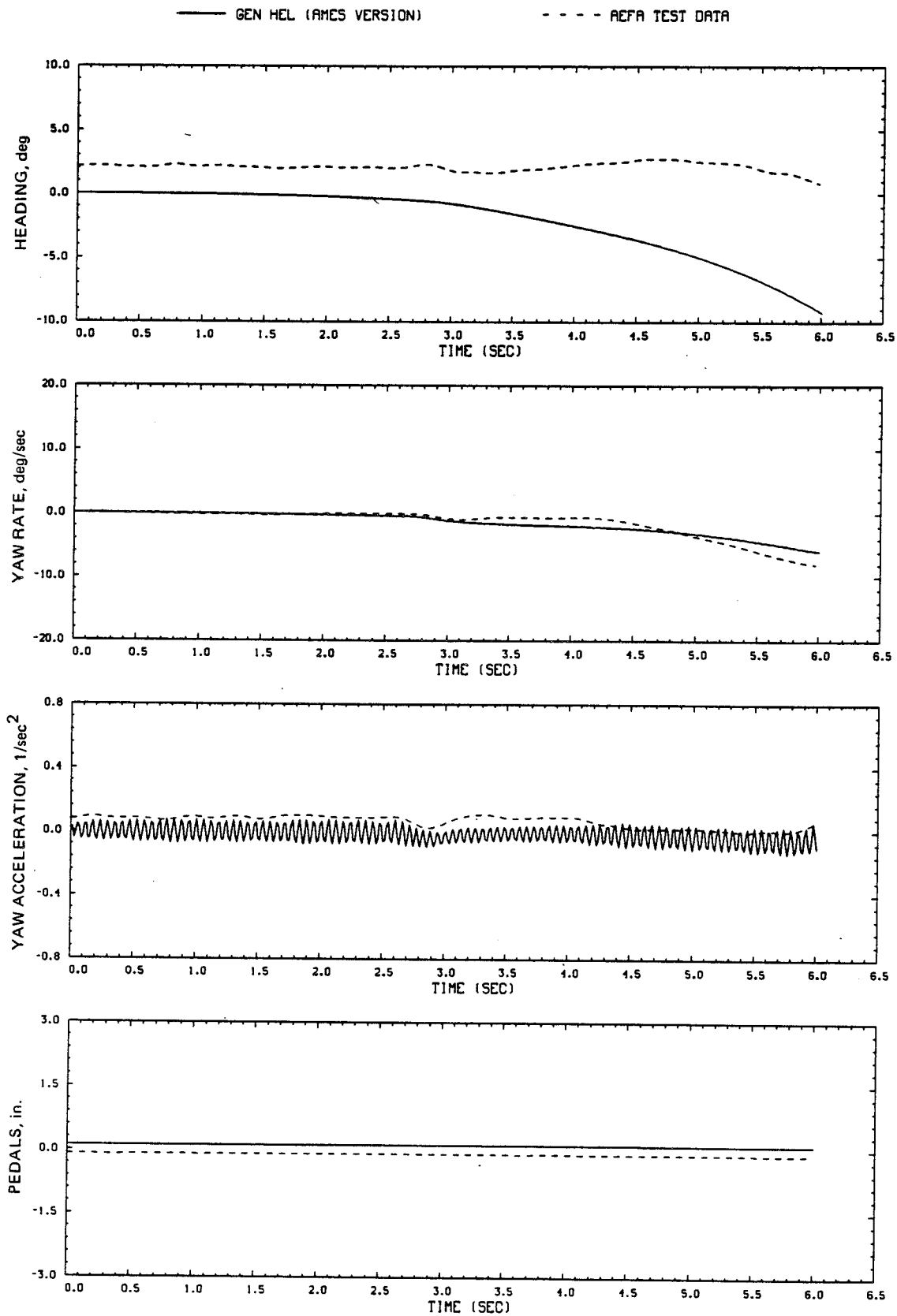


Figure D6.- Continued.

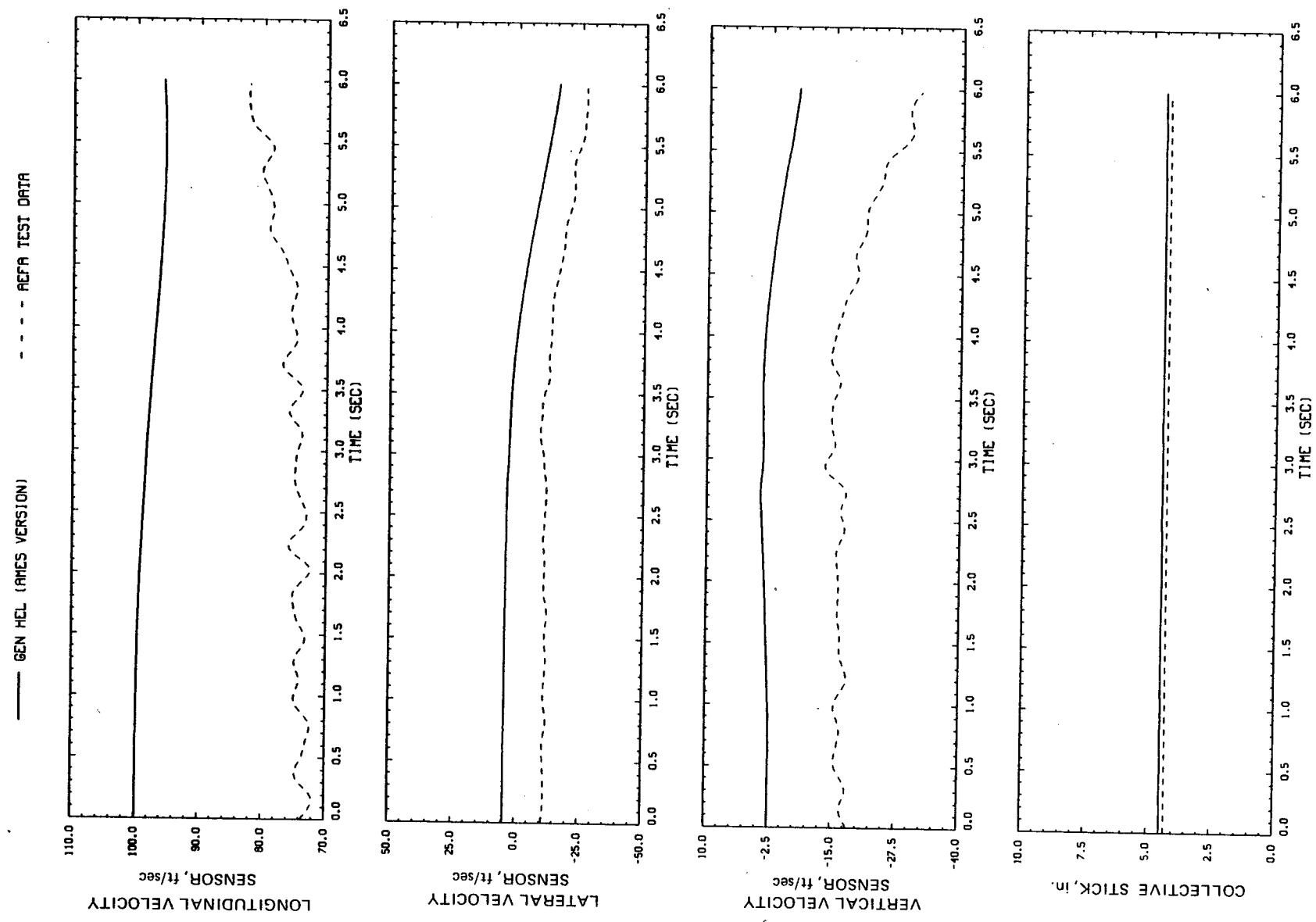


Figure D6.- Continued.

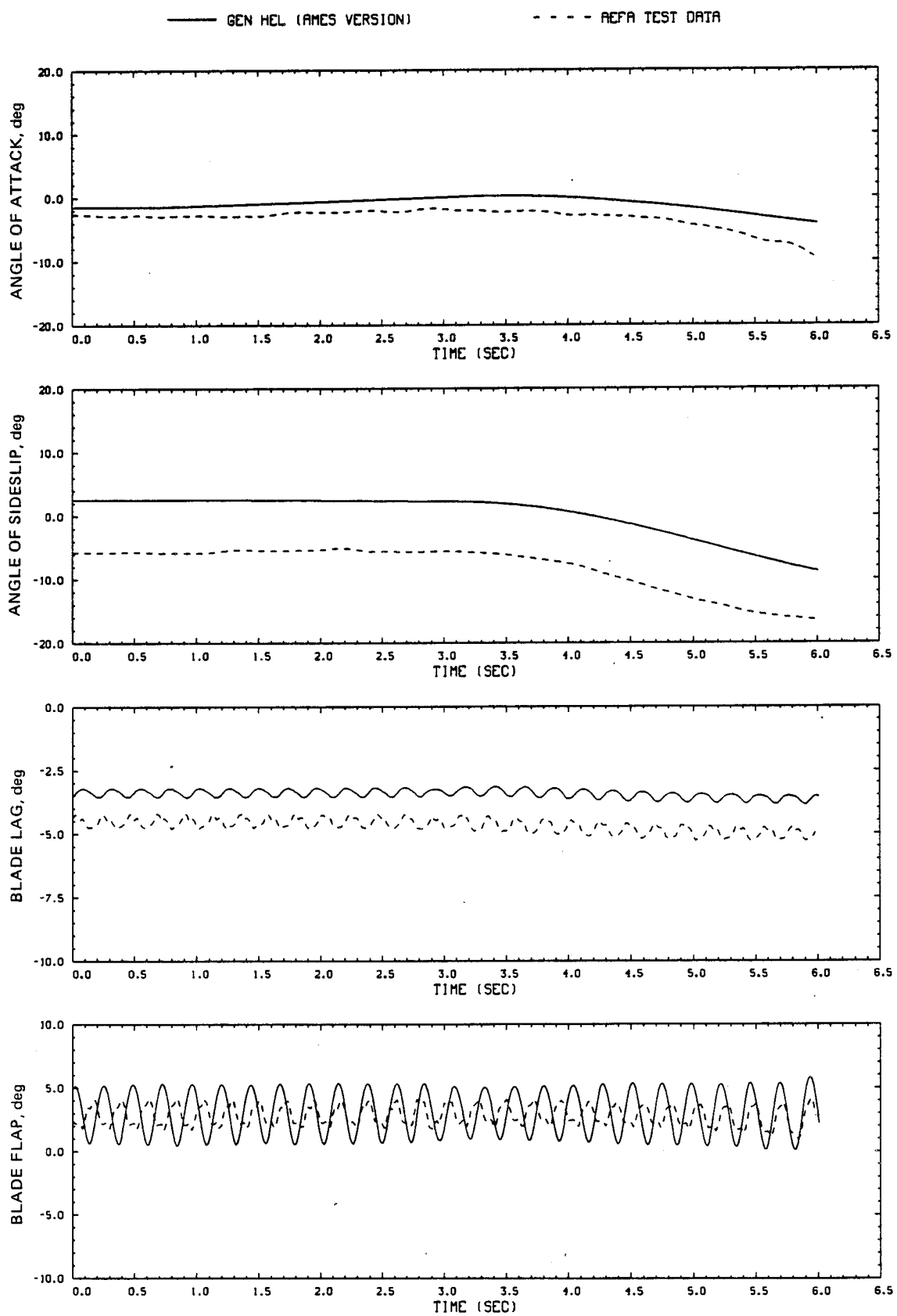


Figure D6.- Continued.

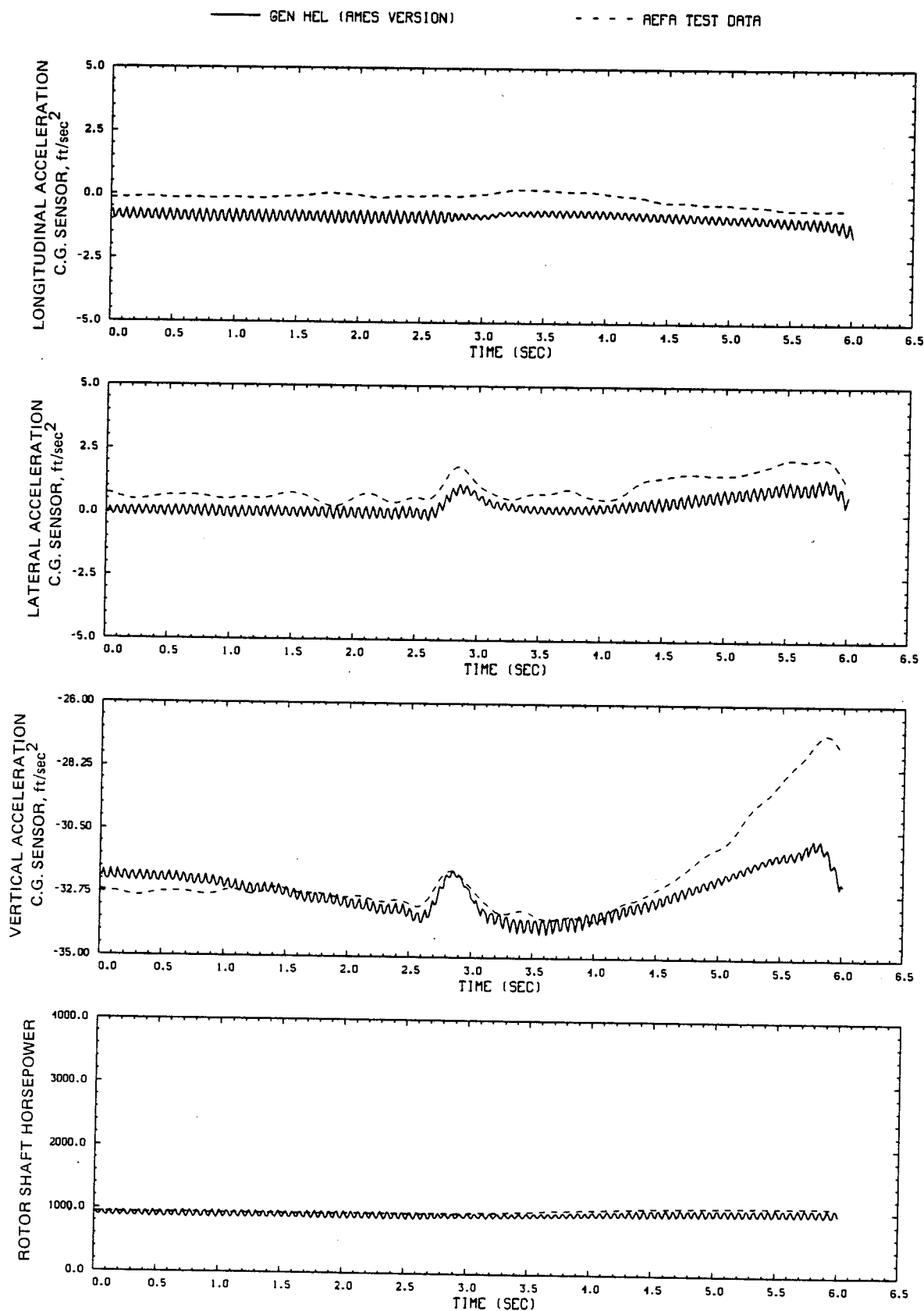


Figure D6.- Continued.

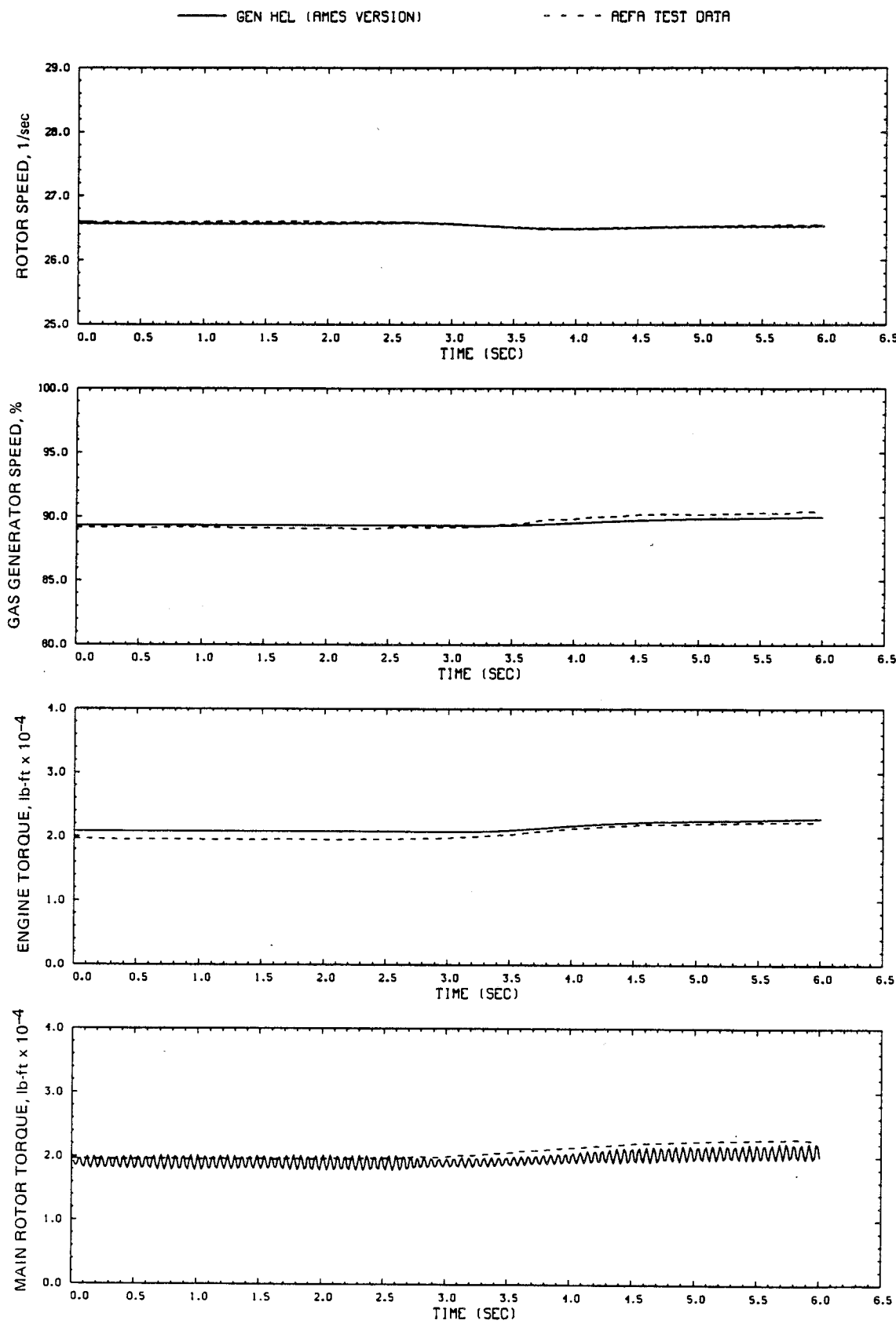


Figure D6.- Concluded.

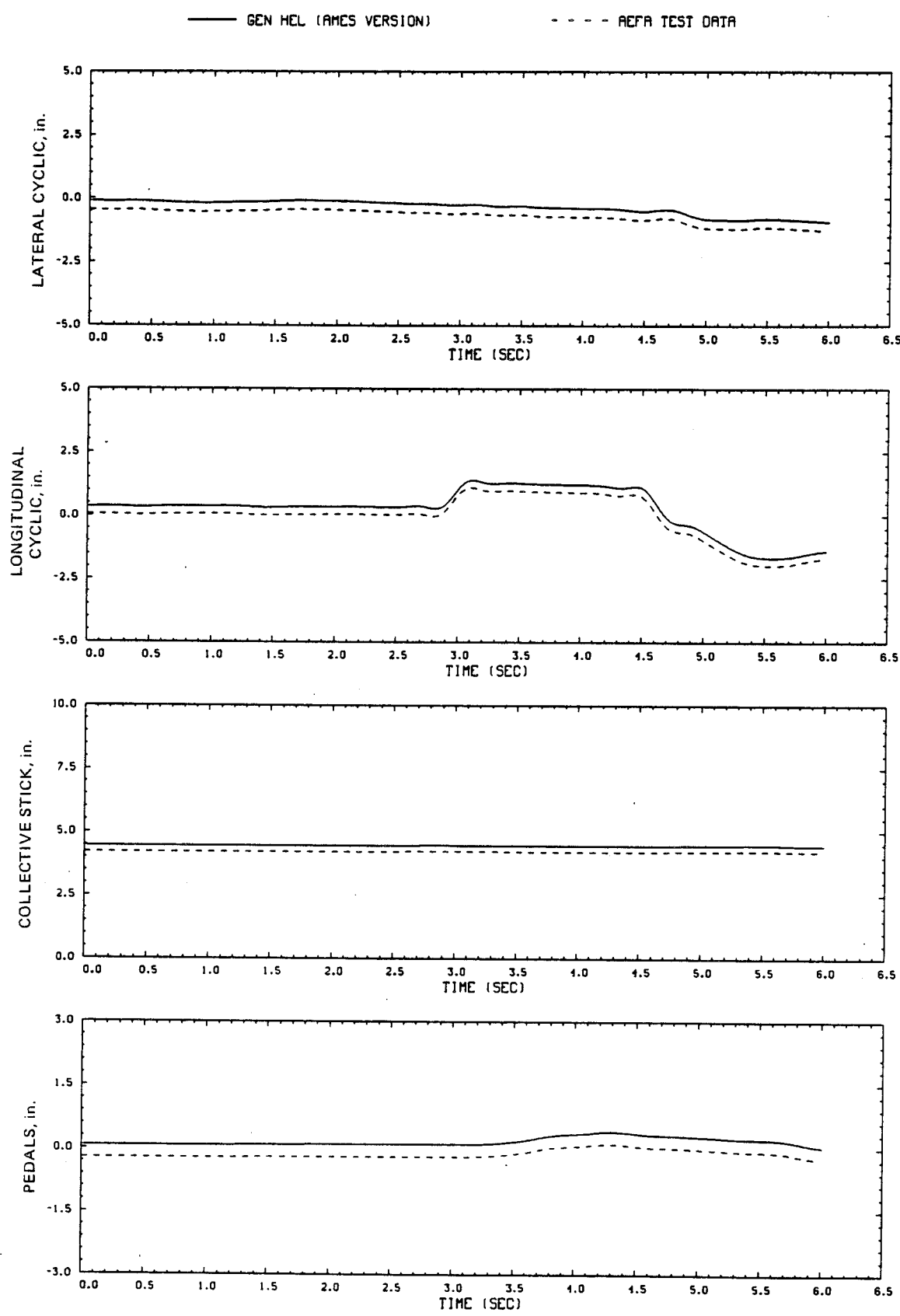


Figure D7.- Comparison of Ames real-time simulation and flight-test data.  
(File 509: 1-in. aft cyclic input, 60 knots)

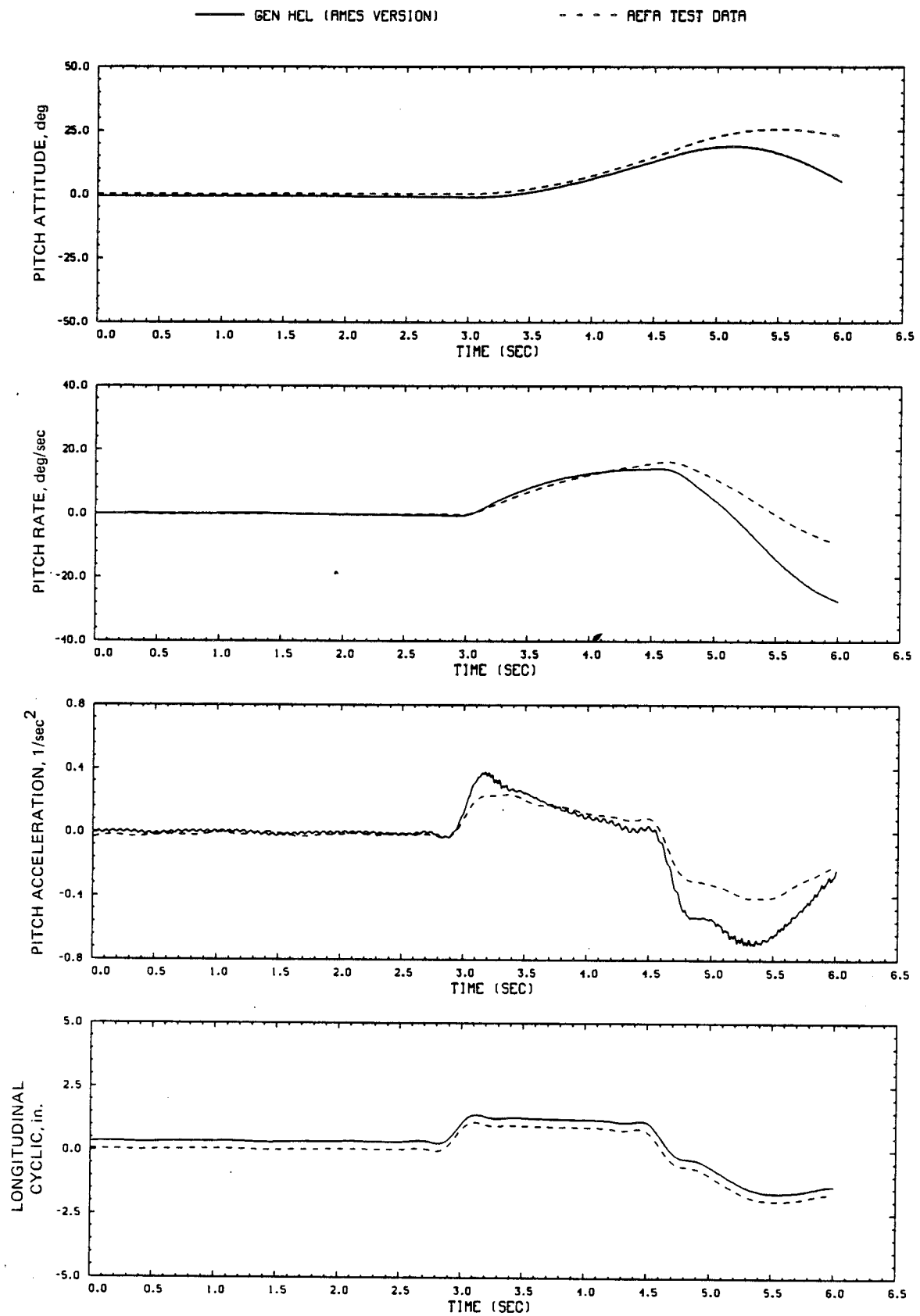


Figure D7.- Continued.

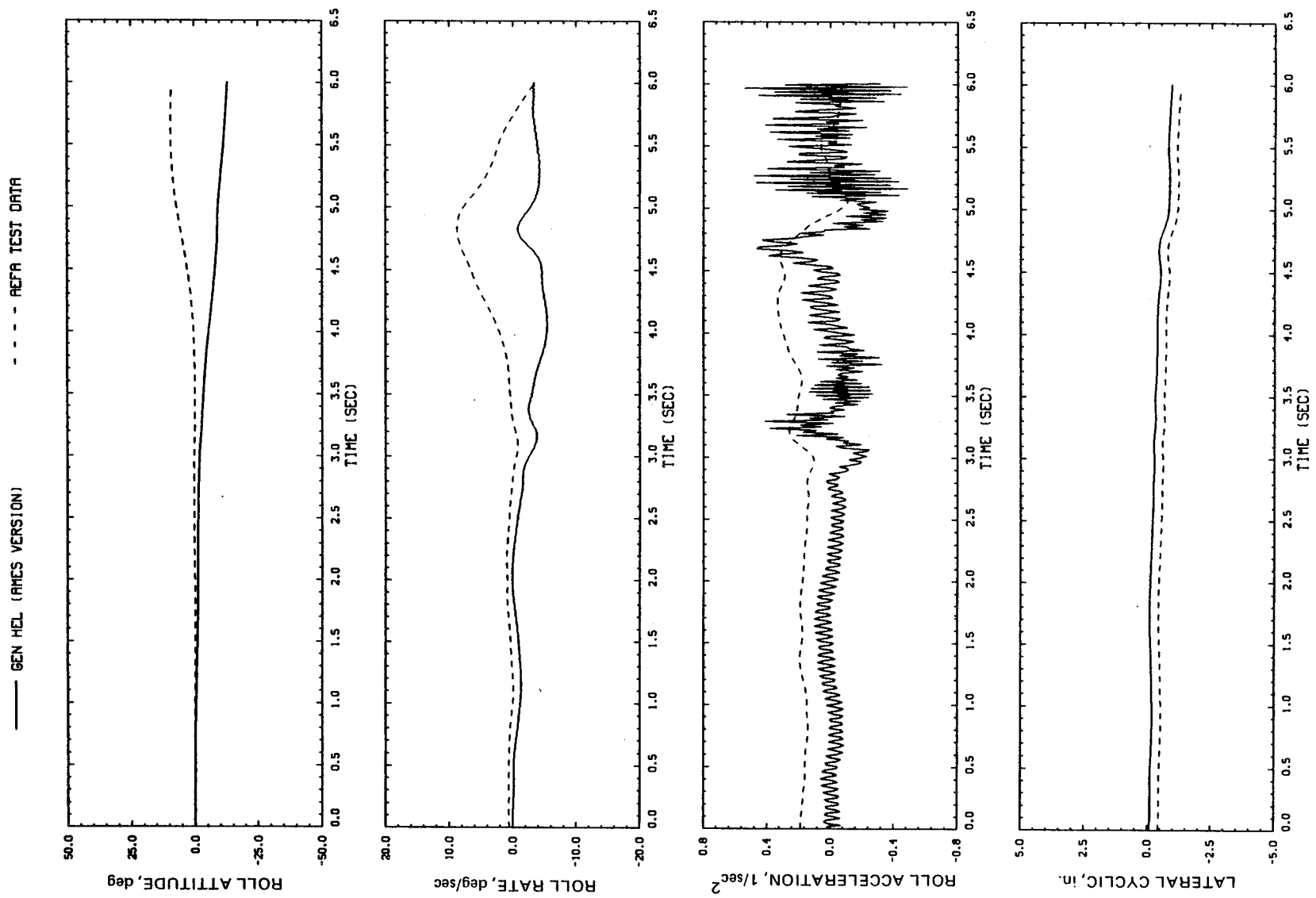


Figure D7. - Continued.

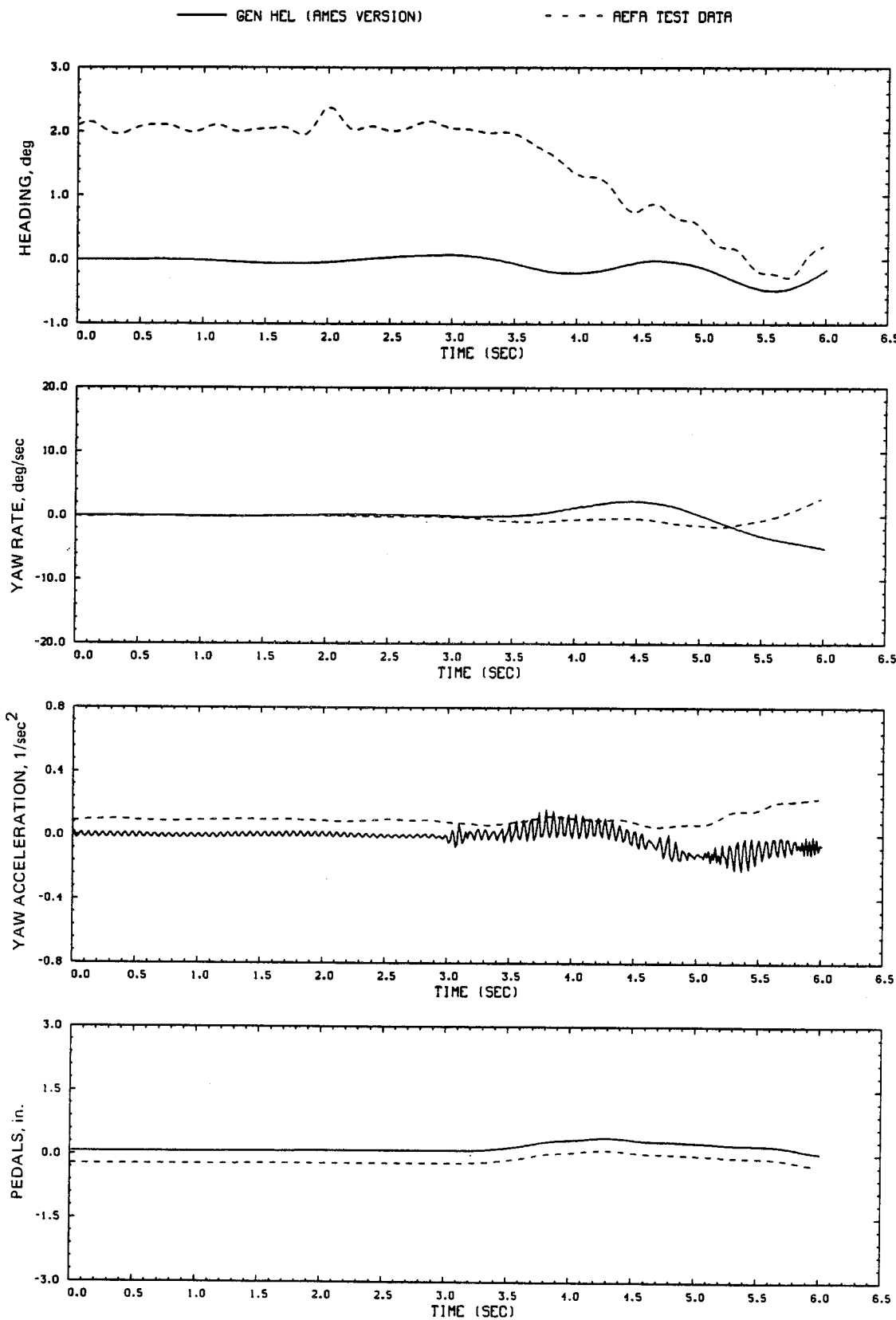


Figure D7.- Continued.

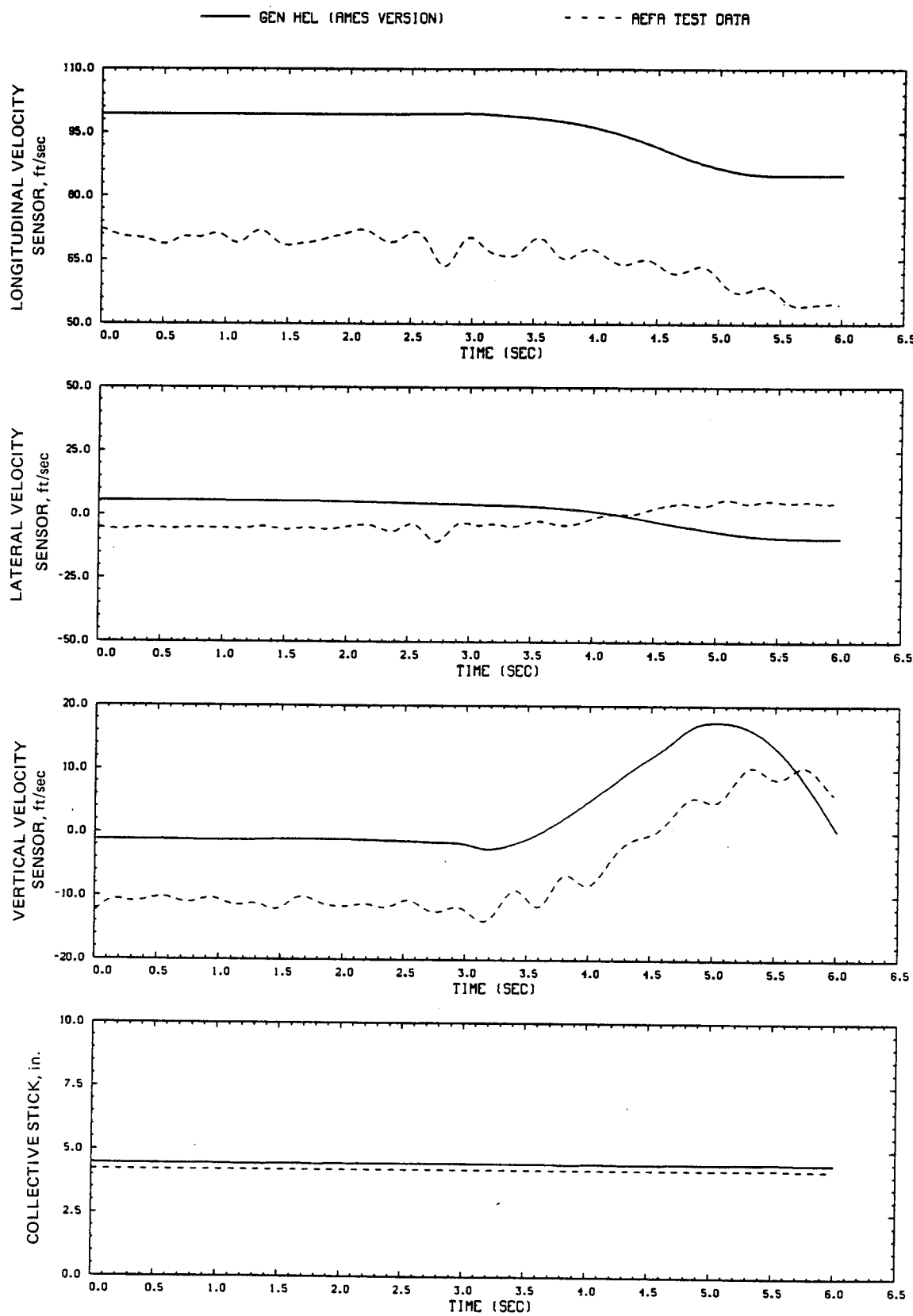


Figure D7.- Continued.

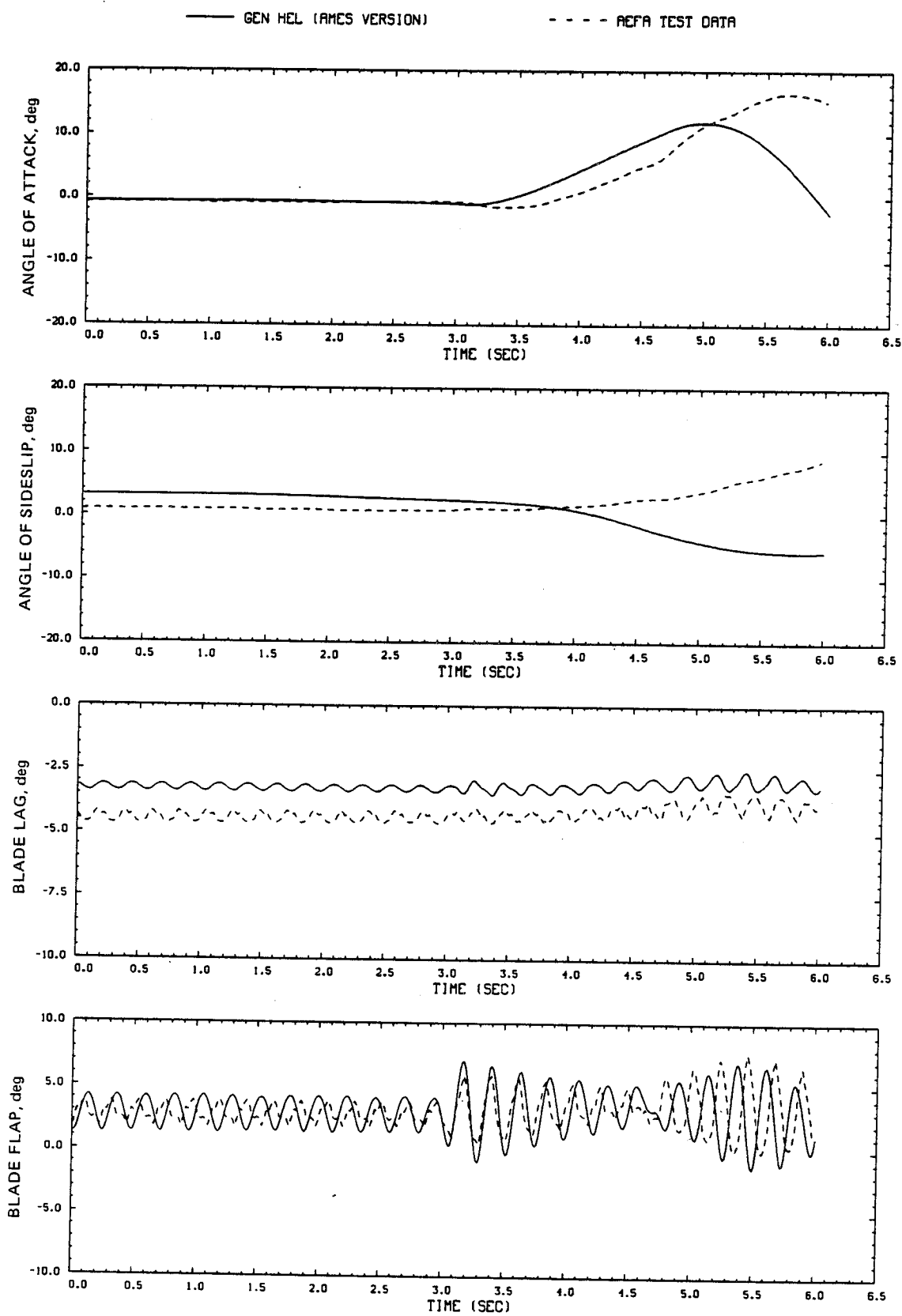


Figure D7.- Continued.

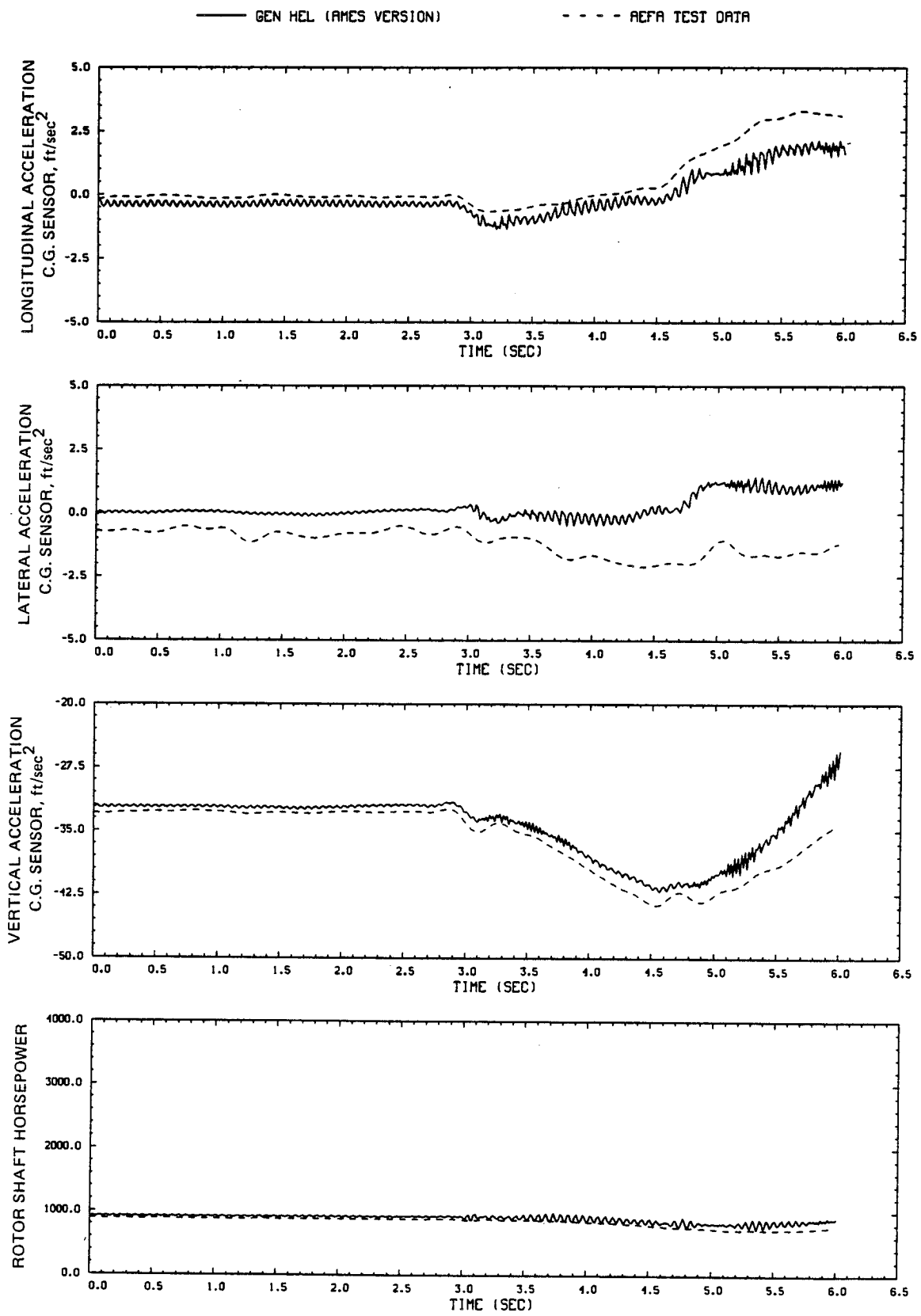


Figure D7.- Continued.

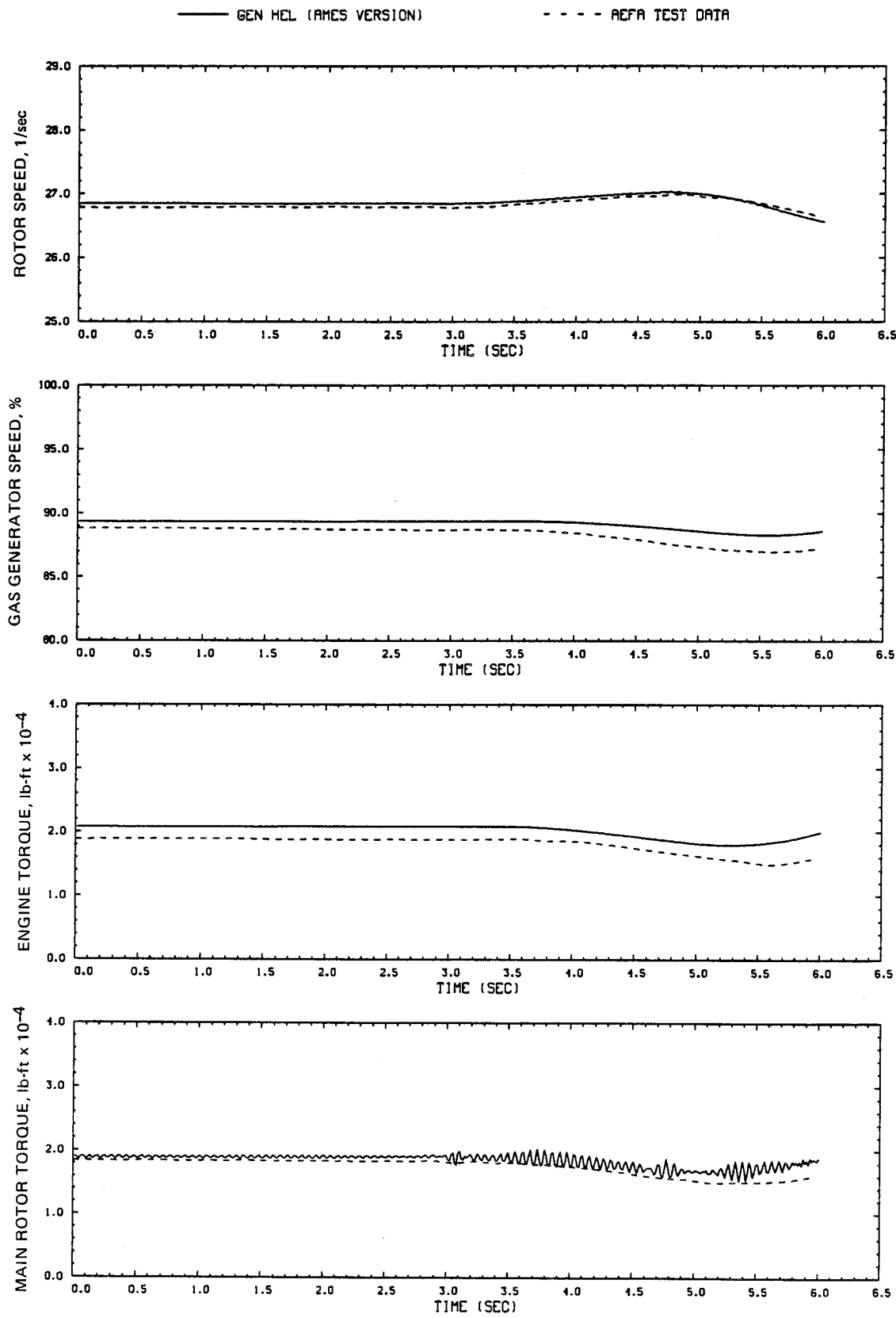


Figure D7.- Concluded.

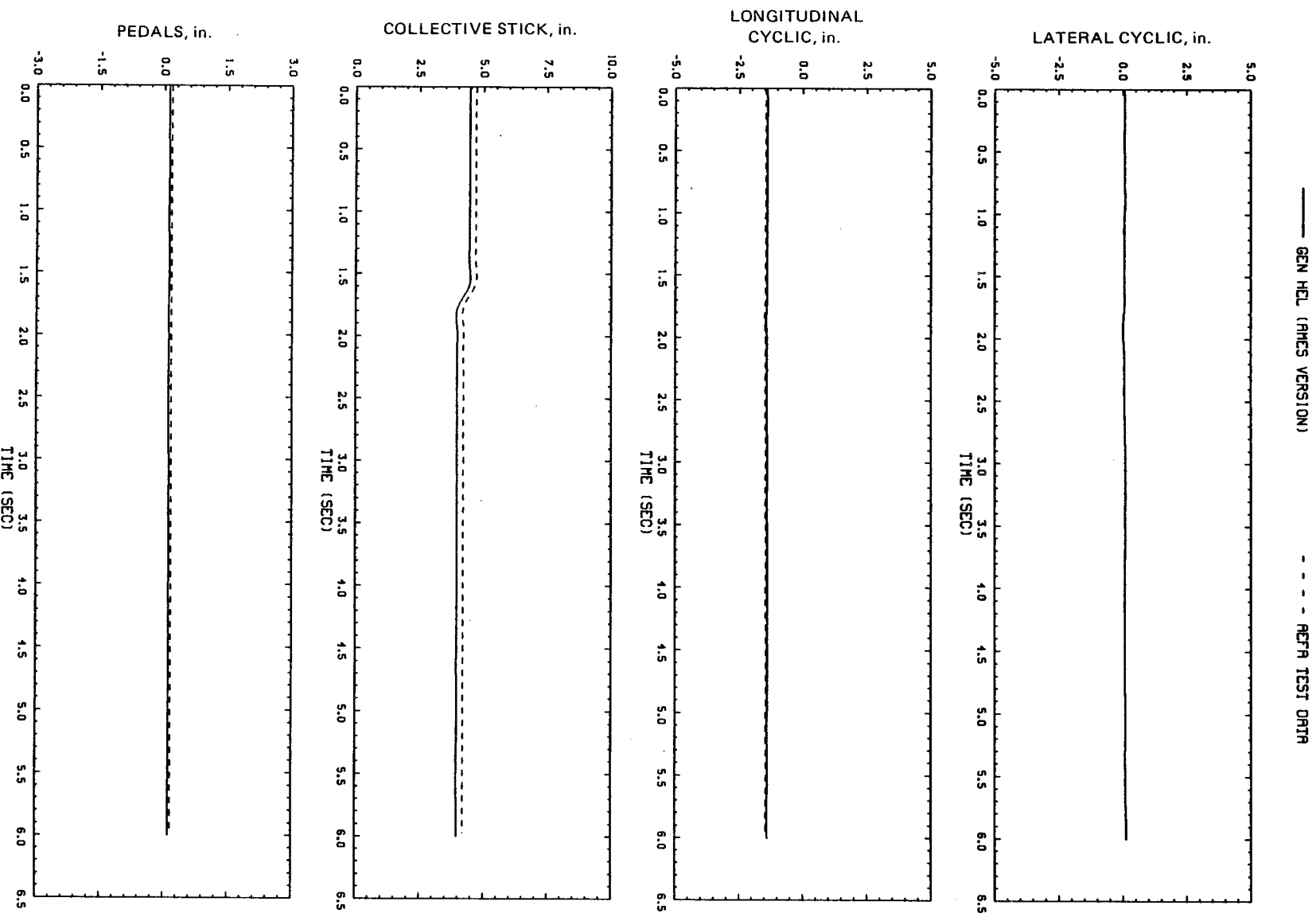


Figure D8.- Comparison of Ames real-time simulation and flight-test data.  
(File 405: 0.5-in. dow collective input, 60 knots, stabilator off nominal)

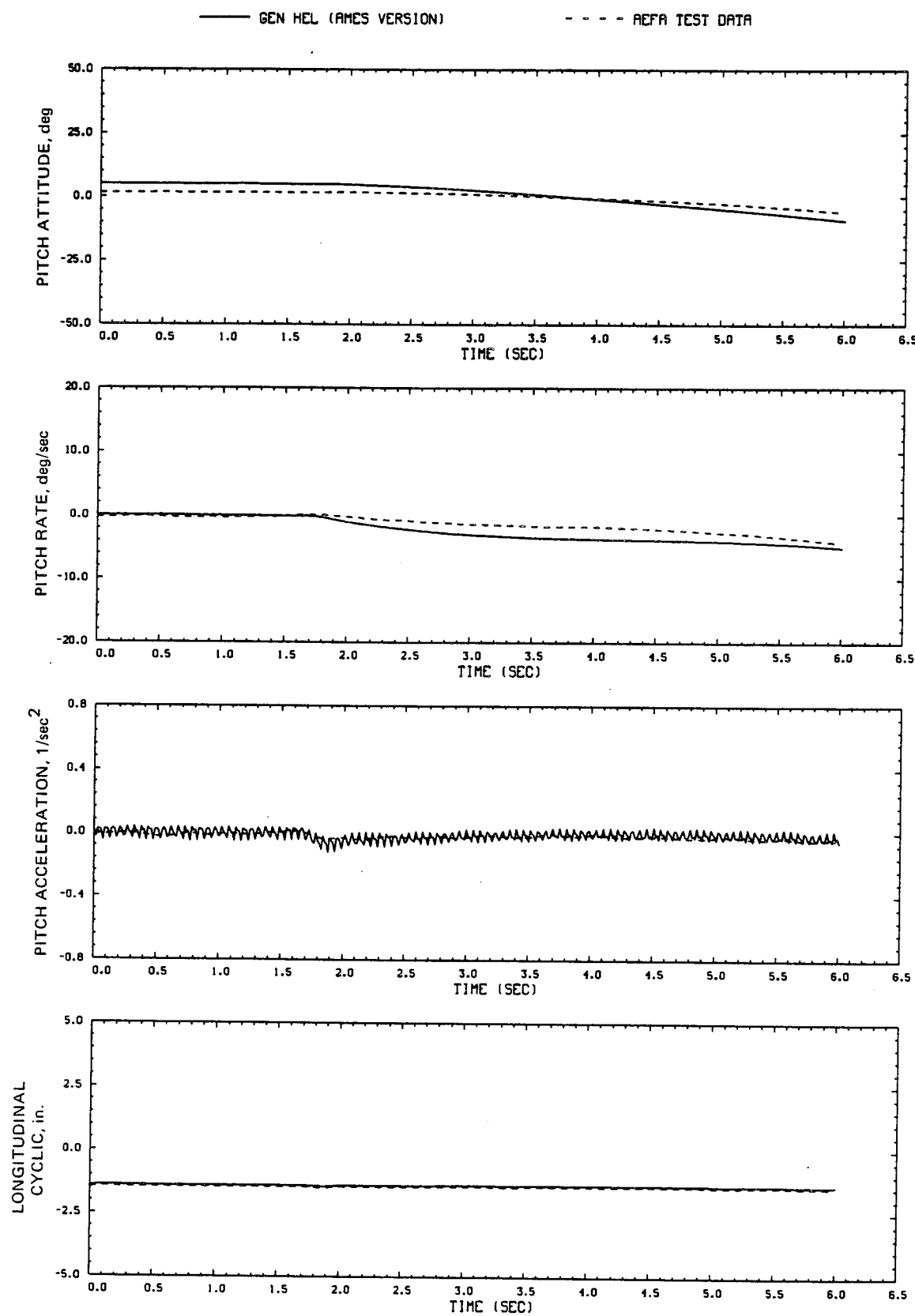


Figure D8.- Continued.

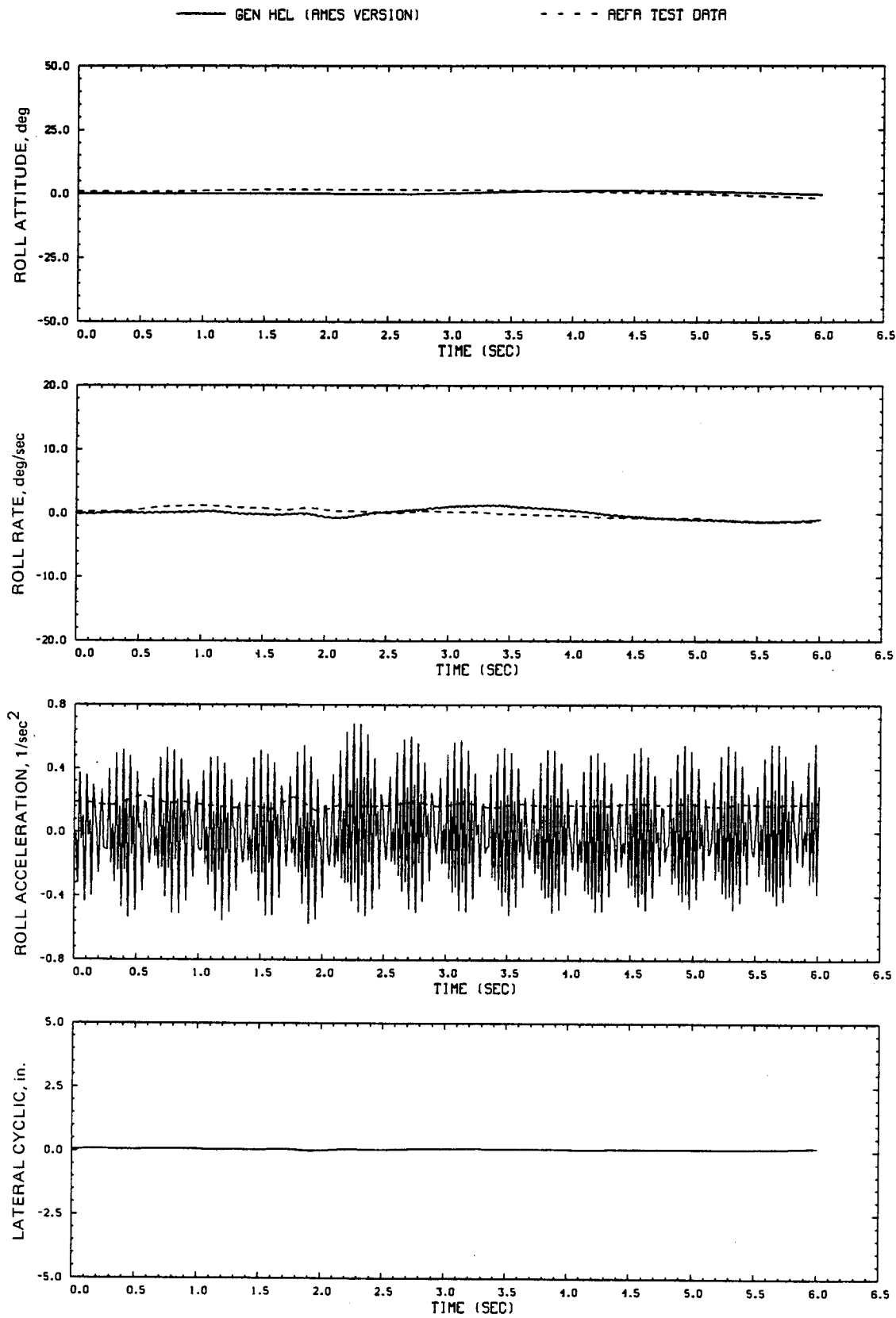


Figure D8.- Continued.

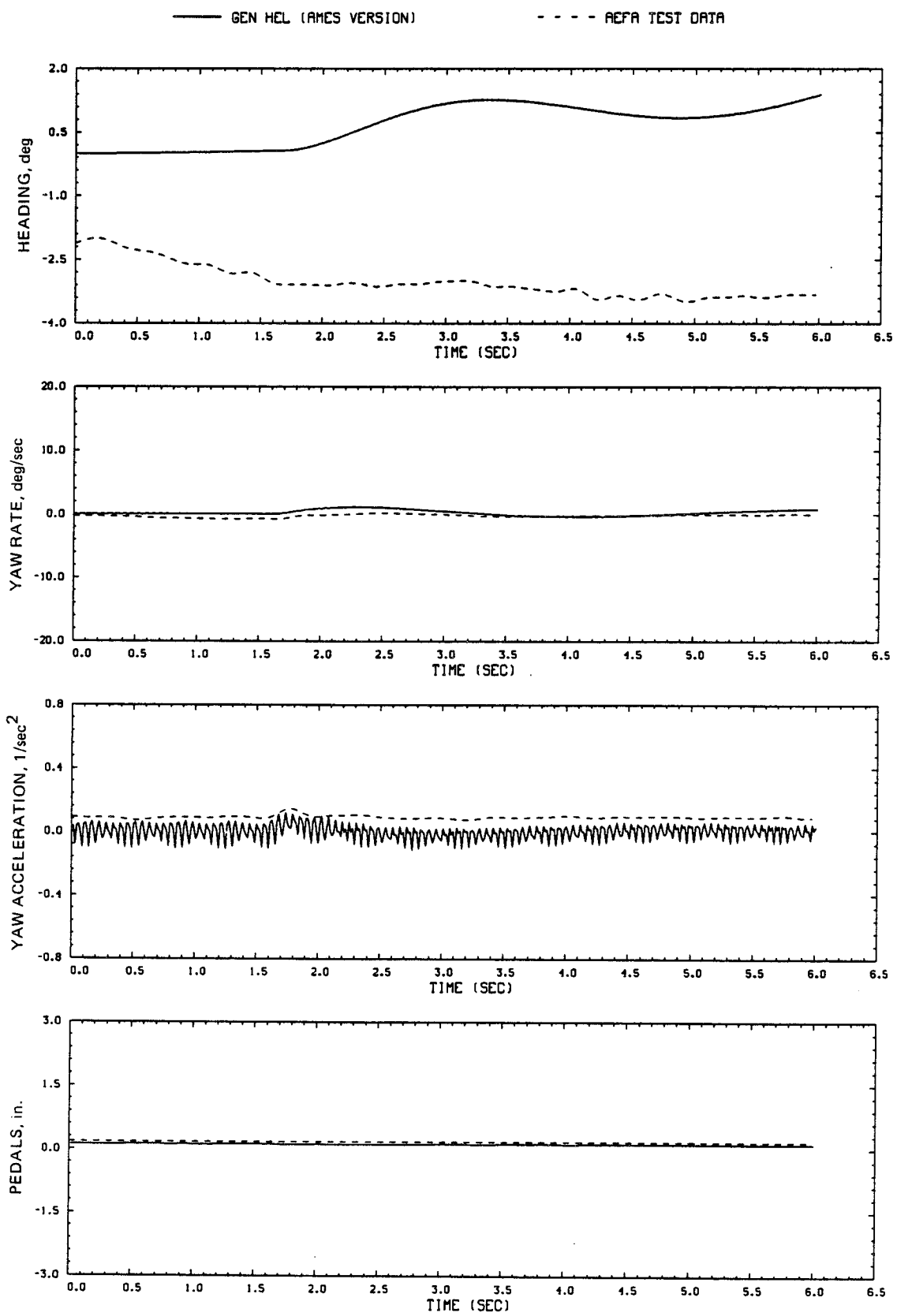


Figure D8.- Continued.

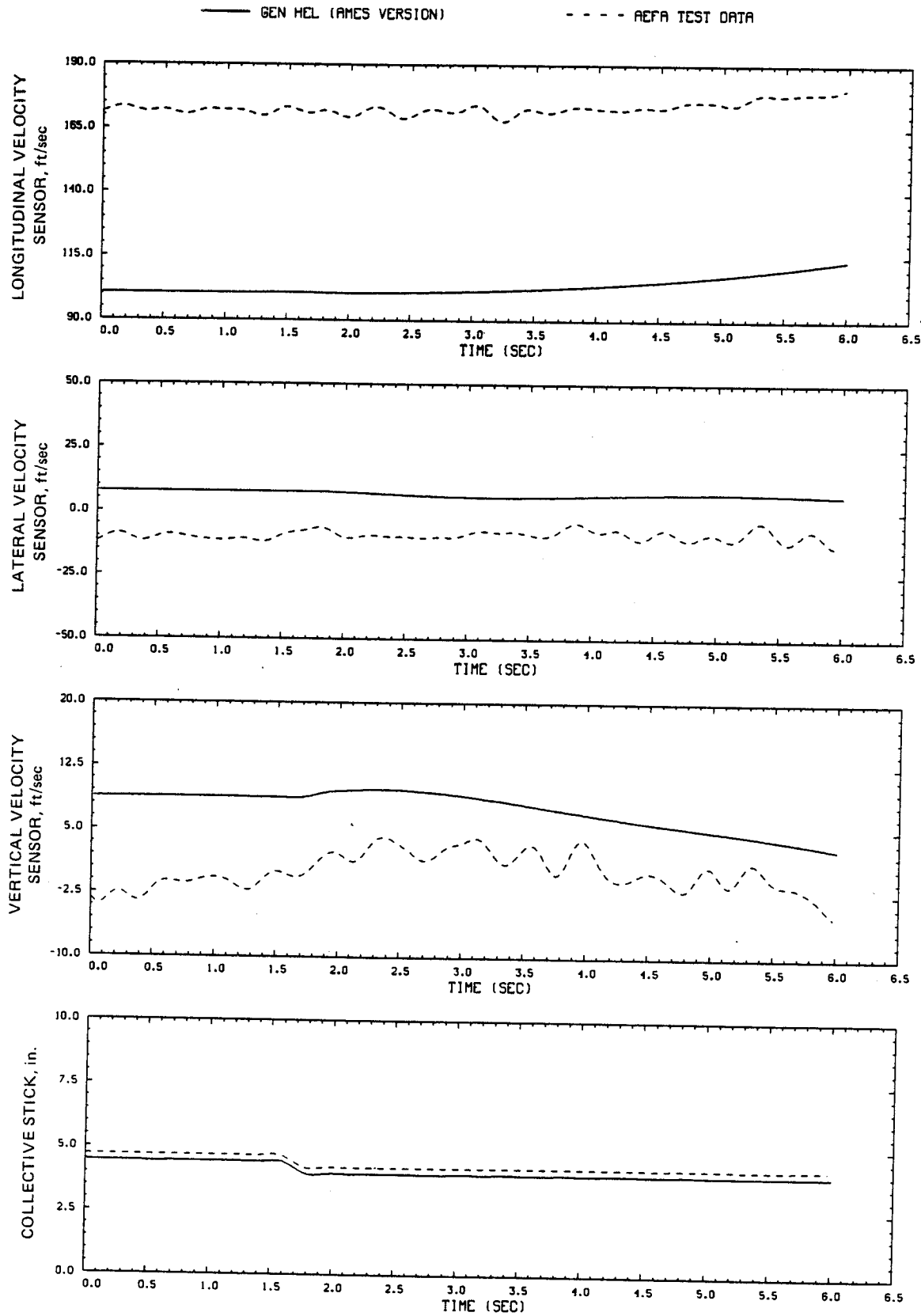


Figure D8.- Continued.

— GEN HEL (AMES VERSION)

- - - - - REFA TEST DATA

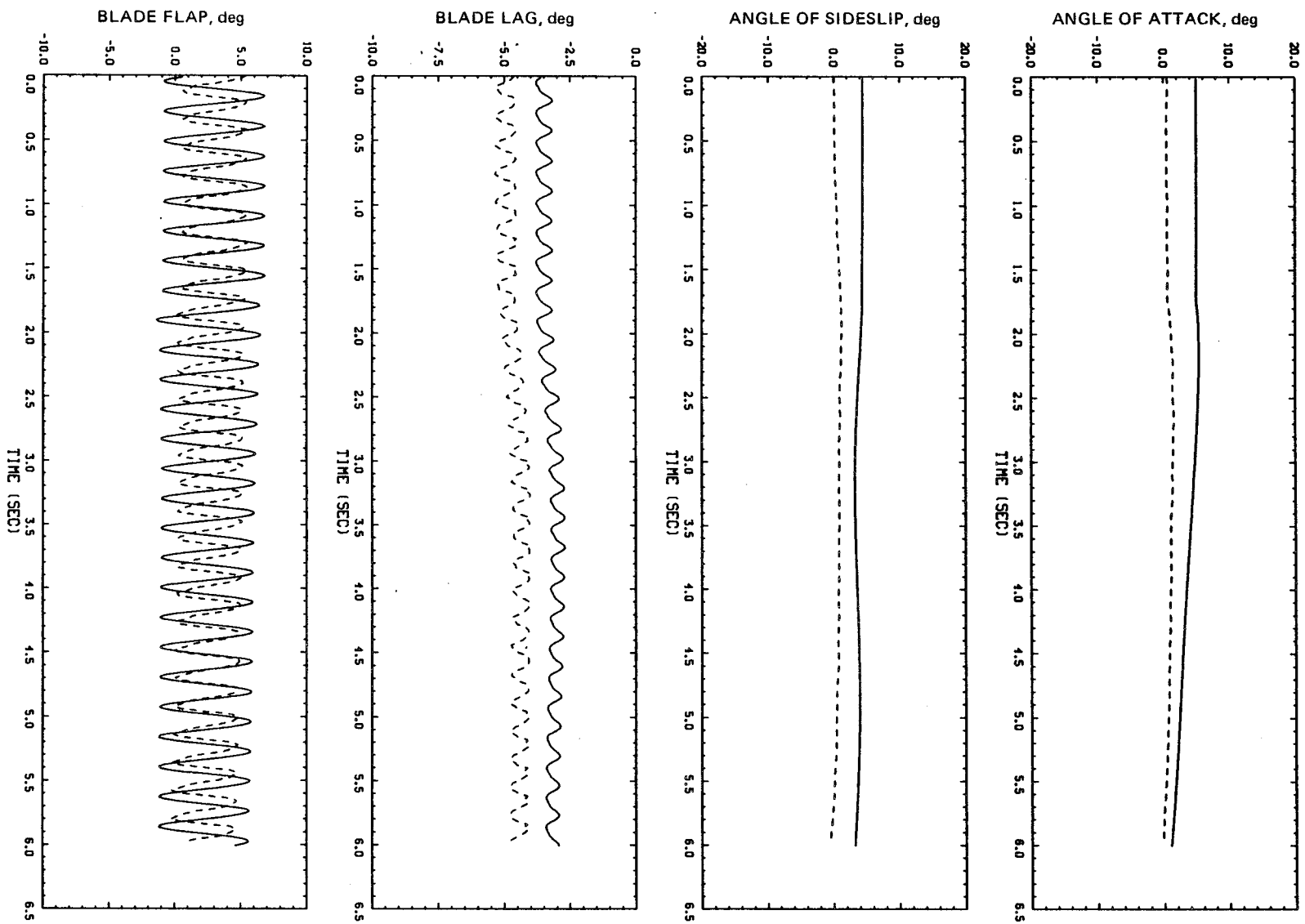


Figure D8.- Continued.

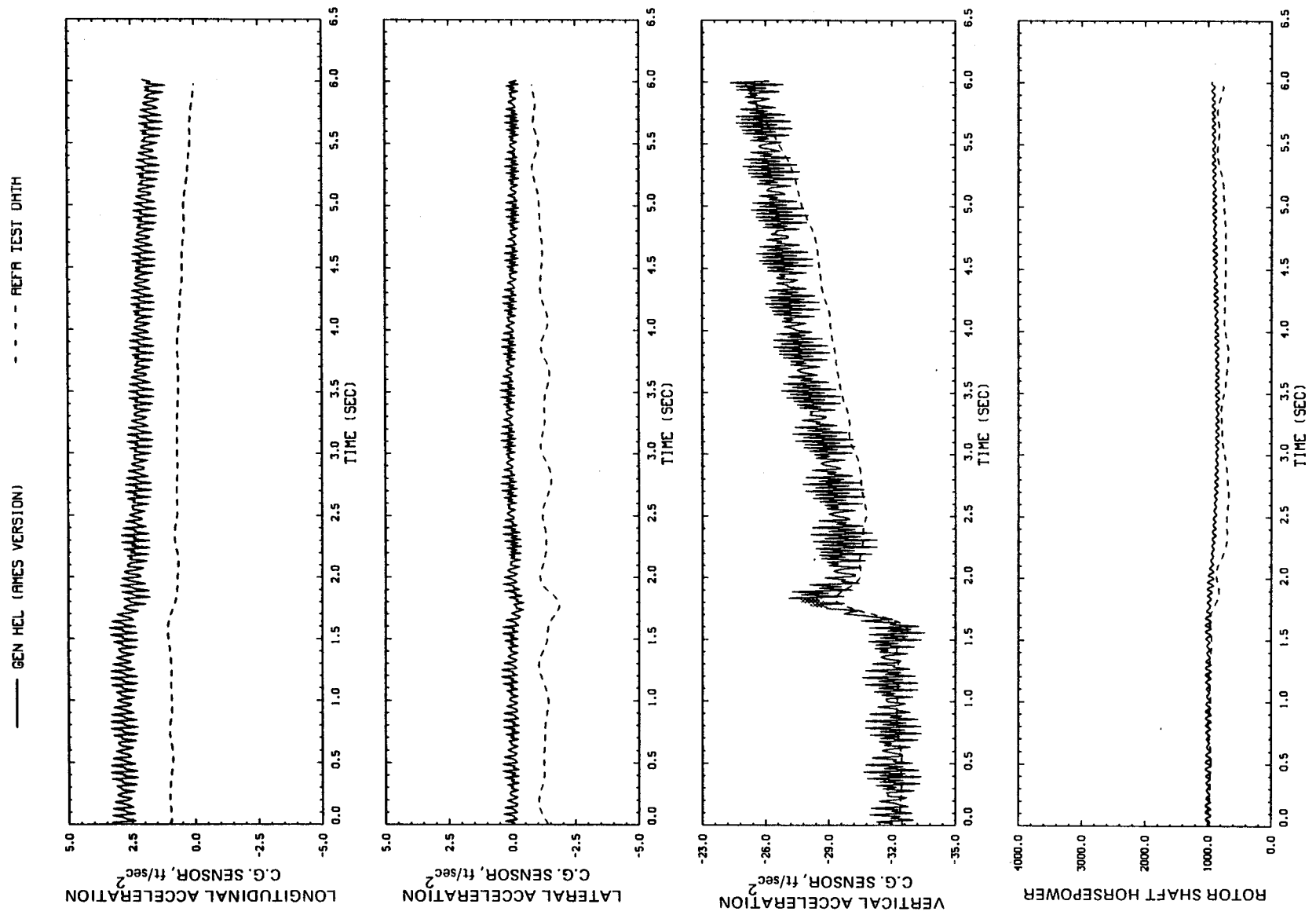


Figure D8.- Continued.

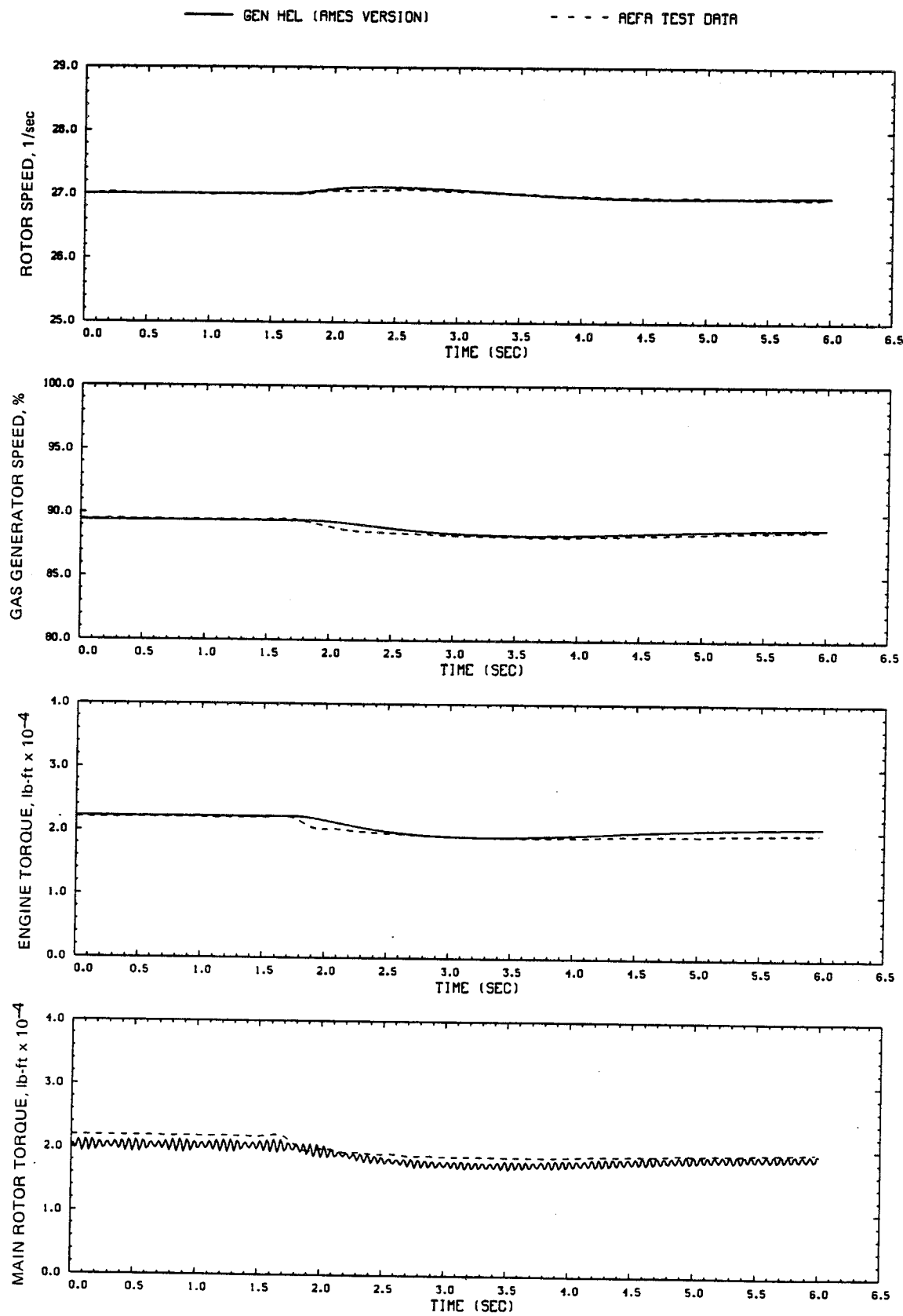


Figure D8.- Concluded.

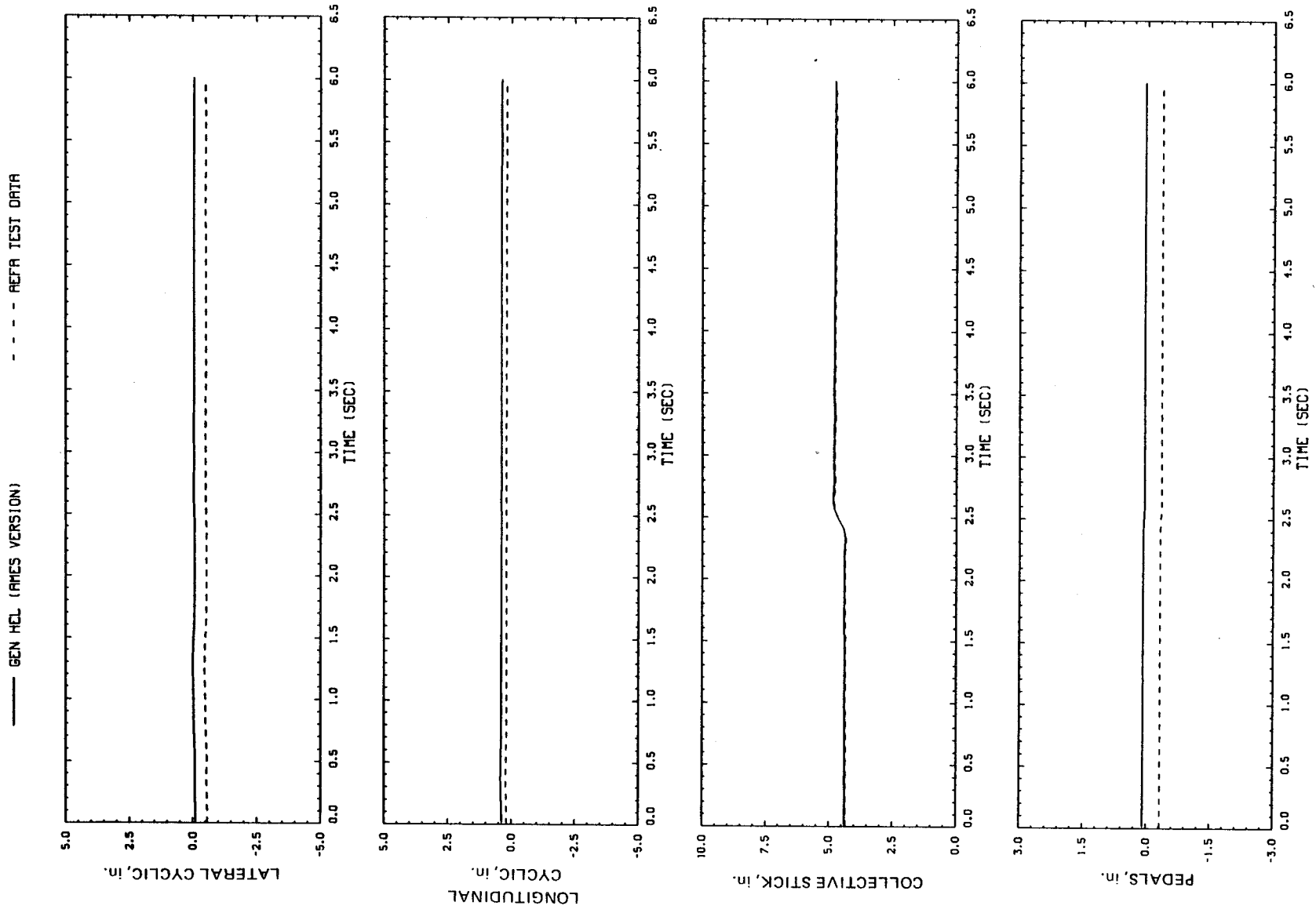


Figure D9.- Comparison of Ames real-time simulation and flight-test data.  
 (File 510: 0.5-in. up collective input, 60 knots)

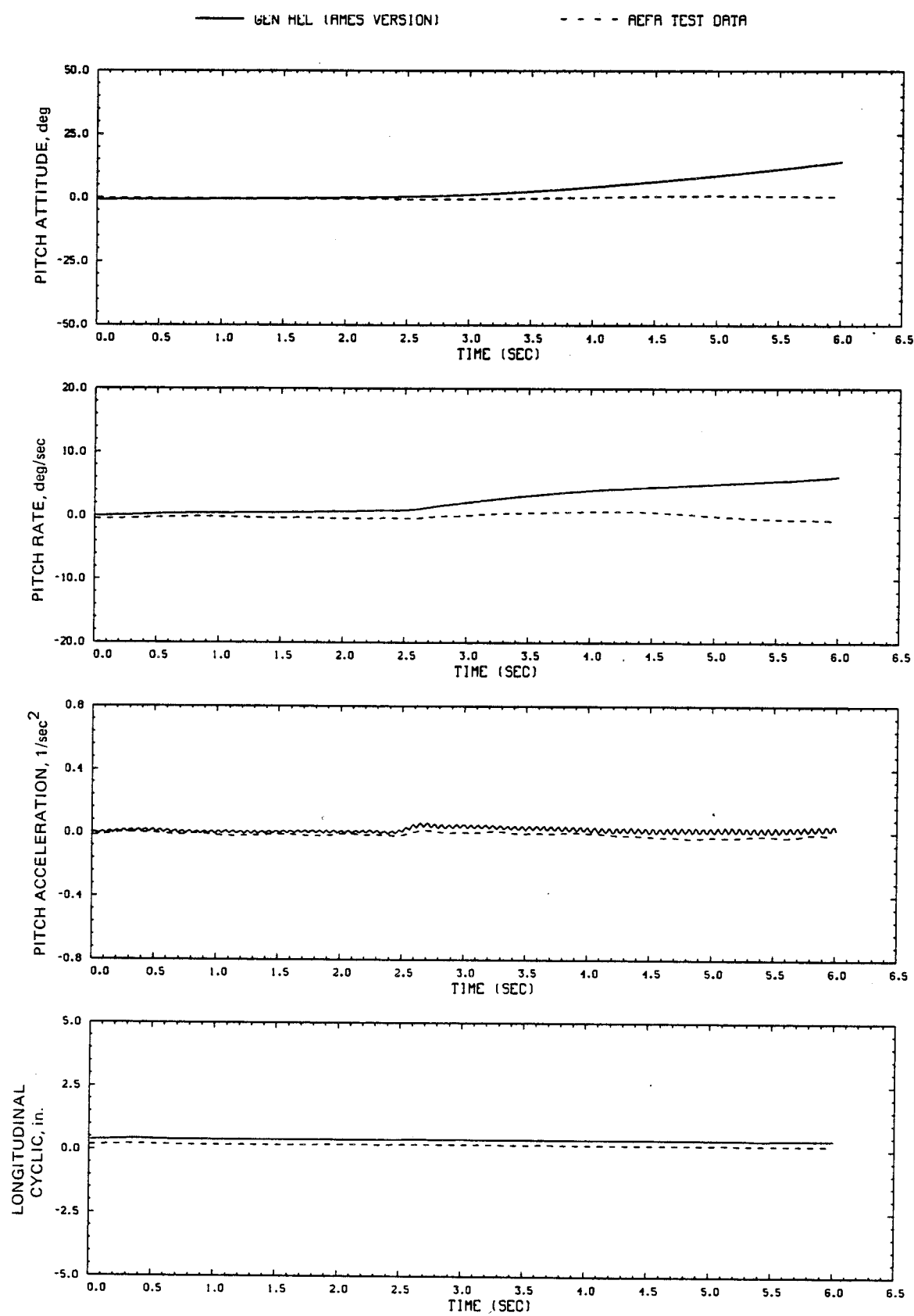


Figure D9.- Continued.

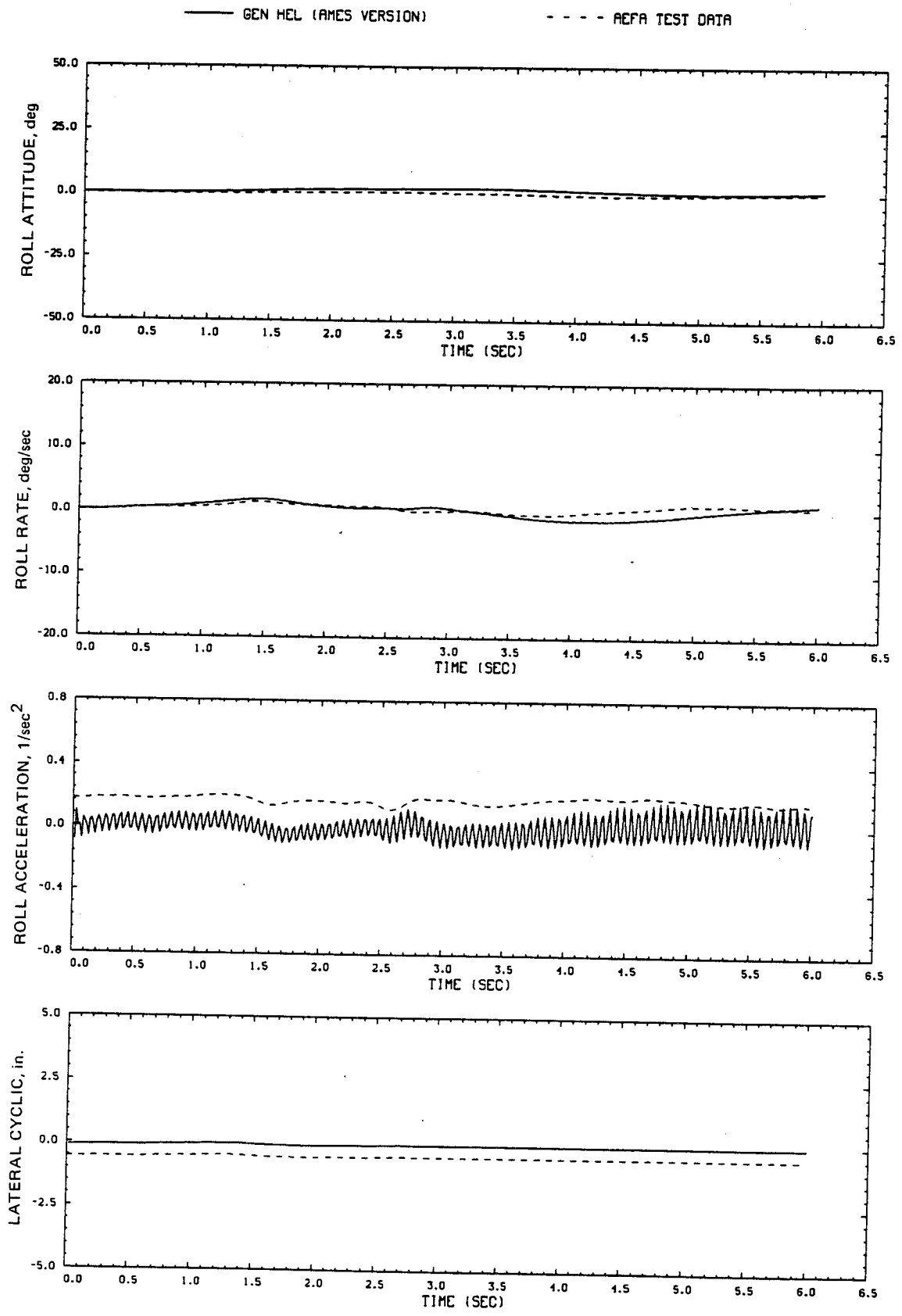


Figure D9.- Continued.

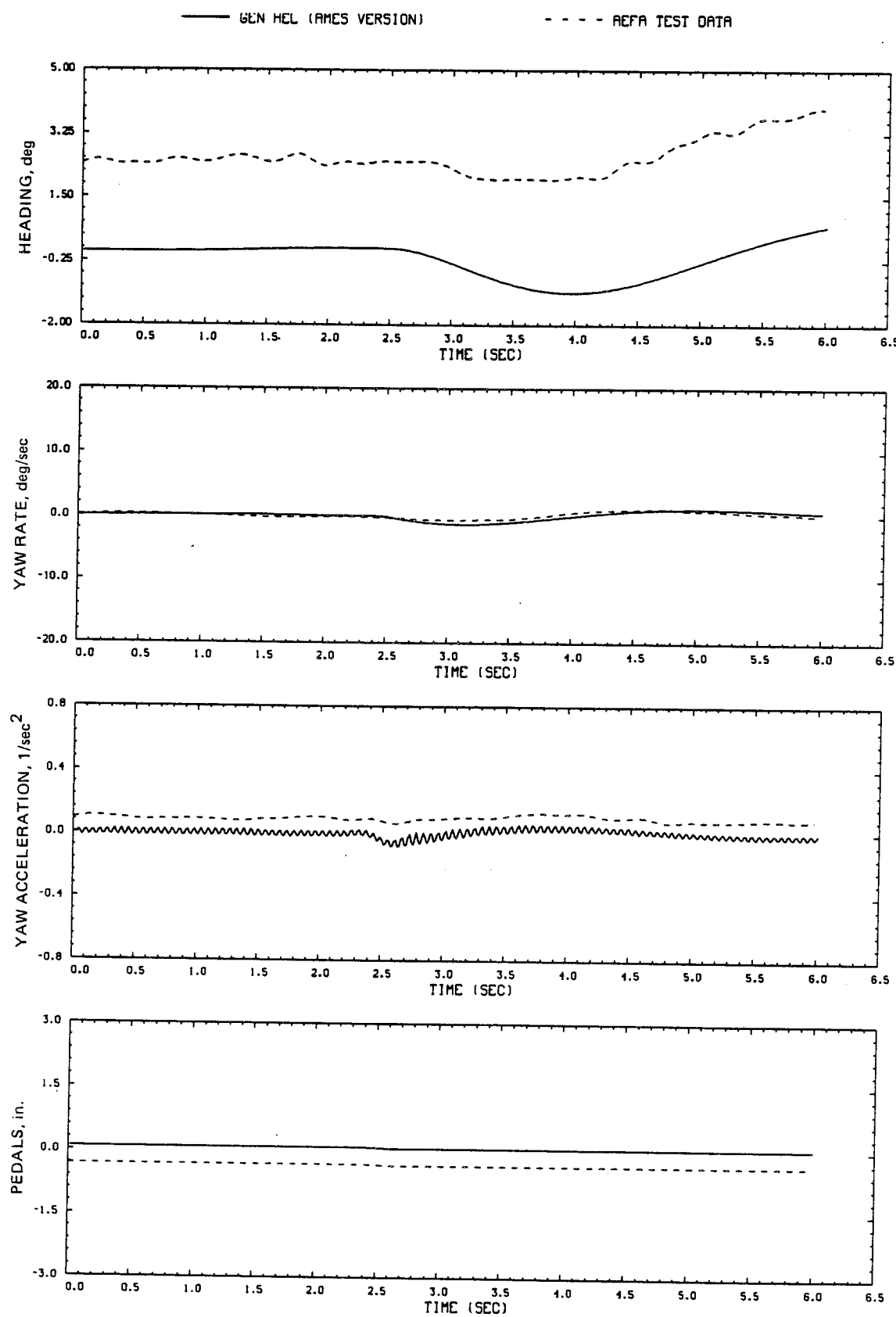
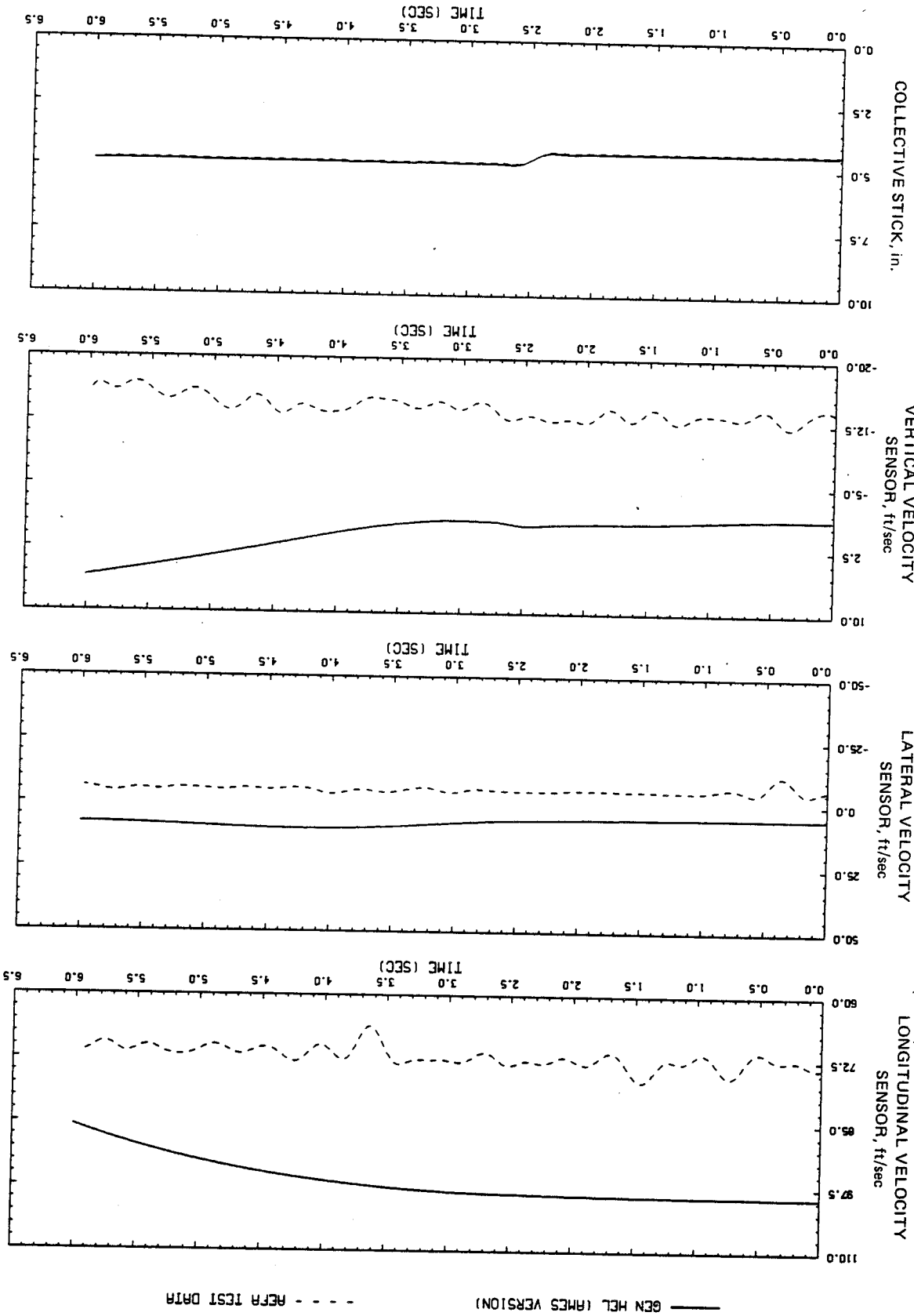


Figure D9.- Continued.

Figure D9.- Continued.



— GEN HEL (ARMES VERSION)      - - - ACFR TEST DATA

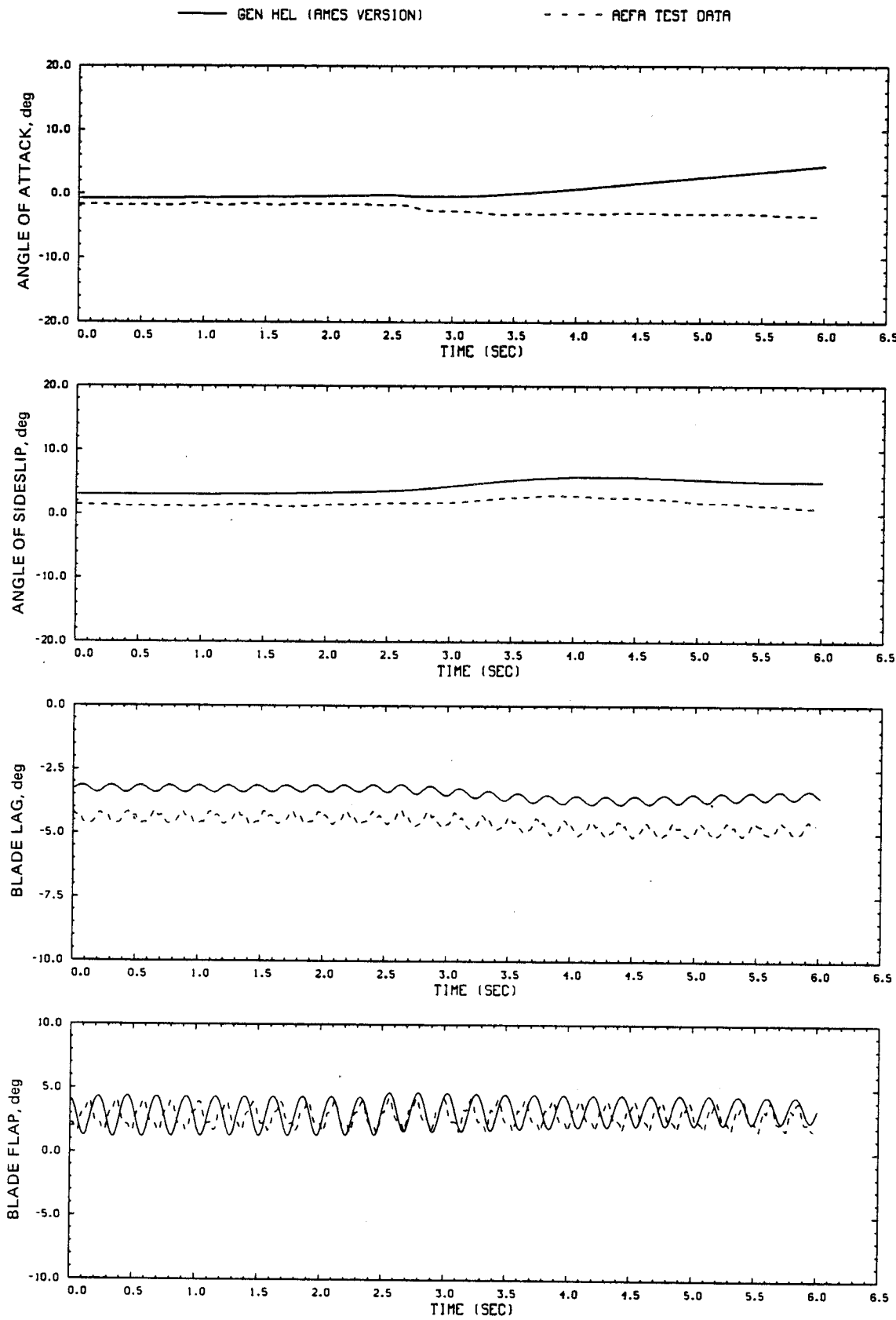


Figure D9.- Continued.

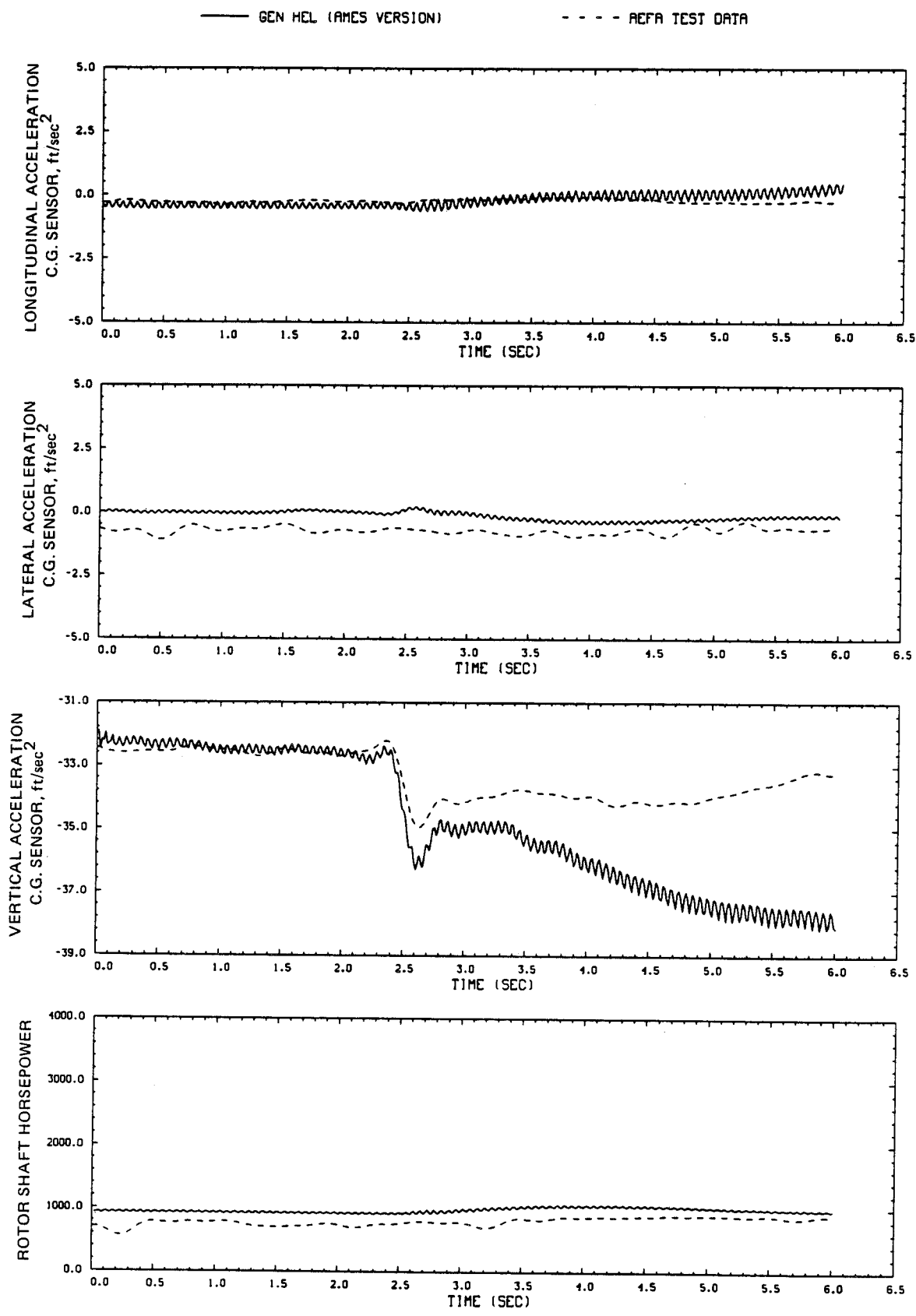


Figure D9.- Continued.

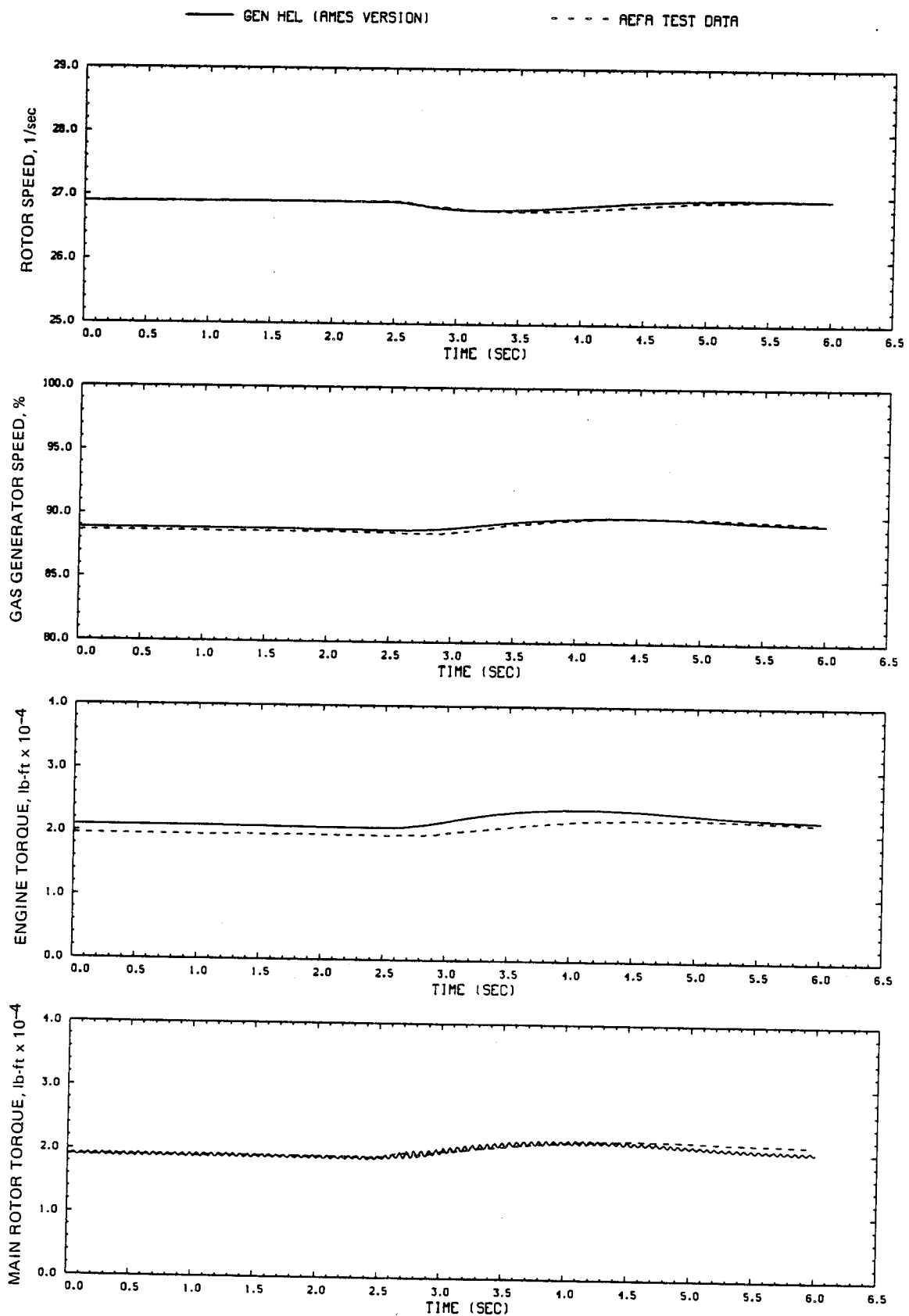


Figure D9.- Concluded.

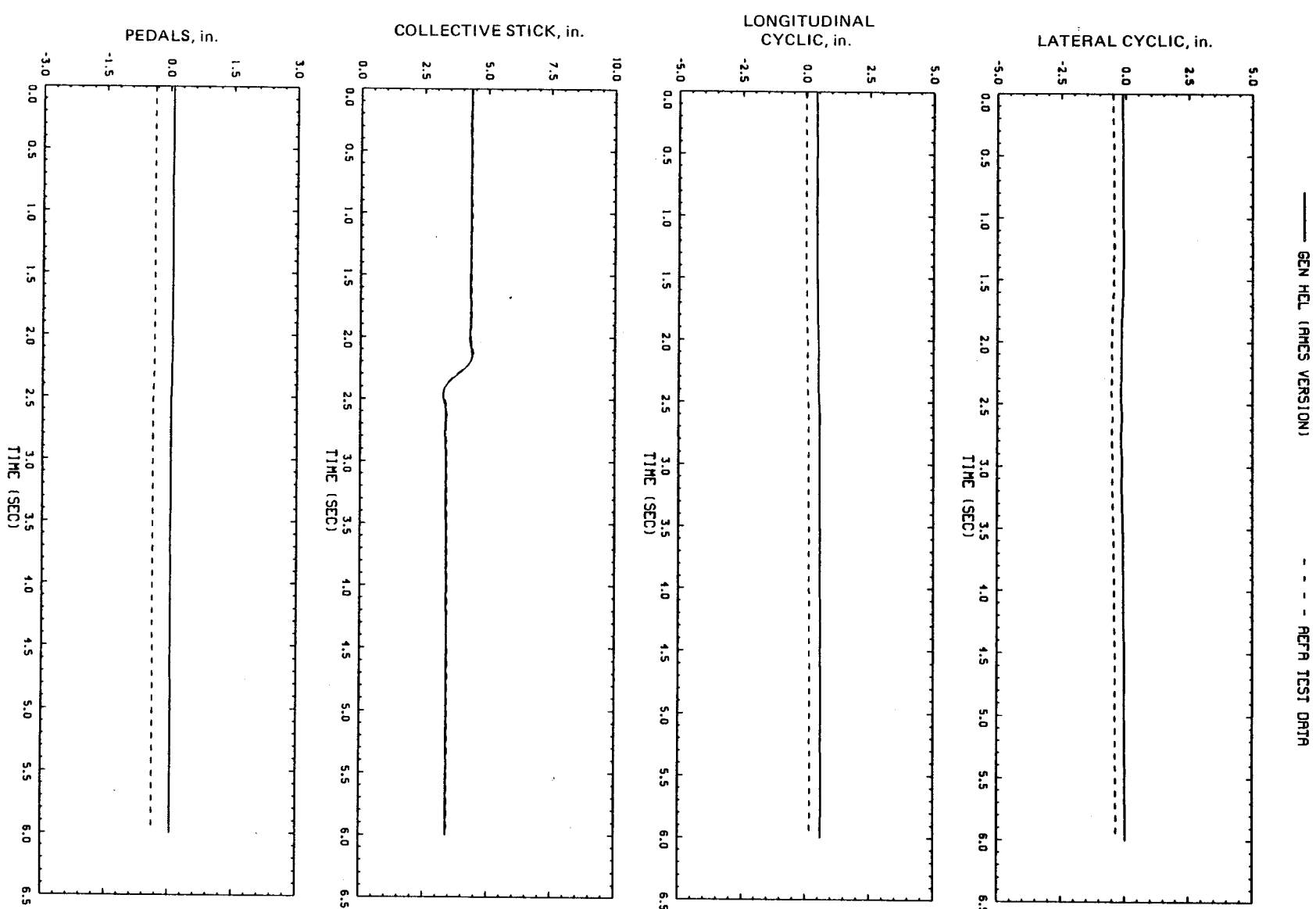


Figure D10.- Comparison of Ames real-time simulation and flight-test data.  
(File 512: 1-in. down collective input, 60 knots)

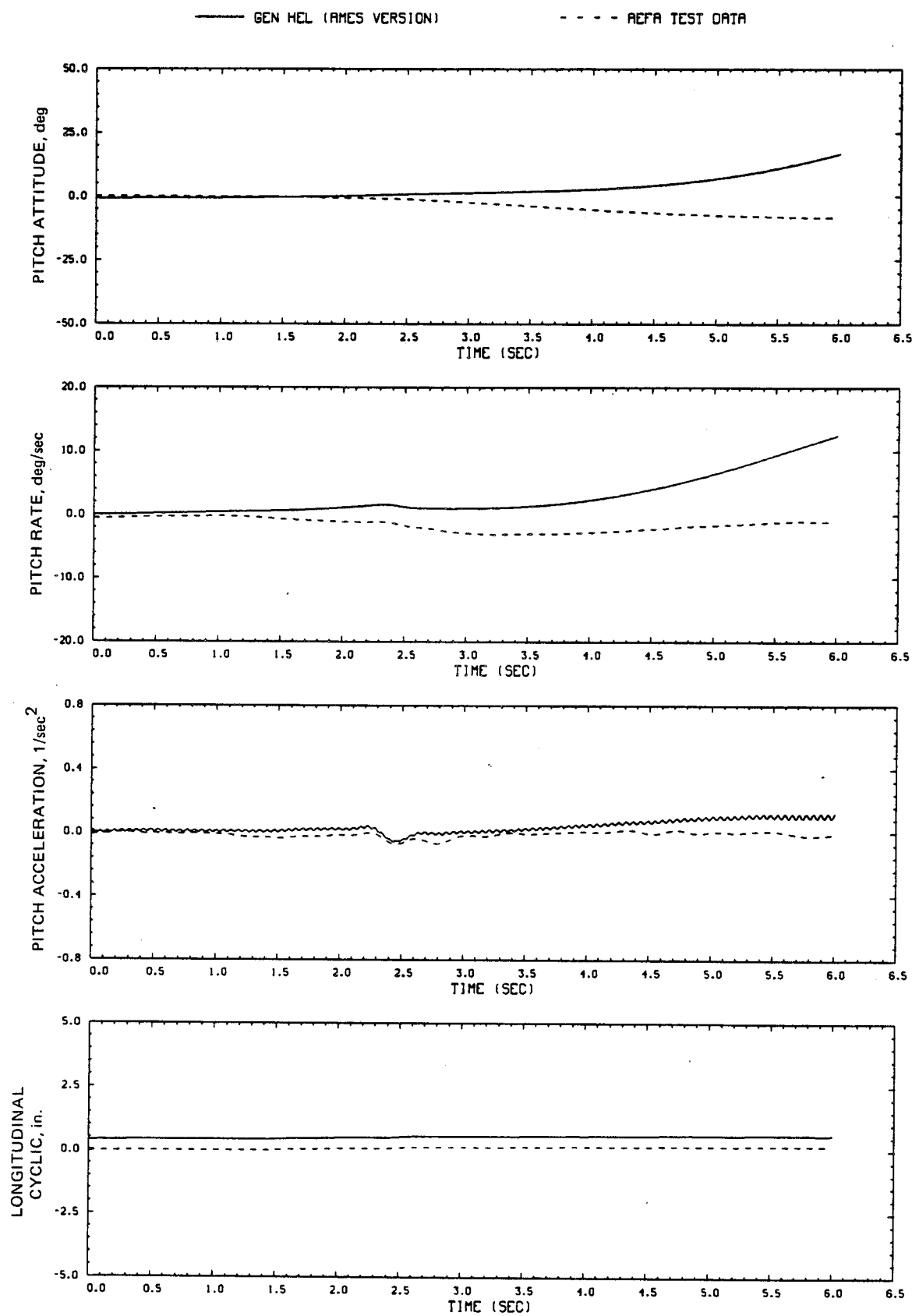


Figure D10.- Continued.

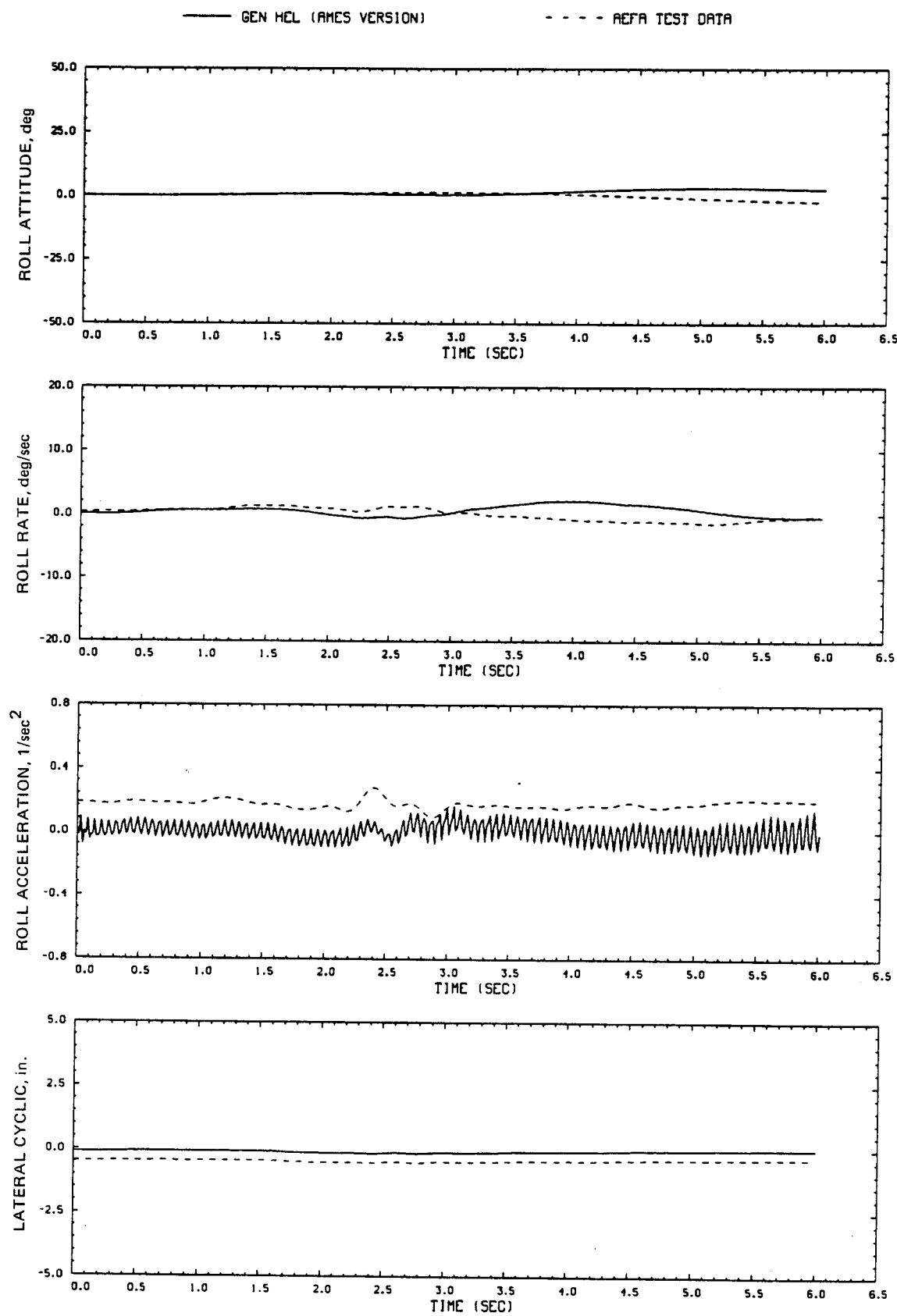
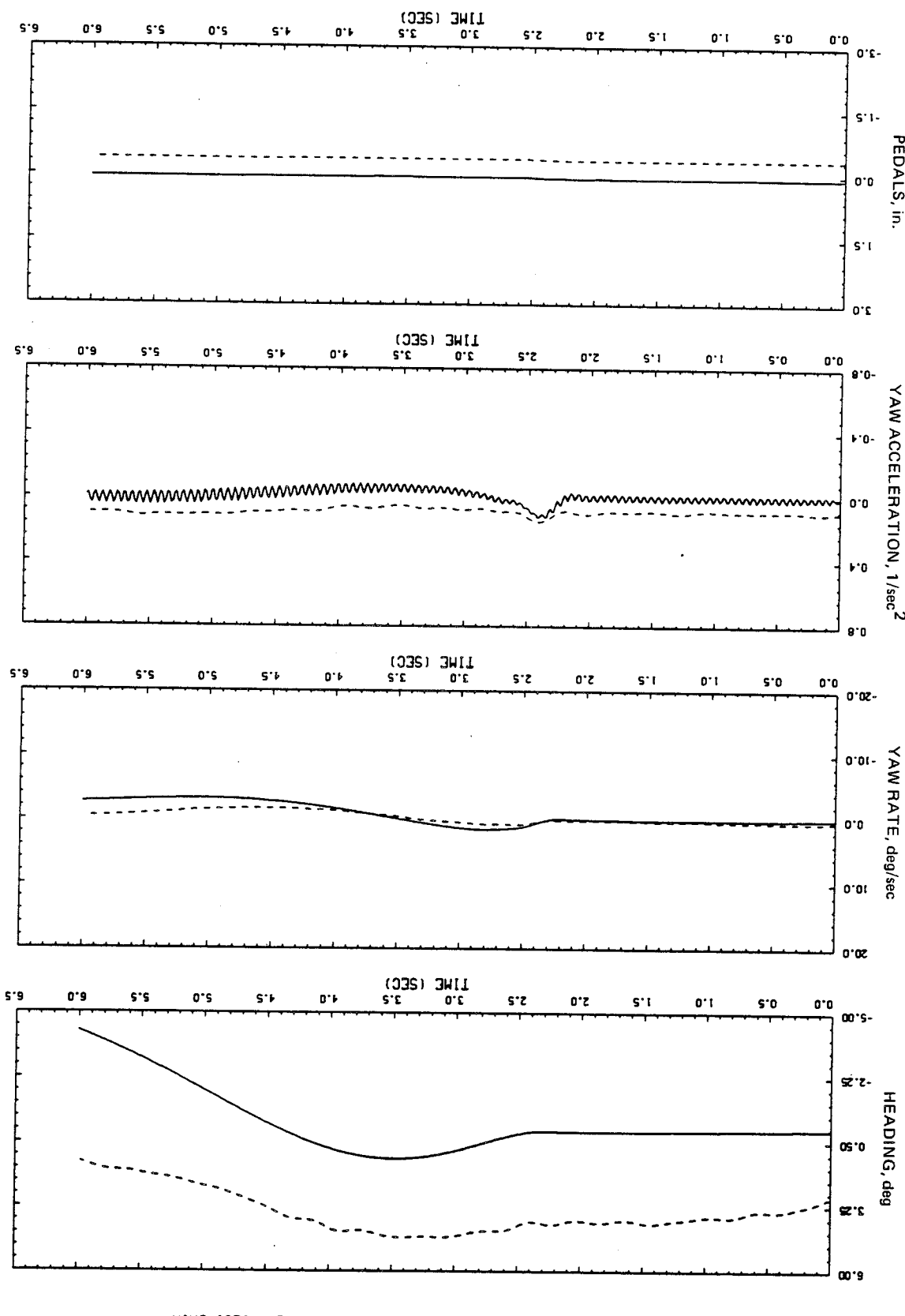


Figure D10.- Continued.

FIGURE D10.- Continued.



— GEN HEL (AMES VERSION)    - - - REFR TEST DATA

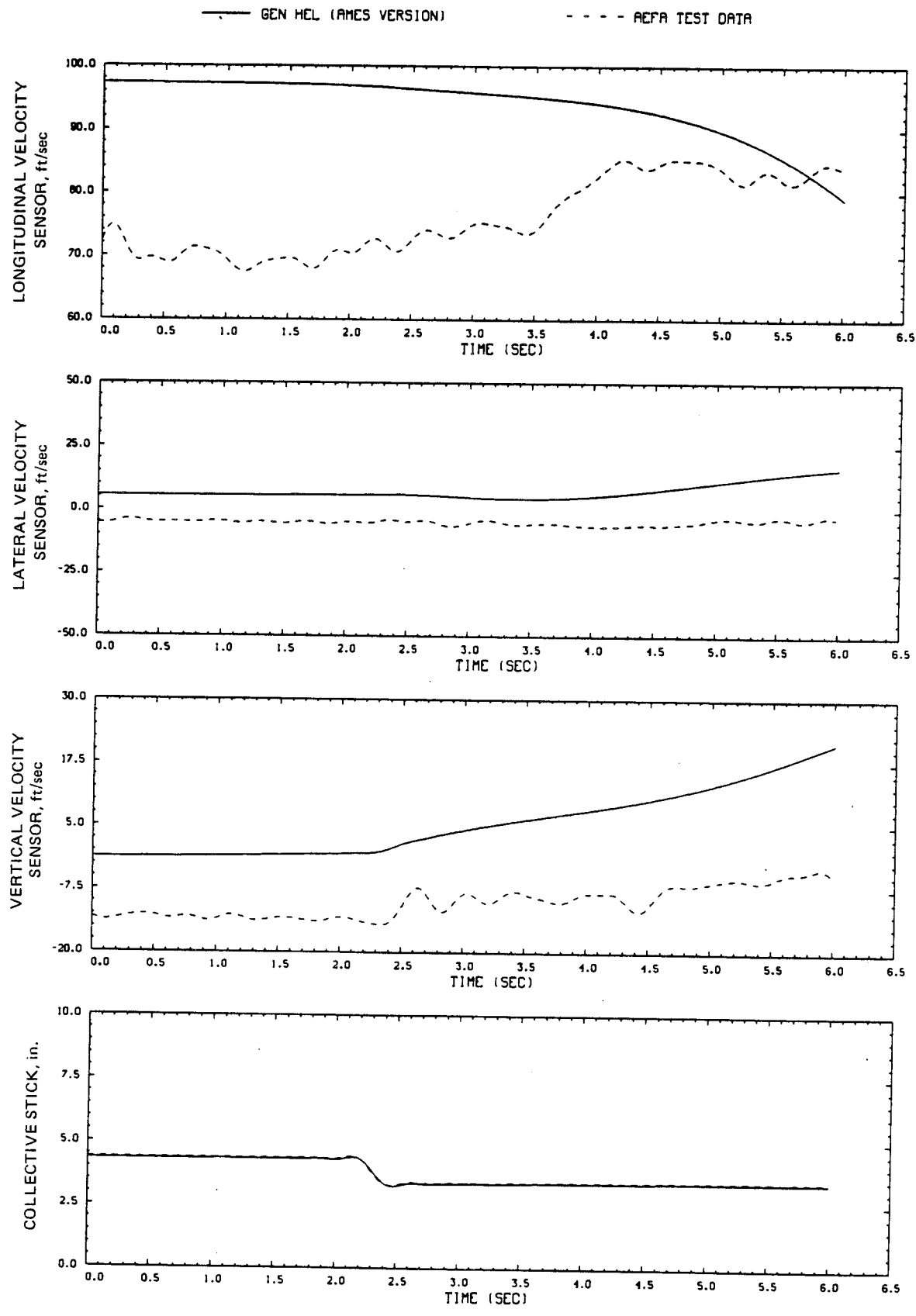


Figure D10.- Continued.

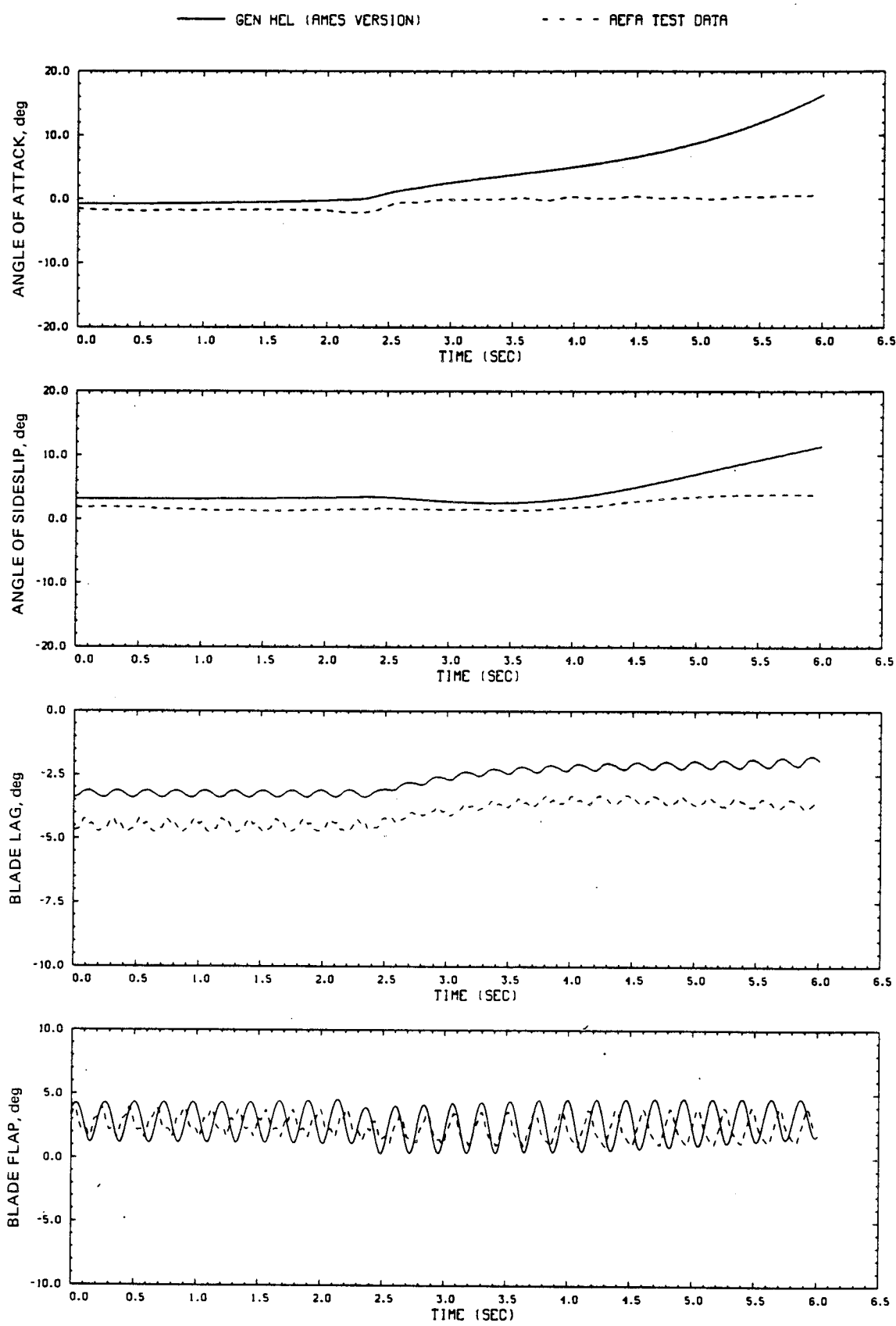


Figure D10.- Continued.

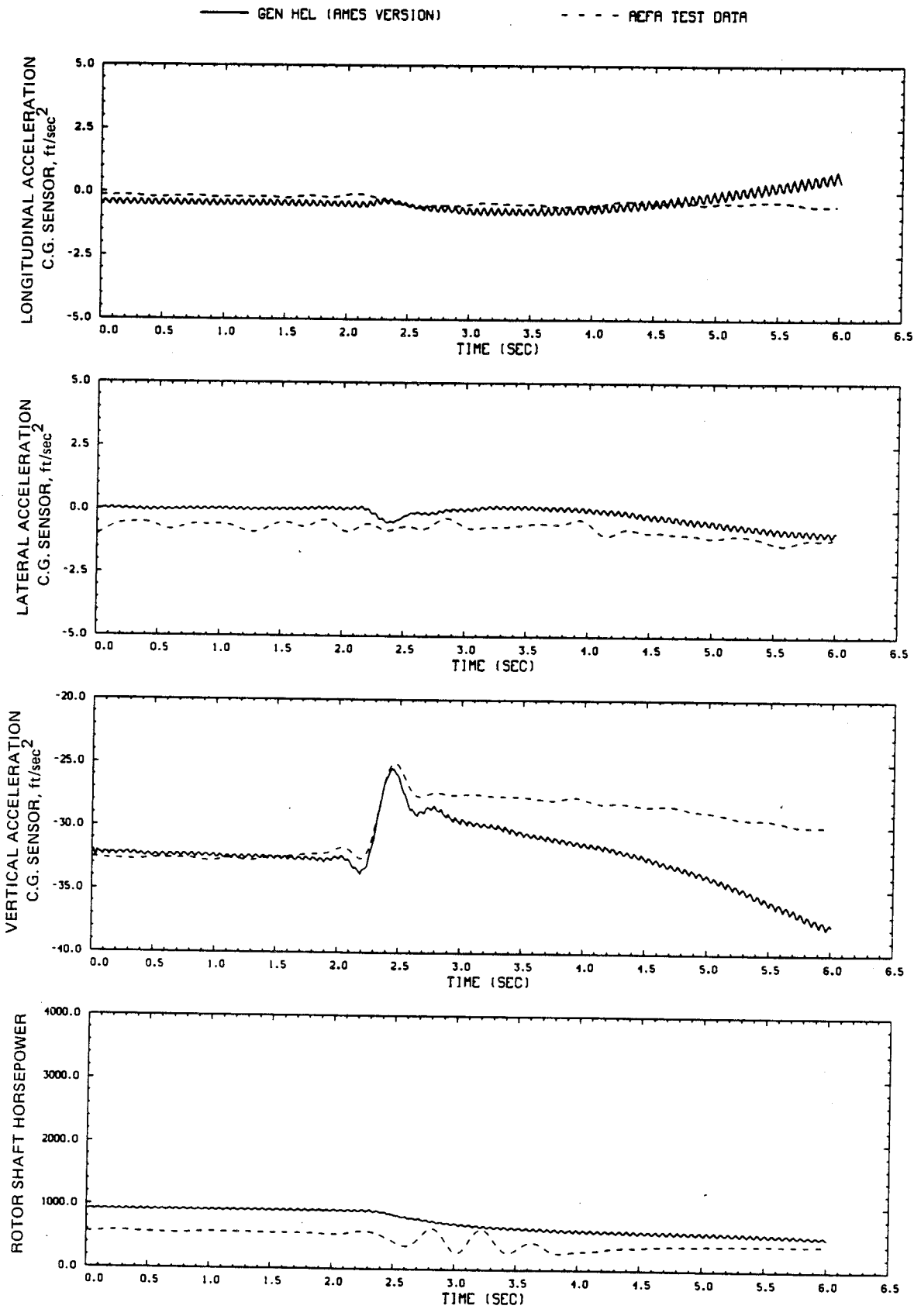


Figure D10.- Continued.

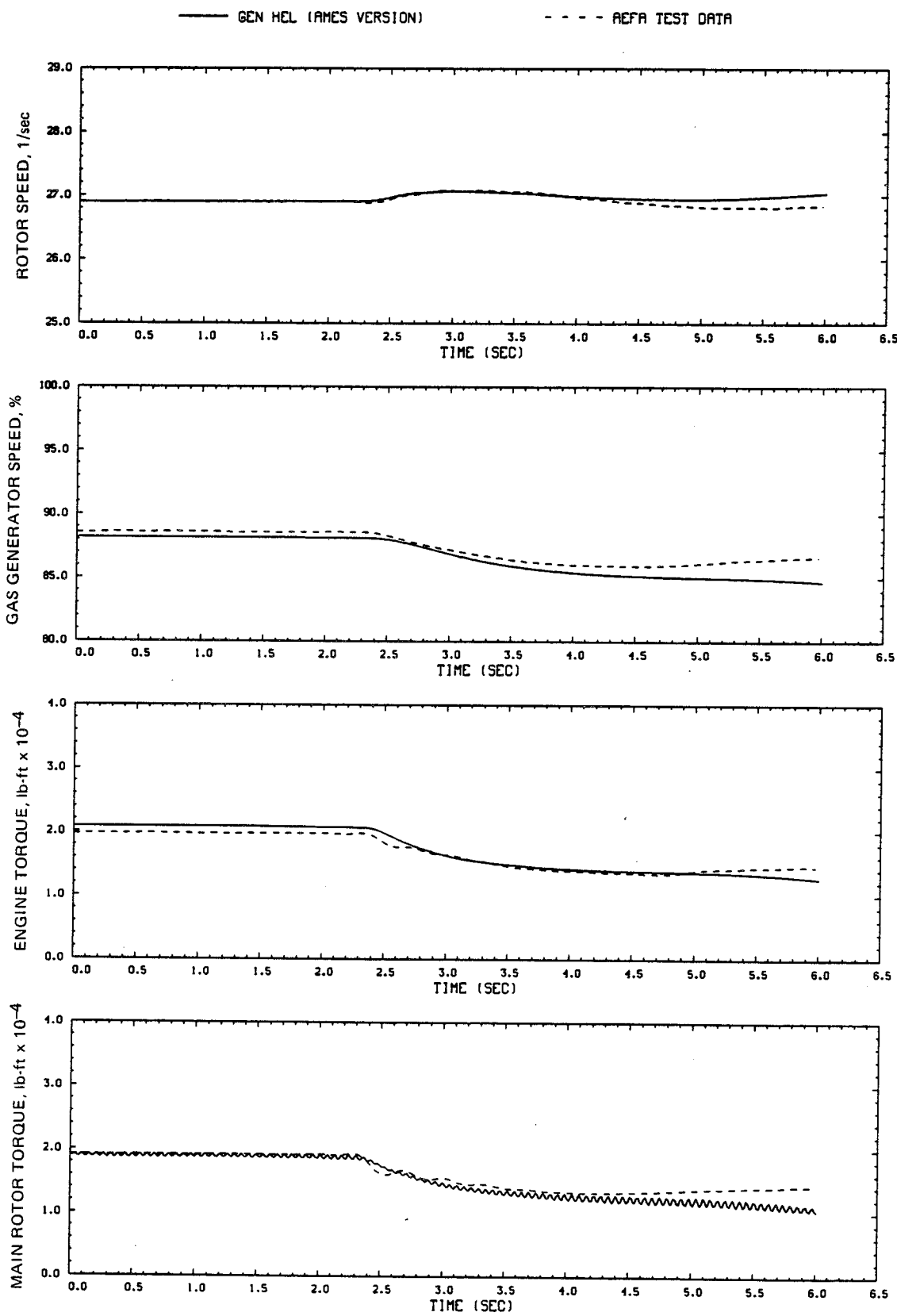


Figure D10.- Concluded.

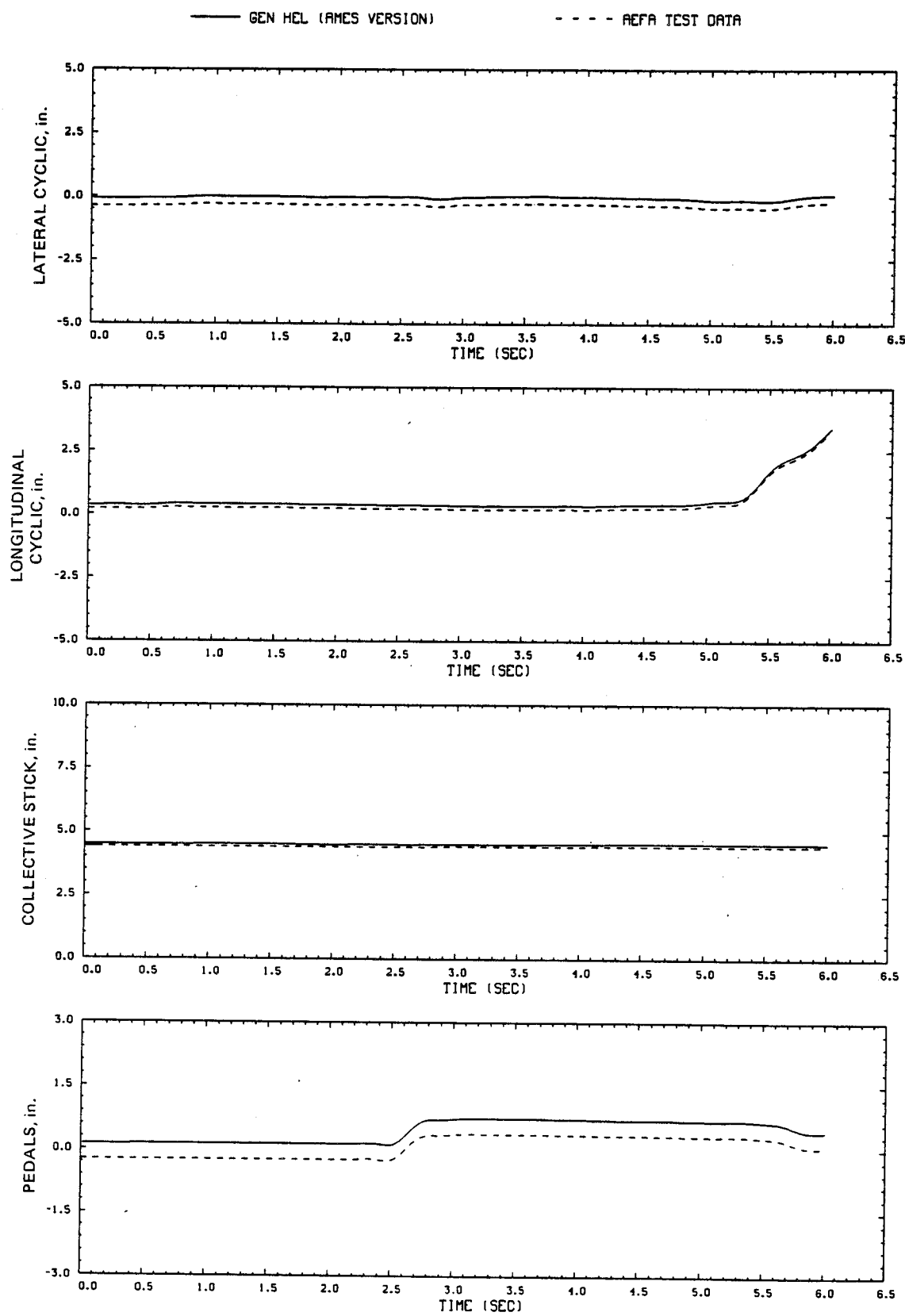


Figure D11.- Comparison of Ames real-time simulation and flight-test data.  
(File 502: 0.5-in. right pedal input, 60 knots)

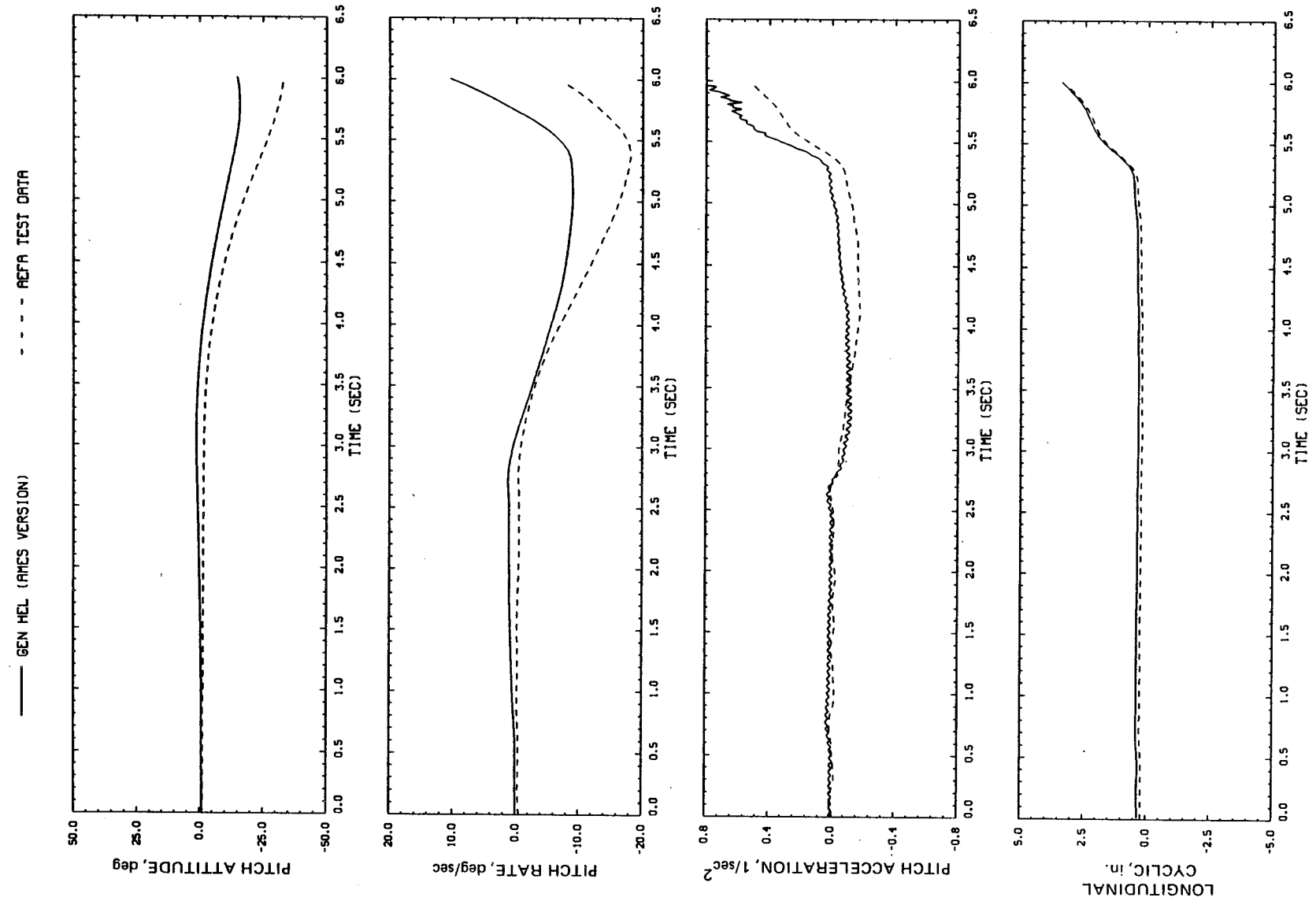


Figure D11.— Continued.

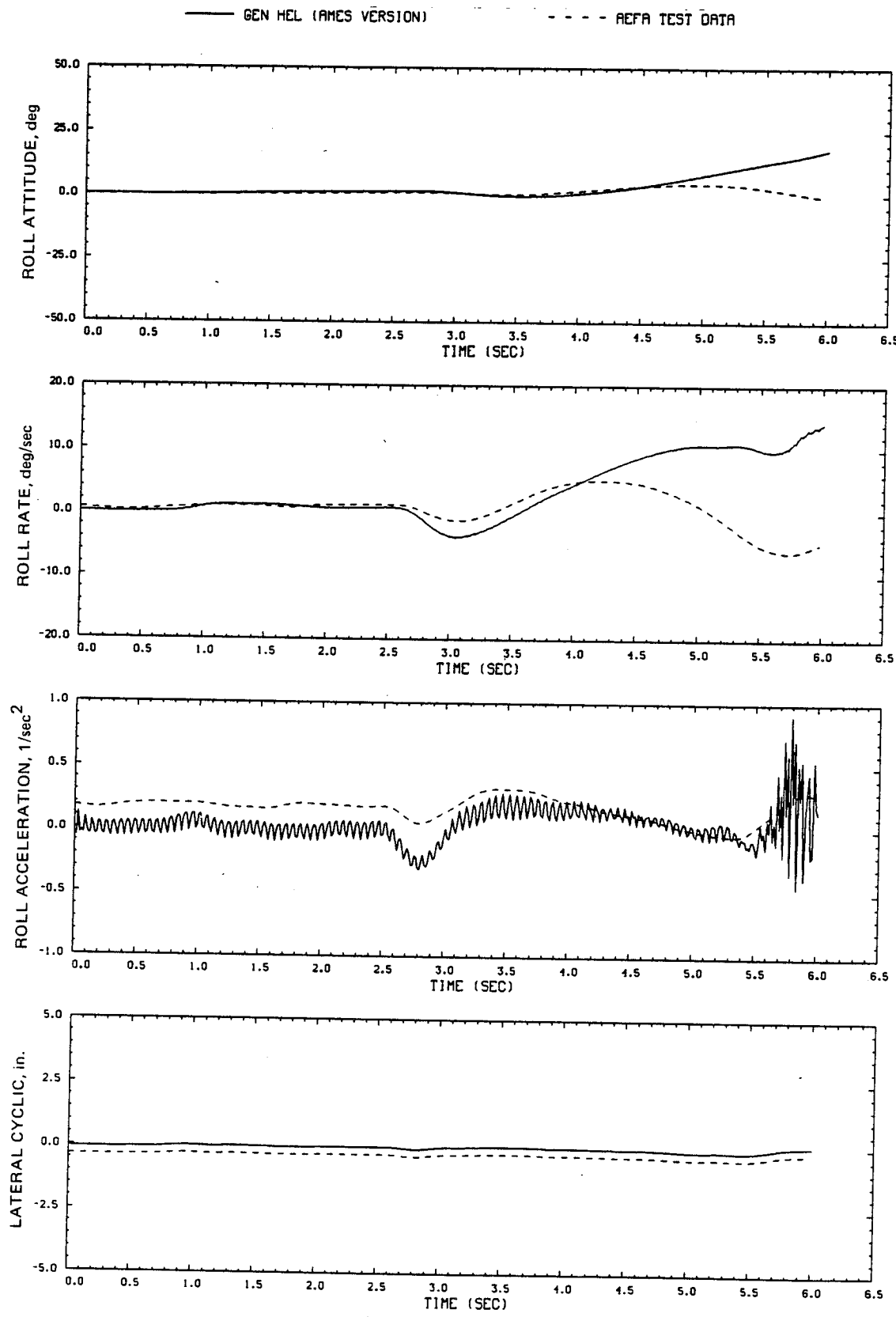


Figure D11.- Continued.

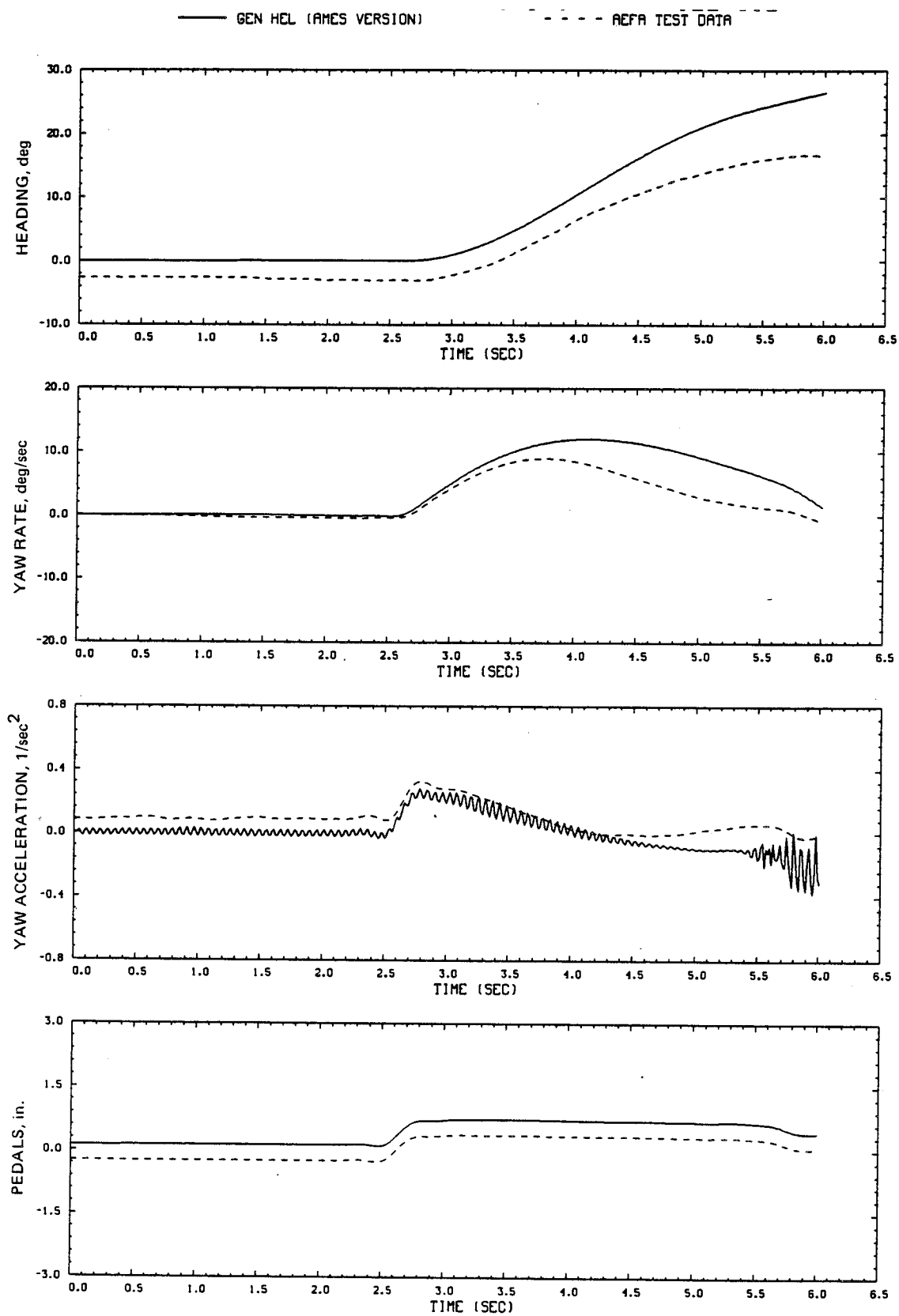


Figure D11.- Continued.

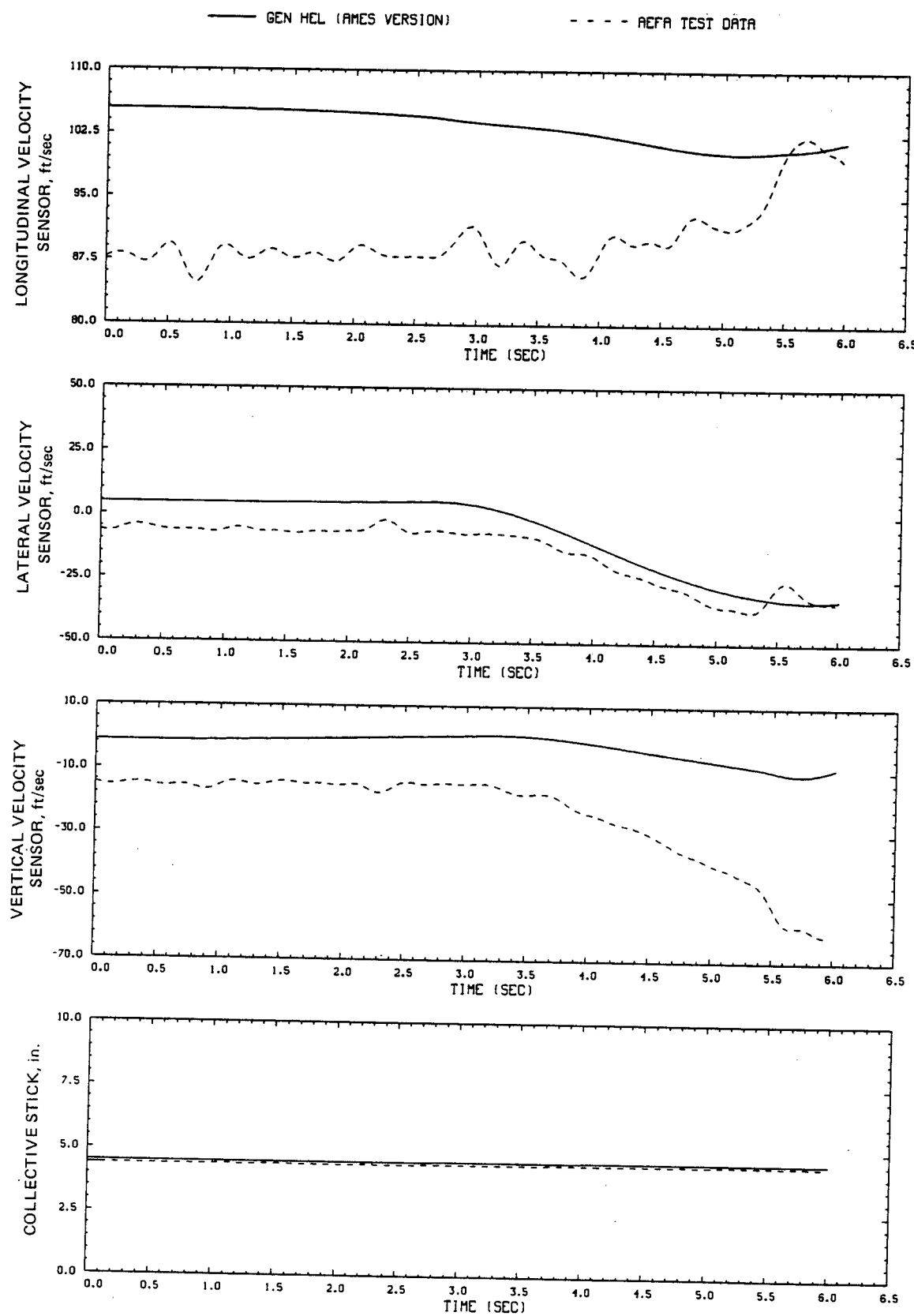


Figure D11.- Continued.

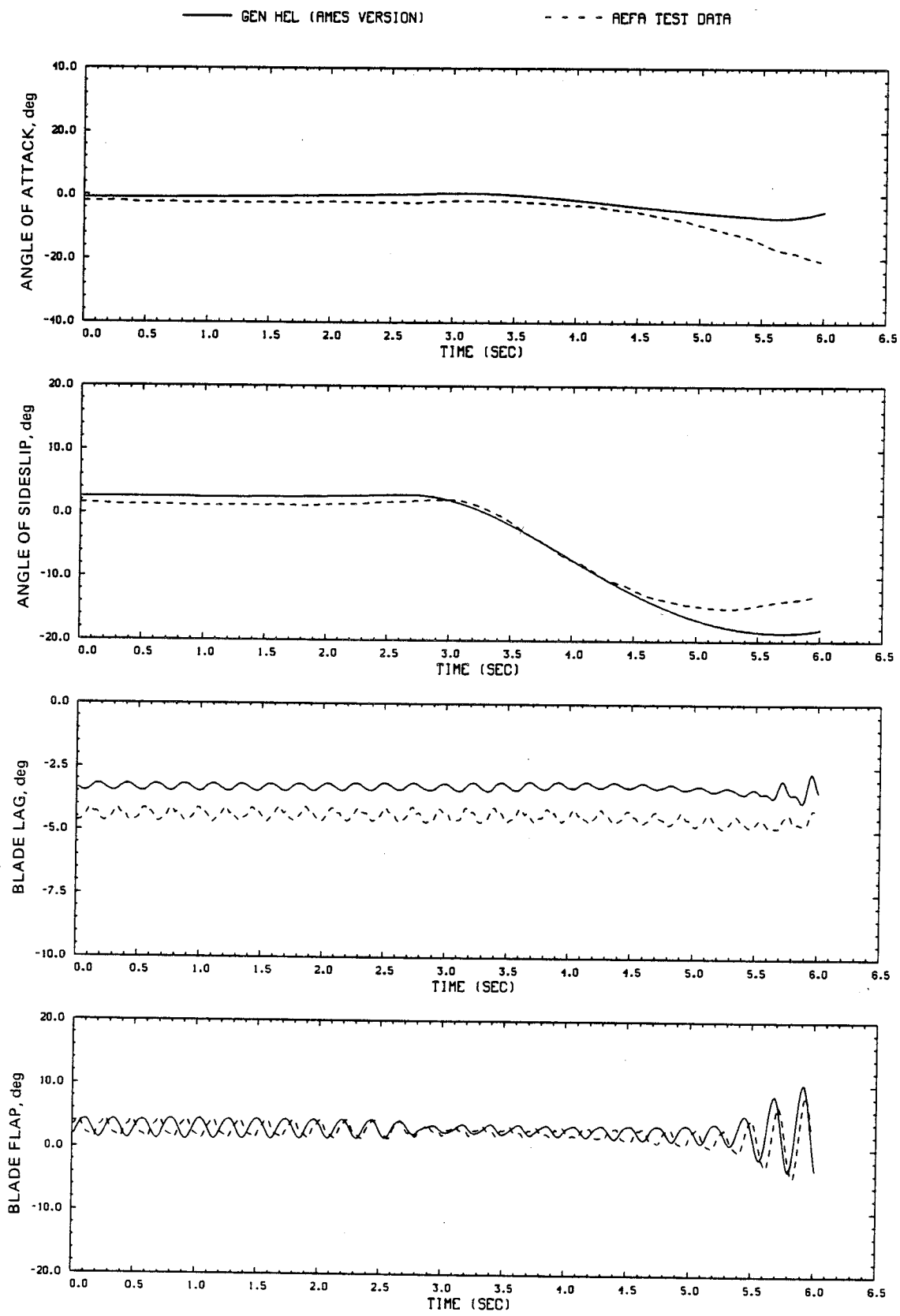


Figure D11.- Continued.

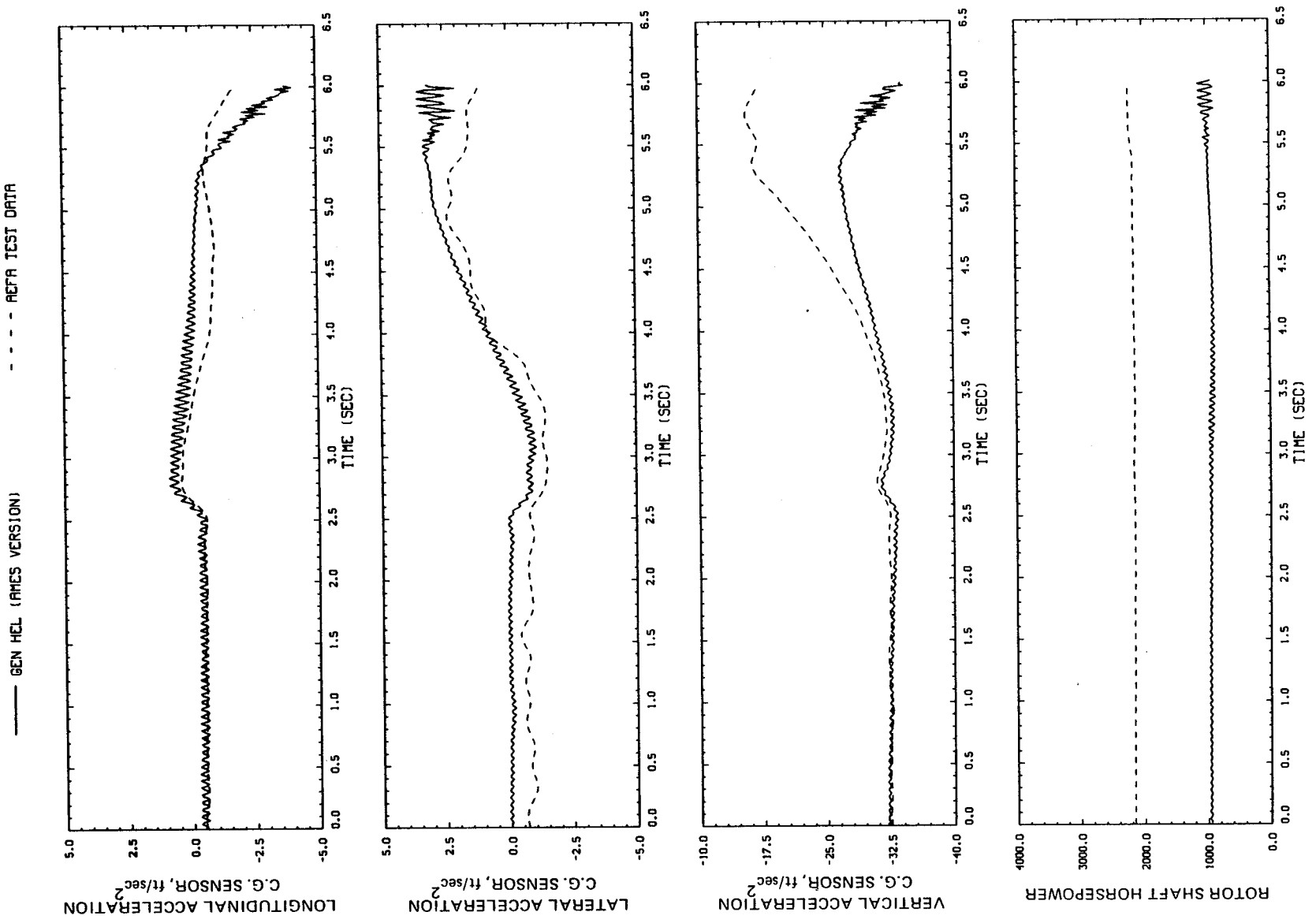


Figure D11.- Continued.

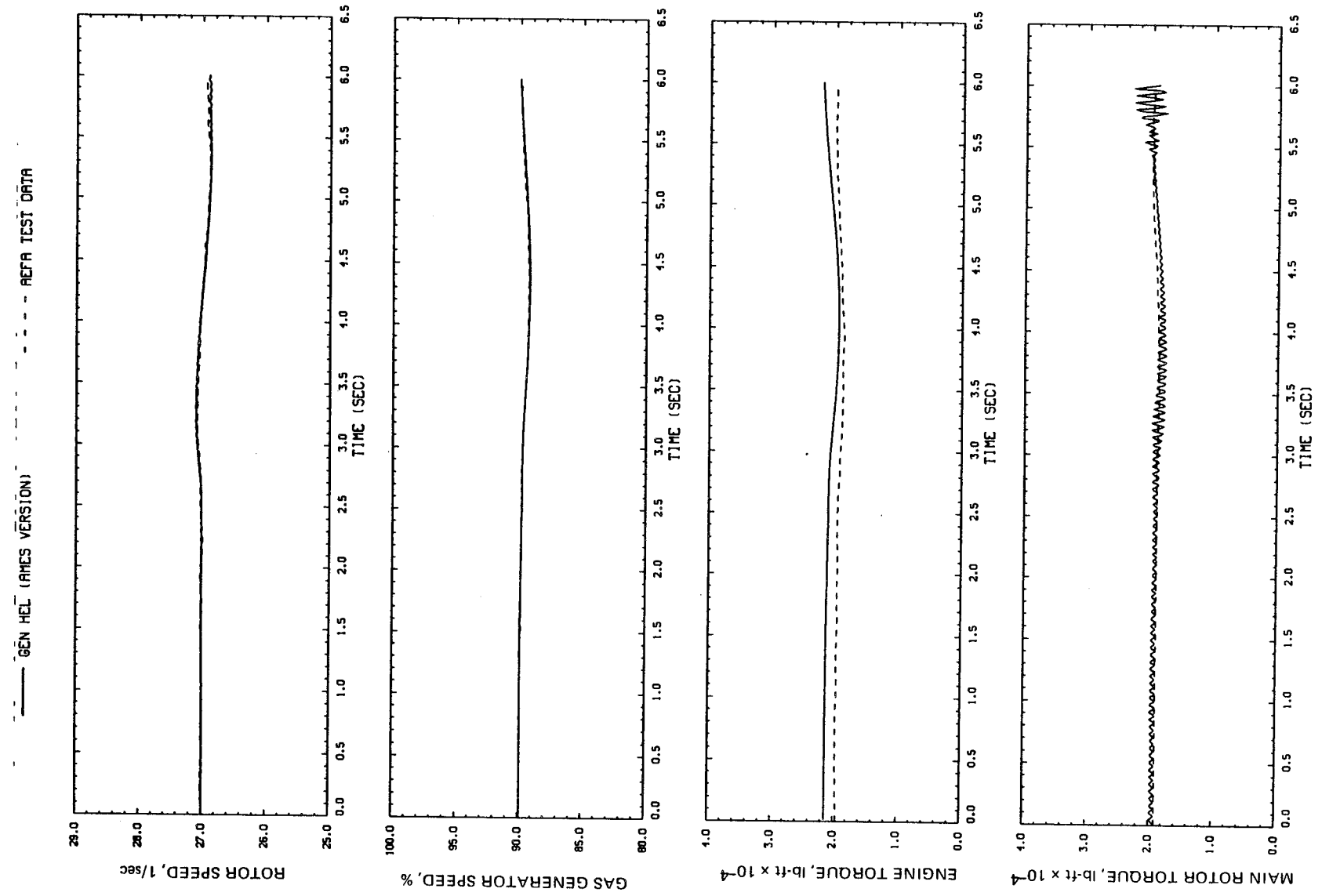


Figure D11.— Concluded.

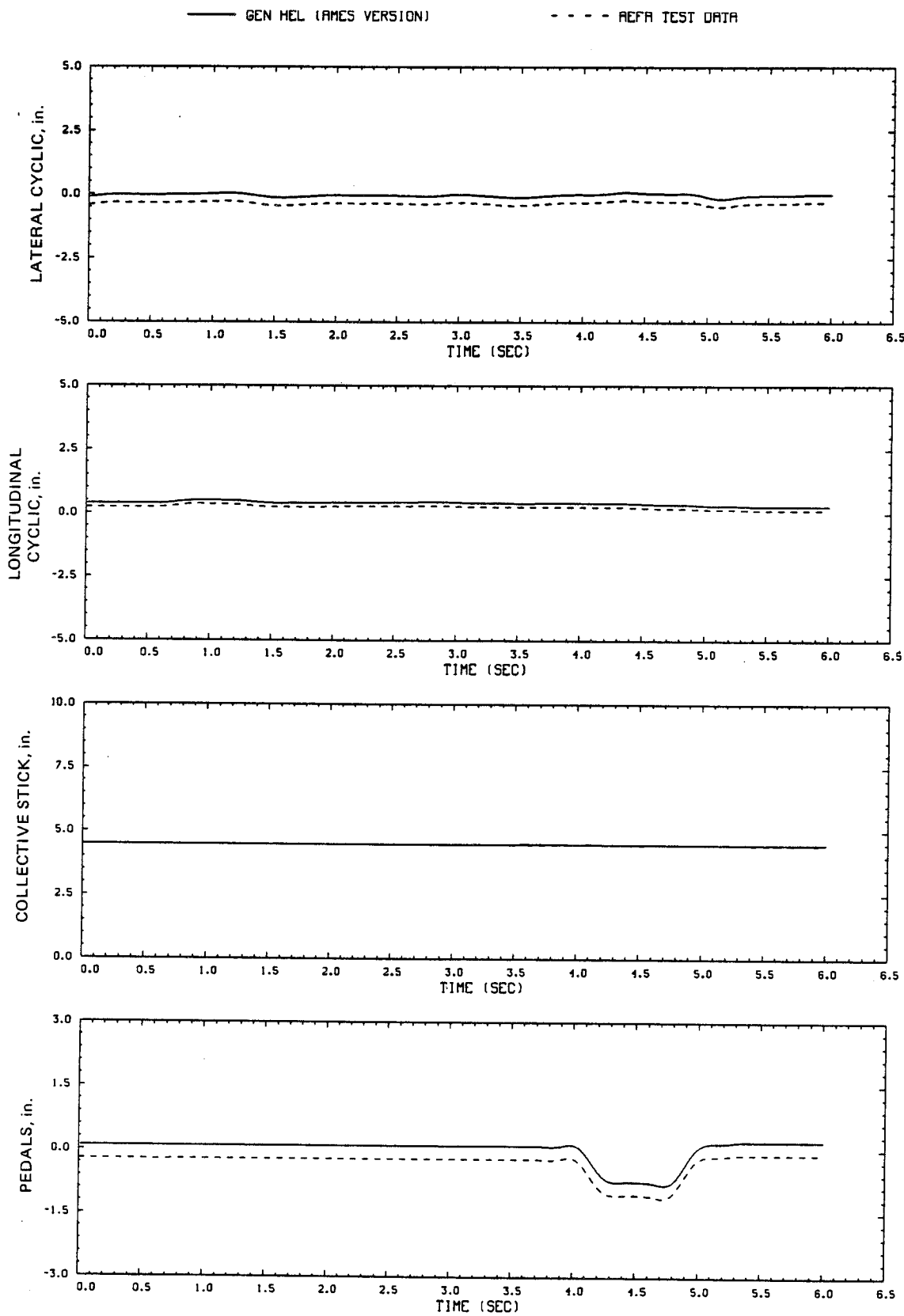


Figure D12.- Comparison of Ames real-time simulation and flight-test data.  
(File 503: 1-in. left pedal input, 60 knots)

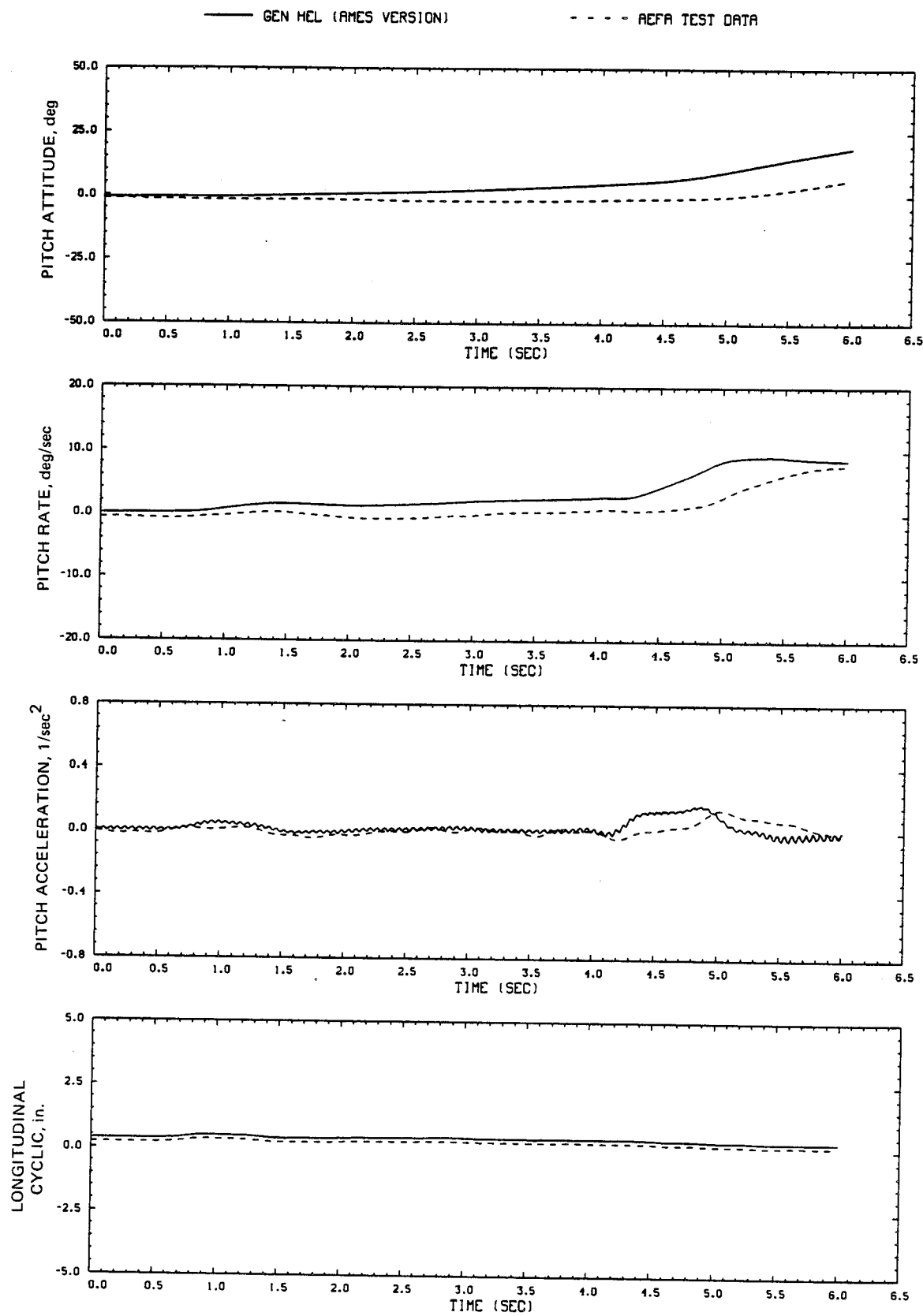


Figure D12.- Continued.

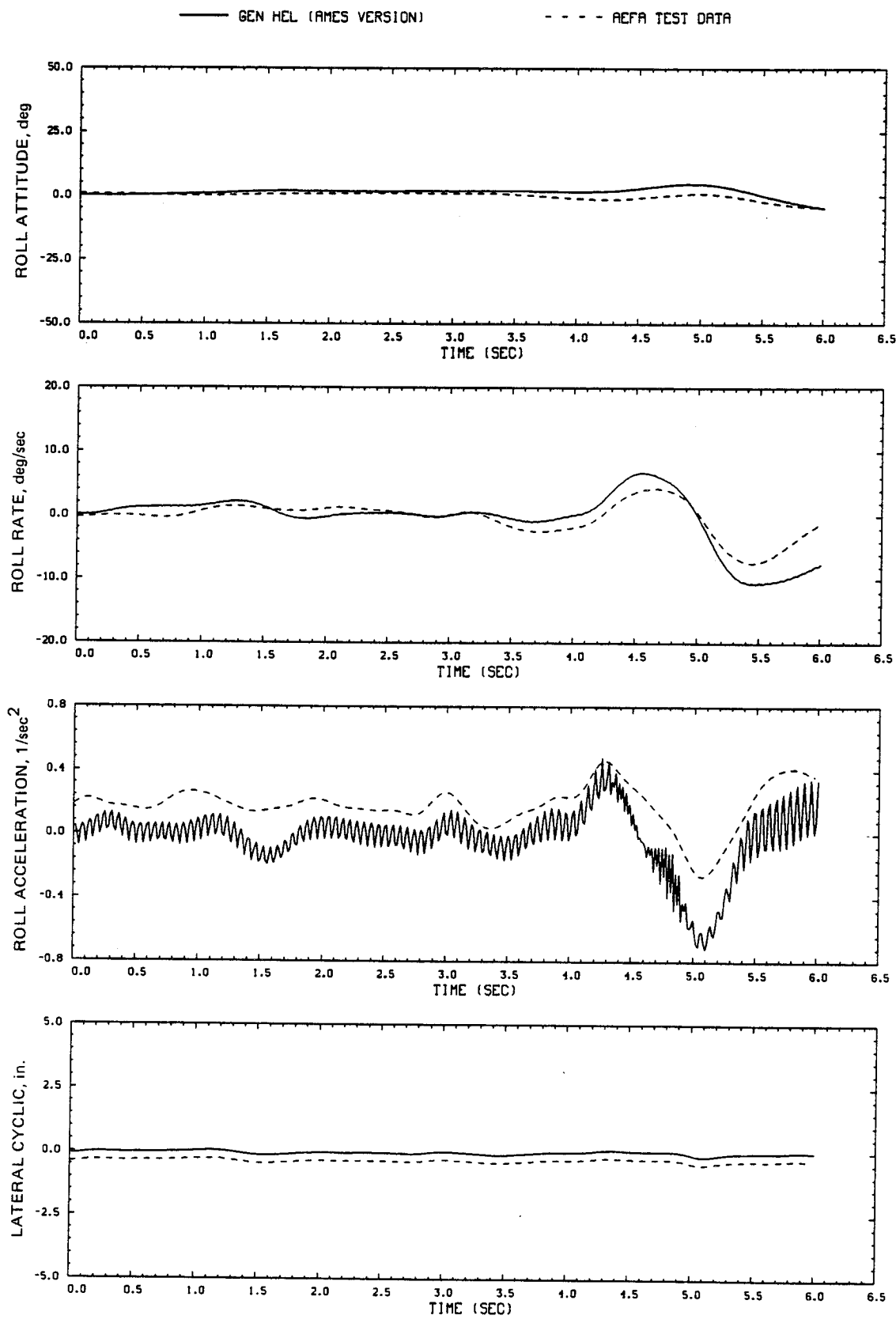


Figure D12.- Continued.

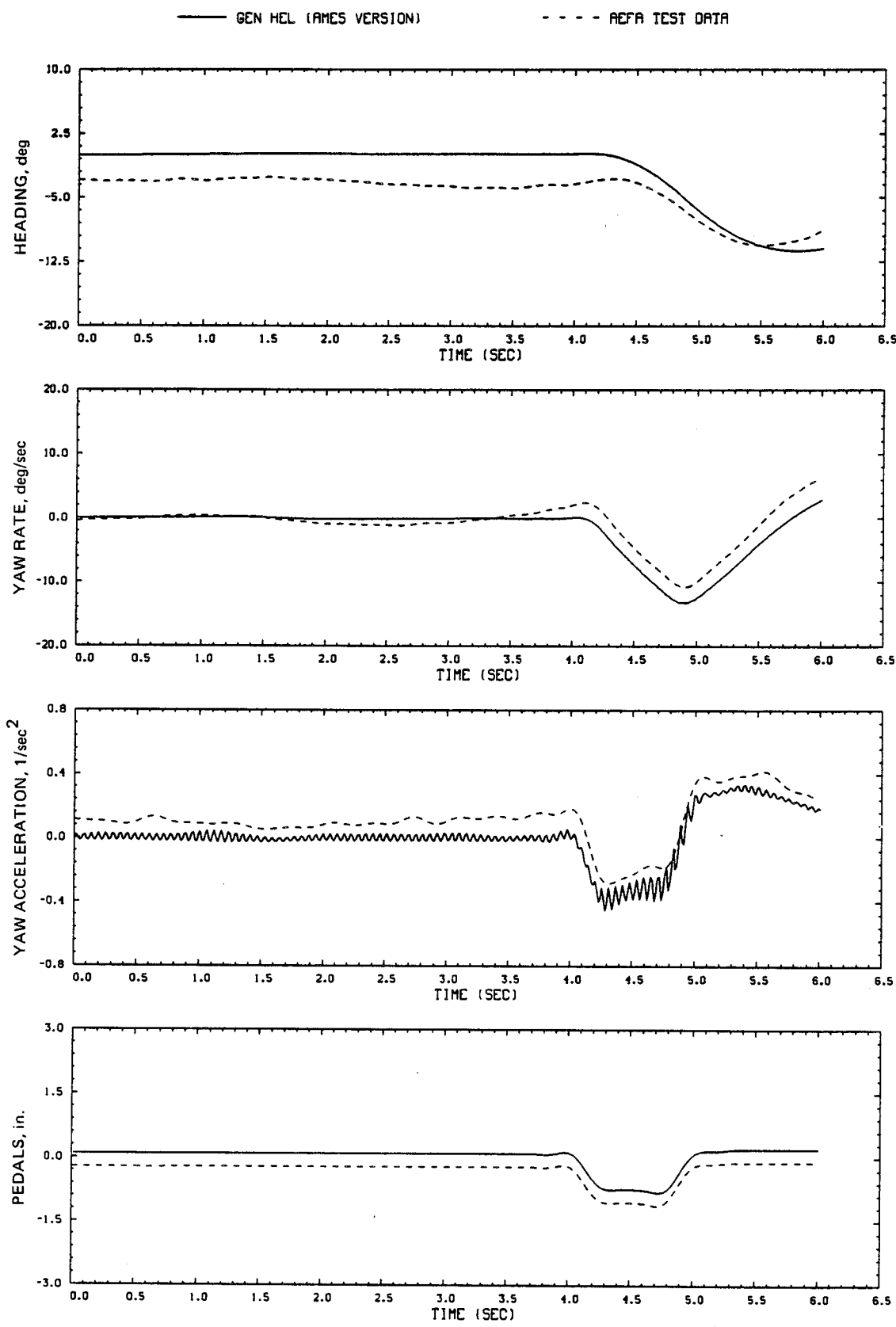


Figure D12.- Continued.

— GEN HEL (AMES VERSION)      - - - REF A TEST DATA

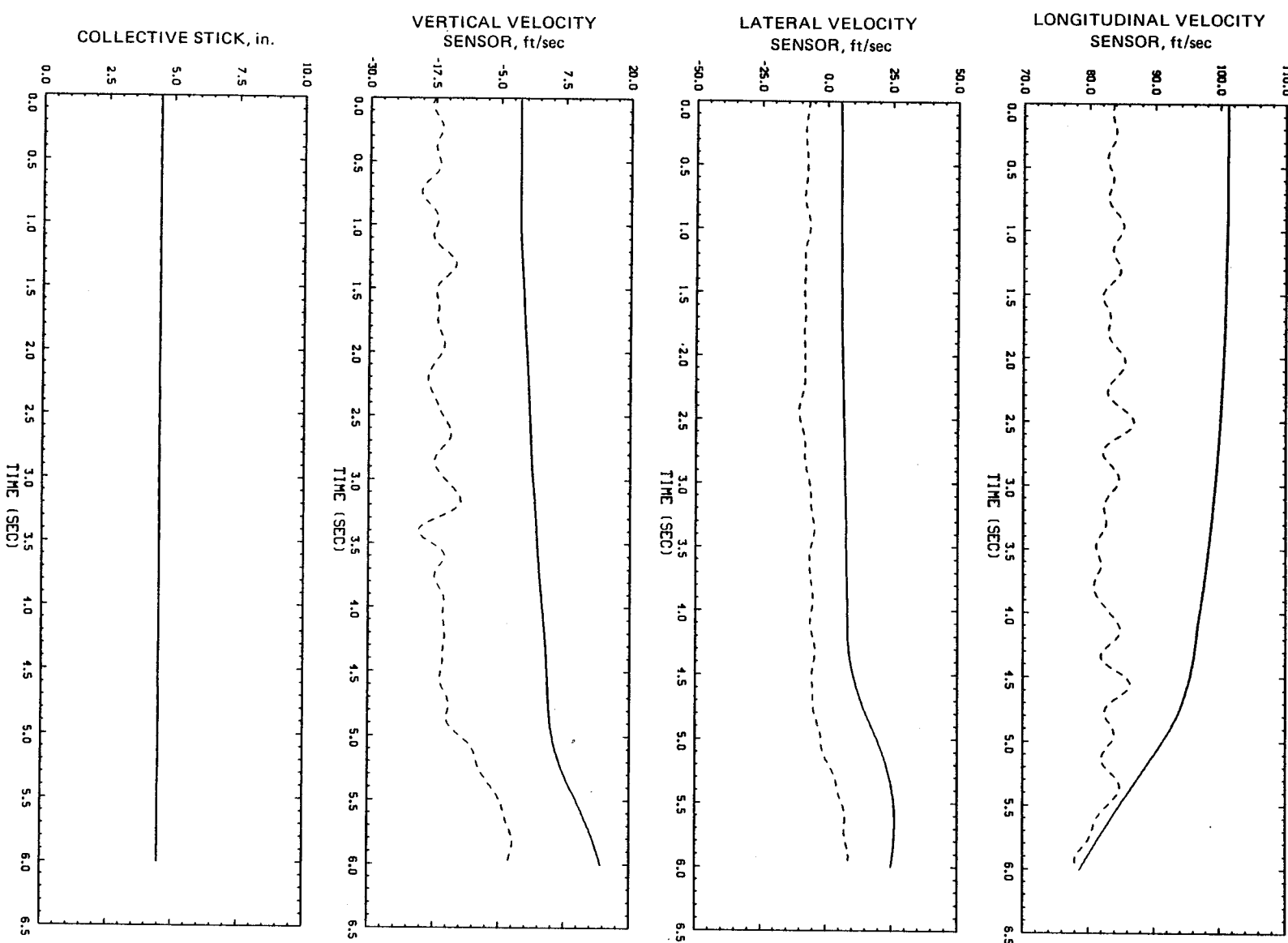


Figure D12.—Continued.

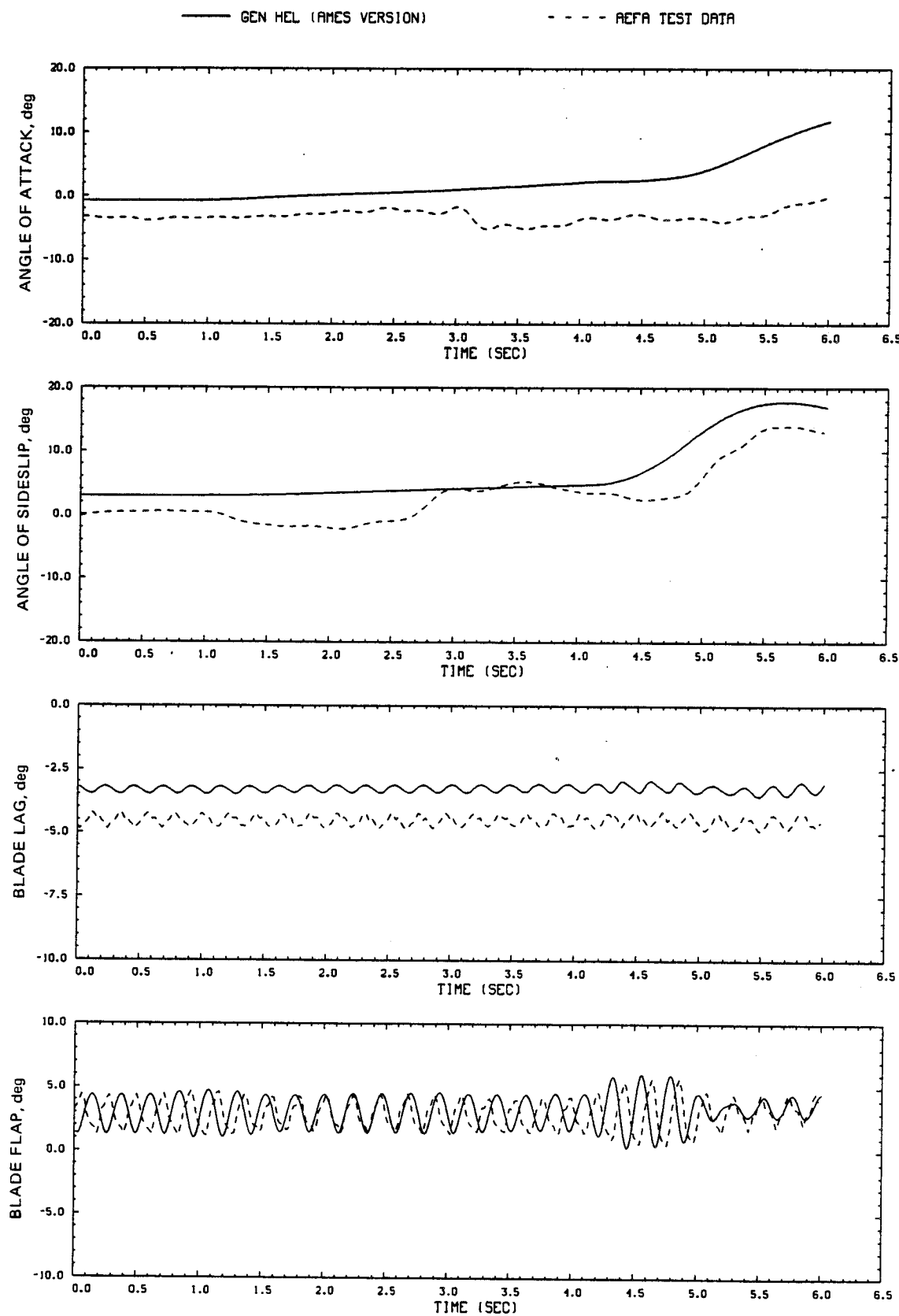


Figure D12.- Continued.

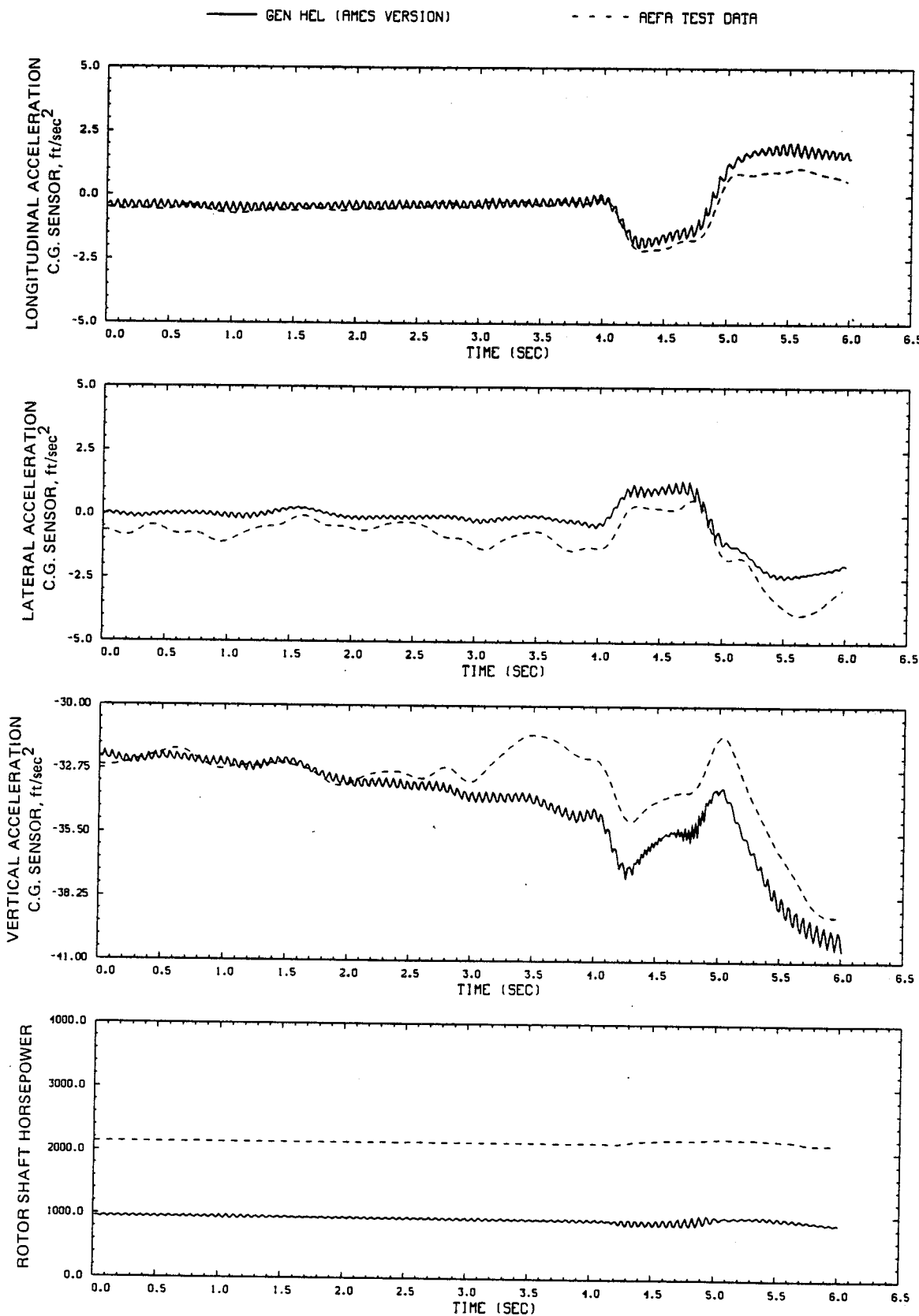


Figure D12.- Continued.

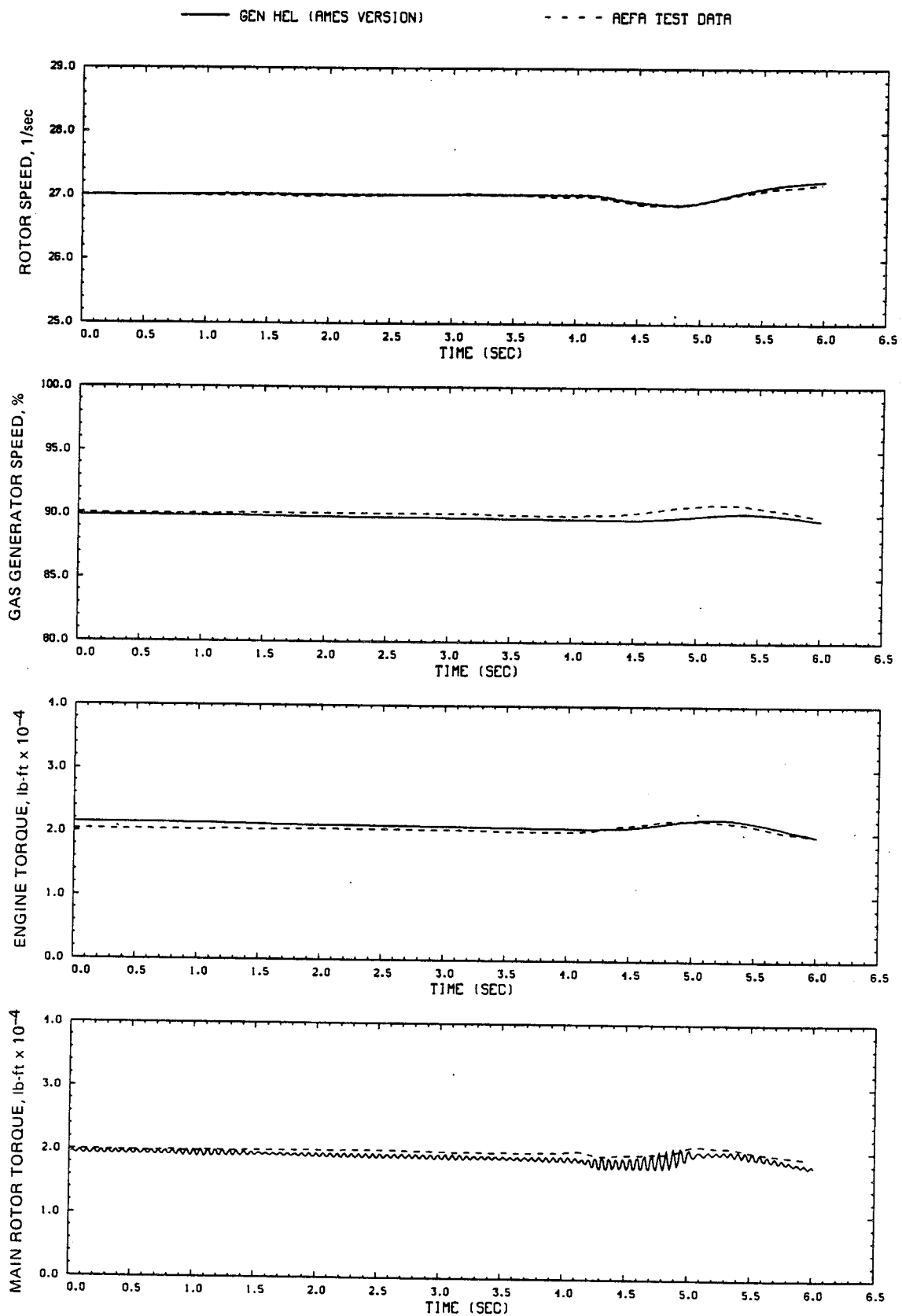


Figure D12.- Concluded.

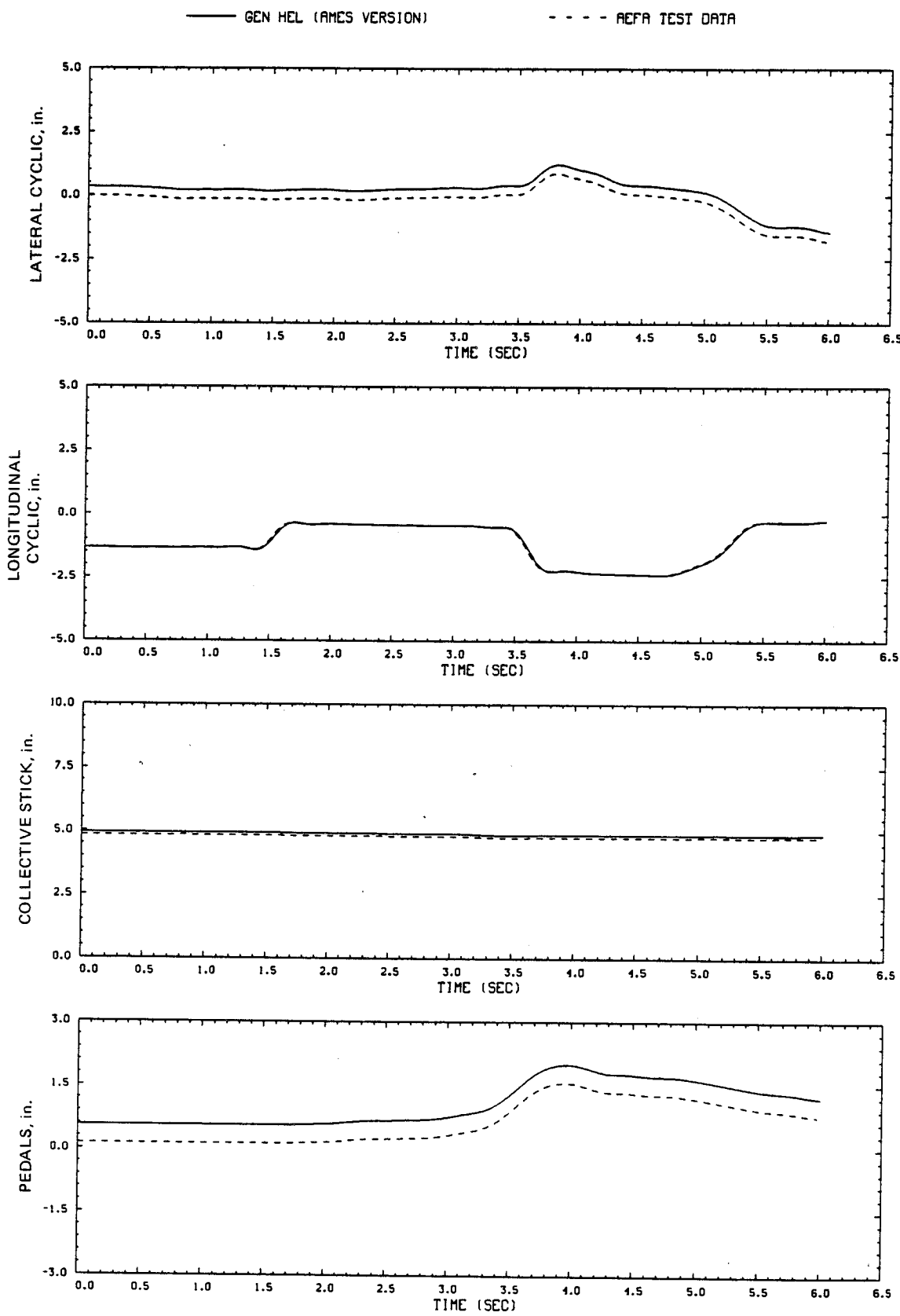


Figure D13.- Comparison of Ames real-time simulation and flight-test data.  
(File 401: 1-in. aft cyclic input, 100 knots)

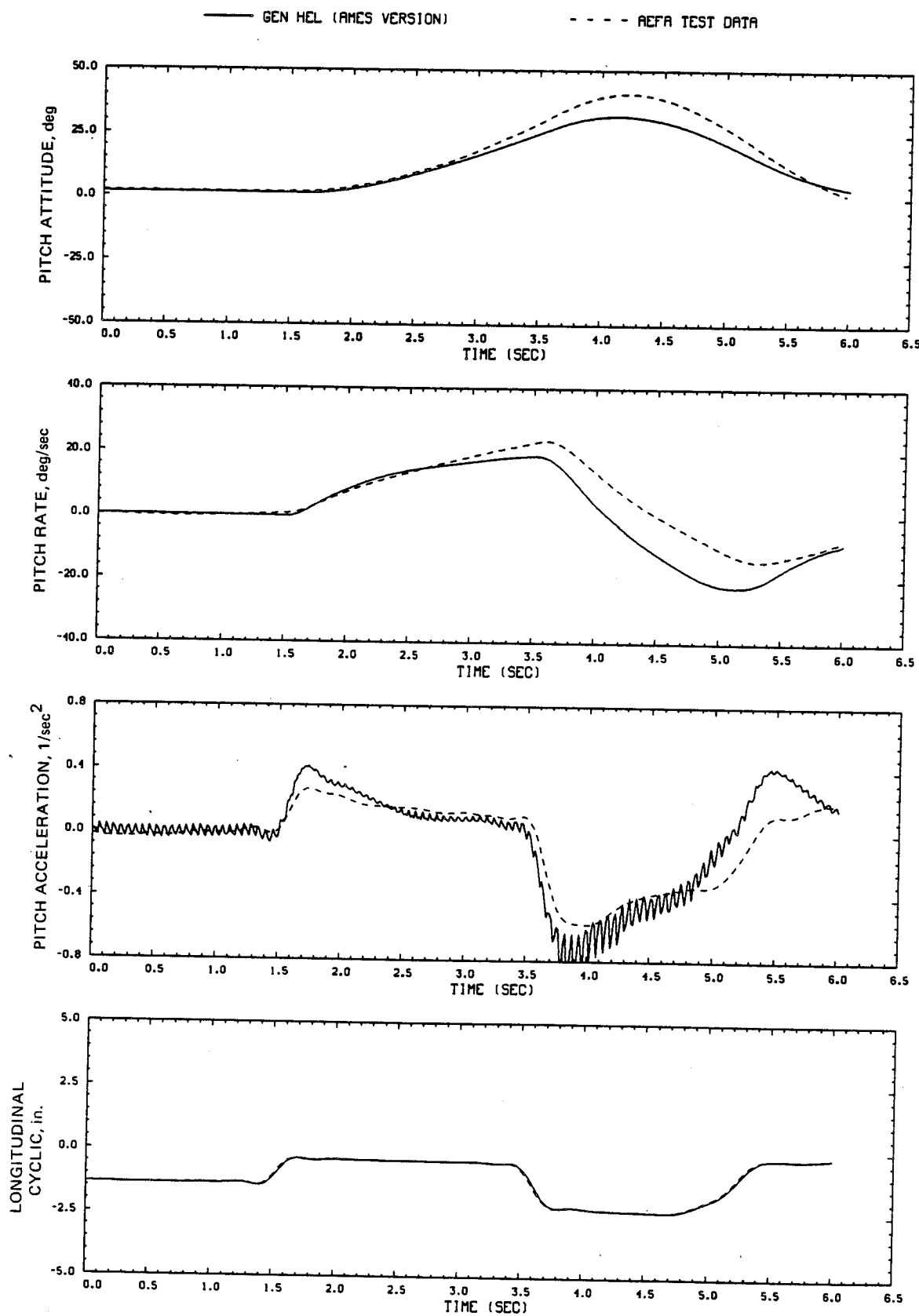


Figure D13.- Continued.

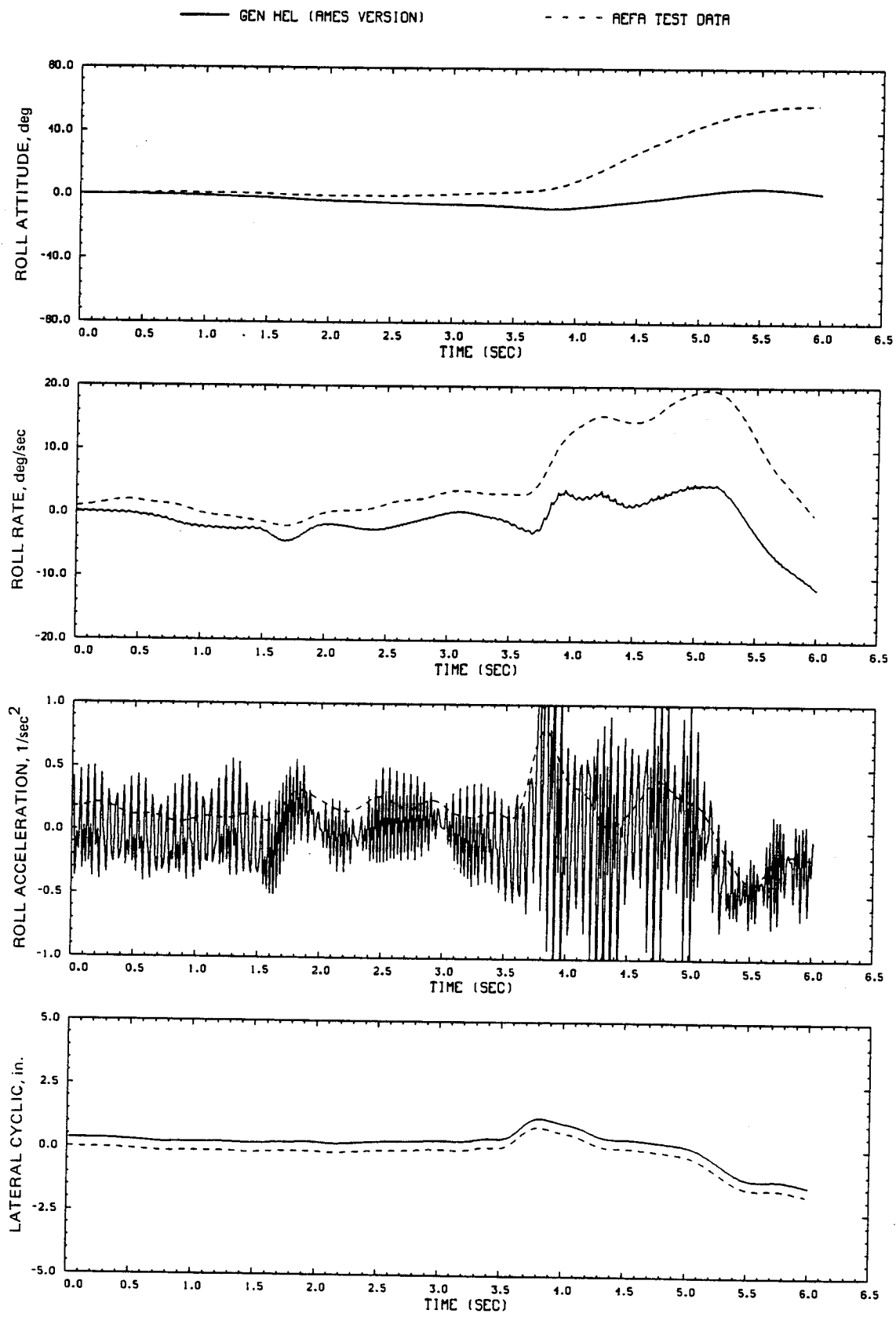


Figure D13.- Continued.

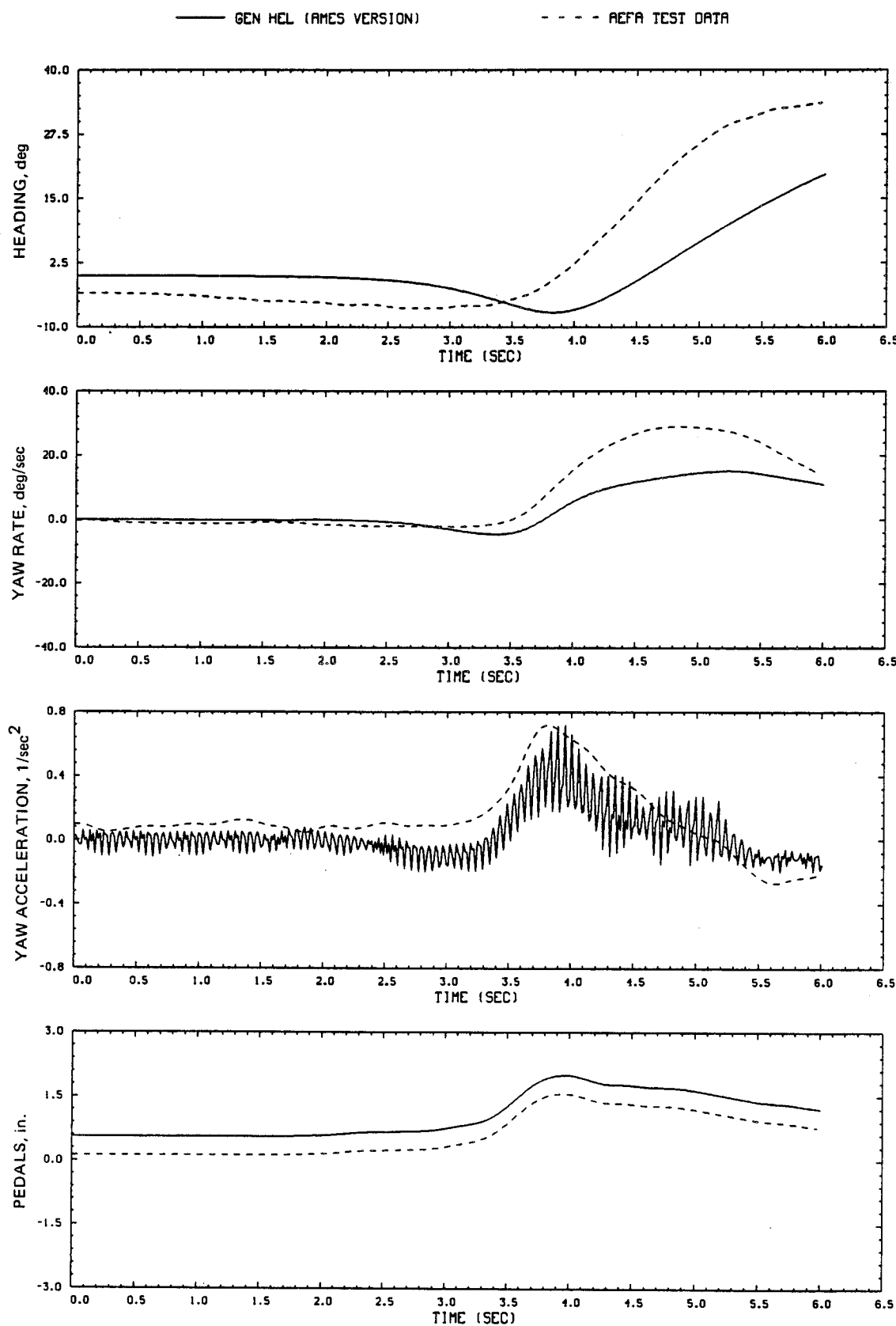


Figure D13.- Continued.

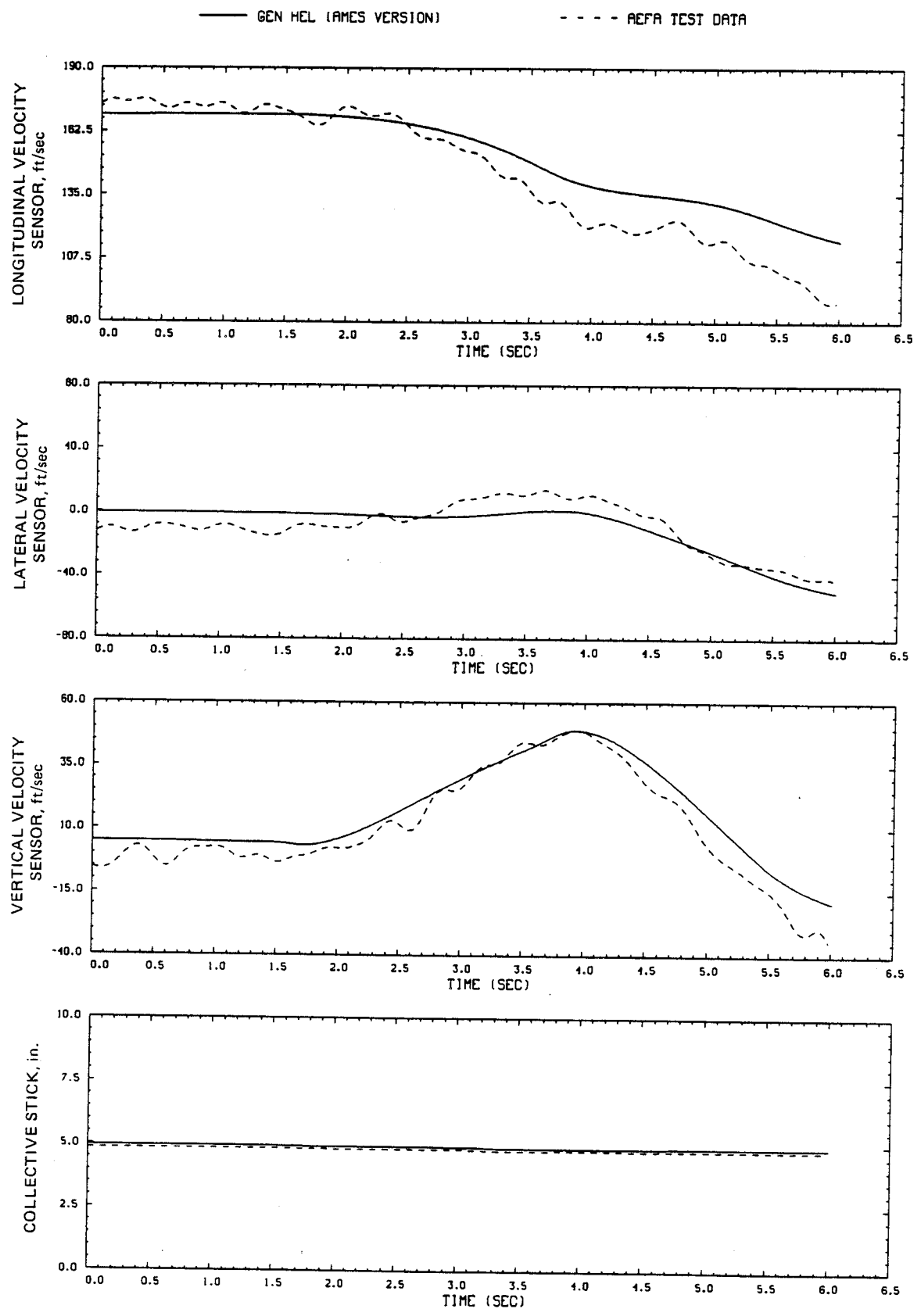


Figure D13.- Continued.

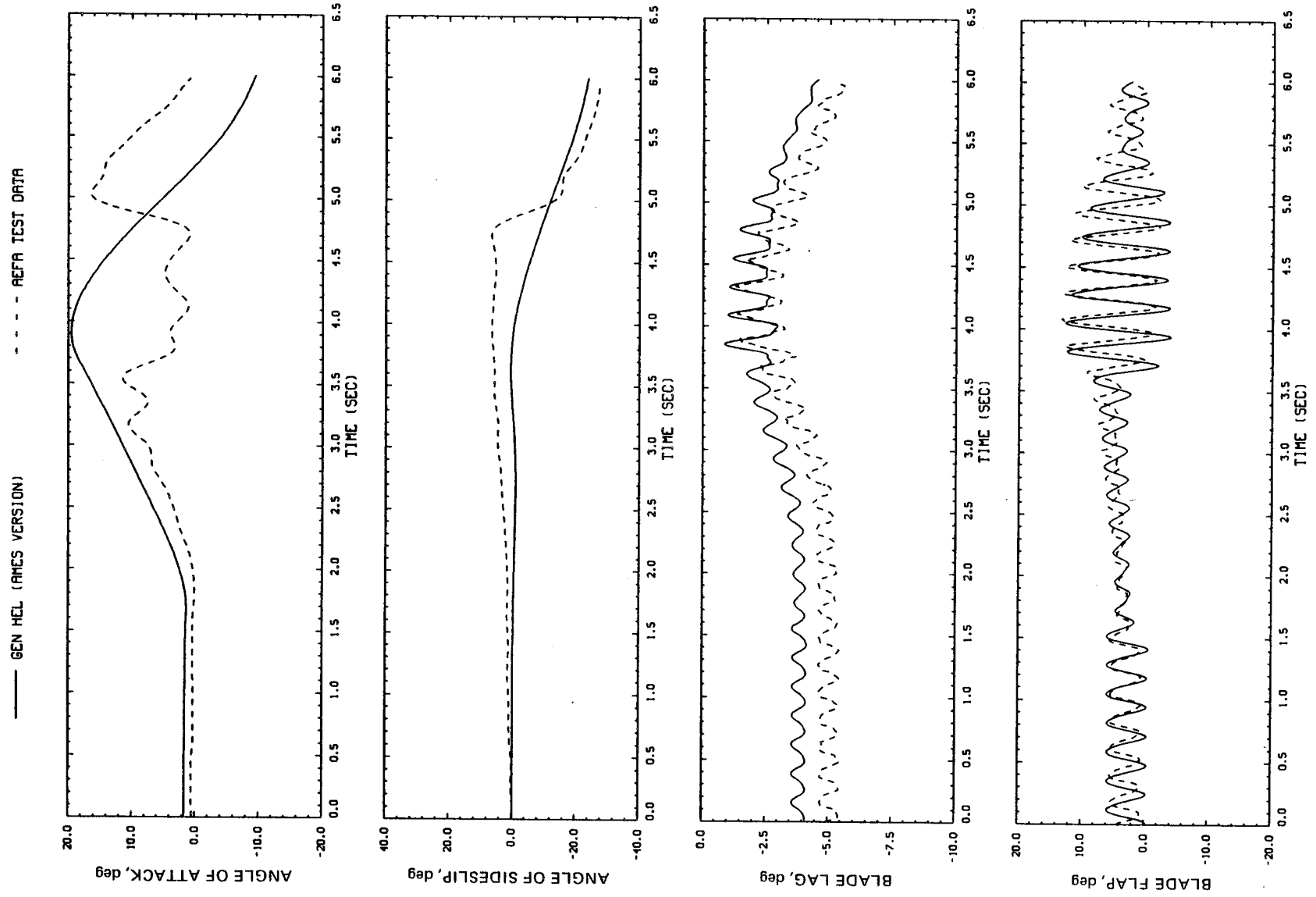


Figure D13.- Continued.

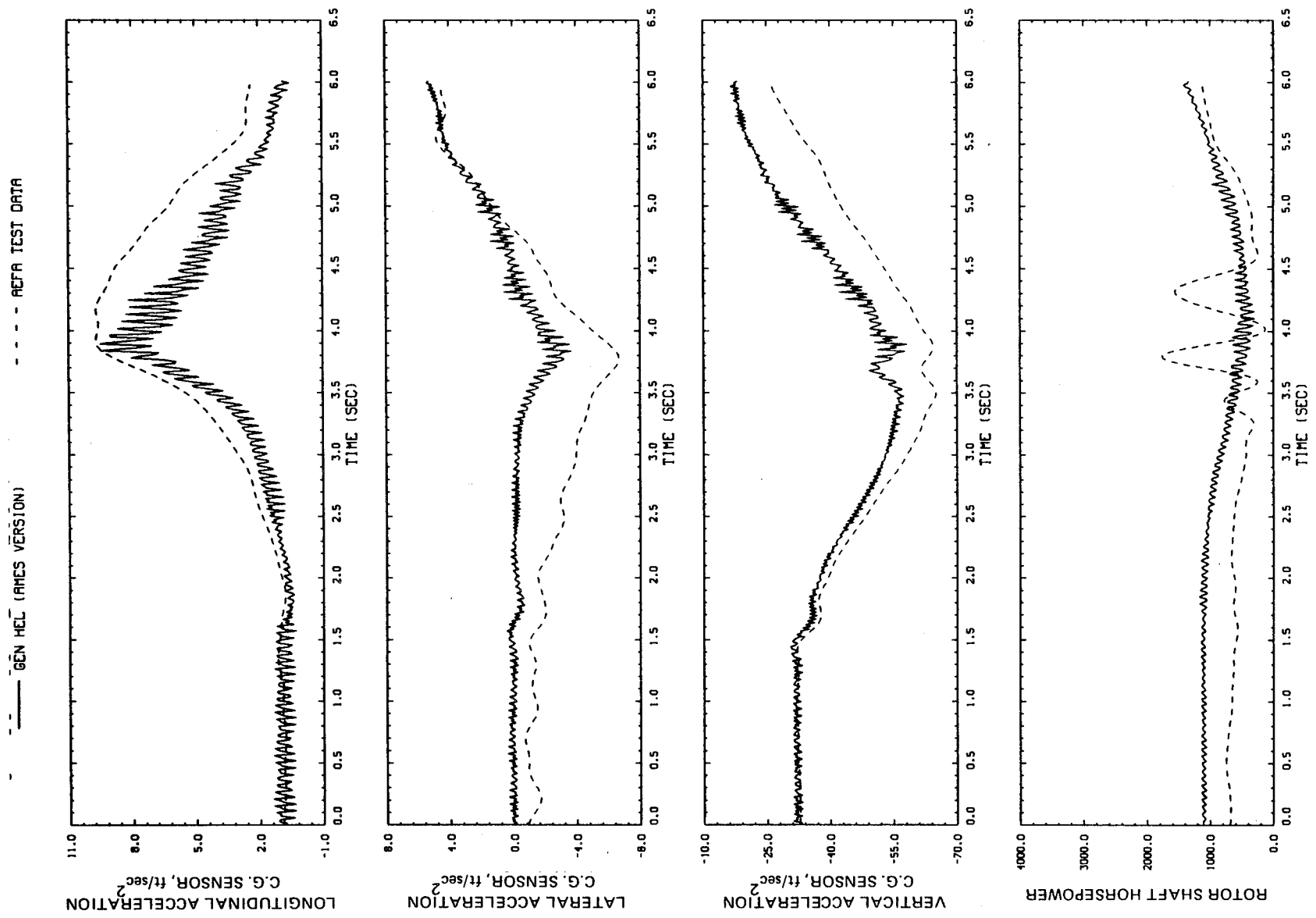


Figure D13.—Continued.

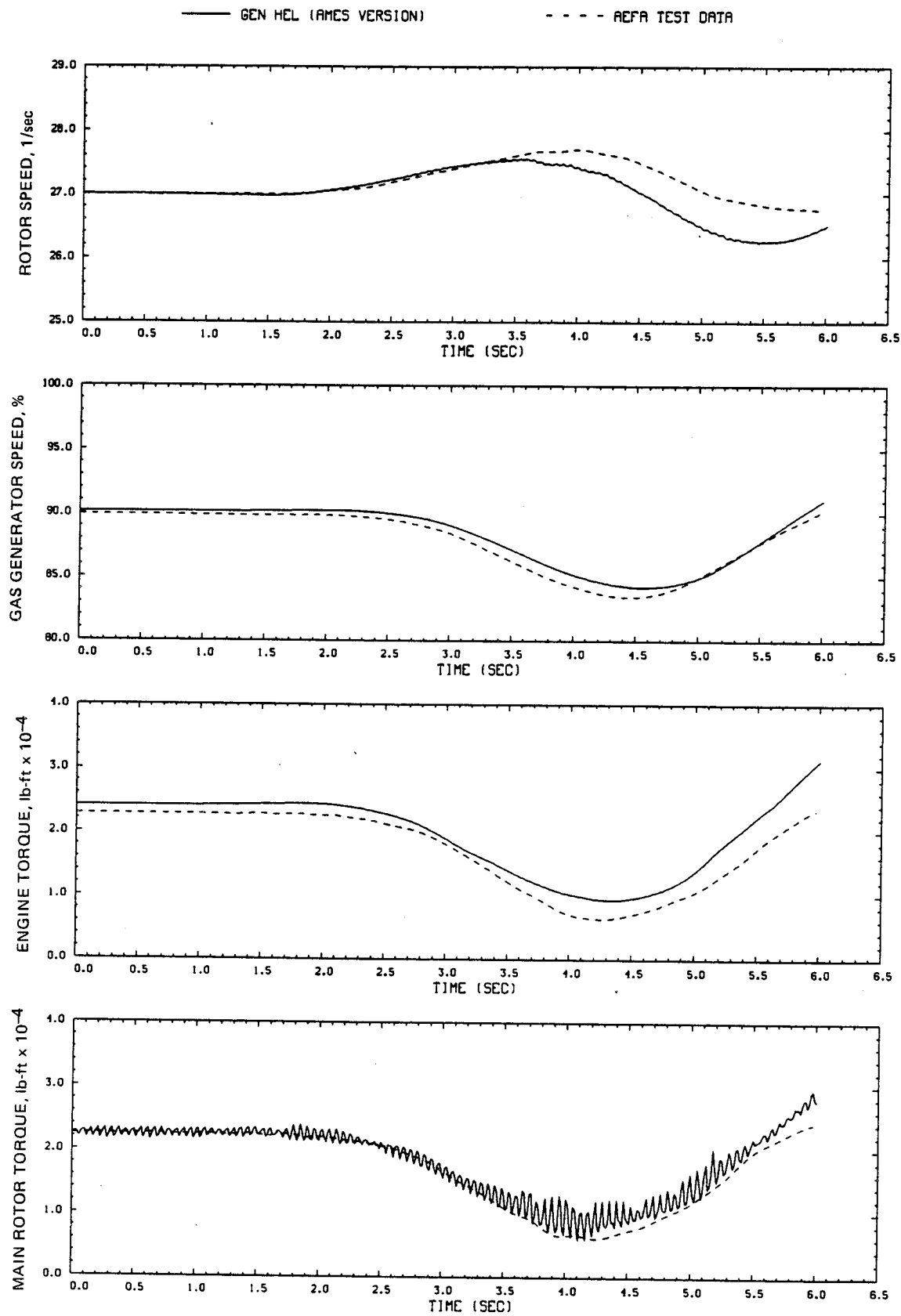


Figure D13.- Concluded.

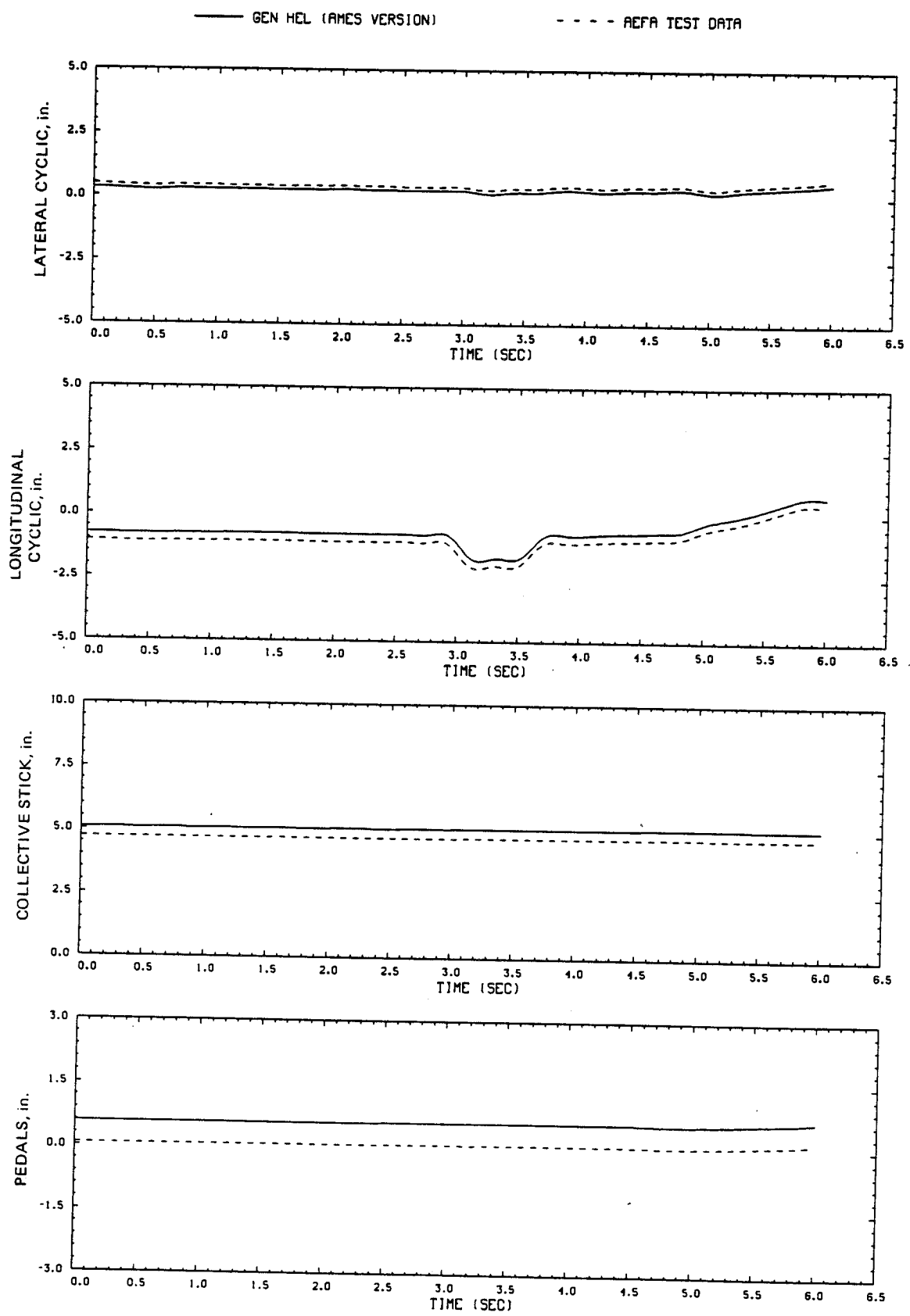


Figure D14.- Comparison of Ames real-time simulation and flight-test data.  
(File 706: 1-in. forward cyclic input, 100 knots)

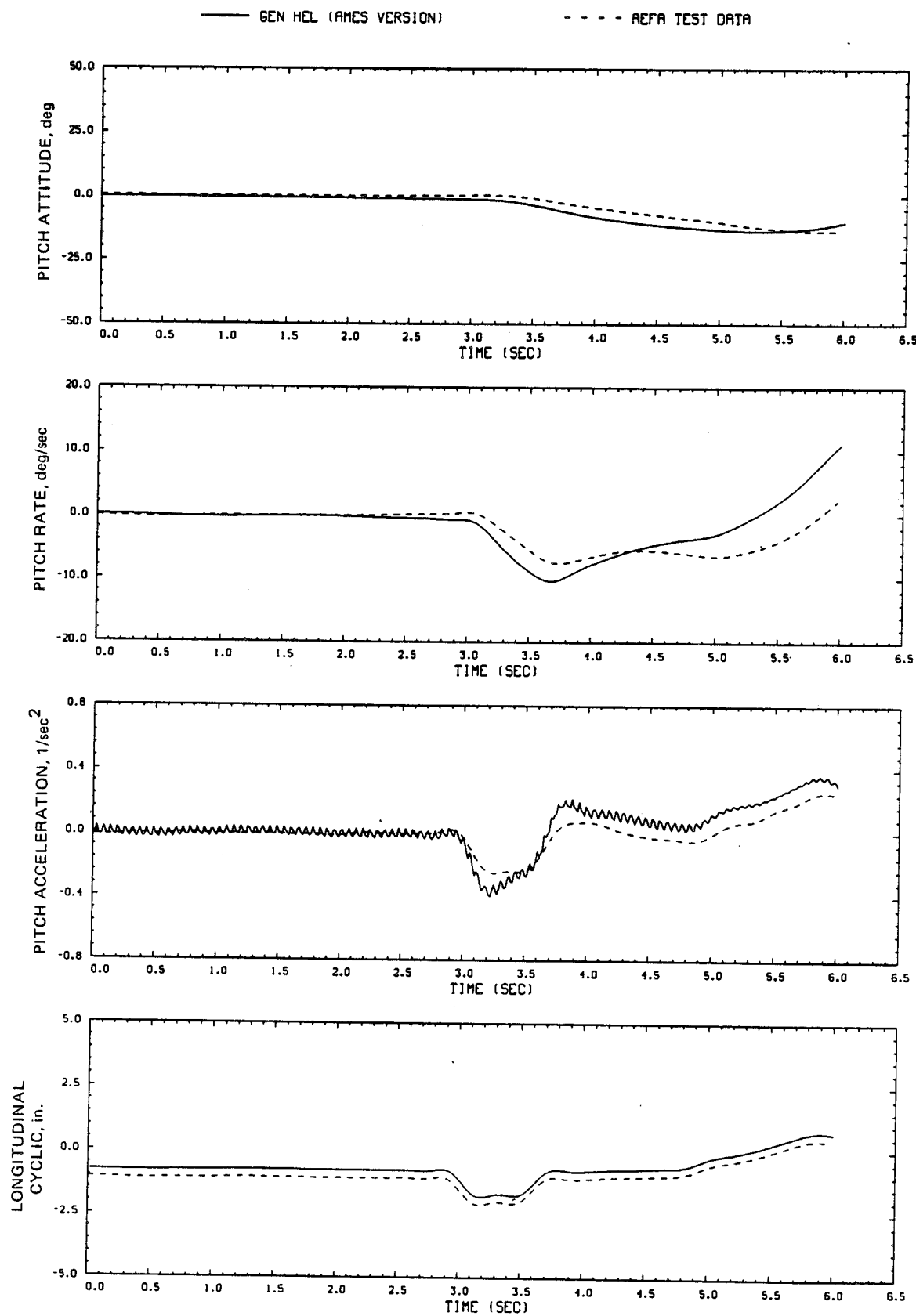


Figure D14.- Continued.

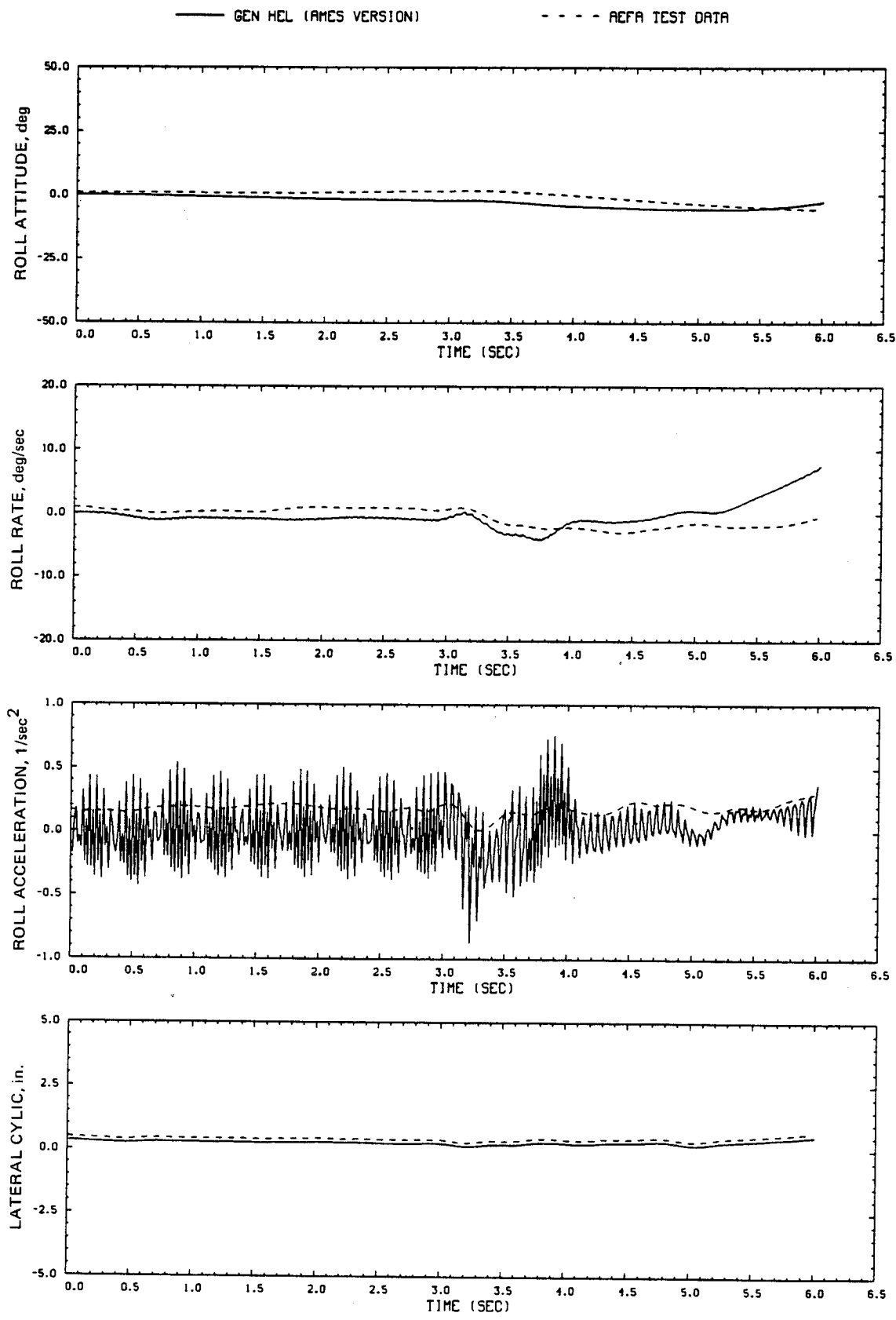


Figure D14.- Continued.

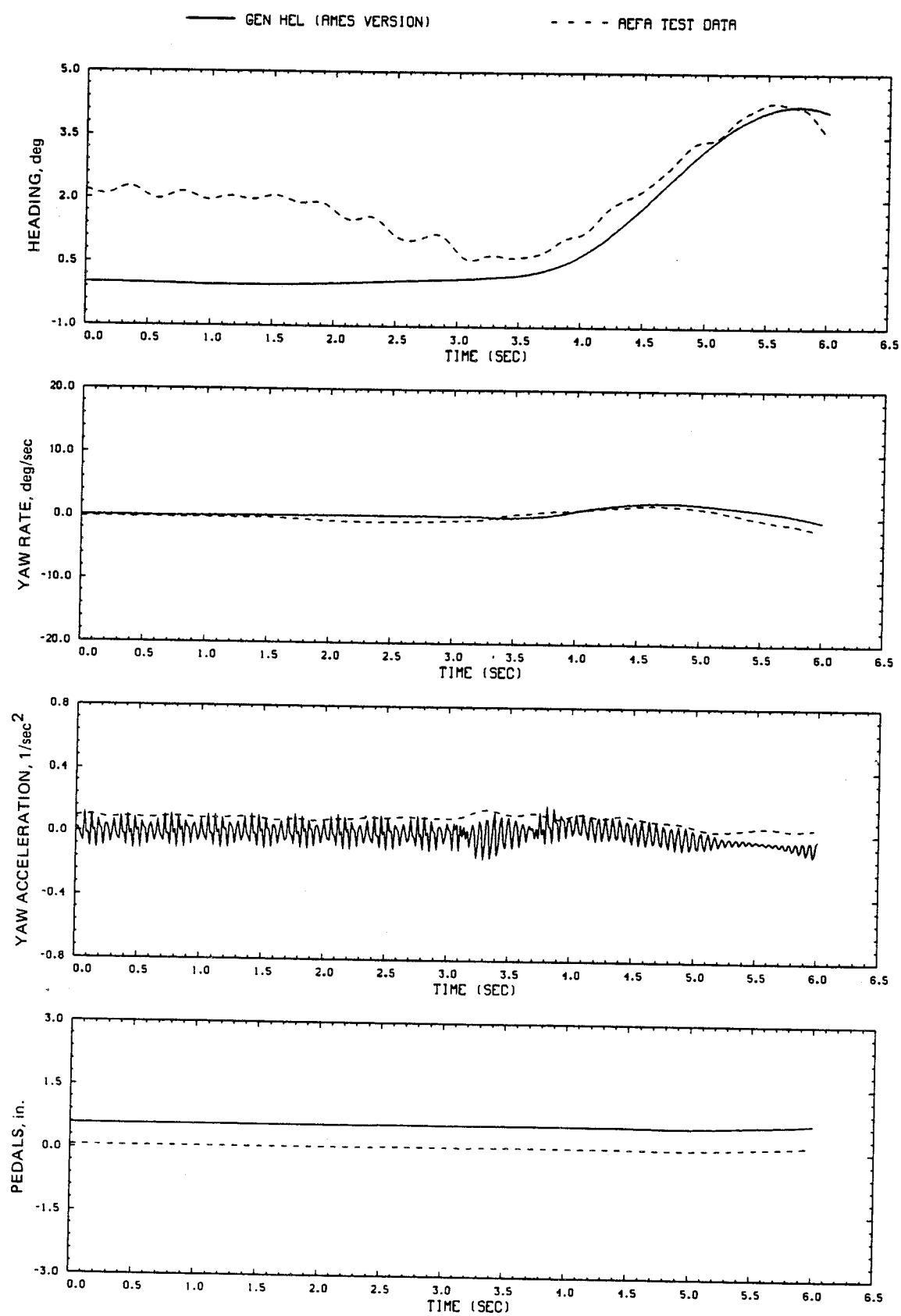


Figure D14.- Continued.

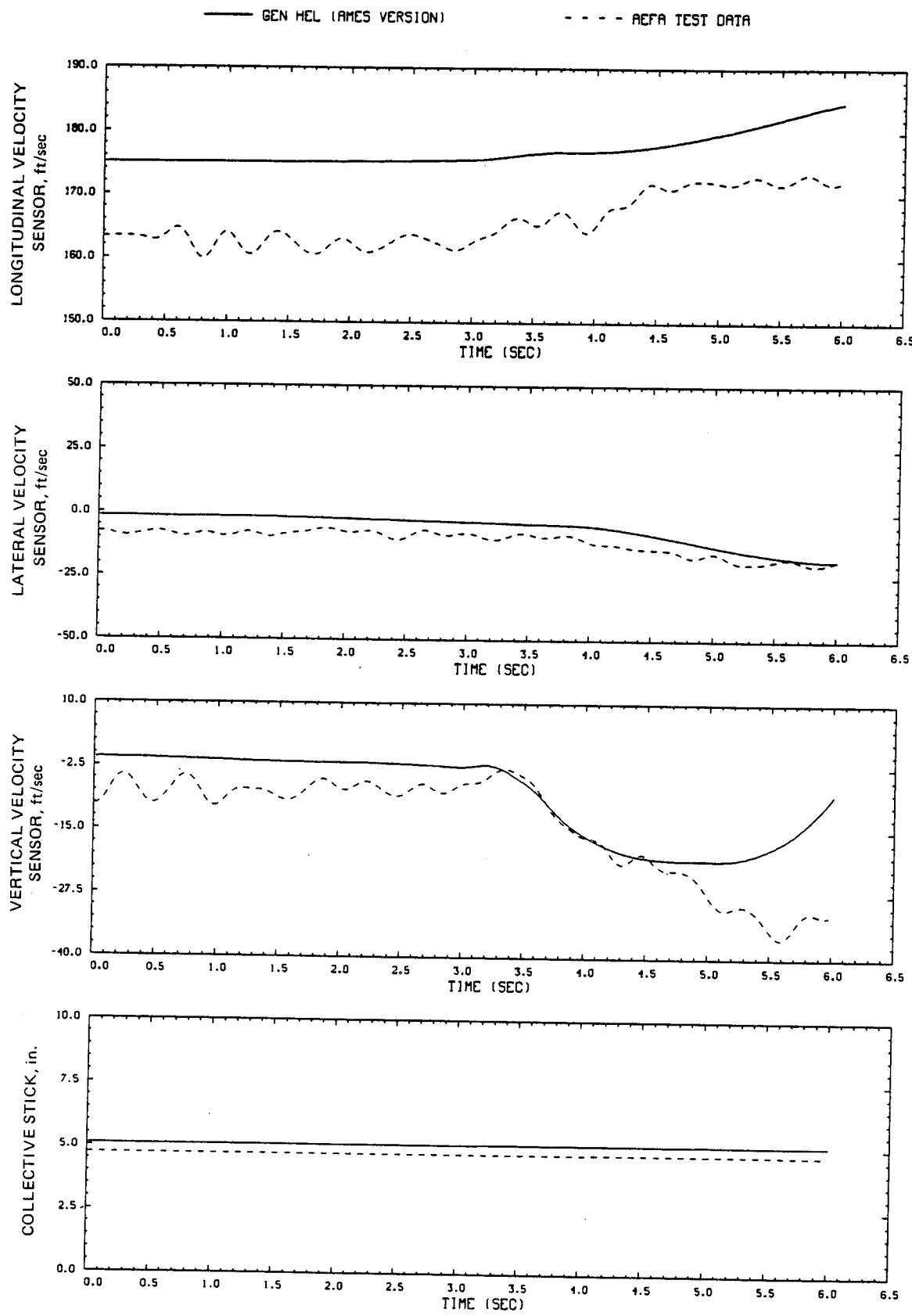


Figure D14.- Continued.

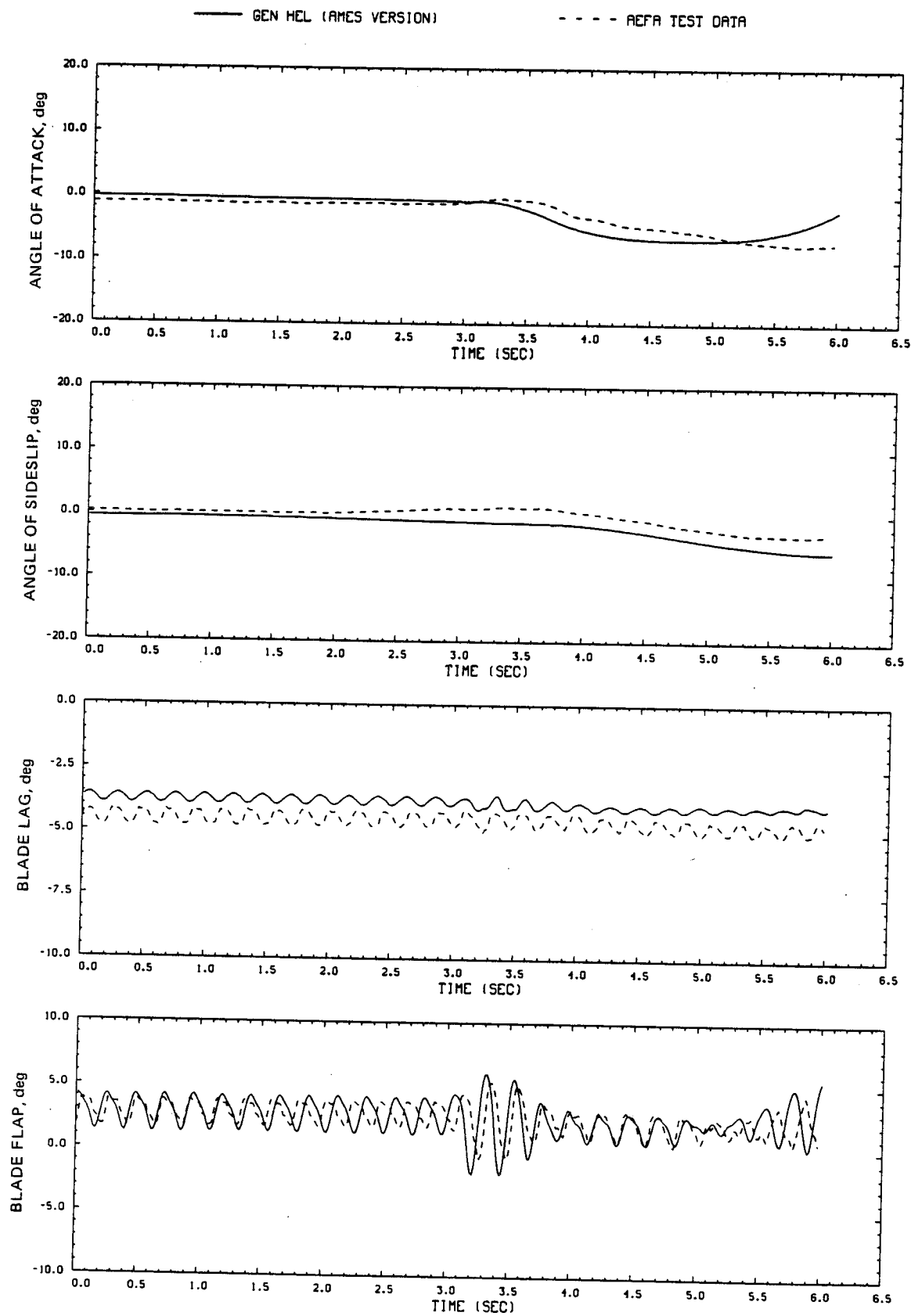


Figure D14.- Continued.

— GEN HEL (AMES VERSION)

- - - RETA TEST DATA

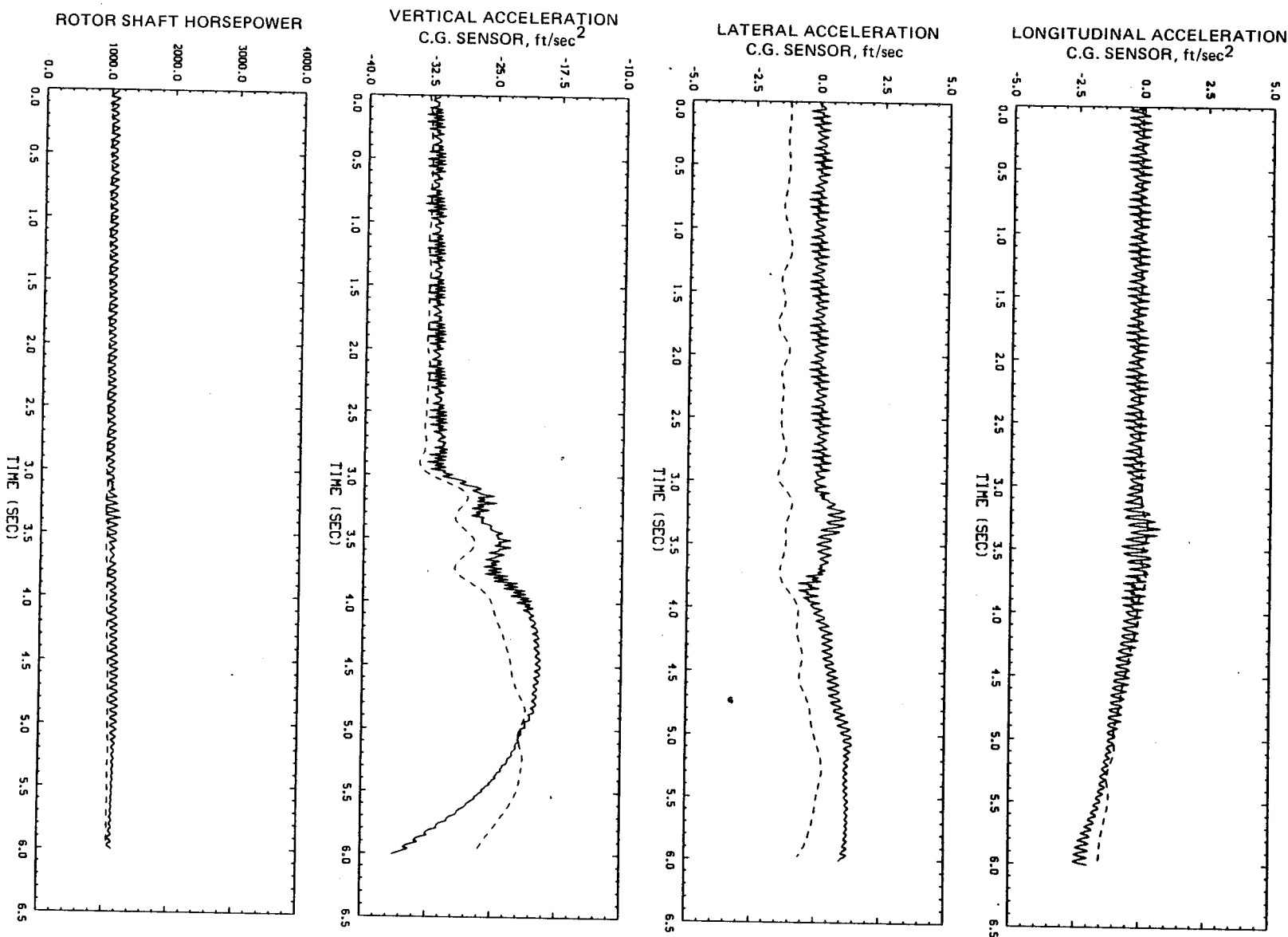


Figure D14.— Continued.

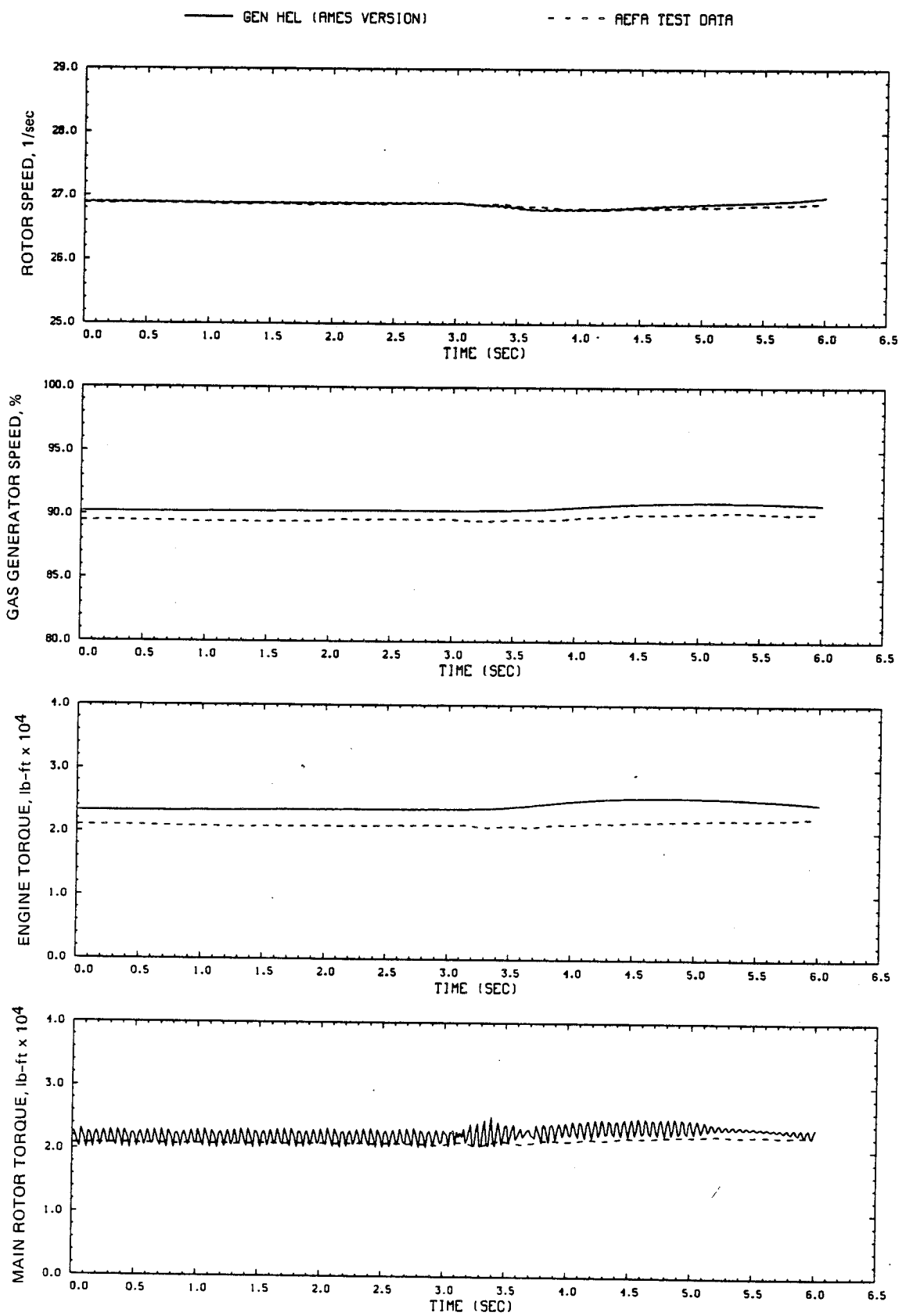


Figure D14.- Concluded.

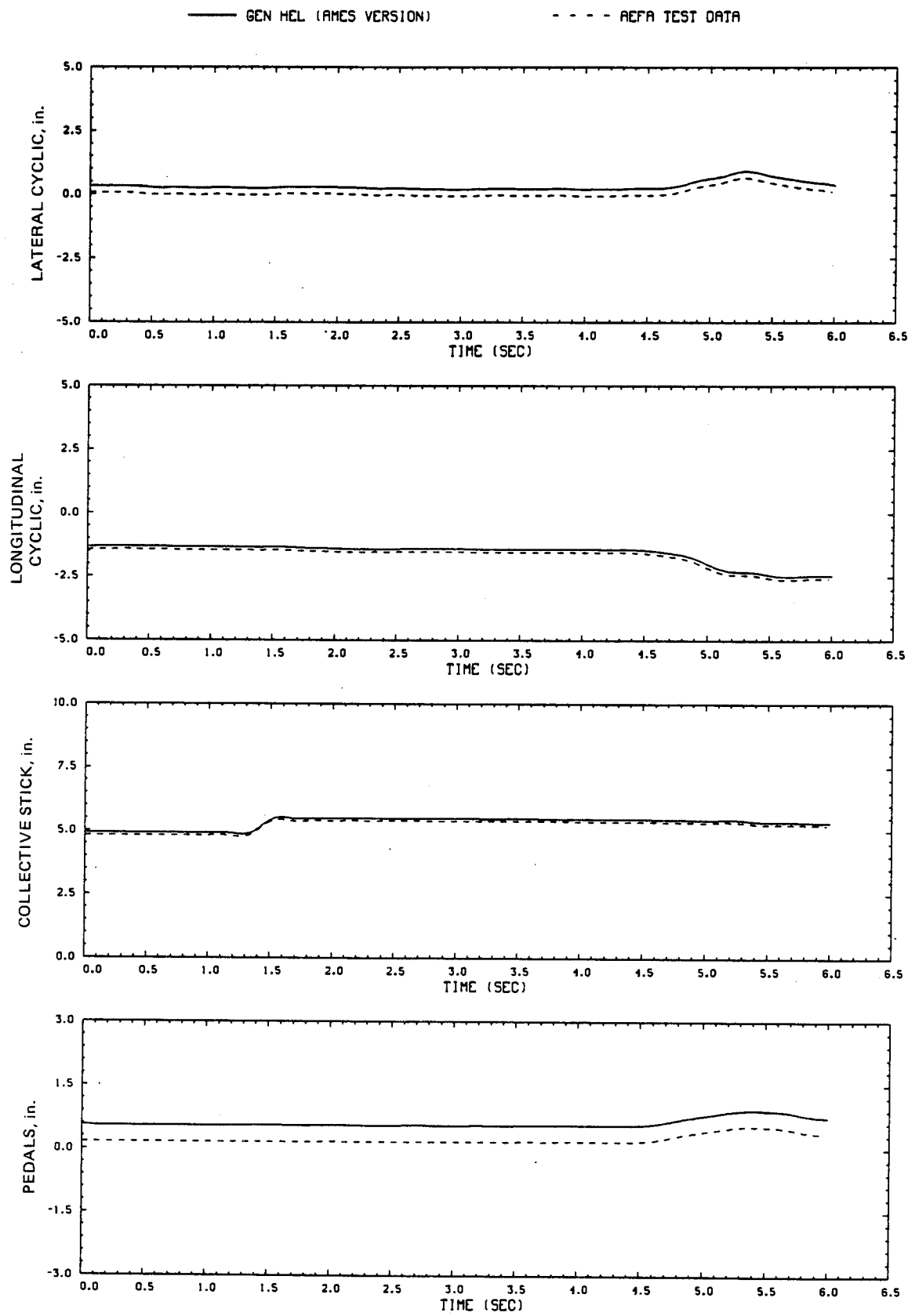


Figure D15.- Comparison of Ames real-time simulation and flight-test data.  
(File 404: 0.5-in. up collective input, 100 knots)

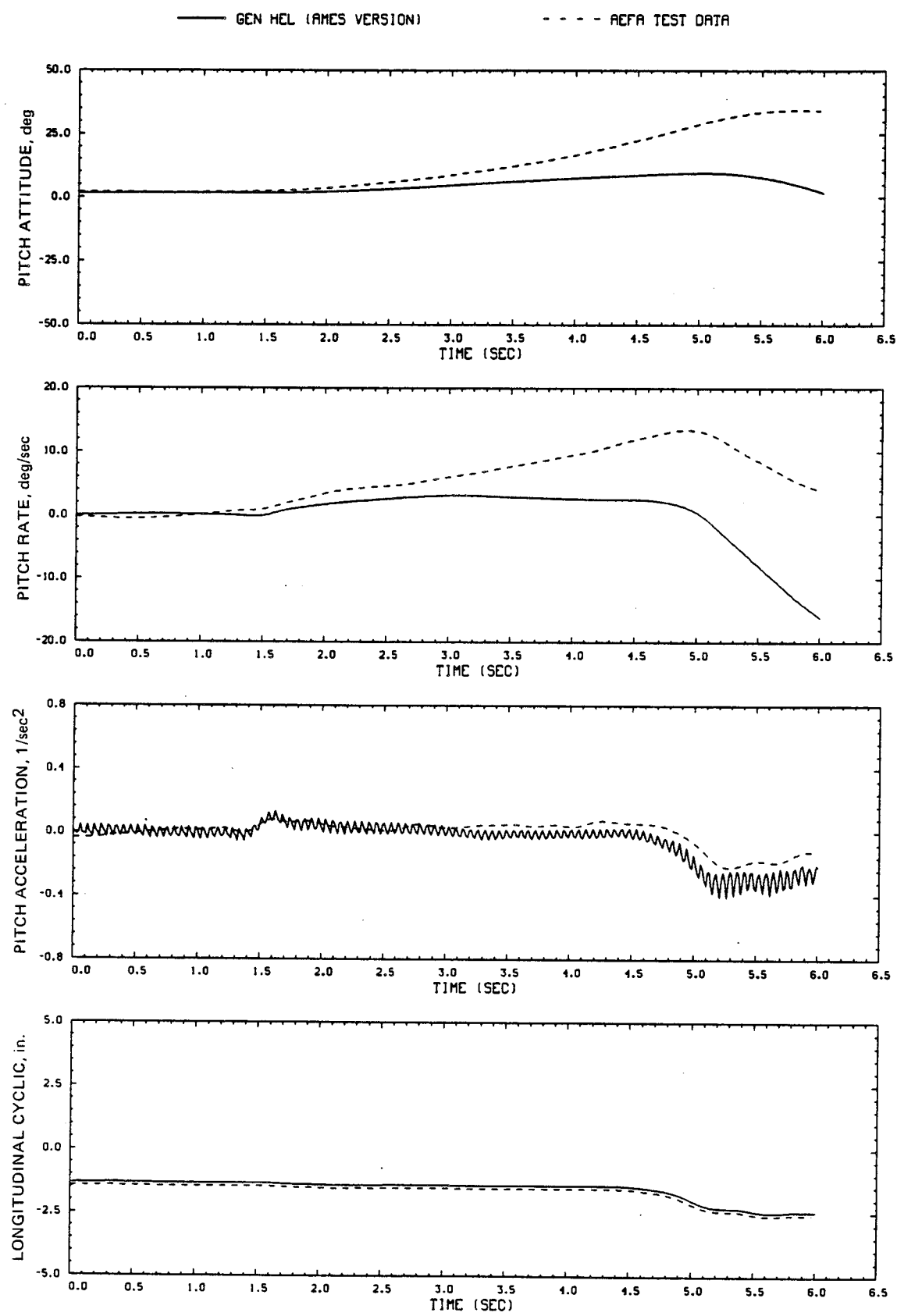


Figure D15.- Continued.

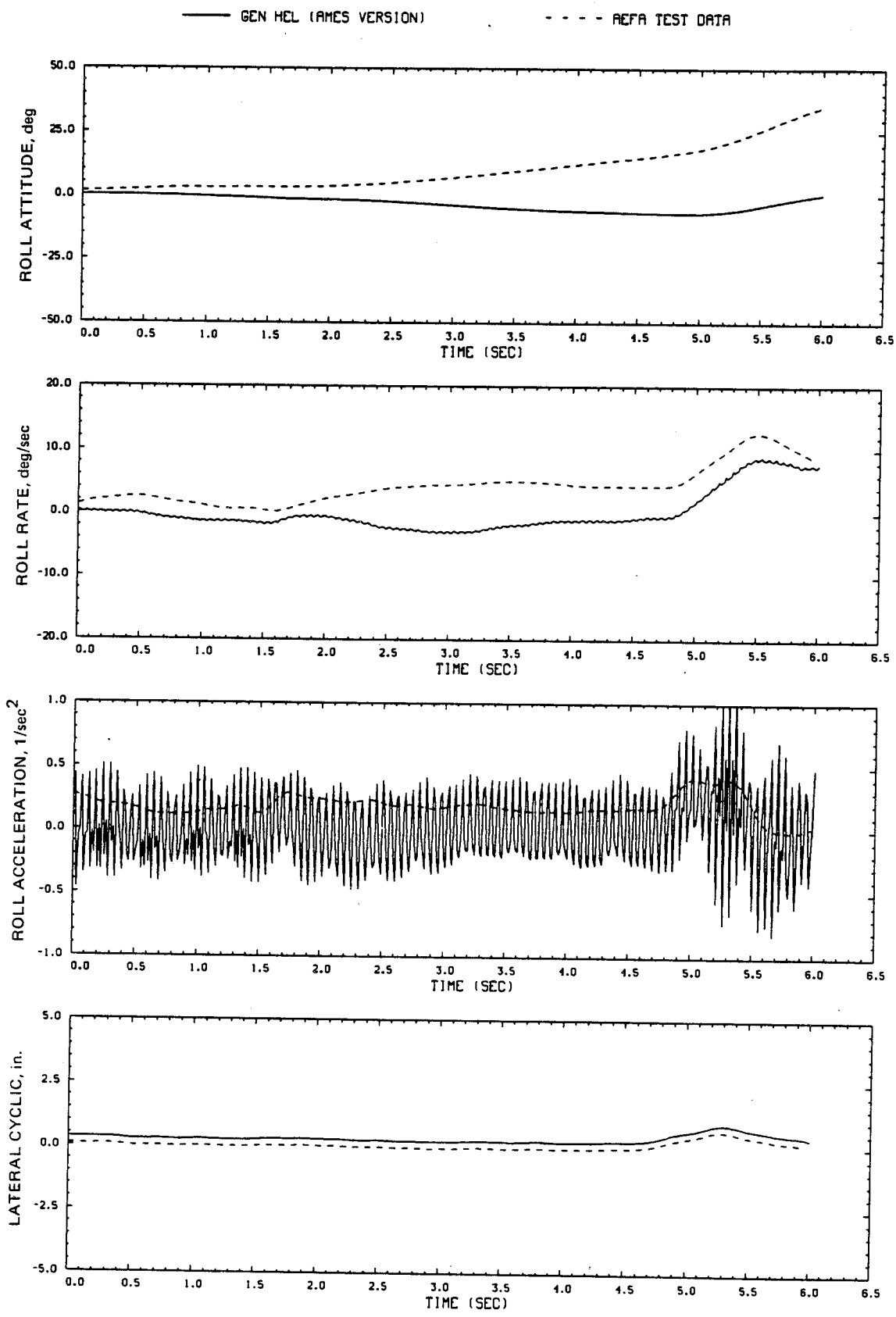


Figure D15.- Continued.

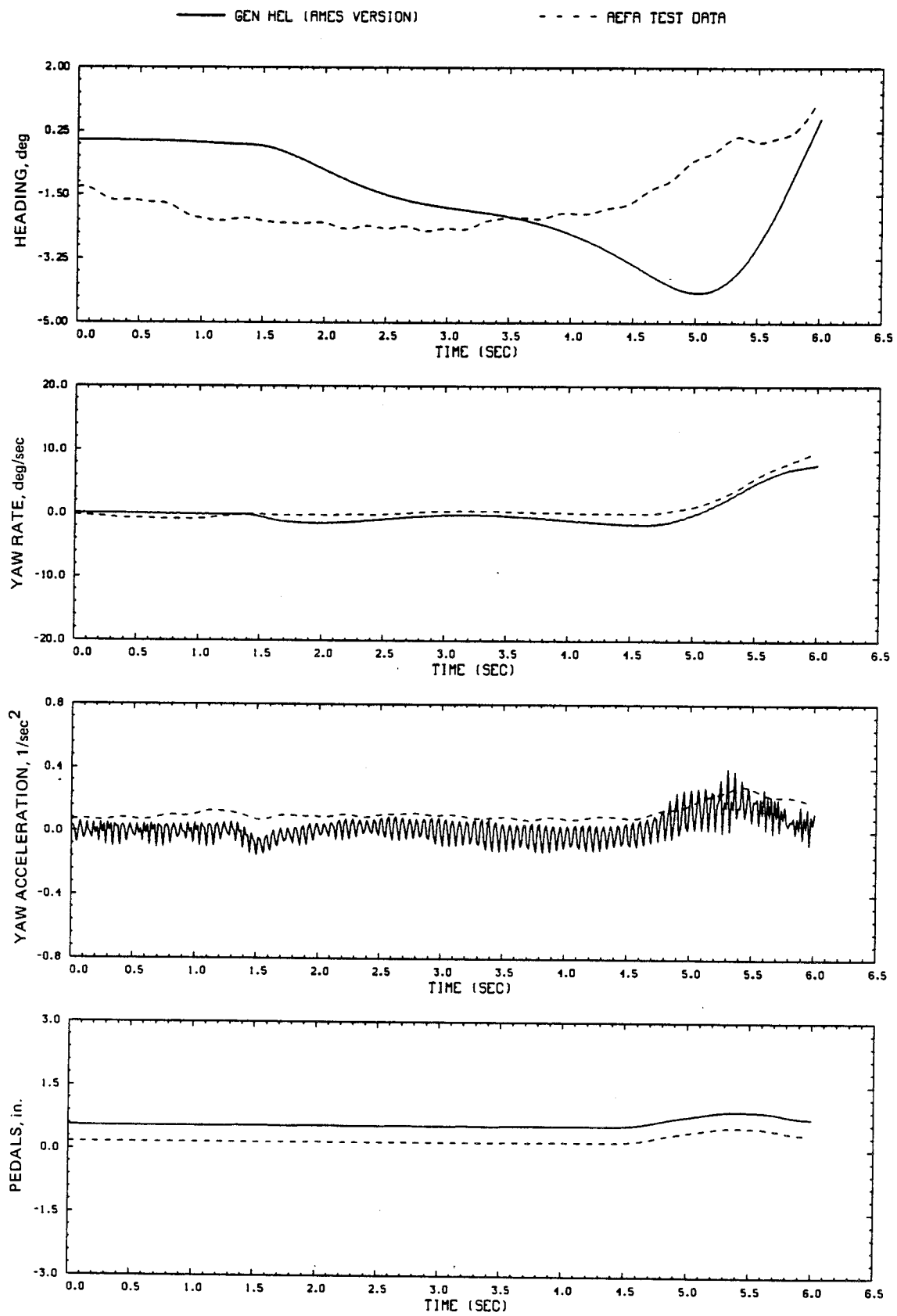
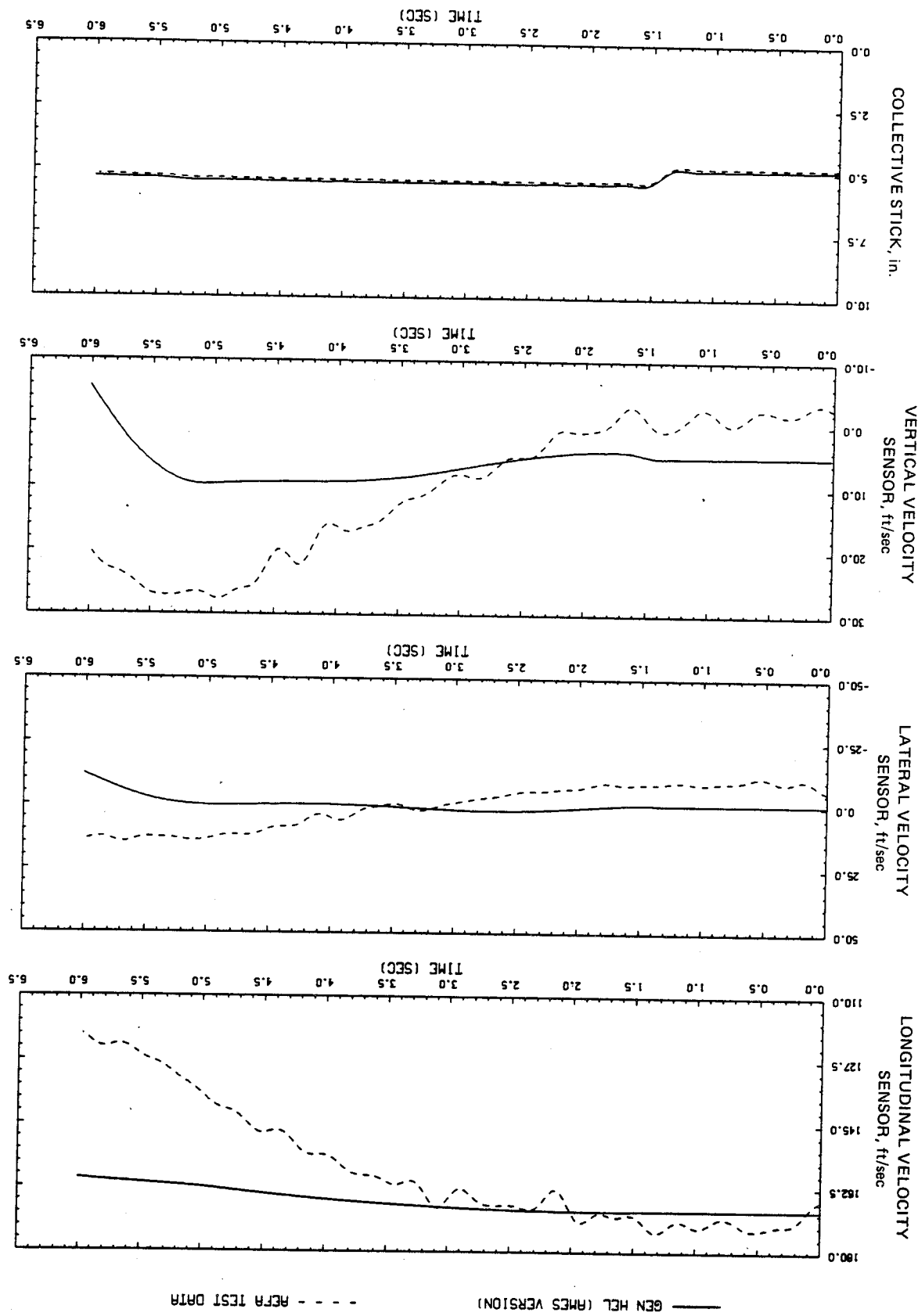


Figure D15.- Continued.

Figure D15. - Continued.



— GEN HCL (AMES VERSION)    - - - ACFR TEST DATA

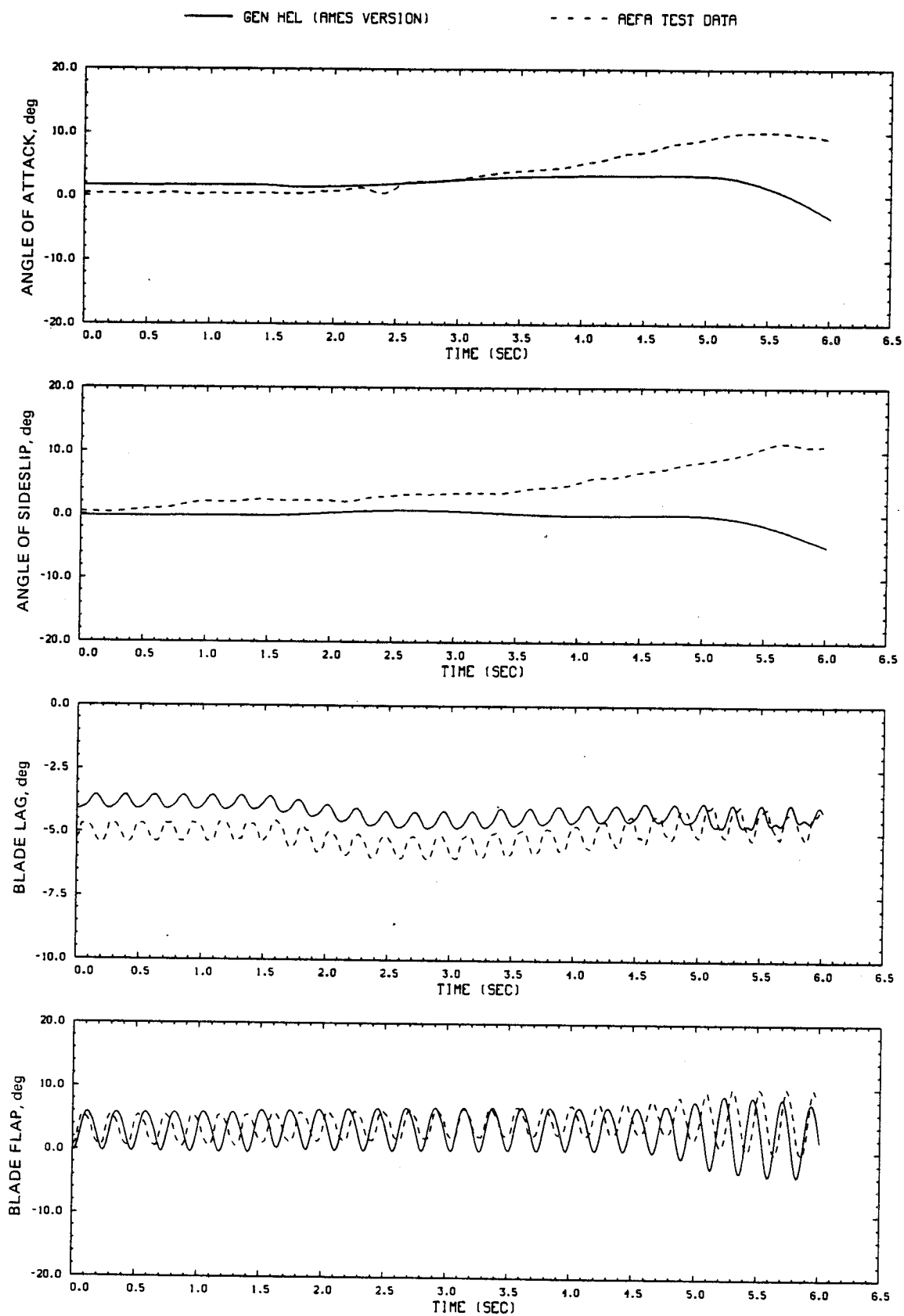


Figure D15.- Continued.

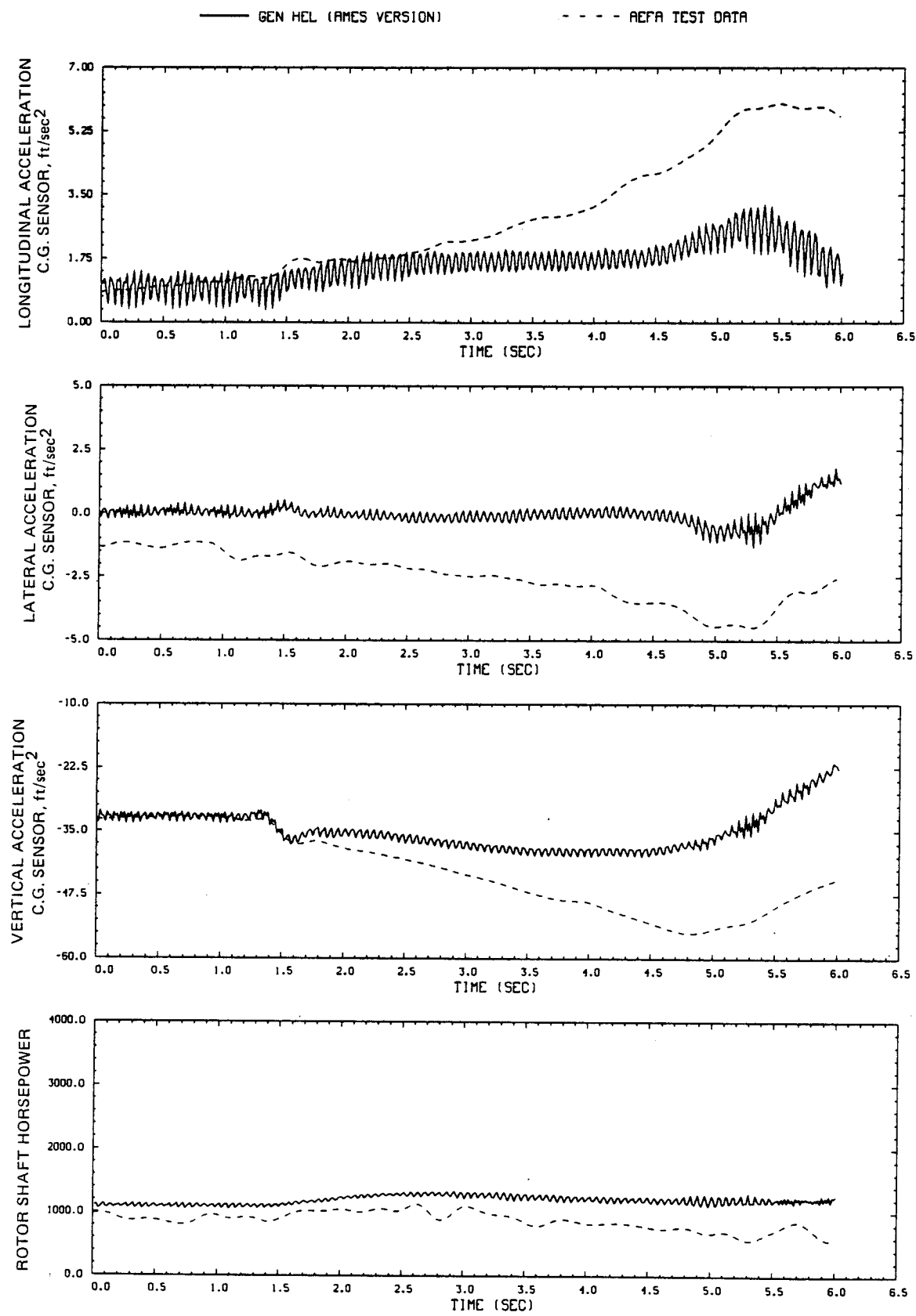


Figure D15.- Continued.

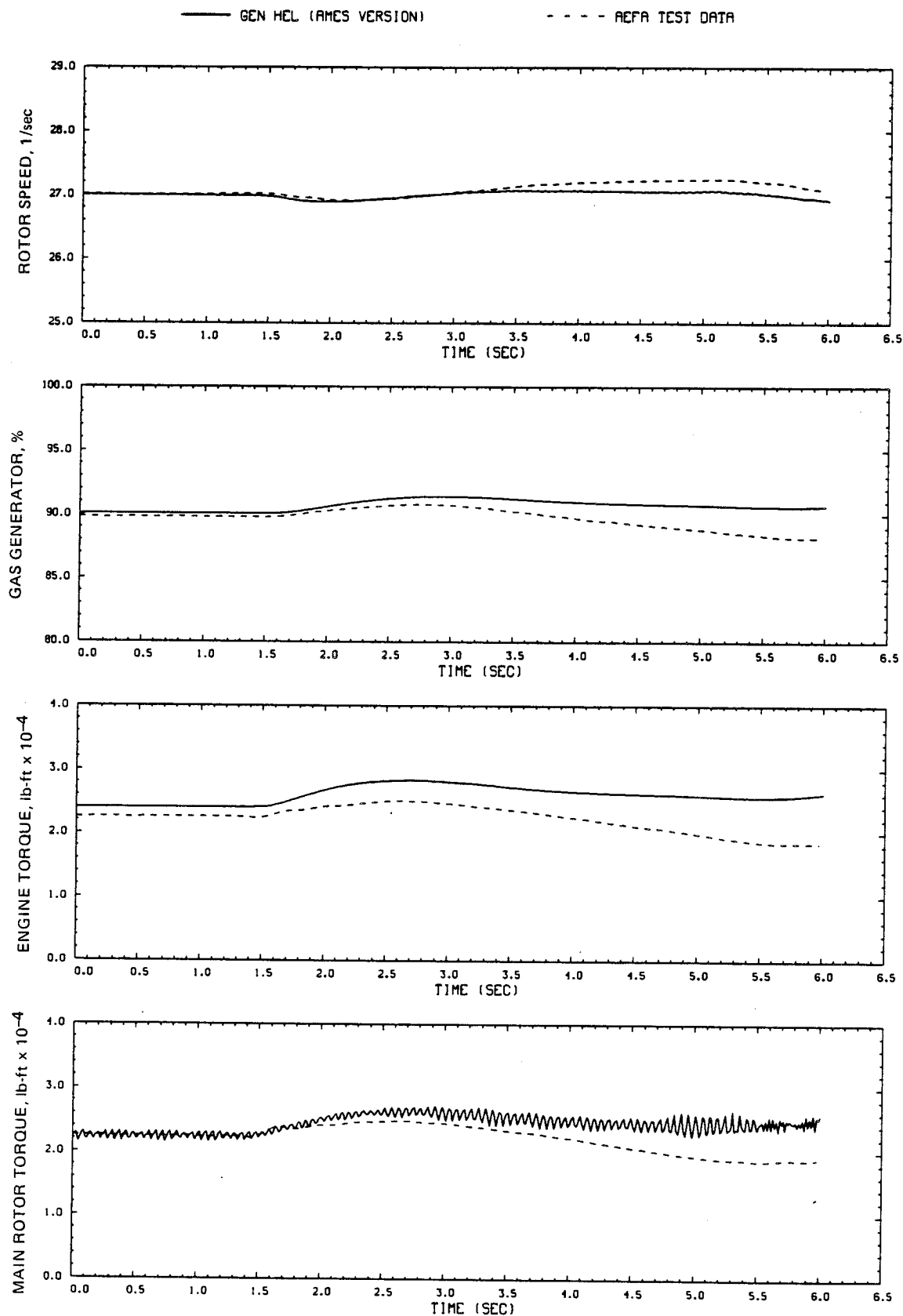


Figure D15.- Concluded.

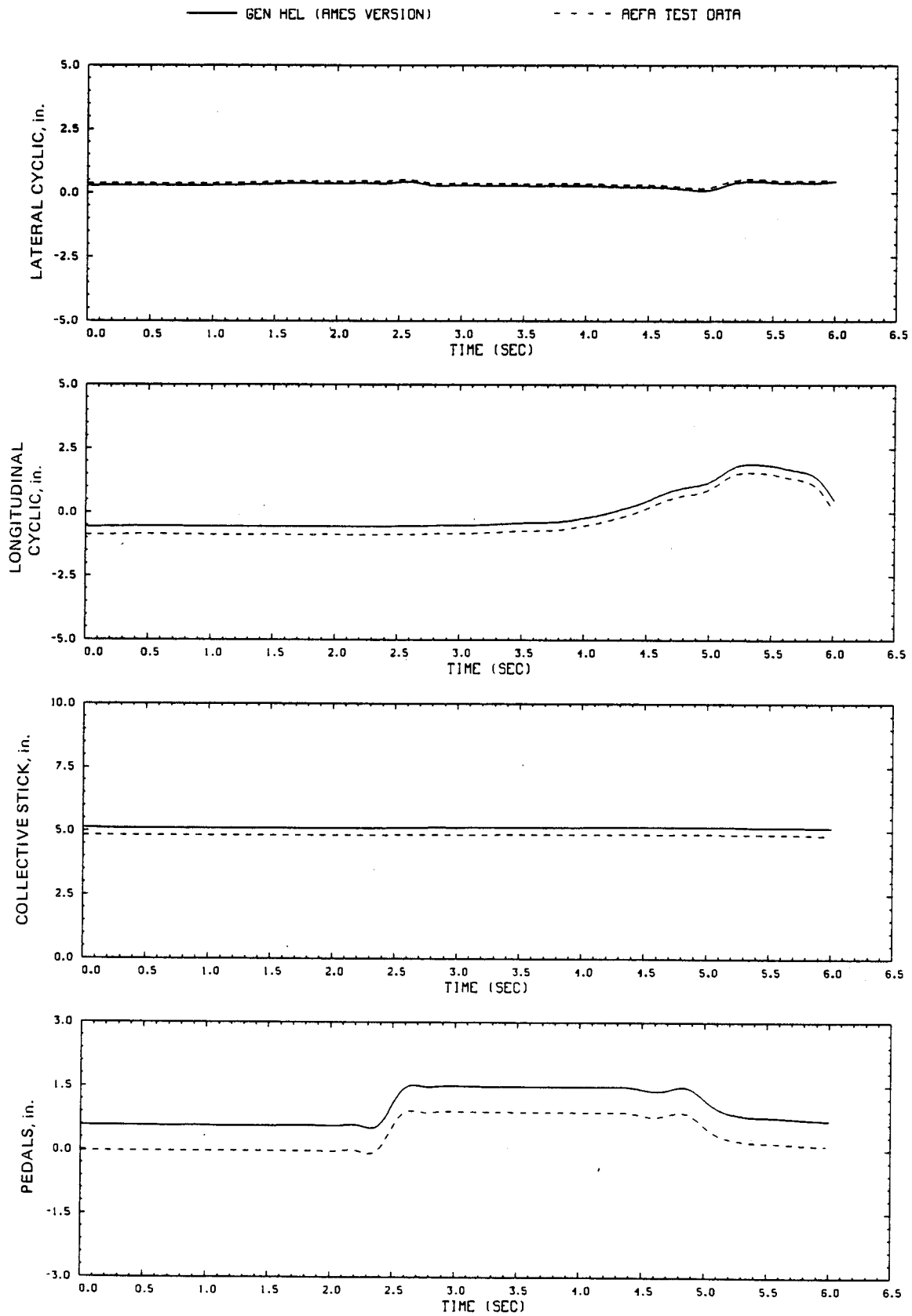


Figure D16.- Comparison of Ames real-time simulation and flight-test data.  
(File 102: 1-in. right pedal input, 100 knots)

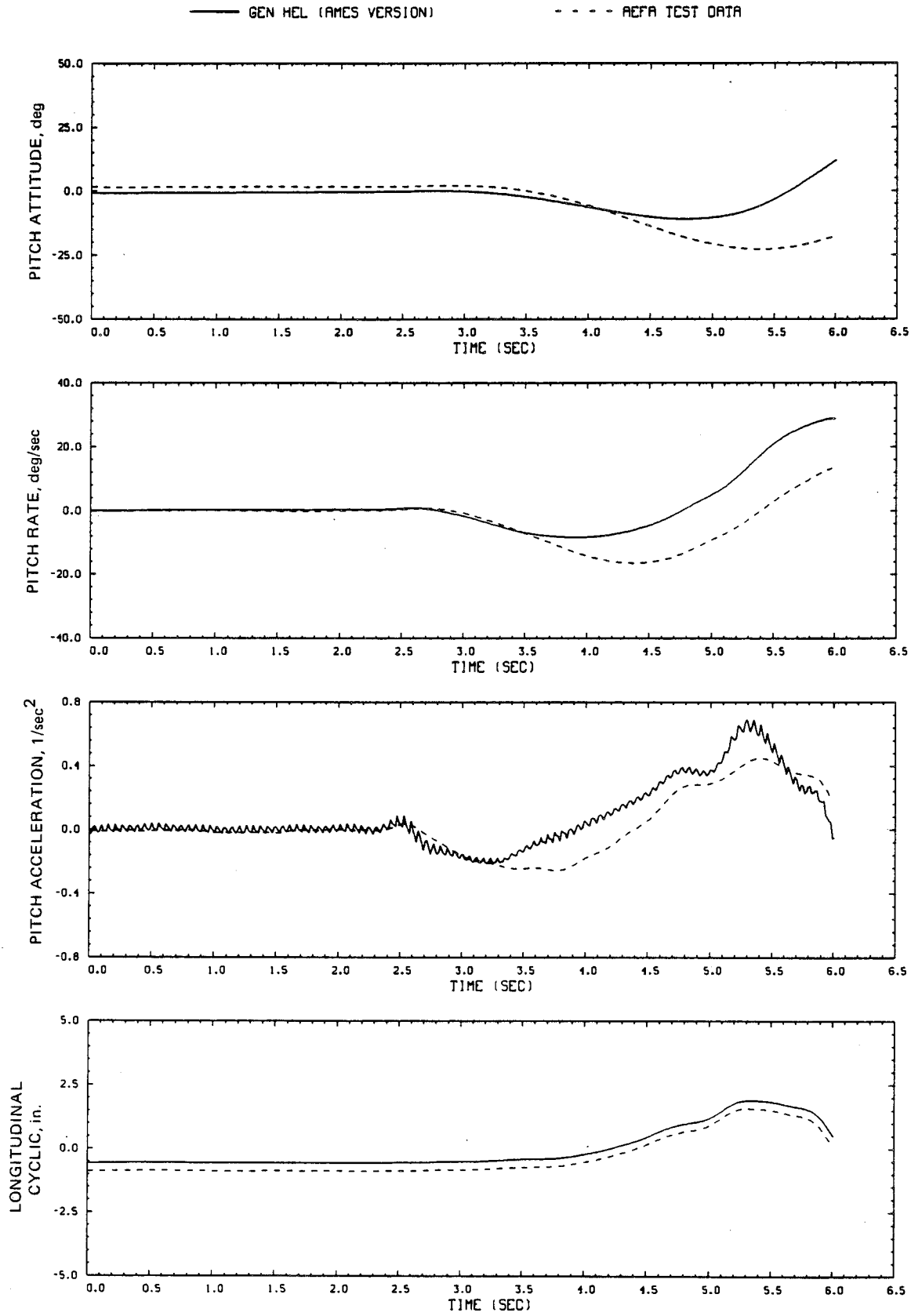


Figure D16.- Continued.

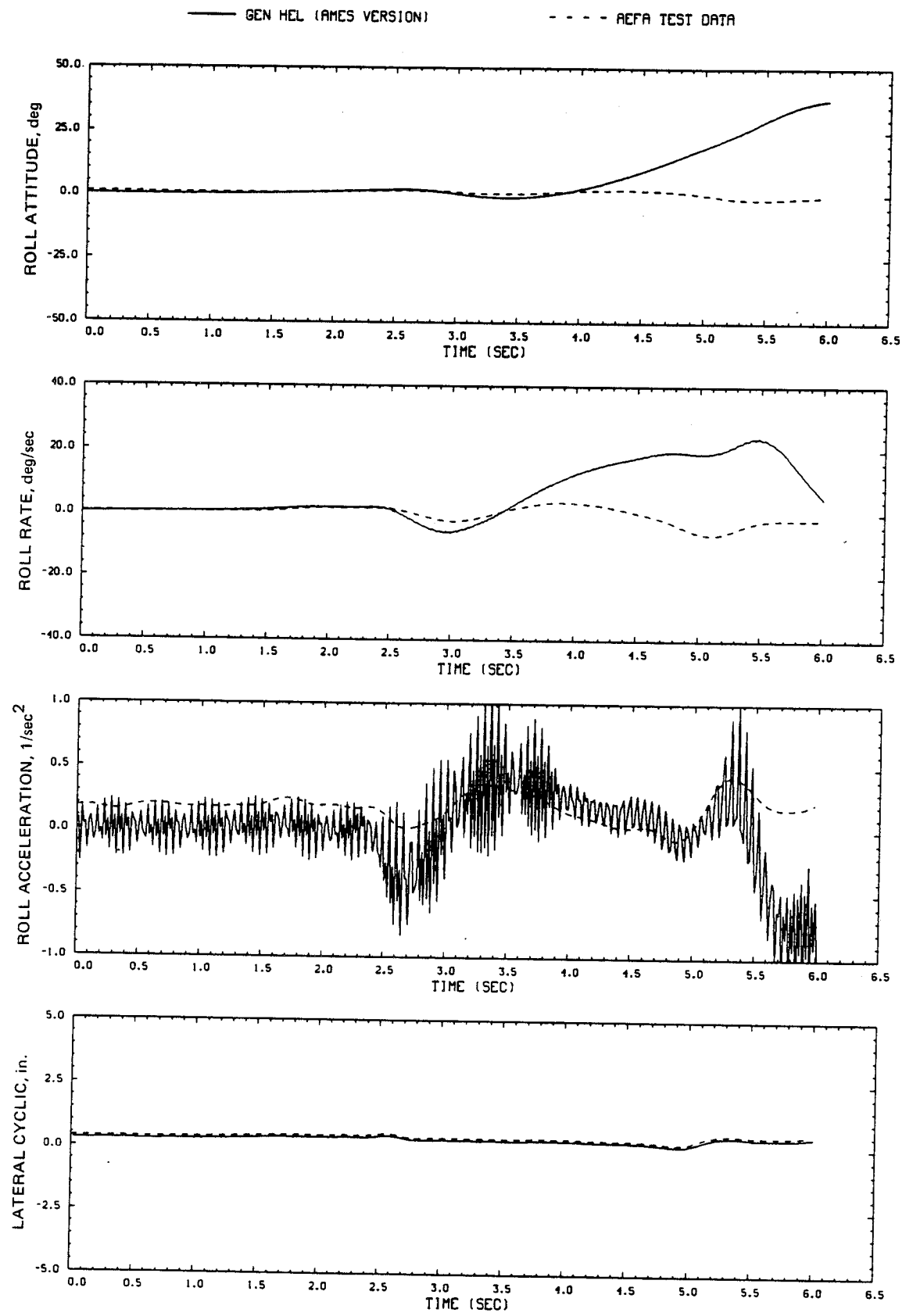


Figure D16.- Continued.

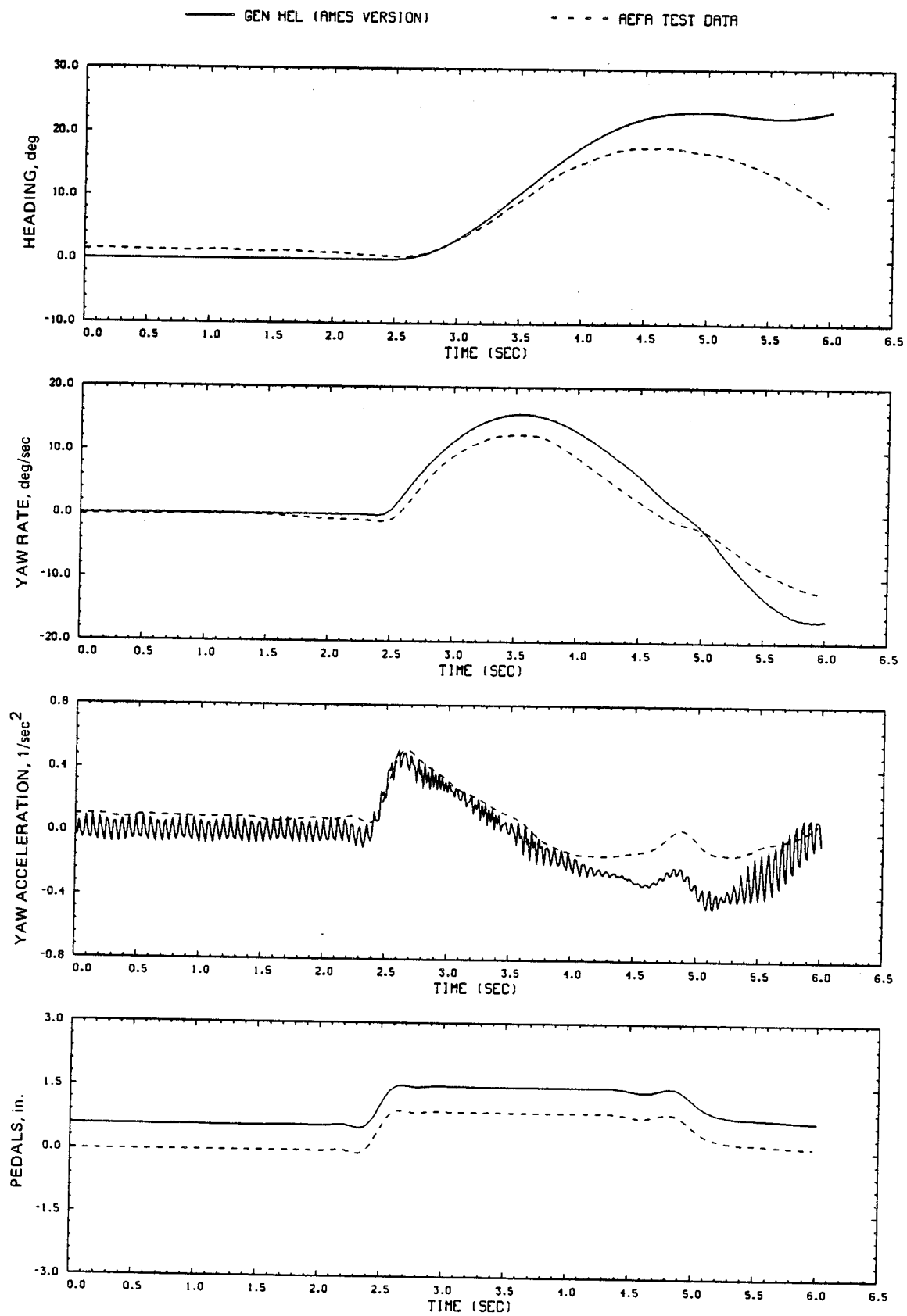


Figure D16.- Continued.

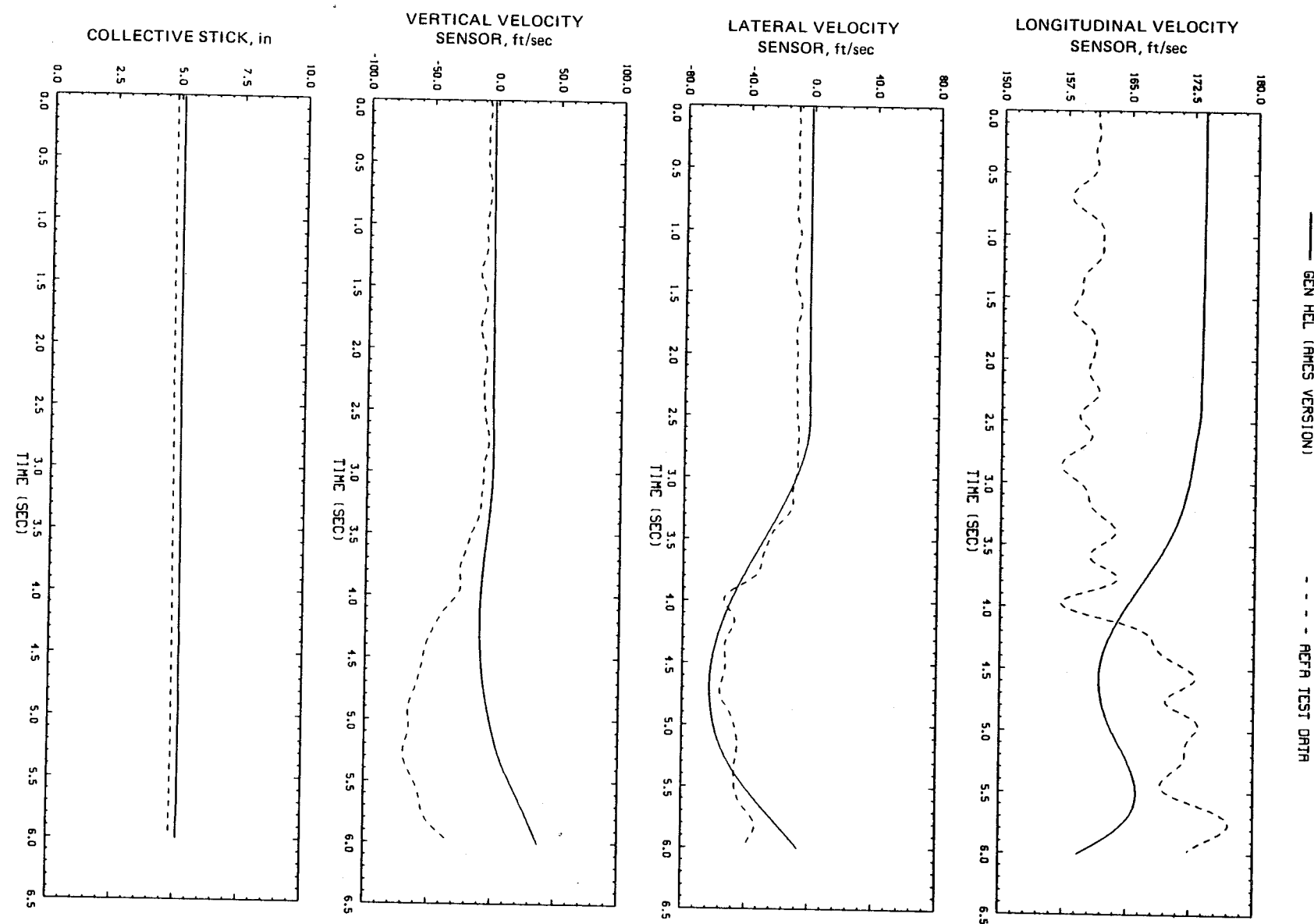


Figure D16.- Continued.

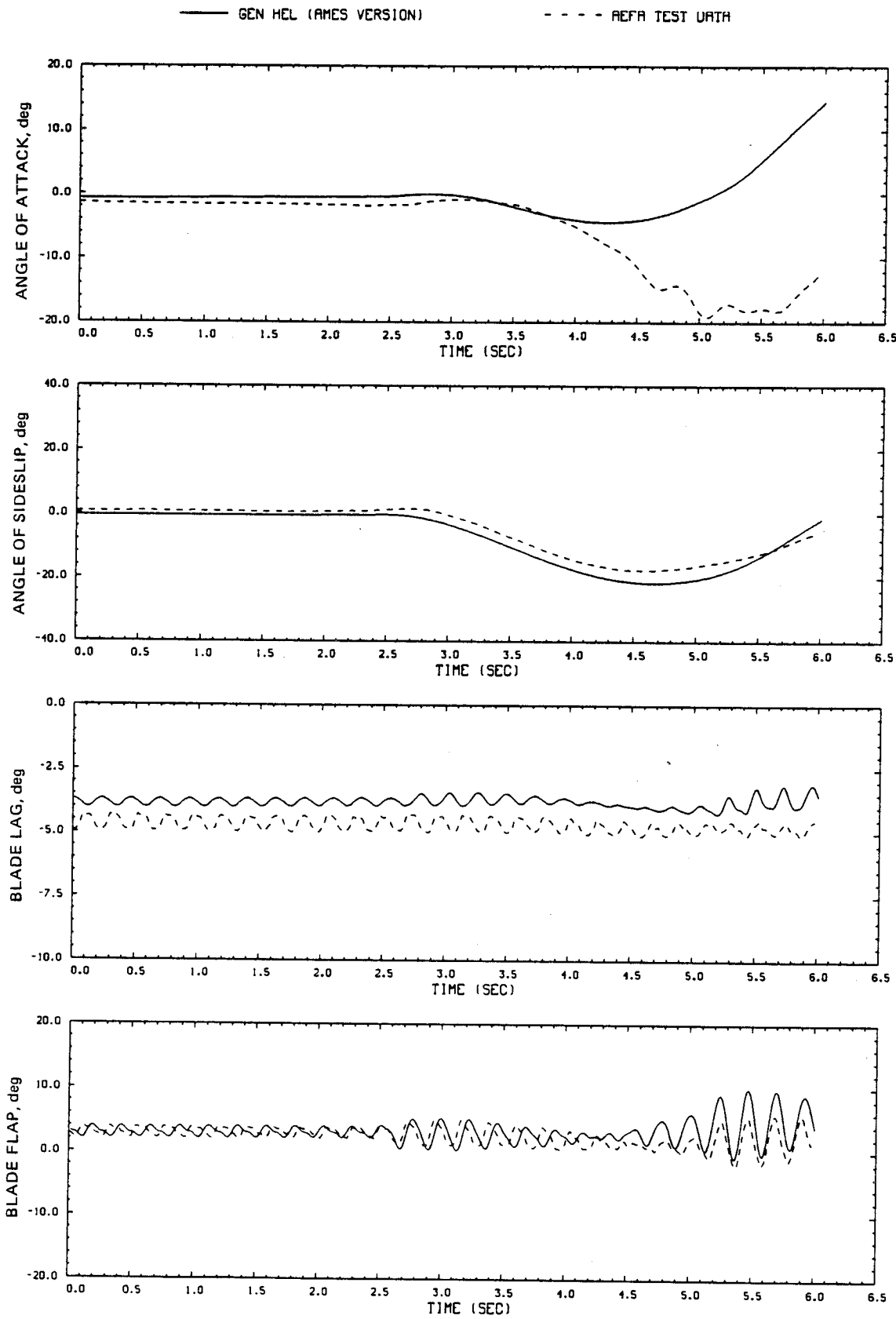


Figure D16.- Continued.

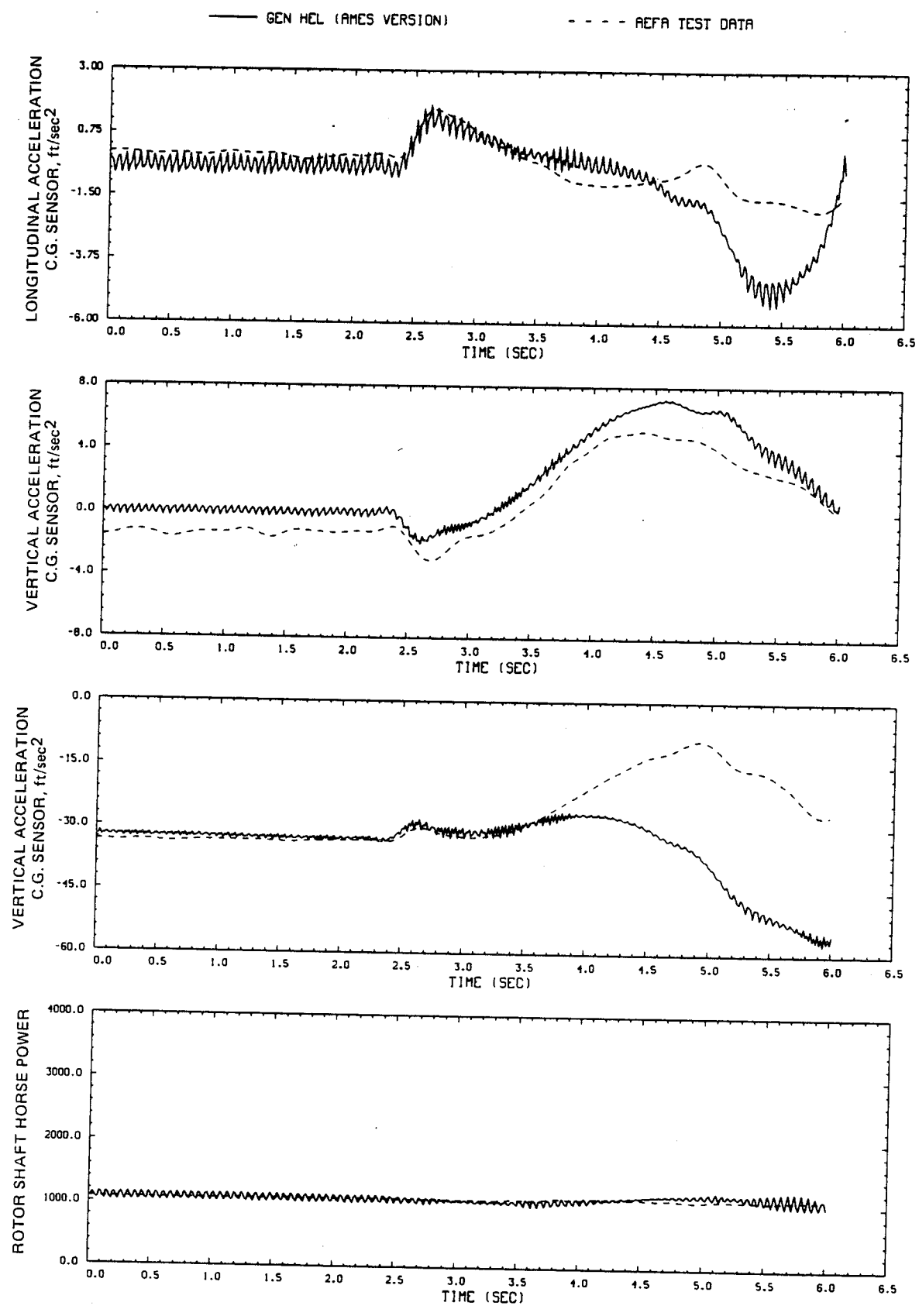


Figure D16.- Continued.

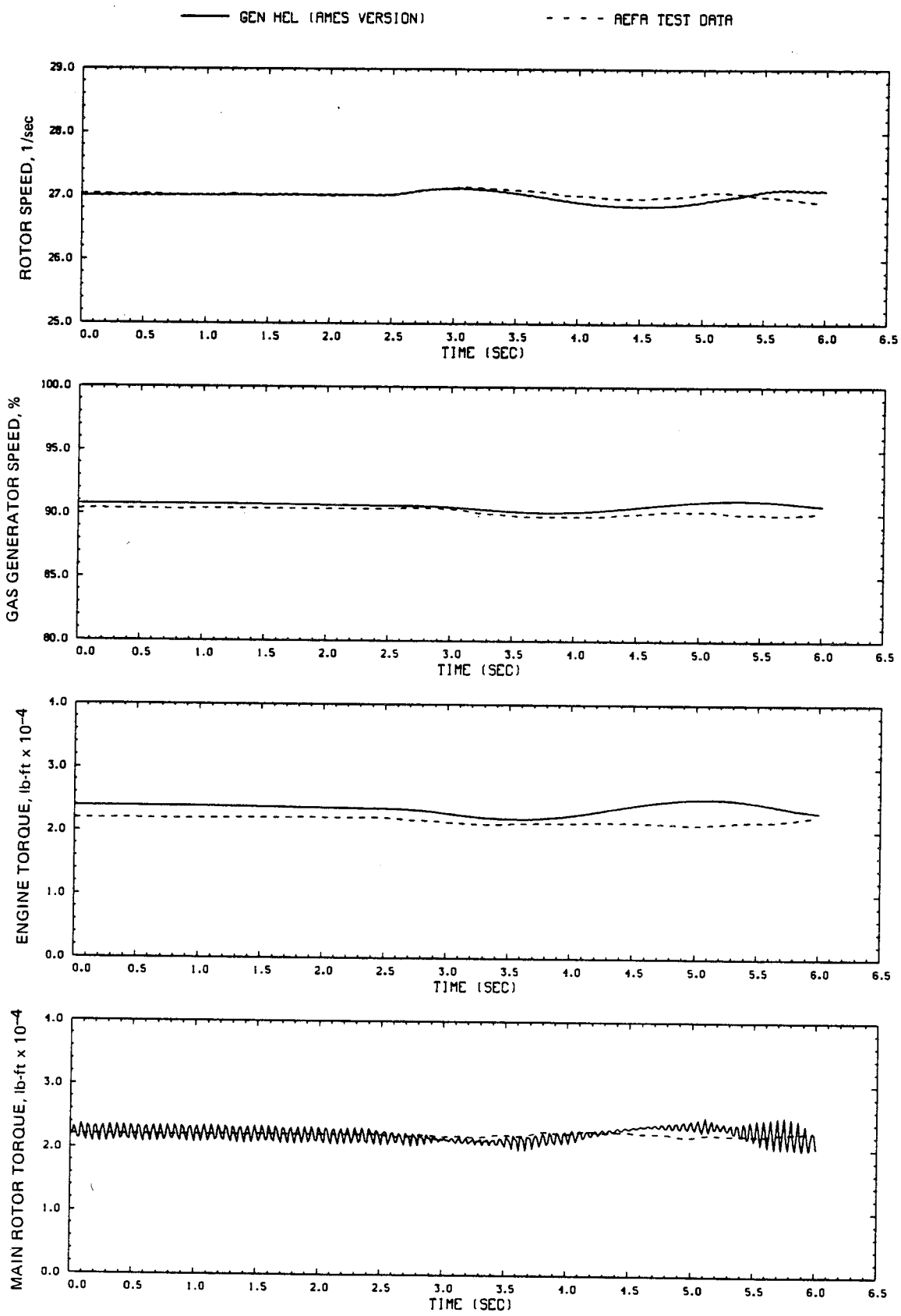


Figure D16.- Concluded.

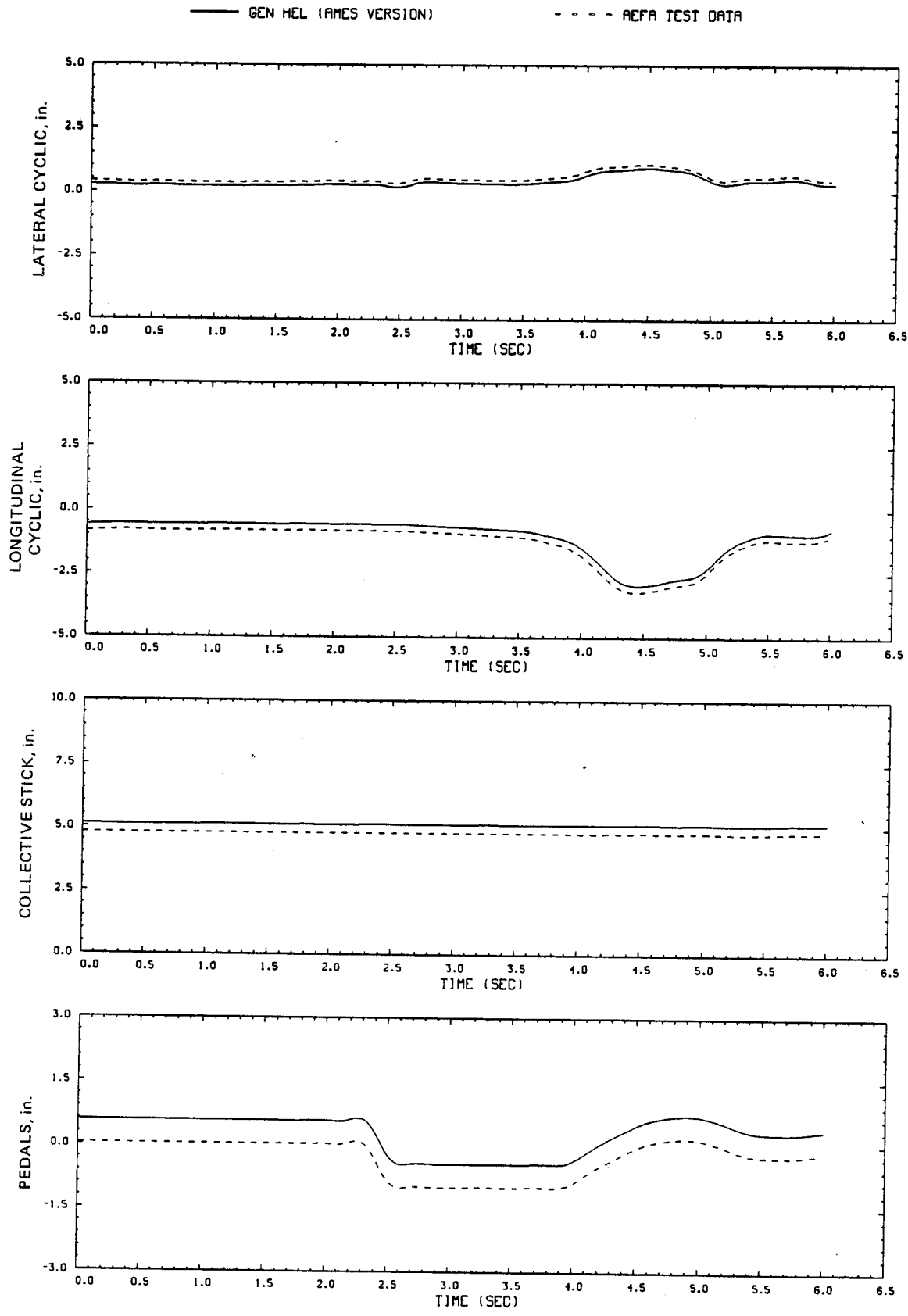


Figure D17.- Comparison of Ames real-time simulation and flight-test data.  
(File 103: 1-in. left pedal input, 100 knots)

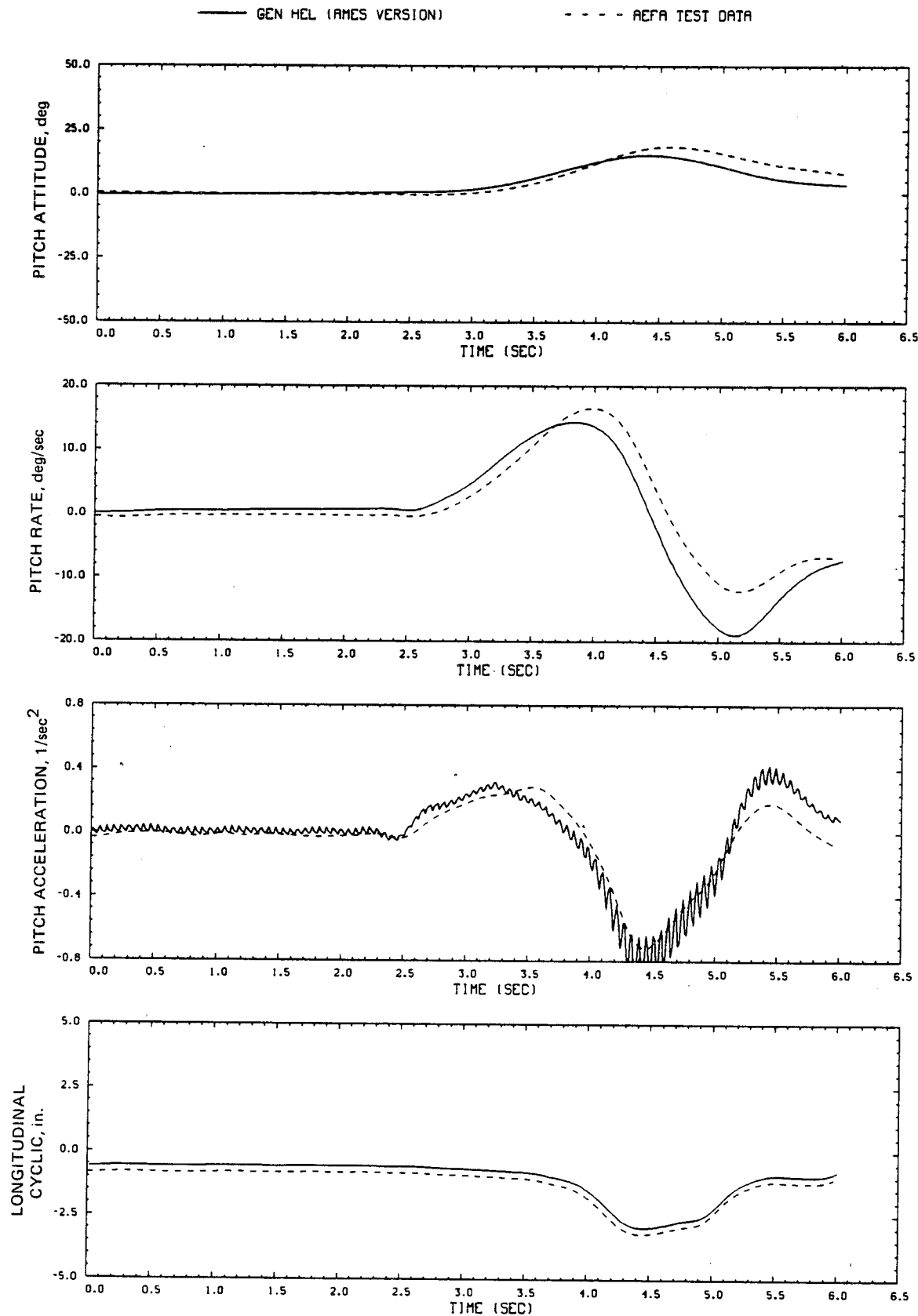


Figure D17.- Continued.

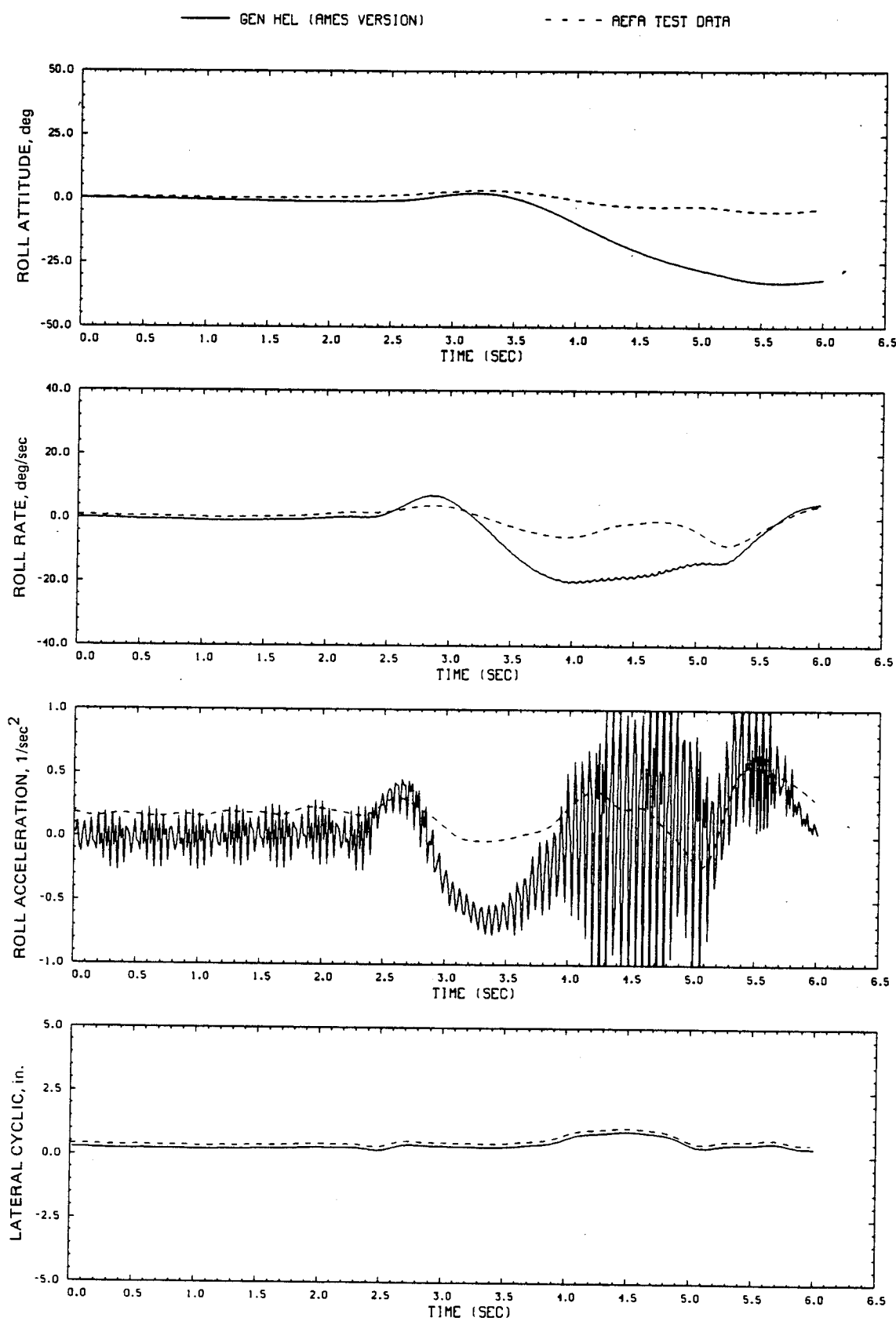


Figure D17.- Continued.

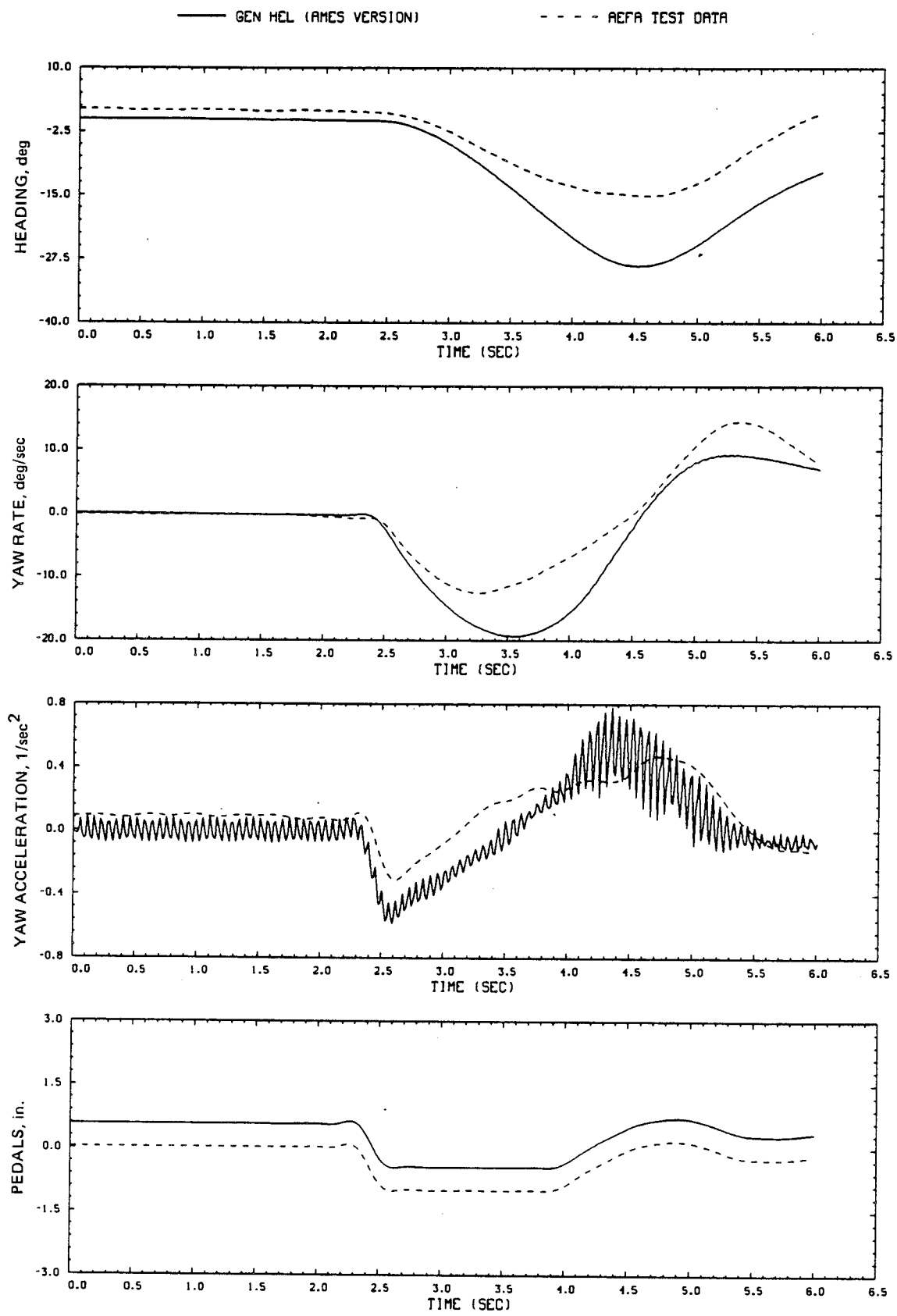


Figure D17.- Continued.

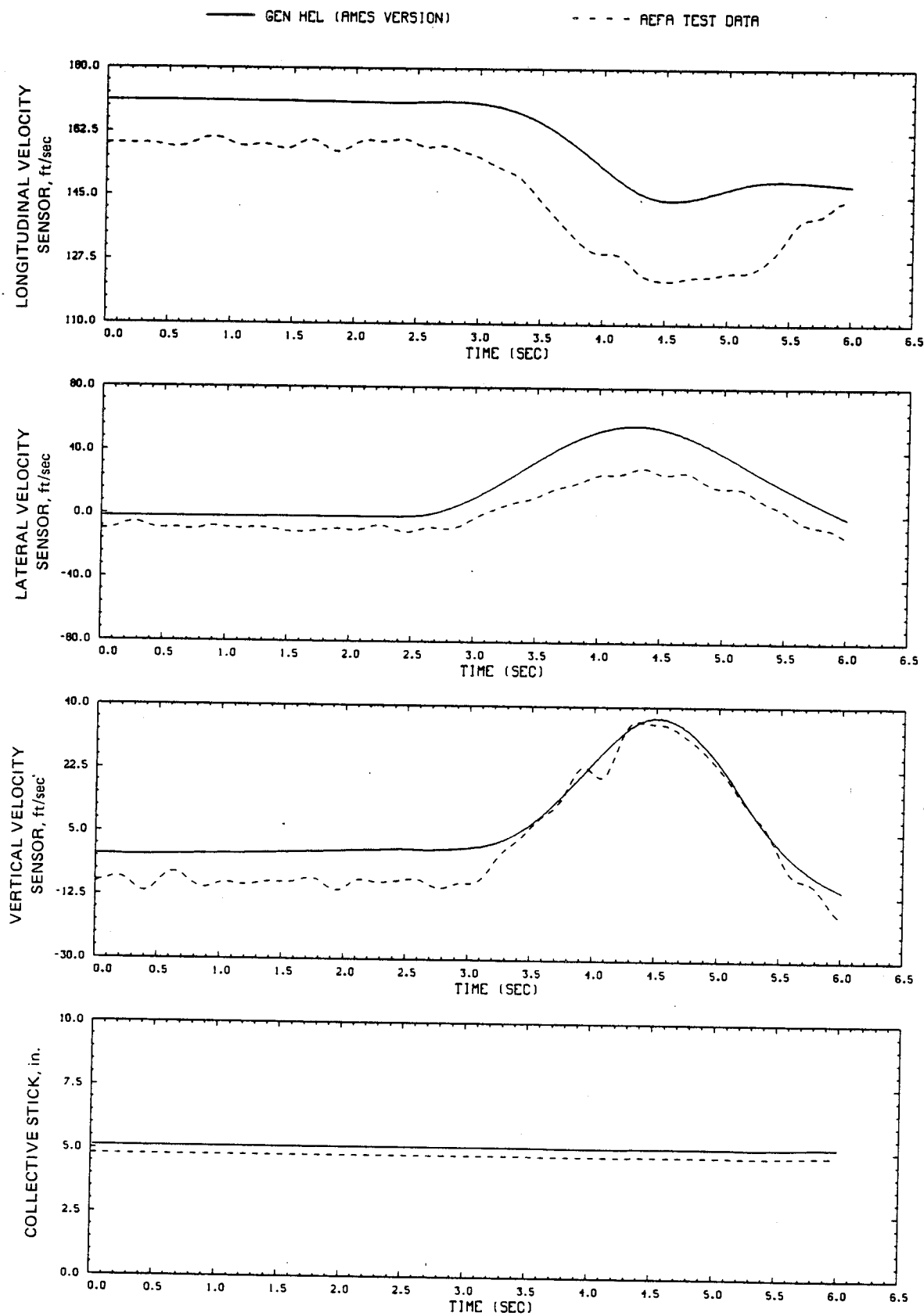


Figure D17.- Continued.

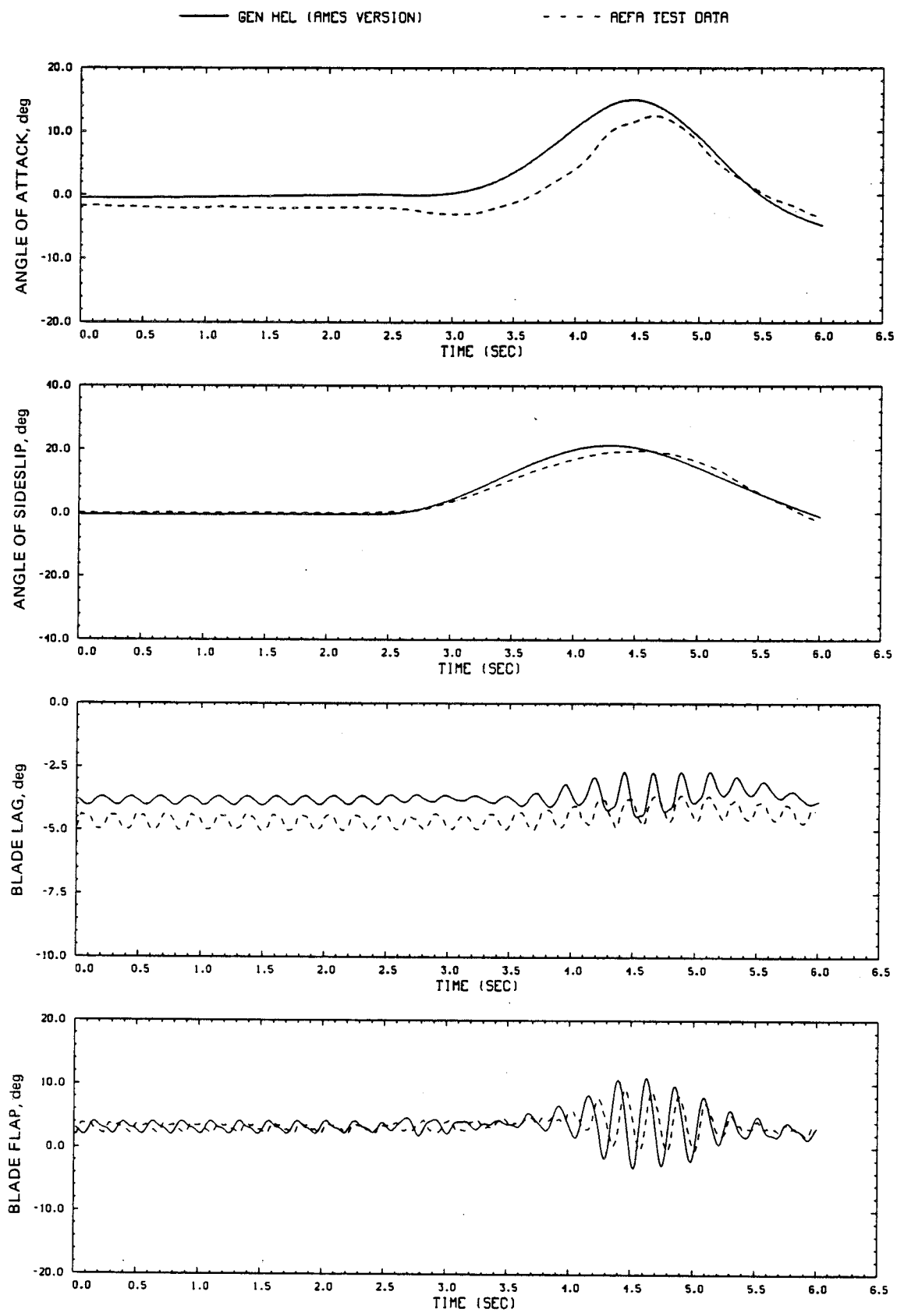


Figure D17.- Continued.

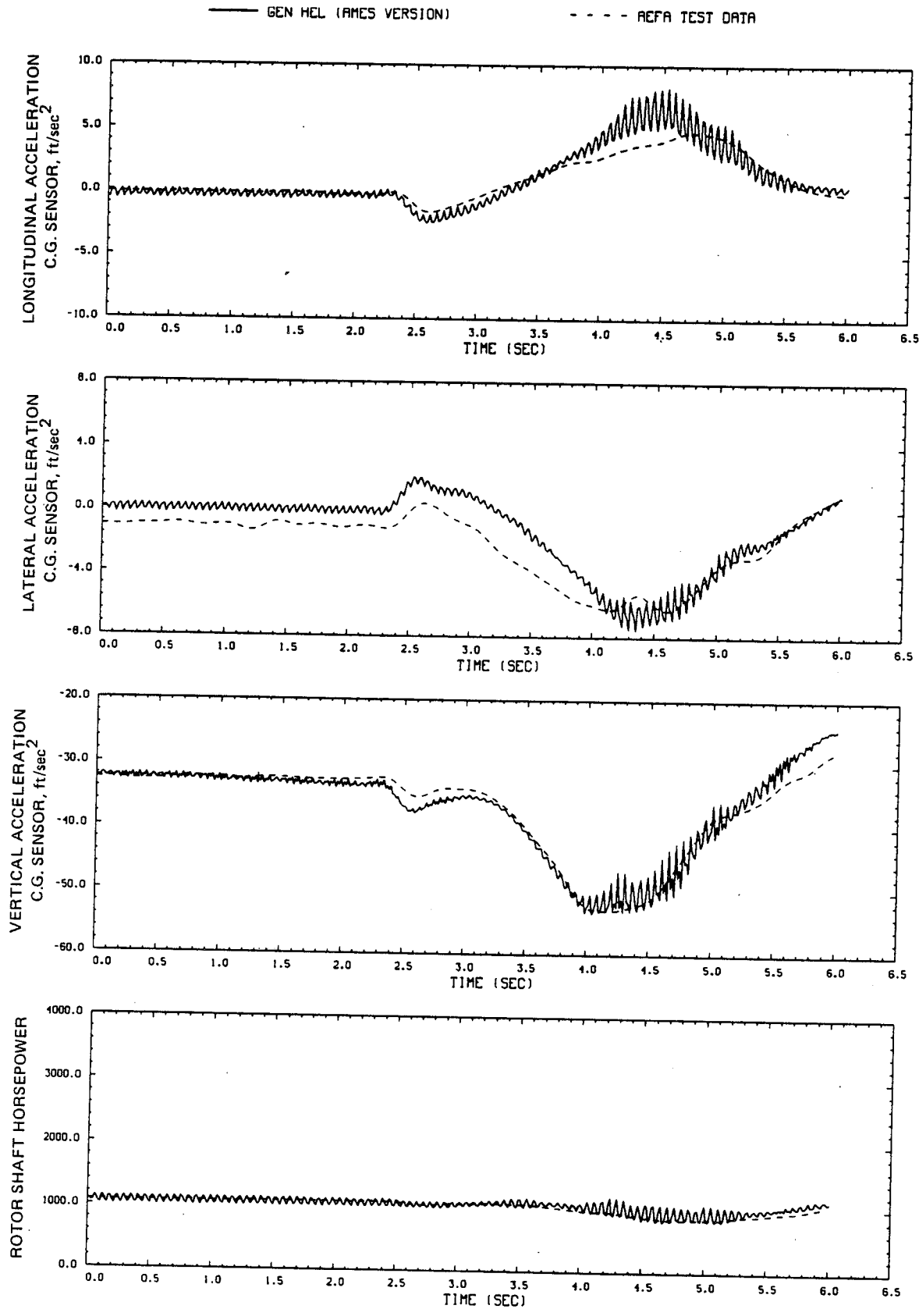


Figure D17.- Continued.

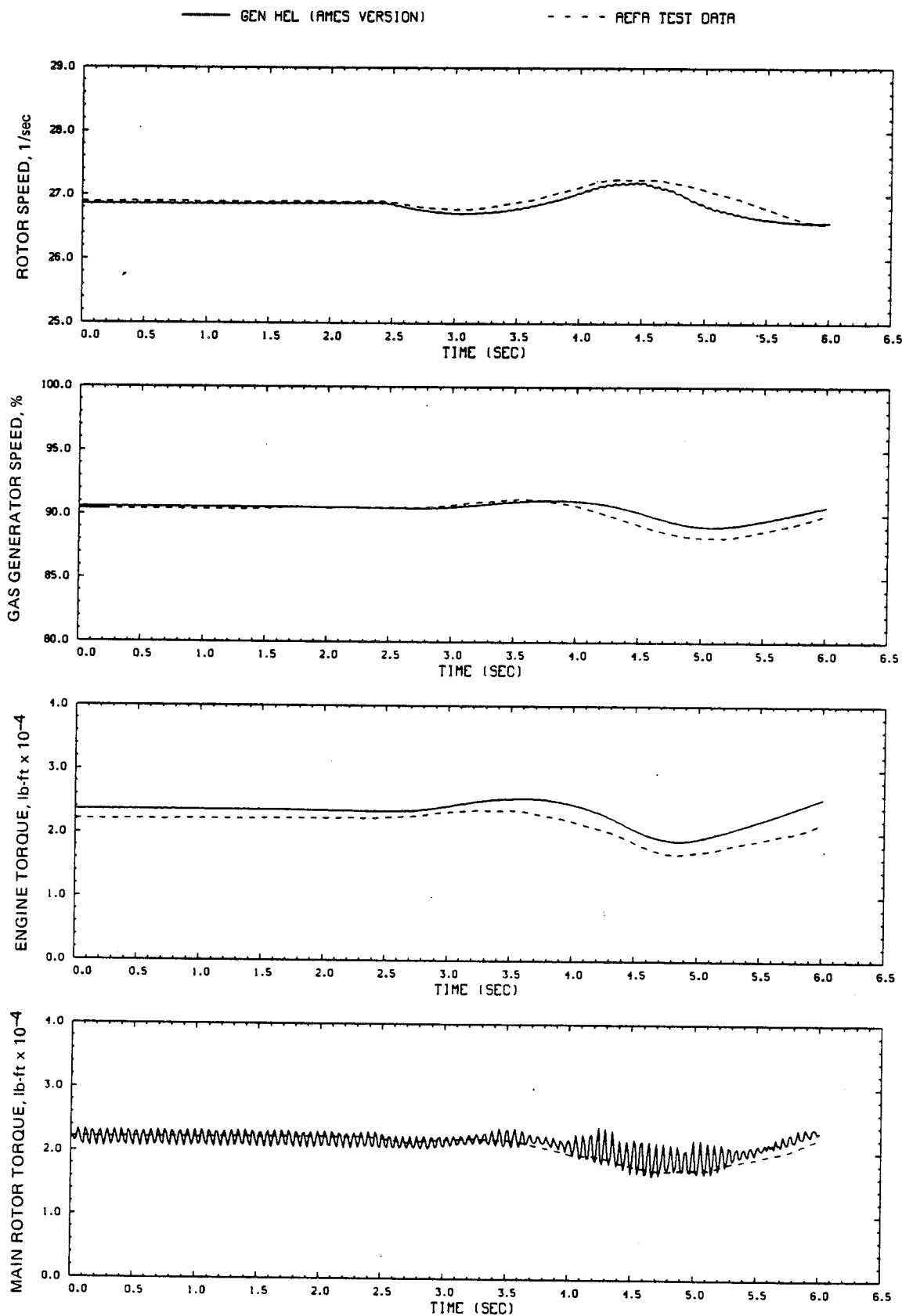


Figure D17.- Concluded.

## APPENDIX E

### SIKORSKY AND AMES GEN HEL DYNAMIC RESPONSE COMPARISONS

Transient responses of the Ames real-time simulation, the Sikorsky Gen Hel simulation, and USAAEFA flight test data of reference 11 are compared for small step-inputs of each control.

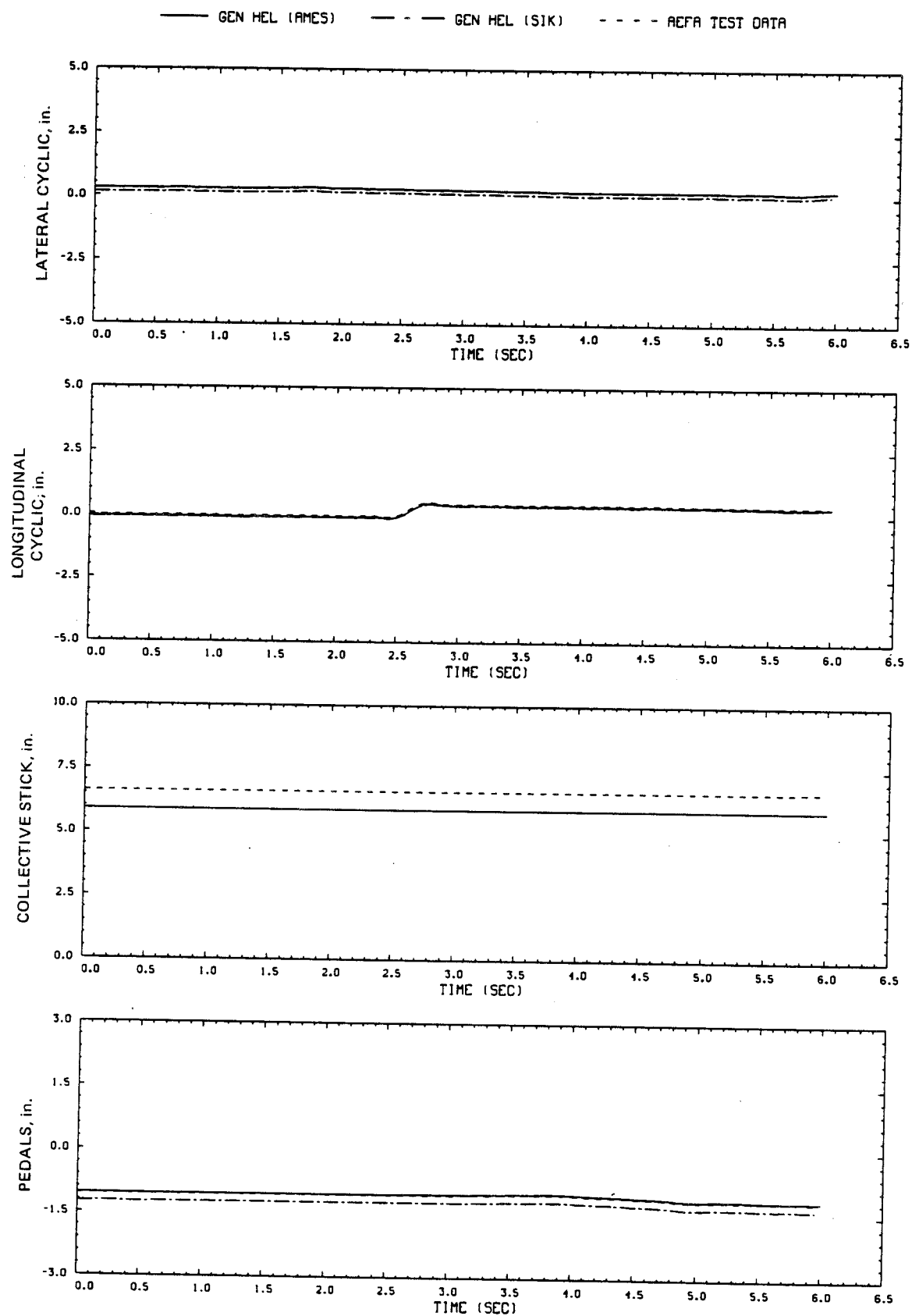


Figure E1.- Comparison of Ames real-time simulation, Sikorsky simulation, and flight-test data. (File 205: 0.5-in. aft cyclic input at hover)

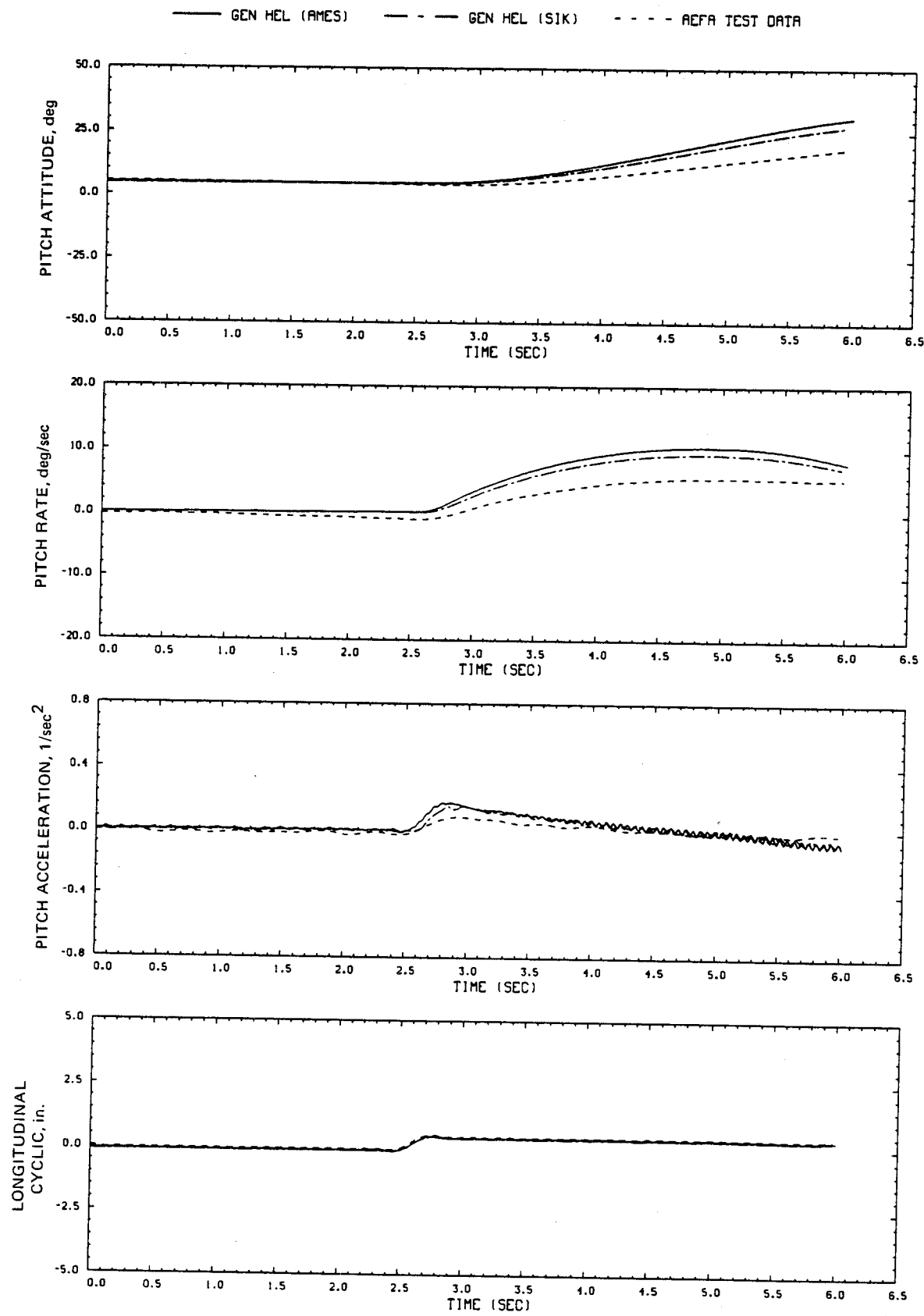


Figure E1.- Continued.

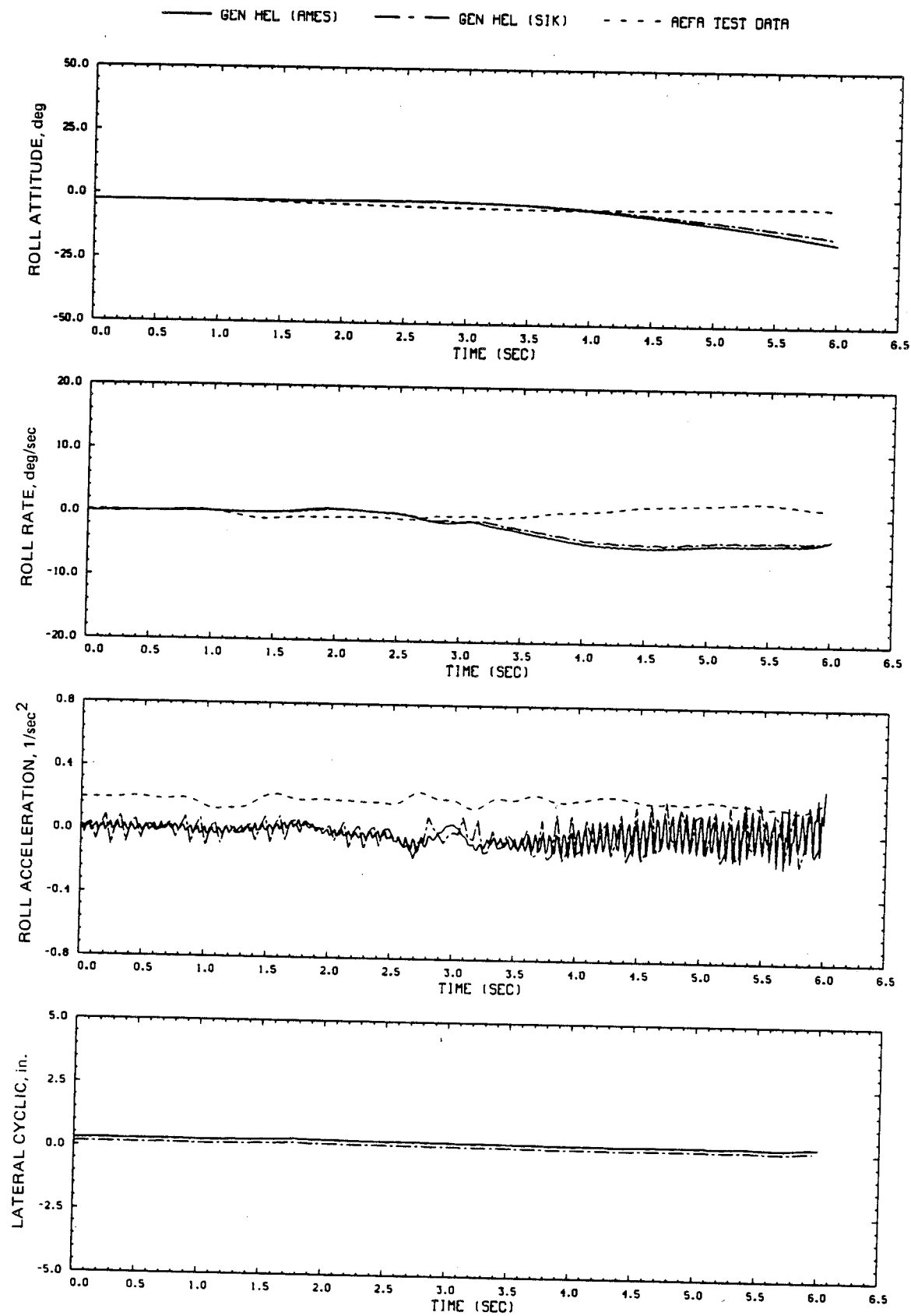


Figure E1.- Continued.

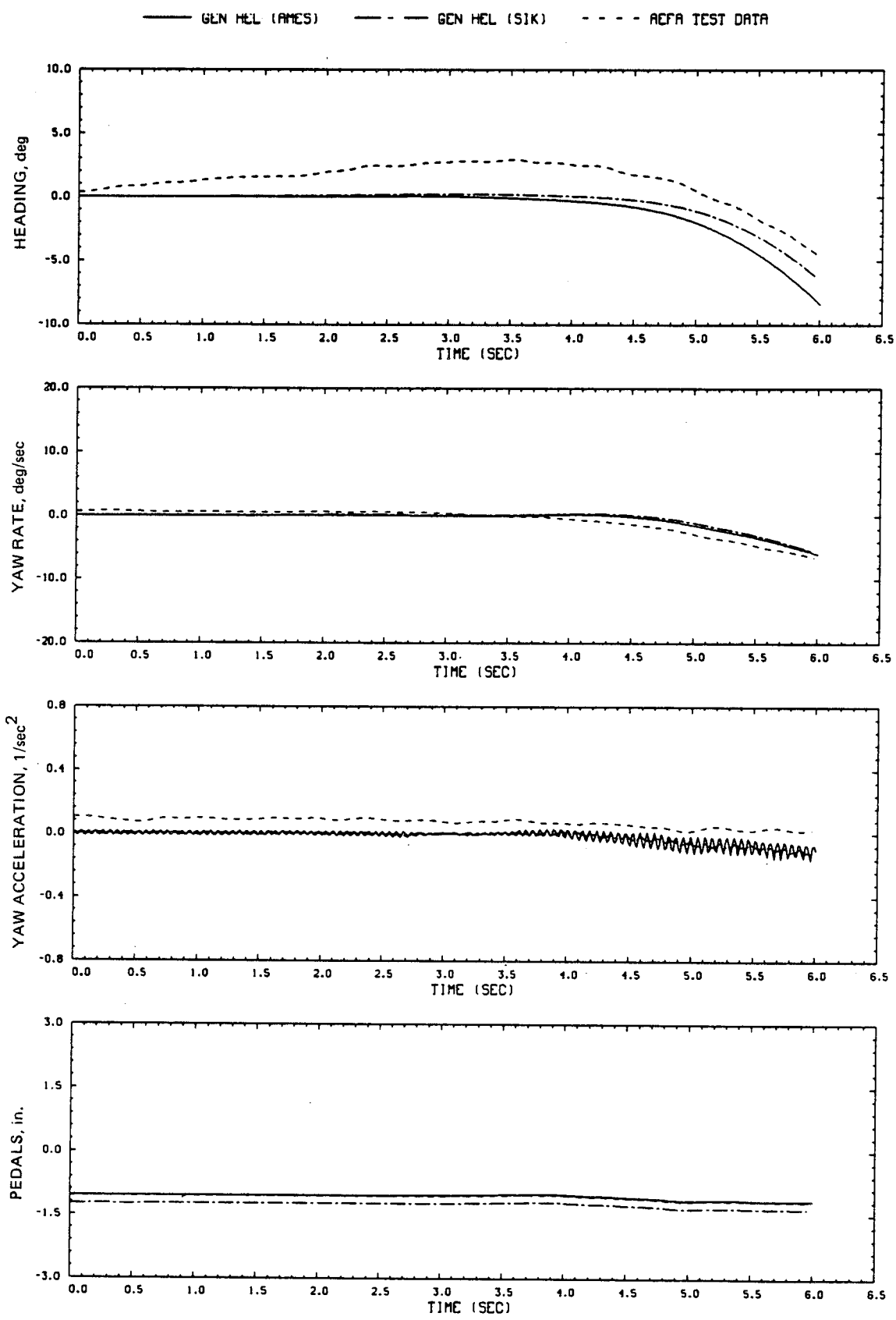


Figure E1.- Continued.

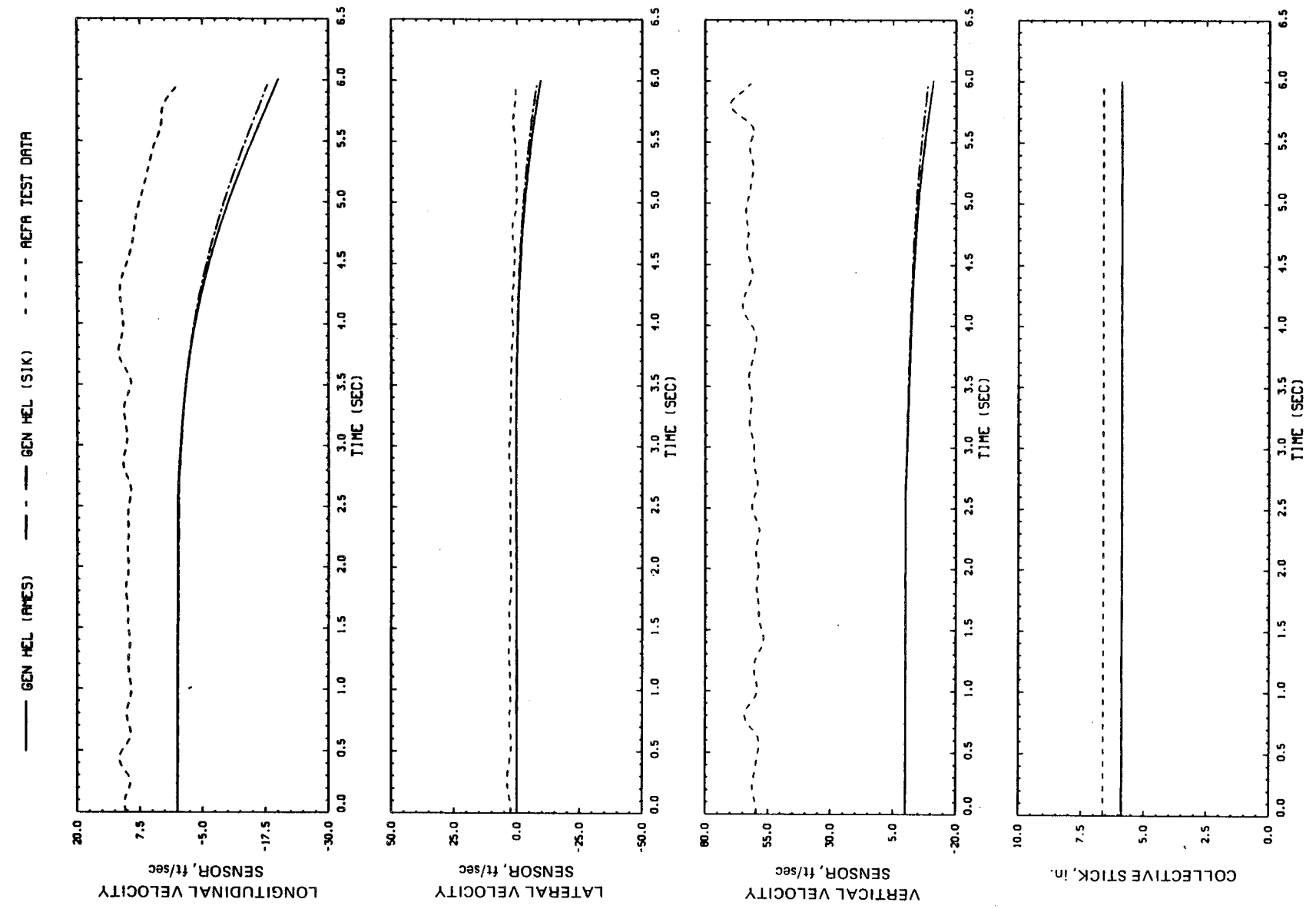


Figure E1.- Continued.

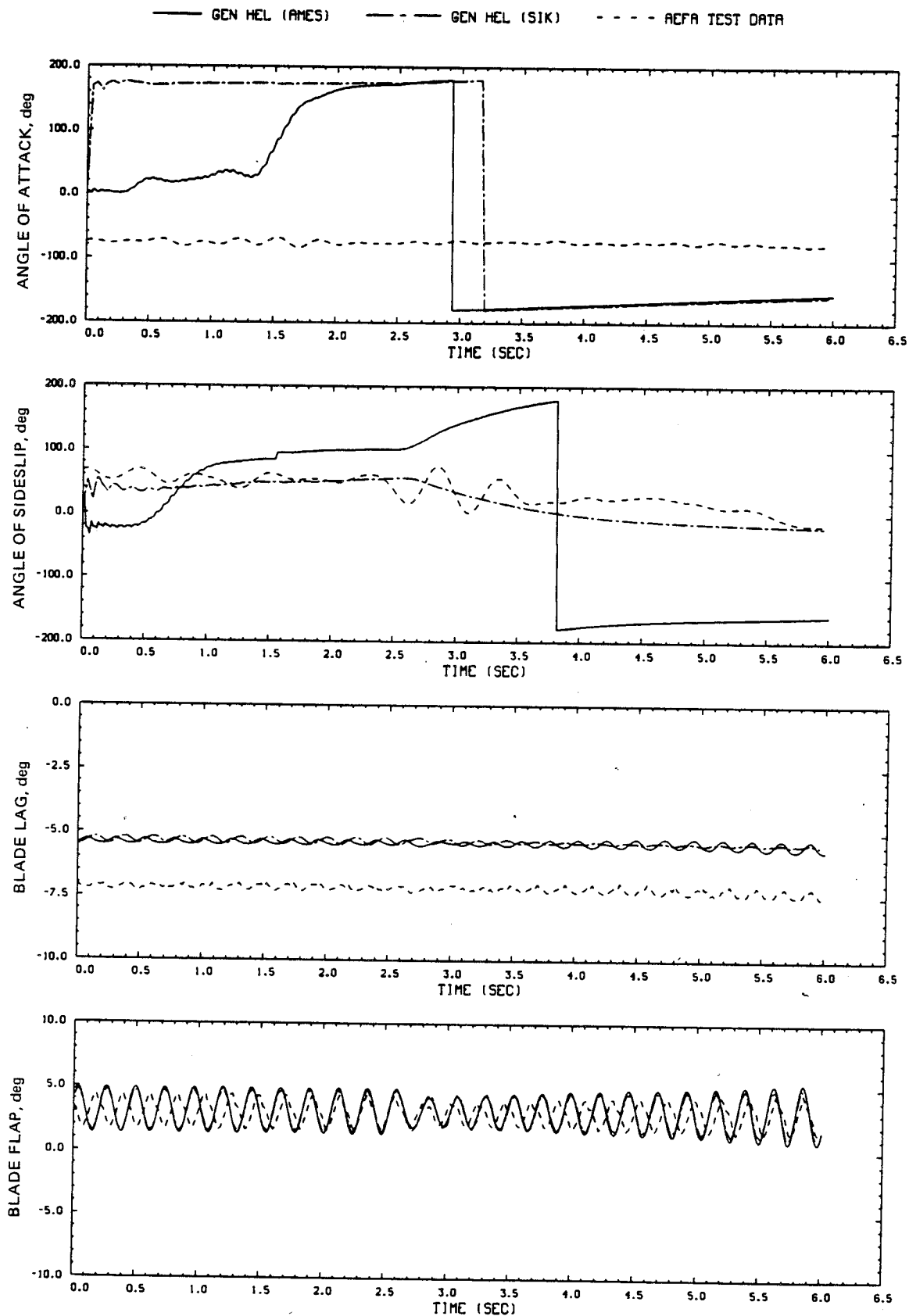


Figure E1.- Continued.

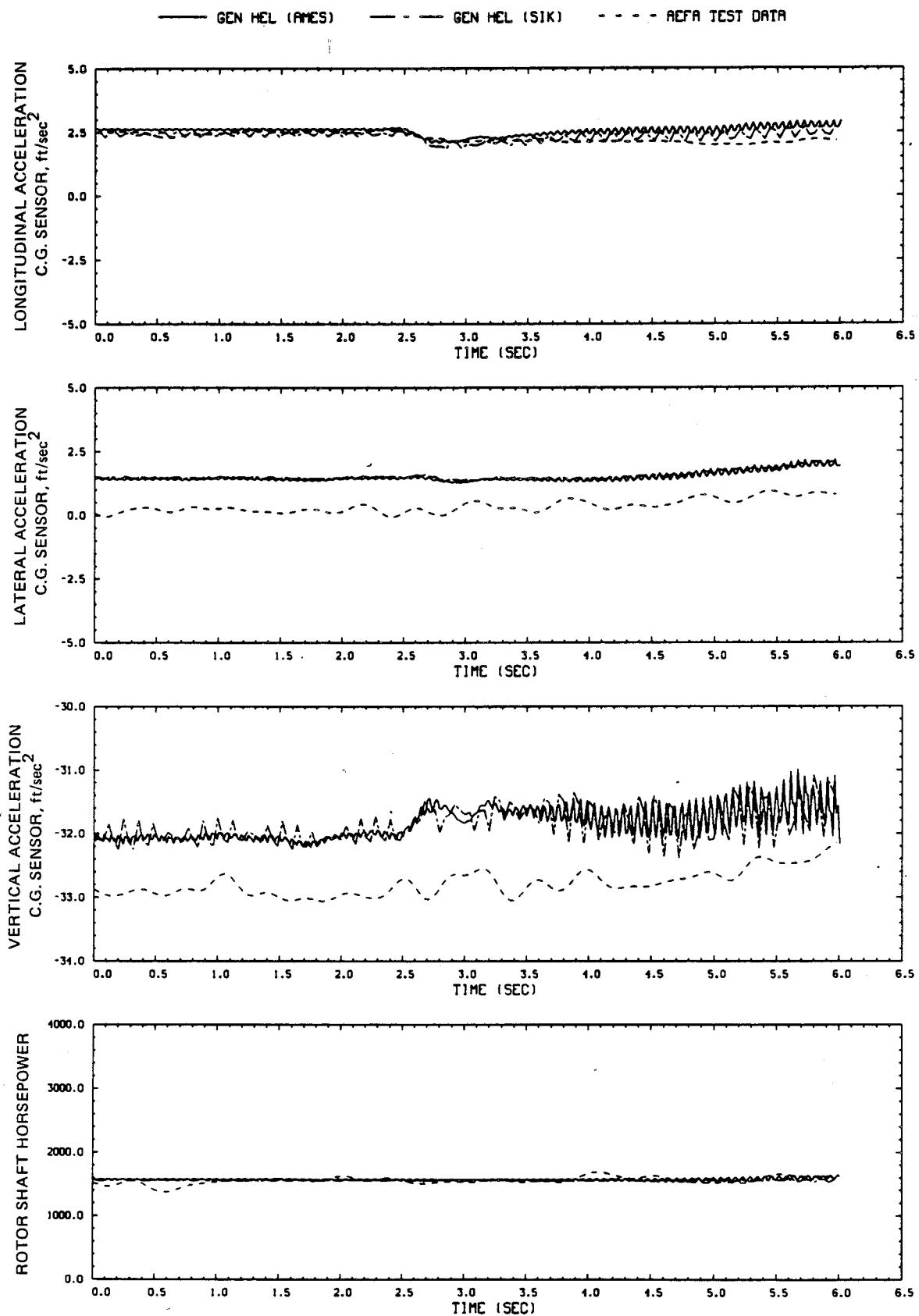


Figure E1.- Continued.

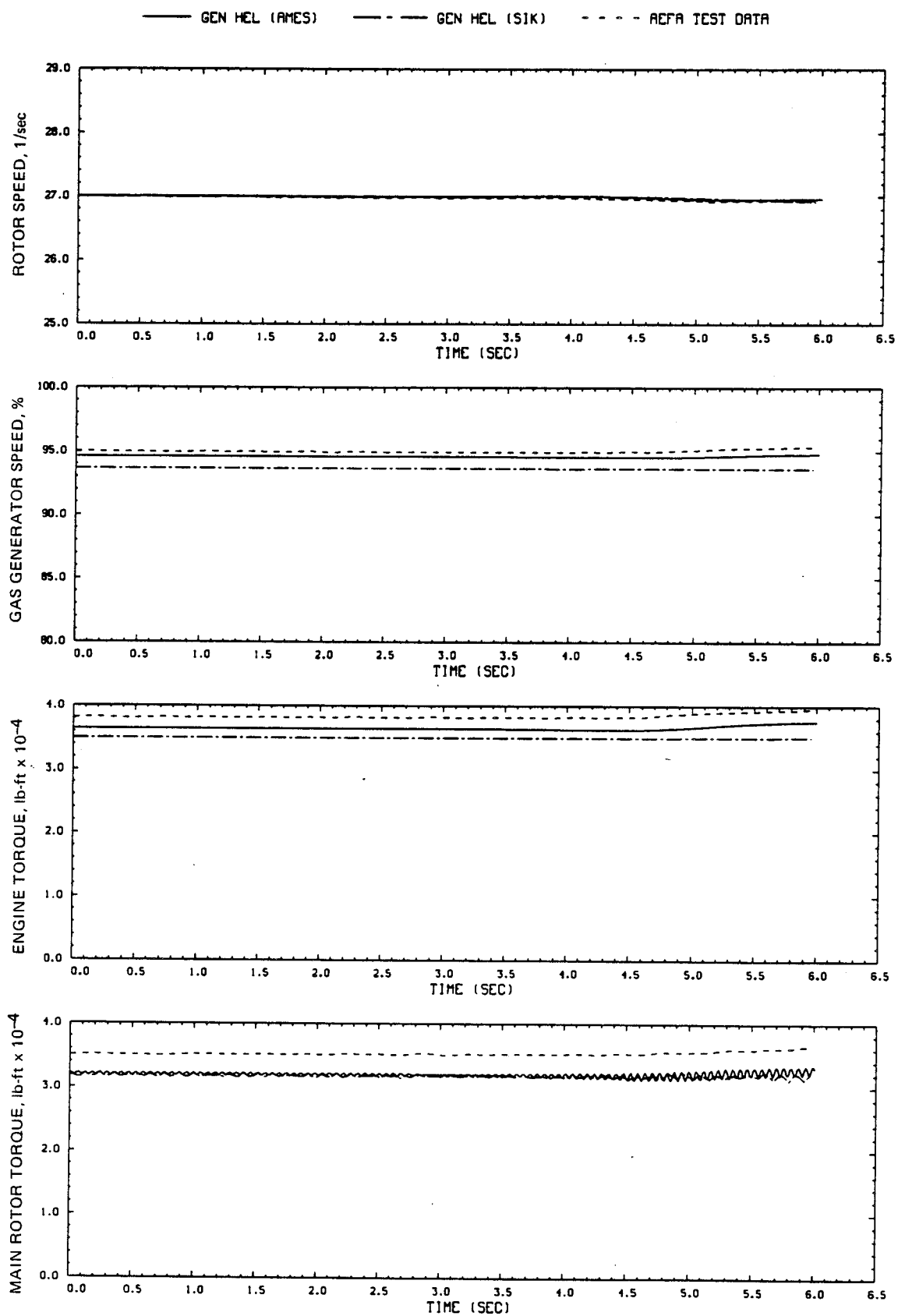


Figure E1.- Concluded.

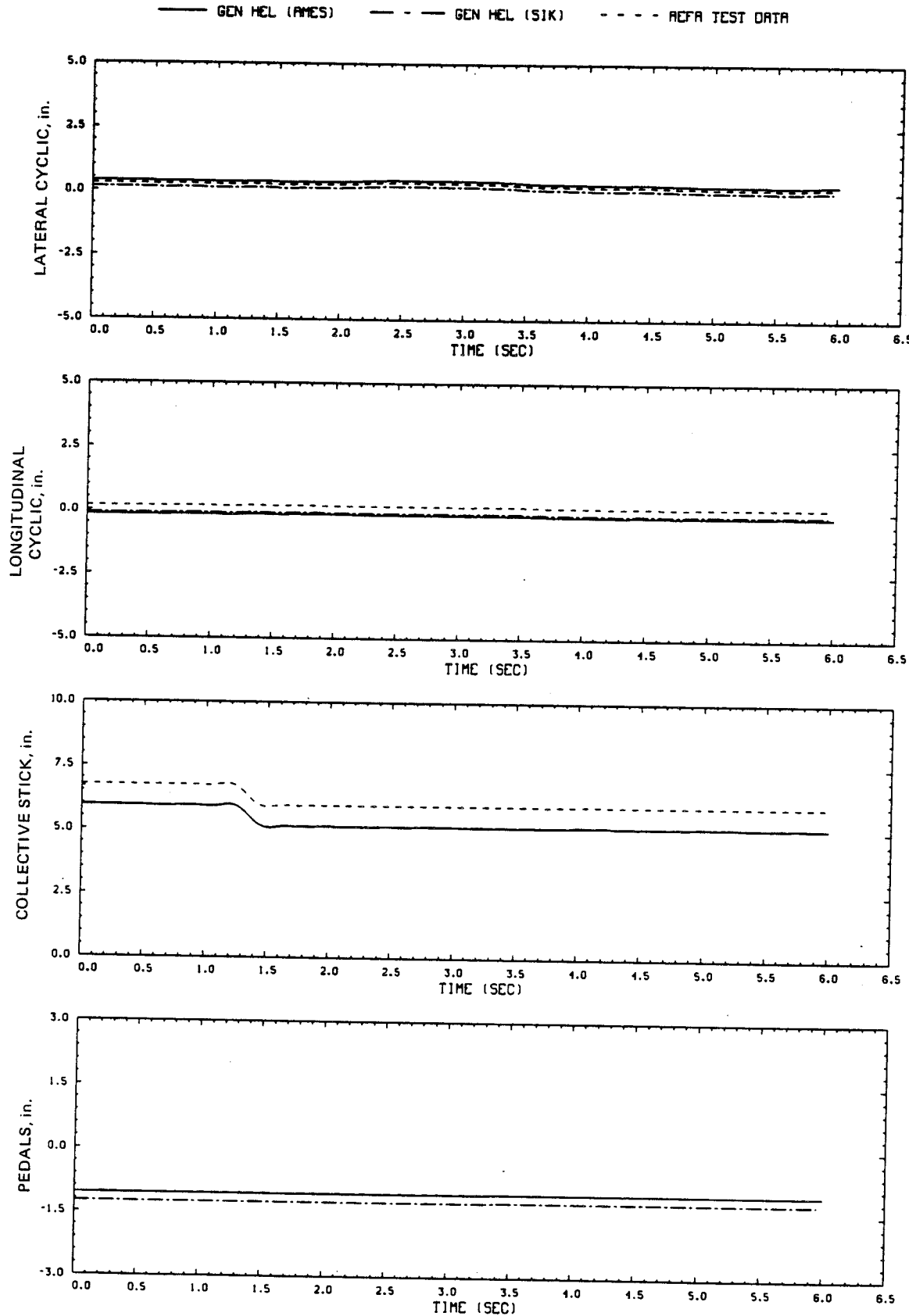


Figure E2.- Comparison of Ames real-time simulation, Sikorsky simulation, and flight-test data. (File 210: 0.5-in. down collective input at hover)

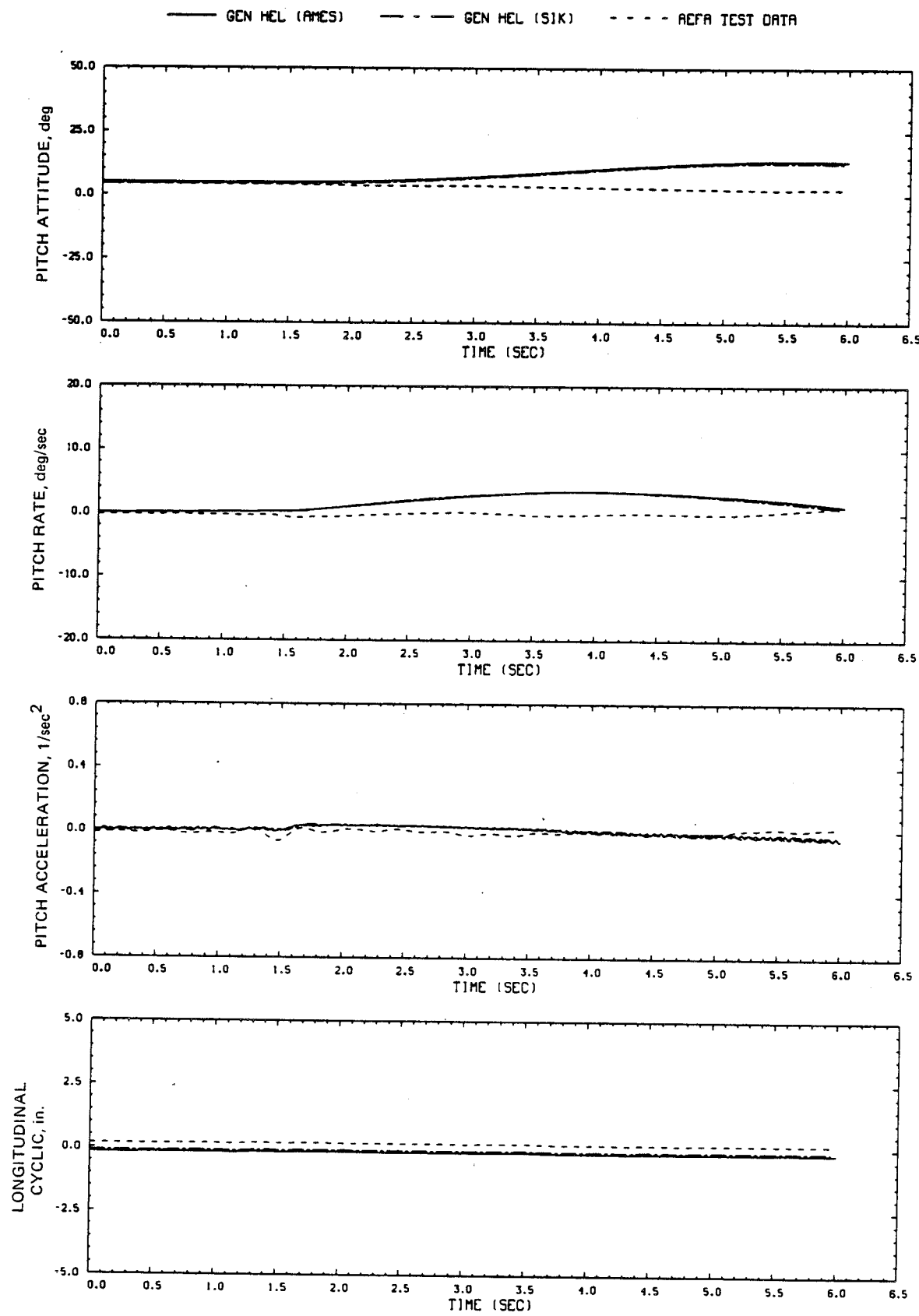


Figure E2.- Continued.

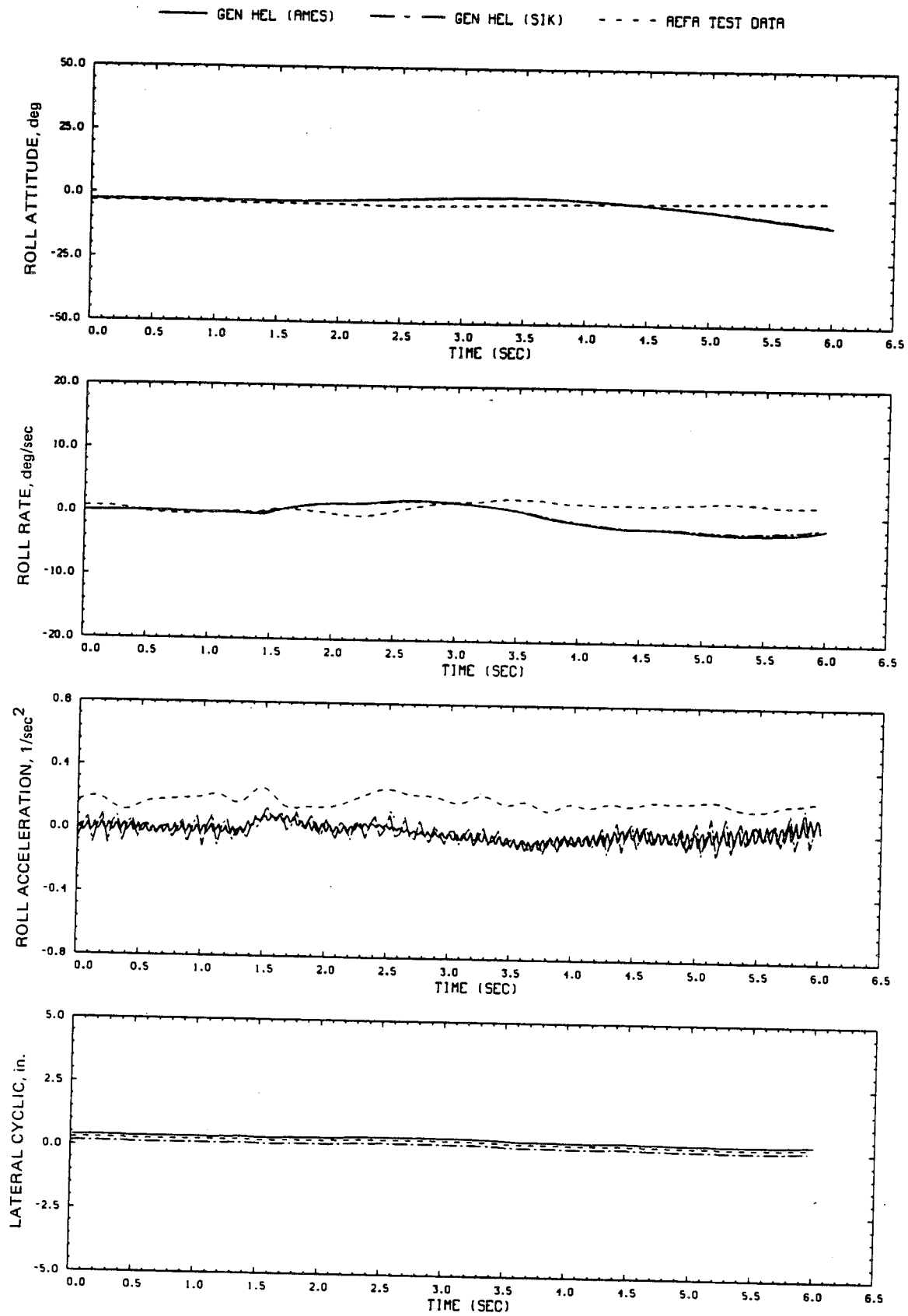


Figure E2.- Continued.

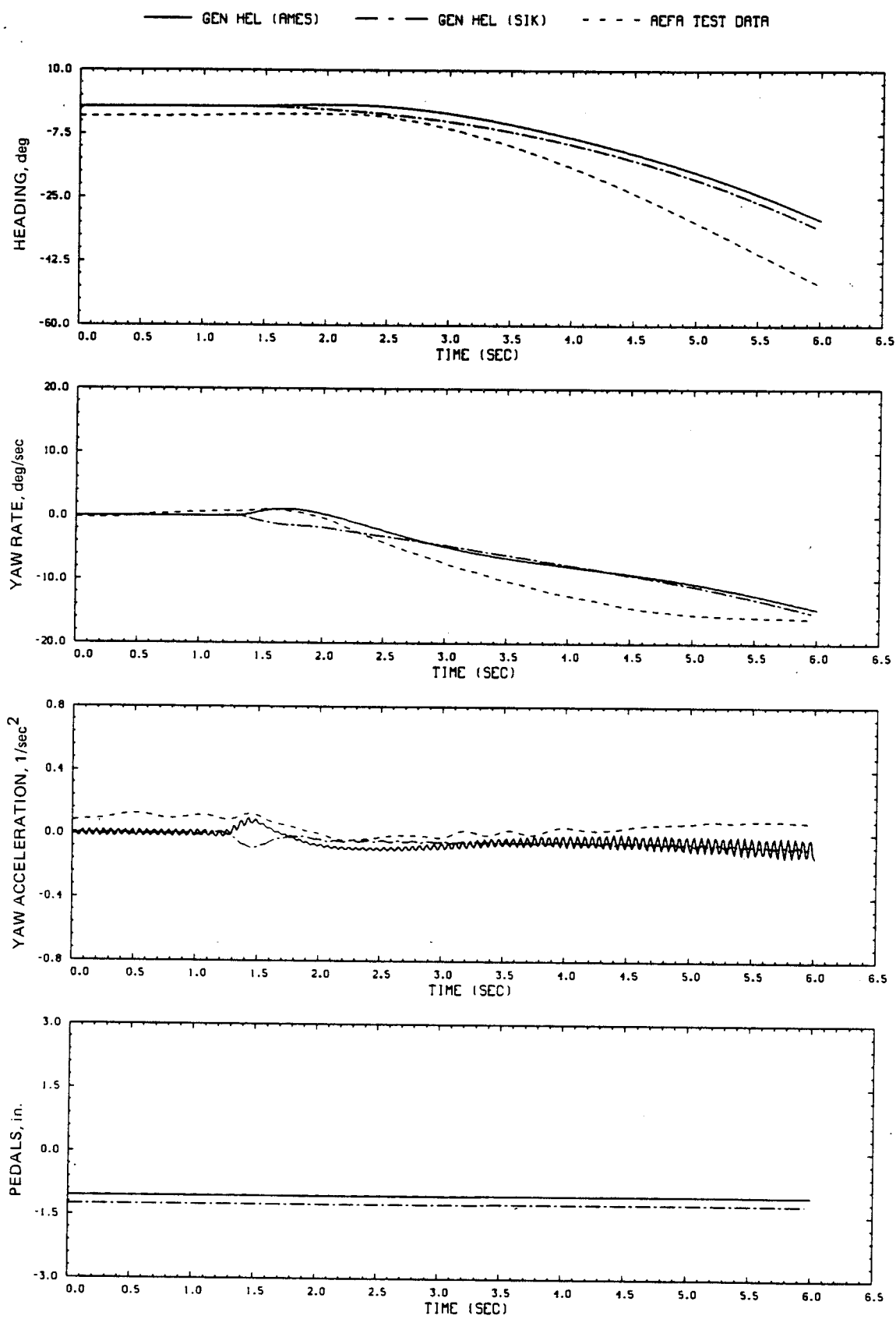


Figure E2.- Continued.

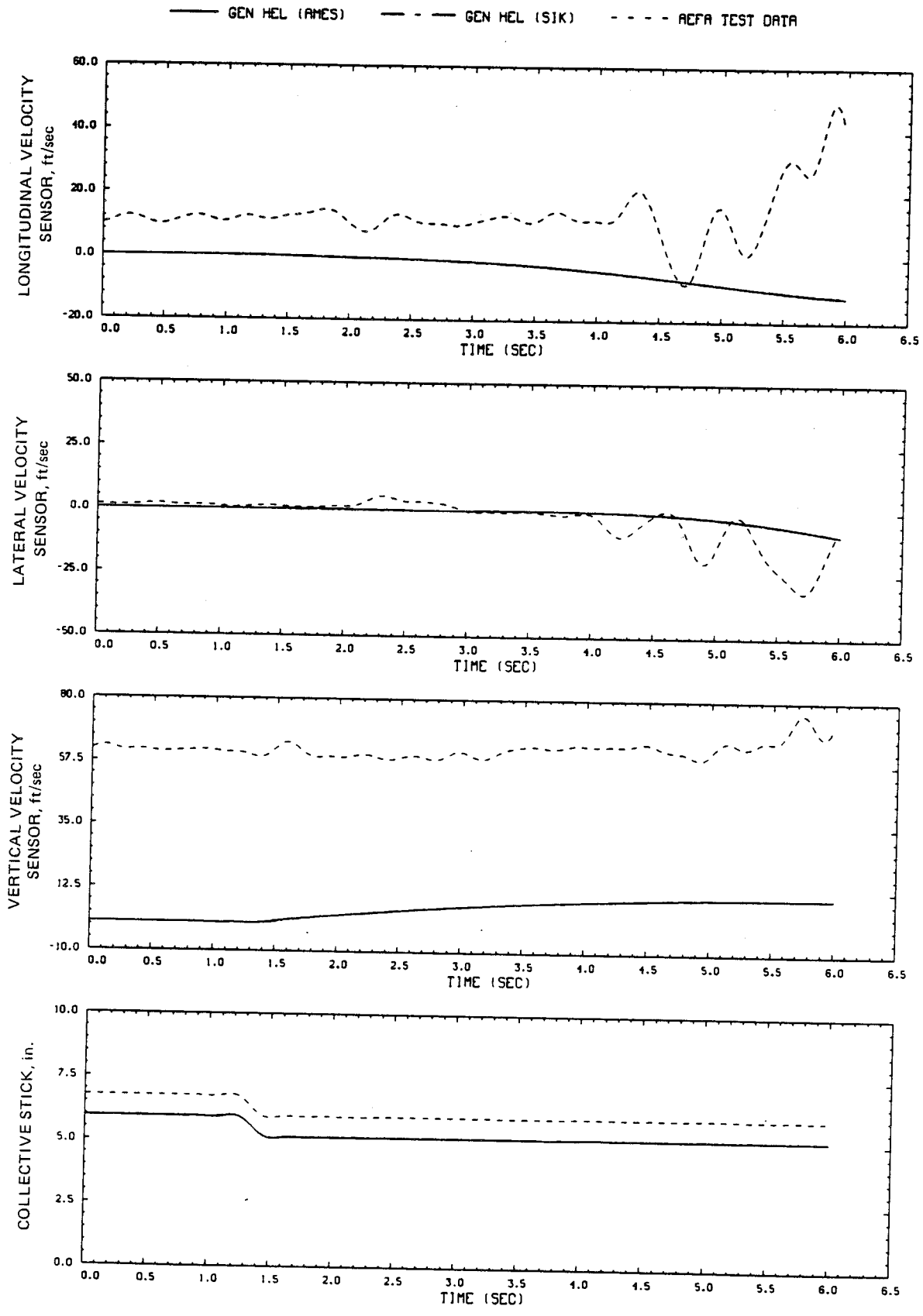


Figure E2.- Continued.

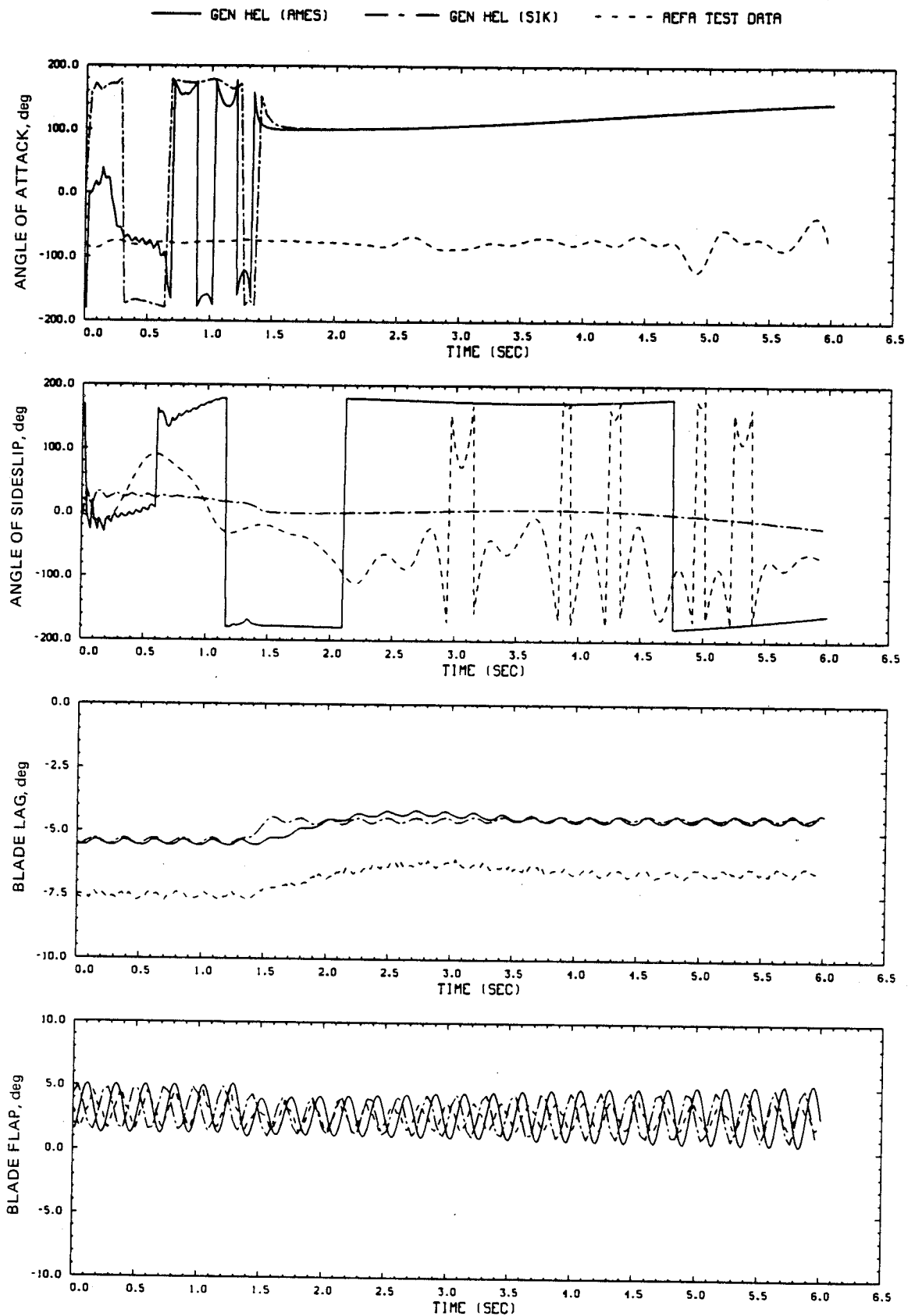


Figure E2.- Continued.

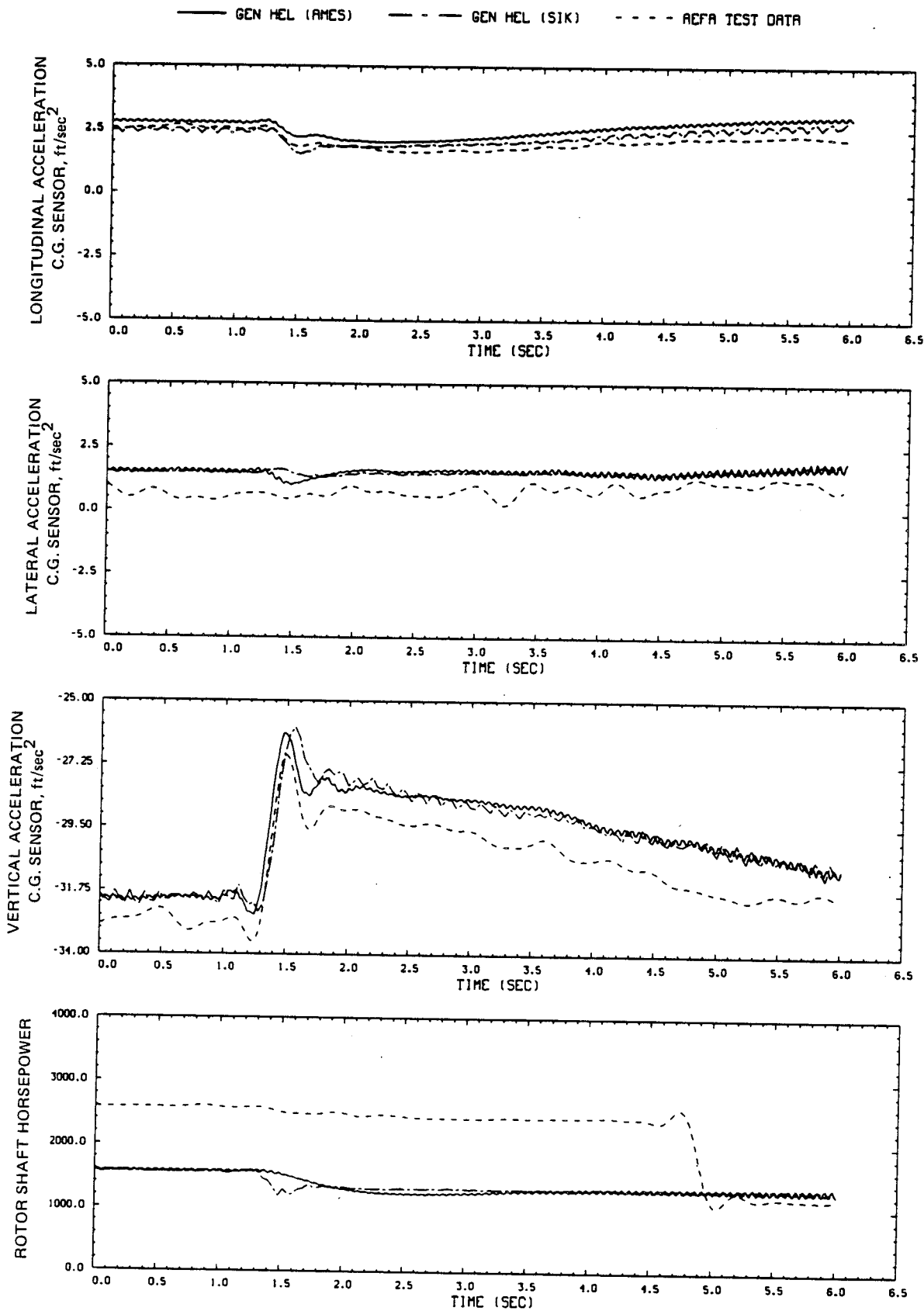


Figure E2.- Continued.

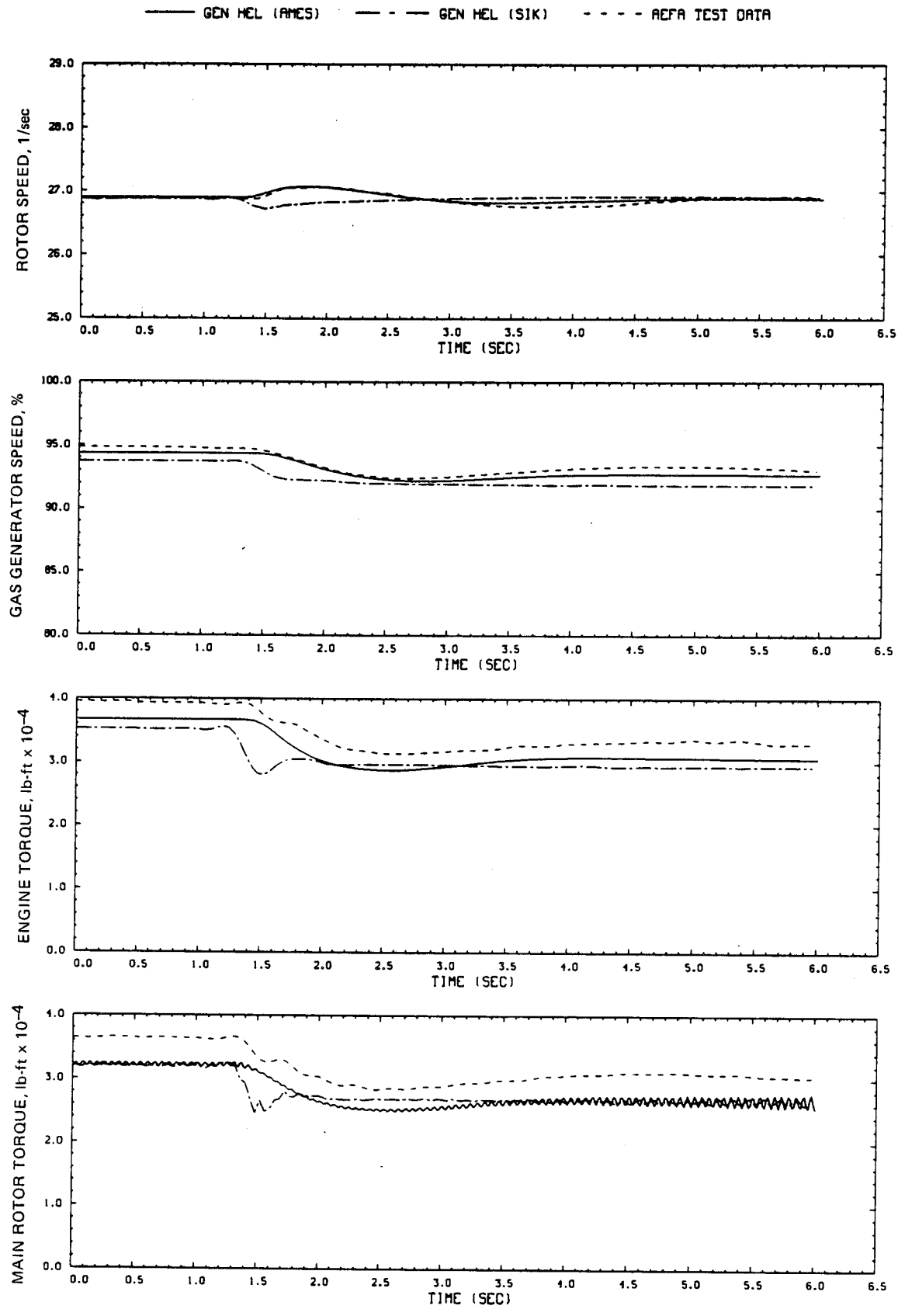


Figure E2.- Concluded.

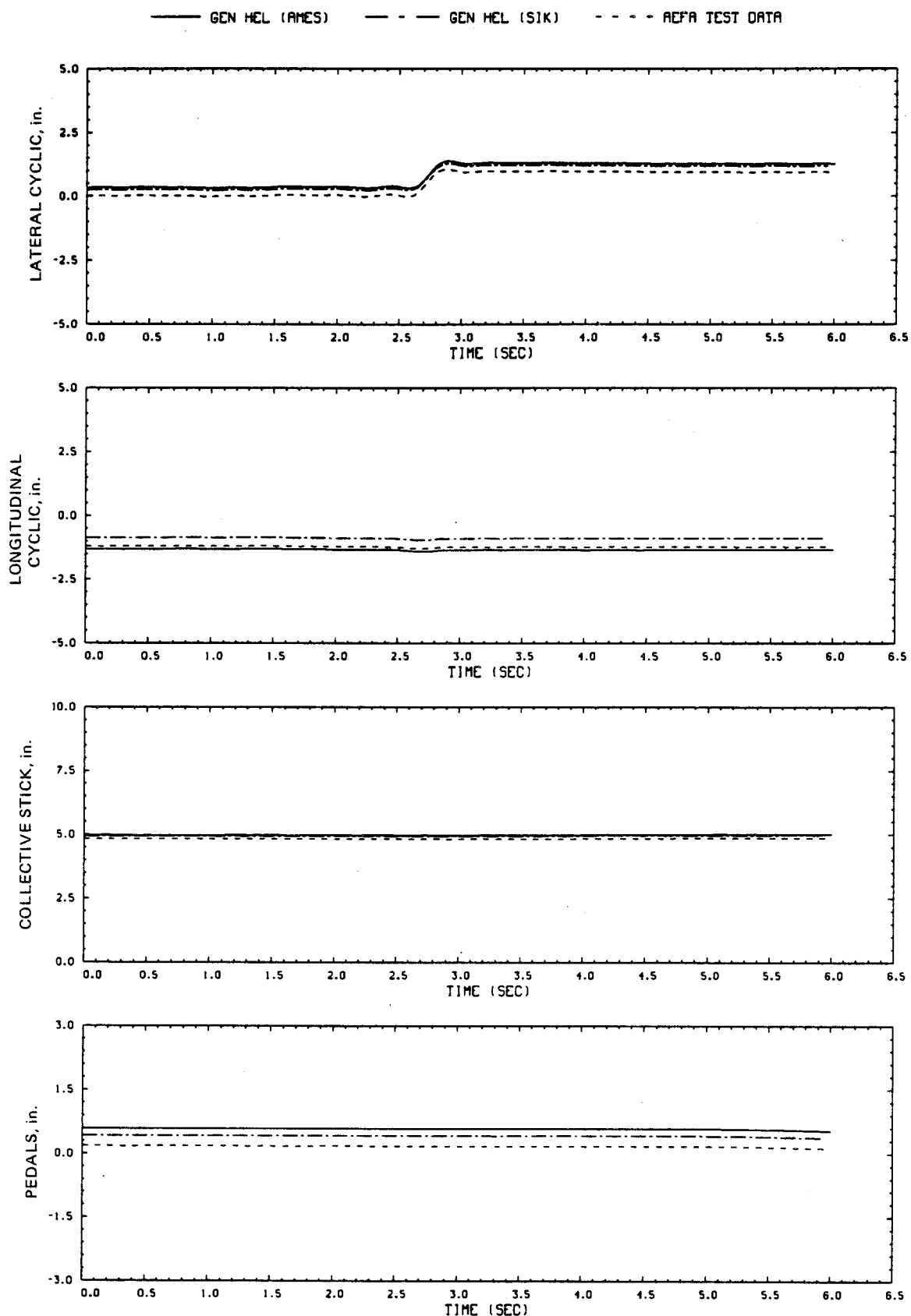
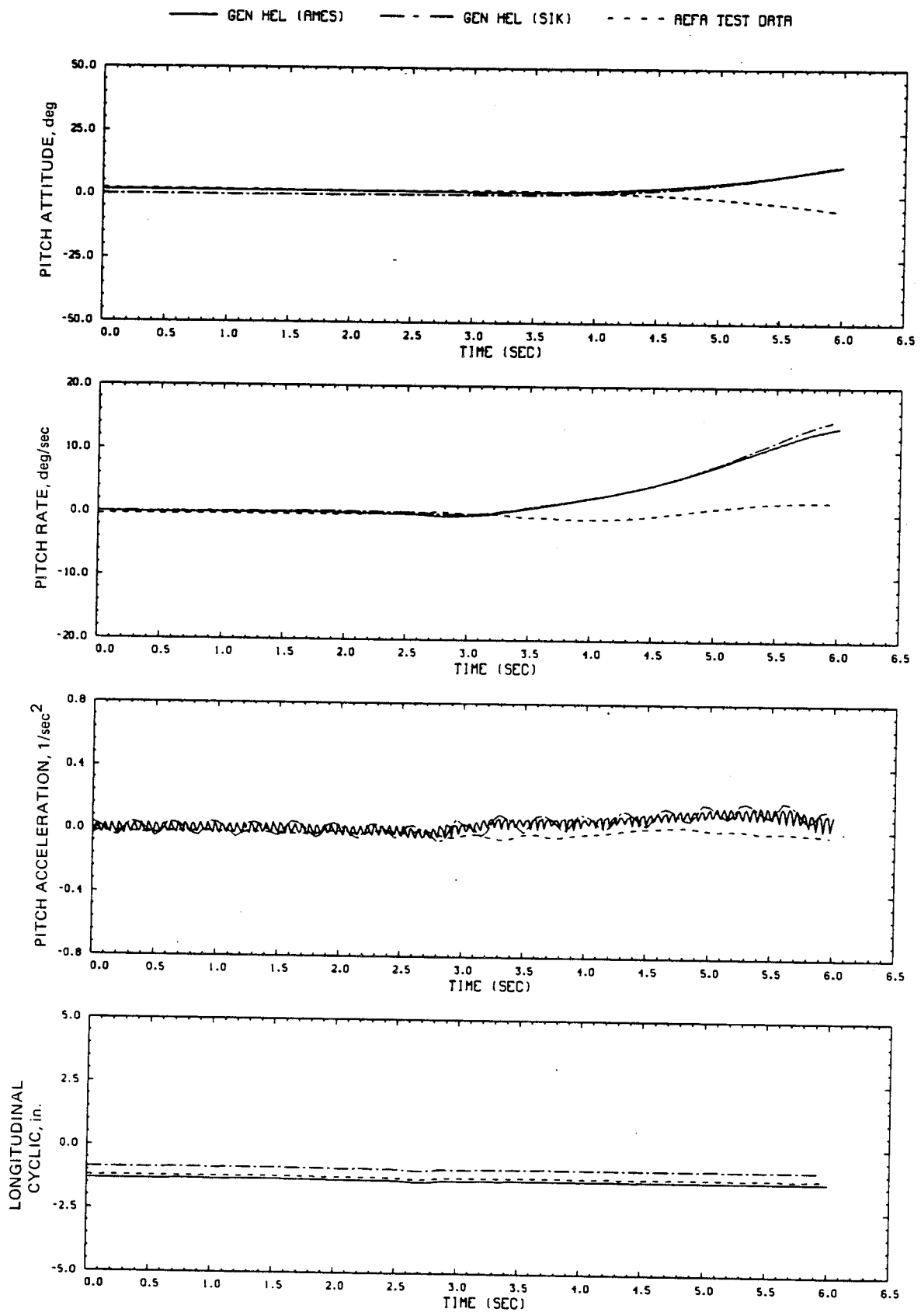


Figure E3.- Comparison of Ames real-time simulation, Sikorsky simulation, and flight-test data. (File 409: 1-in. right lateral input, 100 knots)



C 13

Figure E3.- Continued.

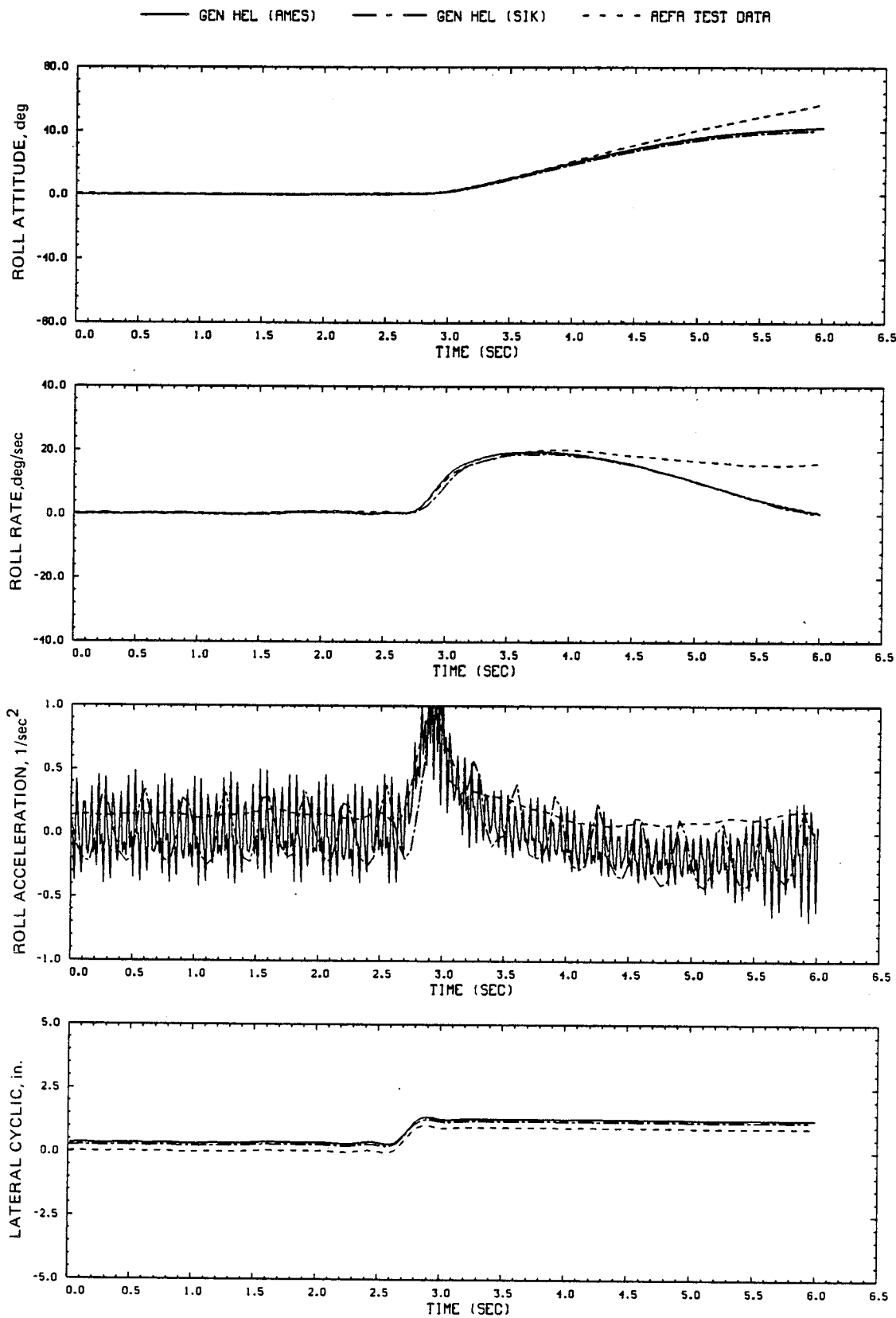


Figure E3.- Continued.

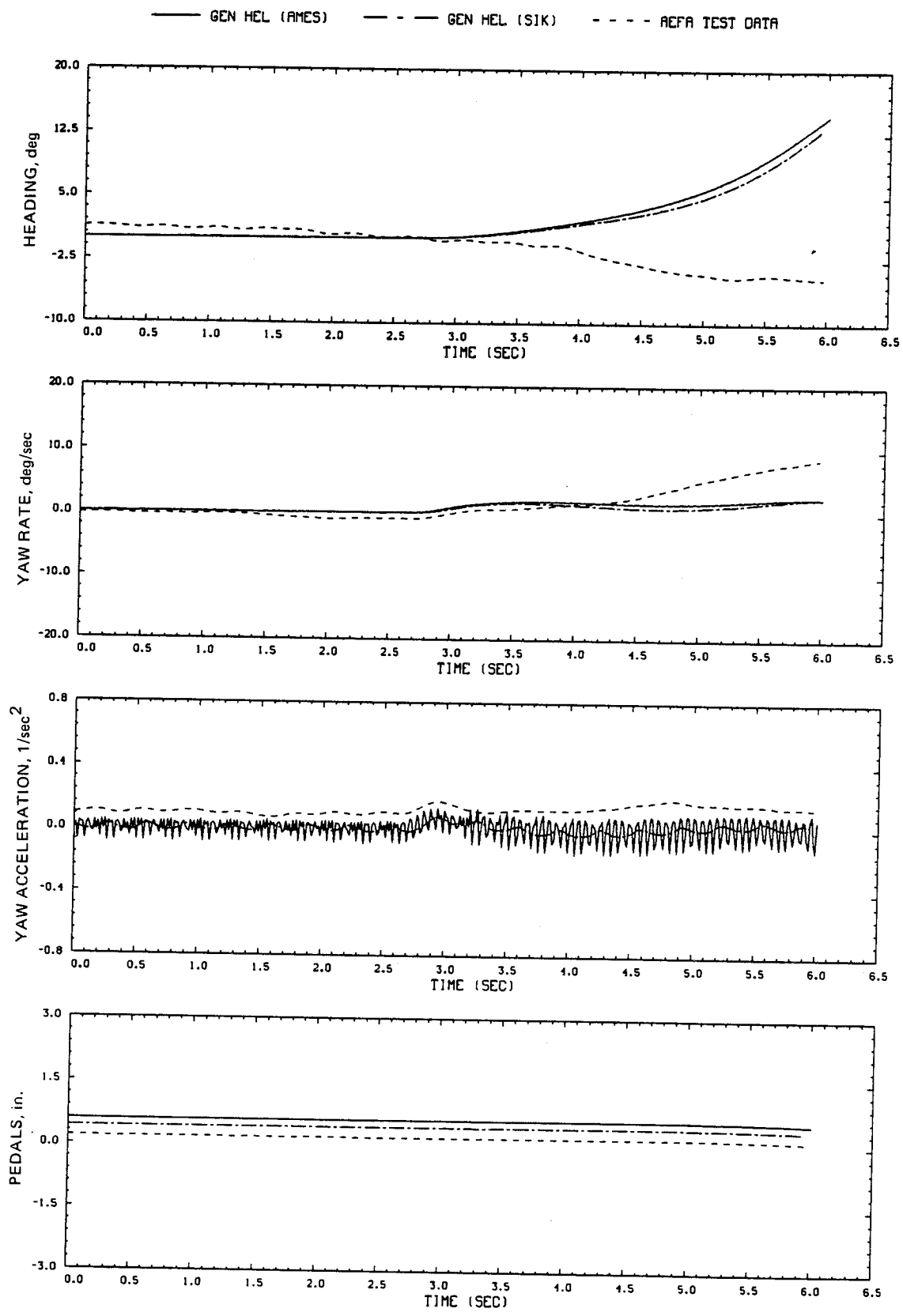


Figure E3.- Continued.

— GEN HEL (AMES) — GEN HEL (SIK) - - - REFL TEST DATA

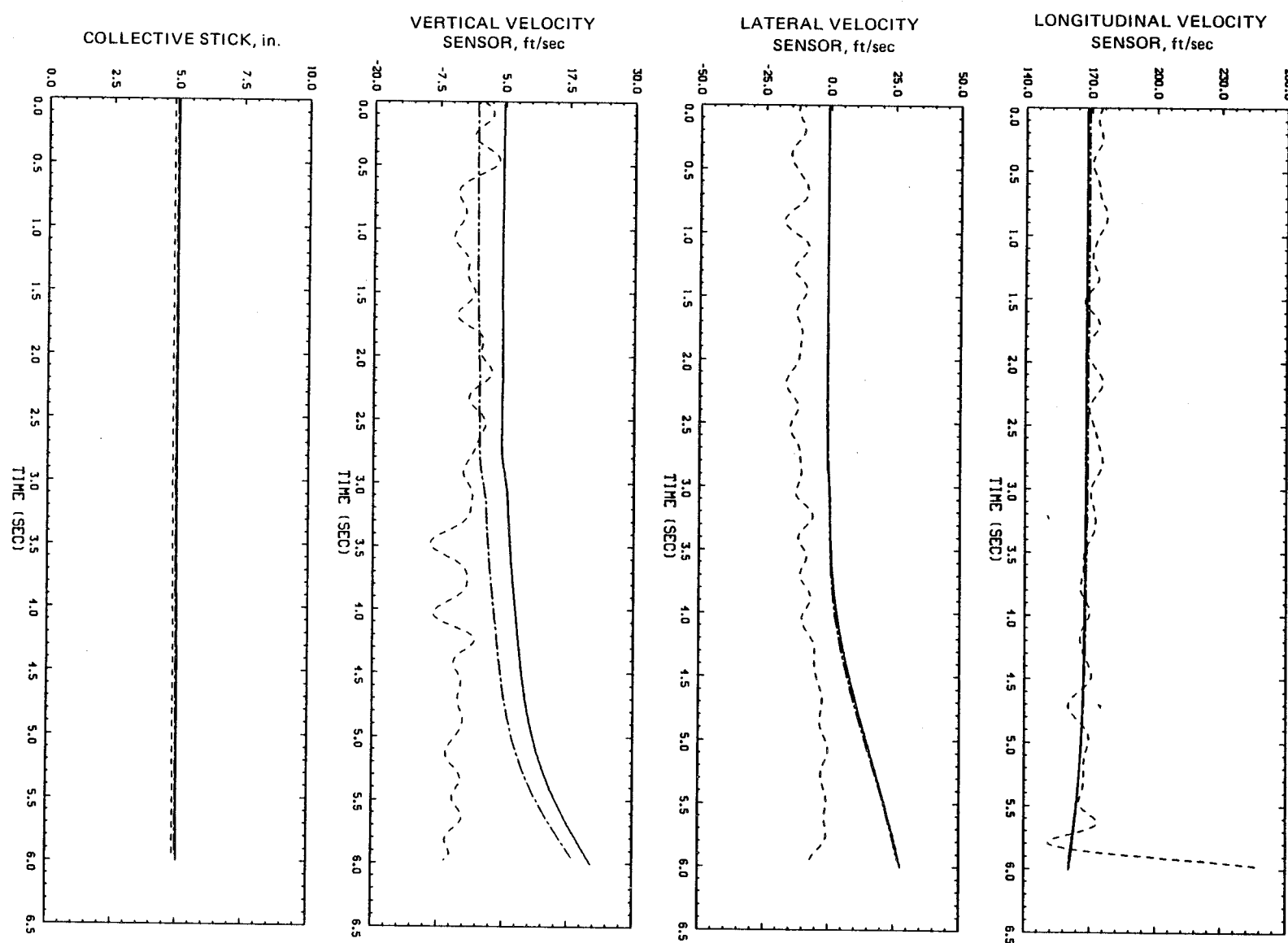


Figure E3.- Continued.

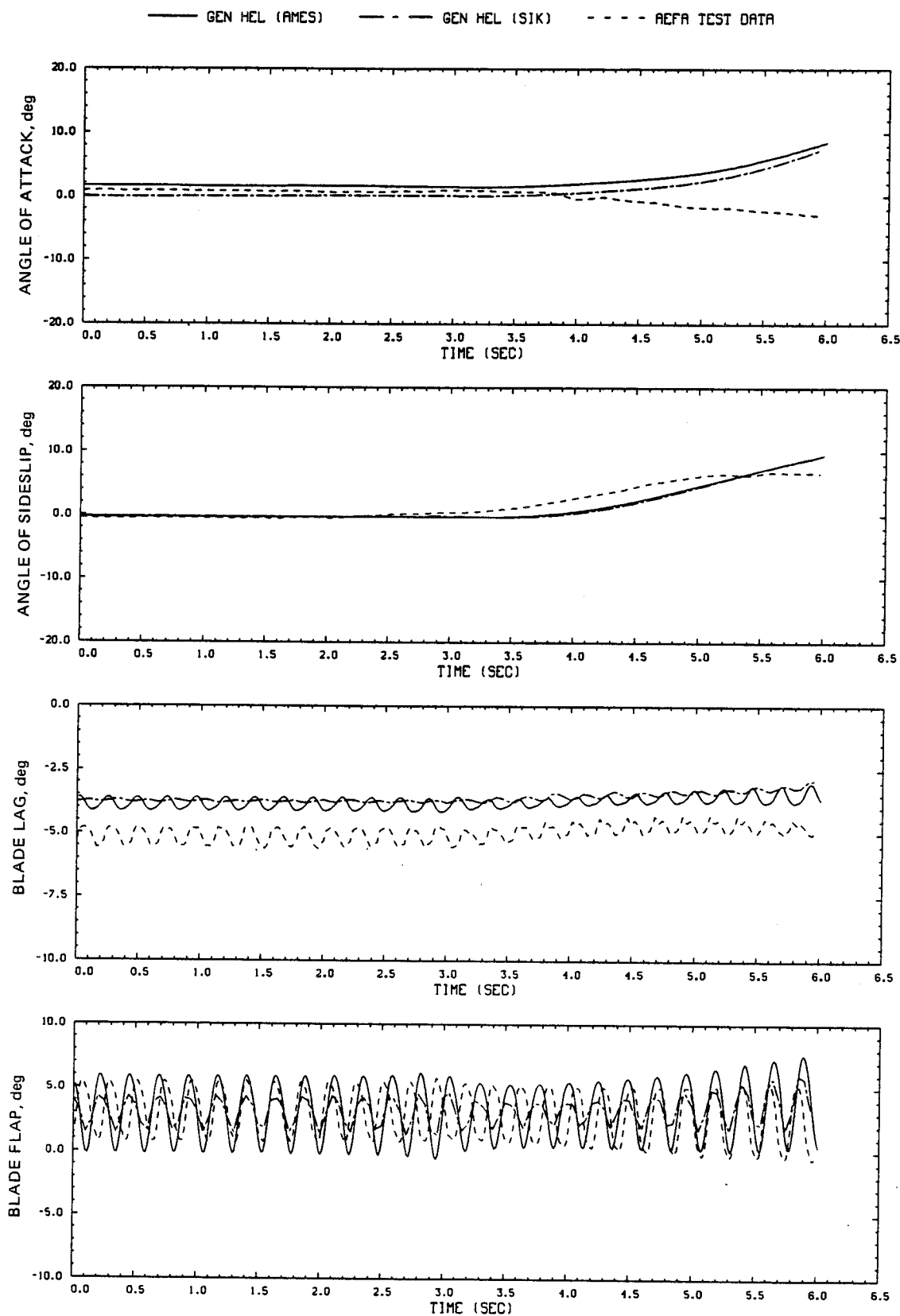


Figure E3.- Continued.

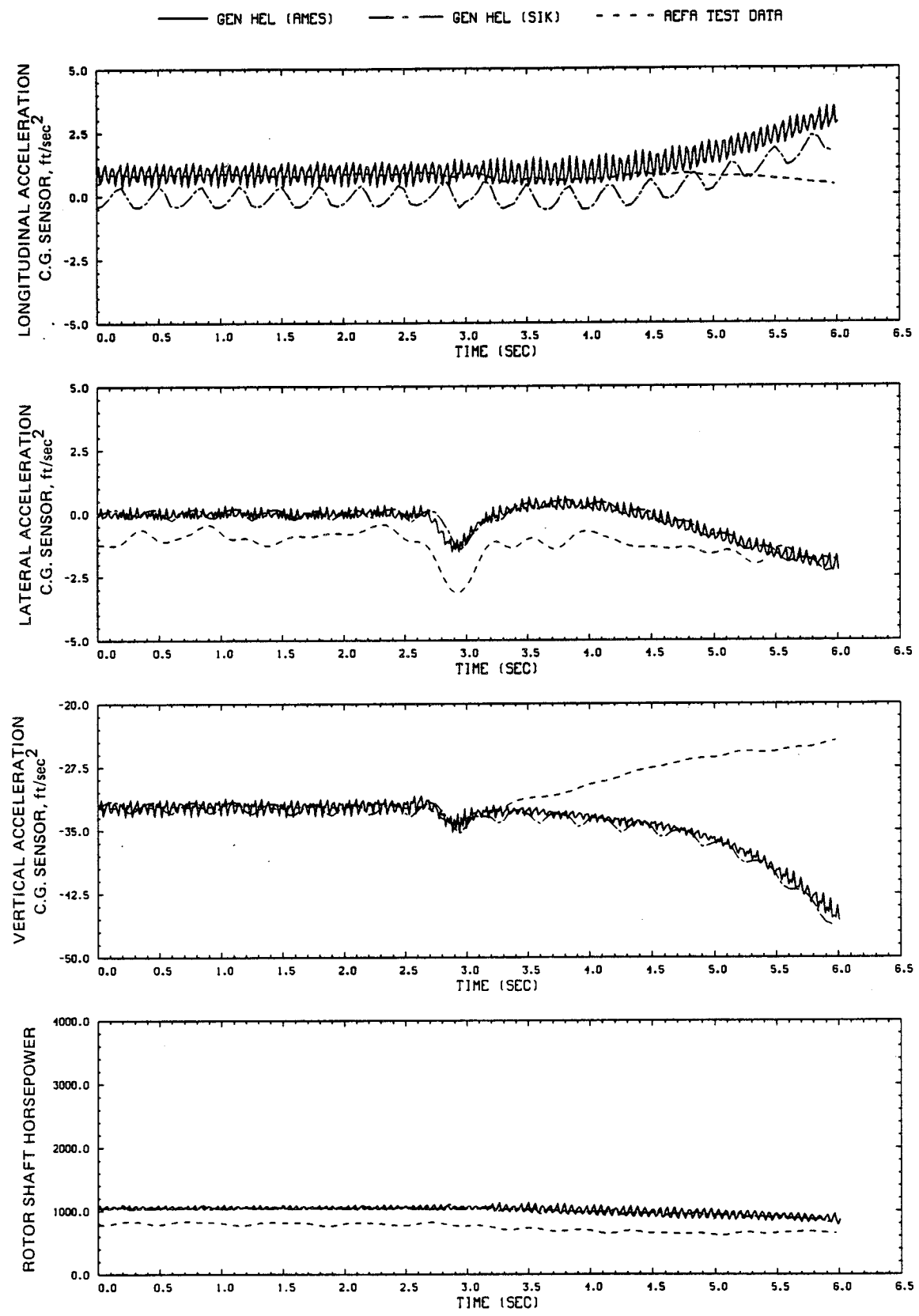


Figure E3.- Continued.

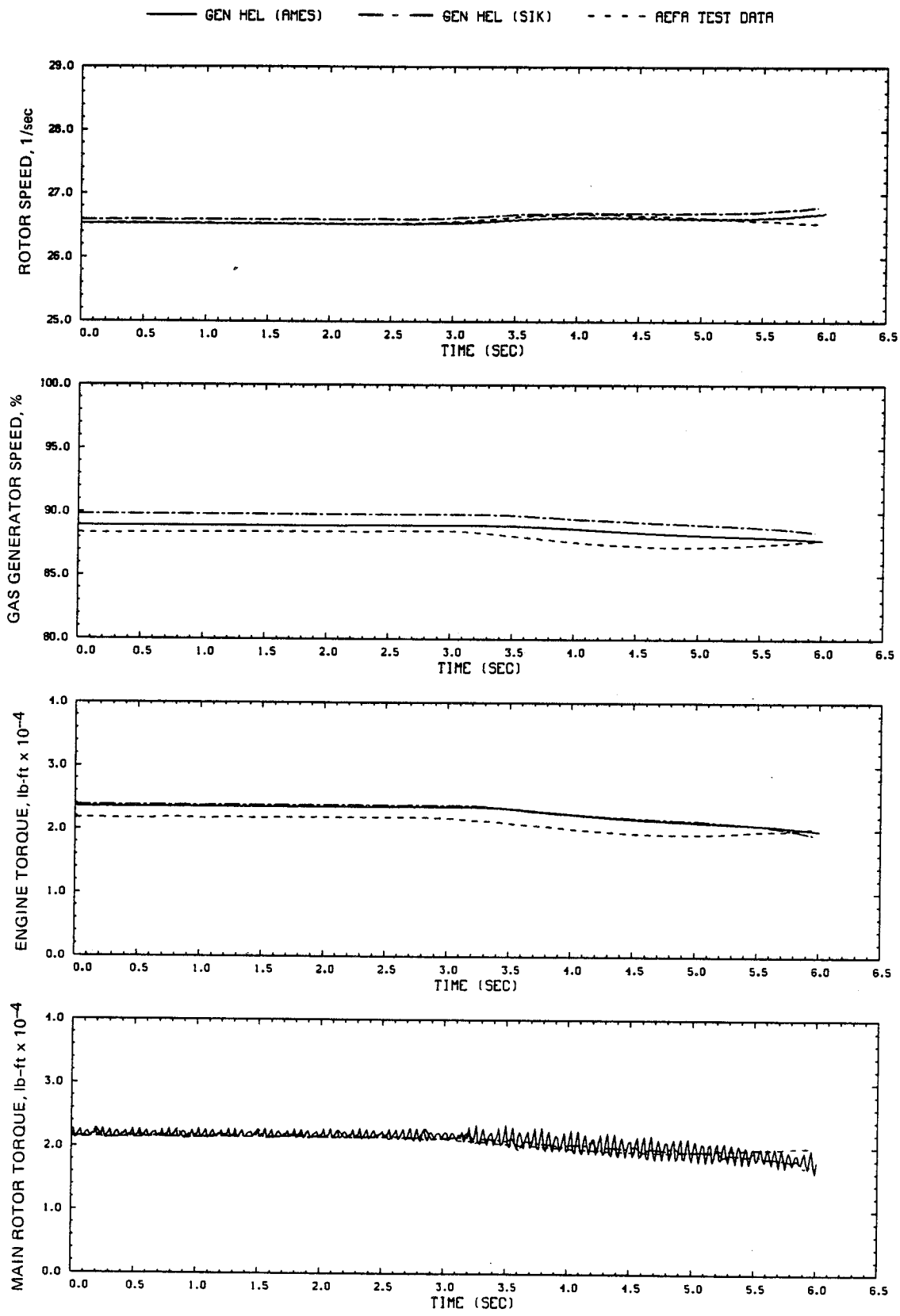


Figure E3.- Concluded.

## REFERENCES

1. Kaplita, T. T.: UH-60A Black Hawk Engineering Simulation Model Validation and Proposed Modifications. Tech. Rep. SER-70982, United Technologies Sikorsky Aircraft, 1984.
2. Howlett, J. J.: UH-60A Black Hawk Engineering Simulation Program: Volume I-- Mathematical Model. NASA CR-166309, 1981.
3. Ellison, D.; and Mattham, L.: USAF Stability and Control DATCOM. Proj. 8219, Wright-Patterson Air Force Base, 1970.
4. Houck, J. A.; Moore, F. L.; Howlett, J. J.; Pollock, K. S.; and Browne, M. M.: Rotor Systems Research Aircraft Simulation Mathematical Model. NASA TM-78629, 1977.
5. DuVal, R. W.: Inertial Dynamics of a General Purpose Rotor Model. NASA TM-78557, 1979.
6. Bailey, F. J., Jr.: A Simplified Theoretical Method of Determining the Characteristics of a Lifting Rotor in Forward Flight. NACA Rep. 716, National Advisory Committee for Aeronautics, 1941.
7. McFarland, R. E.: Establishment of a Rotor Model Basis. NASA TP-2026, 1982.
8. McFarland, R. E.: A Standard Kinematic Model for Flight Simulation at NASA-Ames. NASA CR-2497, 1975.
9. McFarland, R. E.: The N/Rev Phenomenon in Simulating a Blade Element Rotor System. NASA TM-84344, 1983.
10. Abbott, W. Y.; Benson, J. O.; Oliver, R. C.; and Williams, R. A.: Validation Flight Test of UH-60A for Rotorcraft Systems Integration Simulator (RSIS). USAAEFA Project 79-24, United States Army Aviation Engineering Flight Activity, 1982.
11. Kaplita, T. T.: UH-60A Black Hawk Engineering Simulation Model Validation Transient Response Comparison Data, Volumes 1 and 2. Tech. Rep. SER-70983, United Technologies Sikorsky Aircraft, 1984.

1. Report No. NASA TM 88360	2. Government Accession No.	3. Recipient's Catalog No.	
4. Title and Subtitle <b>VALIDATION OF A REAL-TIME ENGINEERING SIMULATION OF THE UH-60A HELICOPTER</b>		5. Report Date <b>February 1987</b>	
		6. Performing Organization Code	
7. Author(s) <b>Mark G. Ballin</b>		8. Performing Organization Report No. <b>A-86407</b>	
9. Performing Organization Name and Address <b>Ames Research Center Moffett Field, CA 94035</b>		10. Work Unit No.	
		11. Contract or Grant No.	
12. Sponsoring Agency Name and Address <b>National Aeronautics and Space Administration Washington, DC 20546</b>		13. Type of Report and Period Covered <b>Technical Memorandum</b>	
		14. Sponsoring Agency Code <b>505-61-51</b>	
15. Supplementary Notes <b>Point of Contact: Mark G. Ballin, M/S 211-2, Ames Research Center, Moffett Field, CA 94035, (415)694-6115 or FTS 464-6115</b>			
16. Abstract <p>A real-time simulation of the UH-60A Black Hawk Helicopter based on the Sikorsky Gen Hel mathematical model is compared with flight test data and Sikorsky's nonreal-time computer program. An overview of the mathematical model is given, including a description of updates and expansion of the model by NASA. Also, real-time programming requirements and techniques are explained. The simulation displays very good agreement with flight test data and excellent agreement with the nonreal-time program on which it is based. The large dedication of effort required to develop the real-time program suggests a need for development of generalized techniques for real-time simulation of high-fidelity physical models of rotorcraft.</p>			
17. Key Words (Suggested by Author(s)) <b>Helicopter flight simulation Helicopter flight dynamics Blade-element rotor</b>		18. Distribution Statement <b>Unclassified - Unlimited</b>  <b>Subject category - 08</b>	
19. Security Classif. (of this report) <b>Unclassified</b>	20. Security Classif. (of this page) <b>Unclassified</b>	21. No. of Pages <b>200</b>	22. Price* <b>A09</b>

